THE UNIVERSITY OF MICHIGAN

3477-1-F

SRCS - XXXIX

THE RADAR CROSS SECTION OF THE B-70 AIRCRAFT

by

R. E. Hiatt and T. B. A. Senior

February 1960

3477-1-F = RL-2101

Report No. 3477-1-F

on

Purchase Order No. LOXO-XZ-250631

Prepared for

NORTH AMERICAN AVIATION, INC.
LOS ANGELES DIVISION
INTERNATIONAL AIRPORT
LOS ANGELES 45, CALIFORNIA
(Prime Contract AF 33(600)-38669)

This document contains information affecting the national defense of the United States within the meaning of the Espionage Laws, Title 18, U.S.C., Section 793 and 794, the transmission or revelation of which in any manner to an unauthorized person is prohibited by law.

MISSING PAGE

MISSING PAGE

MISSING PAGE

MISSING PAGE

MISSING PAGE

MISSING PAGE

TABLE OF CONTENTS

1. INTRODUCTION

The purpose of this report is to describe the theoretical and experimental work carried out by the Radiation Laboratory on the radar reflection characteristics of the B-70 aircraft. In addition to finding the radar (backscattering or monostatic) cross section on the basis of the specifications and models made available to us, a considerable amount of effort has been expended in locating the sources of the dominant returns, and hence in finding ways in which the cross section can be reduced to a more desirable level either by structural modification to the aircraft or by the use of radar absorbing materials.

The theoretical work was confined almost exclusively to a consideration of the return at aspects near to broadside, and this analysis is described in detail in Section 2. The major sources of the return here are the sides of the ducts acting either by themselves or in combination with the undersurfaces of the wings to form corner reflectors. Further contributions are provided by the fuselage itself and by the tail fins. The corner reflector effects can be diminished by changing the dihedral angle, and the formulae relating the change in cross section to the dihedral angle were derived by Dr. F. B. Sleator and Mr. D. M. Raybin of this laboratory (see Appendix). As a result of this and other analyses, certain slight structural modifications to the aircraft are suggested which are sufficient to provide a substantial reduction in the beam cross section at those aspects having operational significance. These modifications are summarized

at the end of Section 2, and amount to a tilting of the duct sides and tail fins with respect to the vertical, coupled with a tilting of the wings above the horizontal.

One of the major aims of the experimental program was to study the cross section at aspects near to forward (out to, say, 50^{o} from nose-on) and to determine ways in which this could be reduced to 40 square meters or less. It was immediately recognized that at these aspects the cross section is almost entirely provided by returns from the air intake ducts. The depth of penetration of the field into the ducts is a function of both the frequency and the aspect, and it is clear that the corresponding return could be reduced to a negligible amount by merely blocking up the ducts. Practically, of course, this is not possible, but the equivalent electromagnetic effect can be achieved with the use of suitably shaped screens and meshes over the apertures. Unfortunately, to function satisfactorily at the higher frequencies the grid spacing must be small and this in turn entails a loss in aerodynamic performance which may not be acceptable. Since it was understood that the NAA is investigating the possible use of widely spaced meshes for the lower frequencies, it was decided to concentrate upon the use of radar absorbing materials suitably placed within the ducts in order to achieve the desired reduction in radar cross section.

Section 3 is devoted to a description of the radar absorbing materials which are available at this moment and which are capable of functioning at the temperatures

experienced within the ducts. One of the more promising materials is Ferroxcube 105, a preliminary investigation of which has been made by Professor D. M. Grimes of the Electrical Engineering Department, The University of Michigan.

The experimental work as such is described in Section 4. This work was carried out at K and X band frequencies using mainly an 8 ft (1:25 scale) model, but also on occasions a 4 ft (1:50 scale) model. Cross section patterns were obtained at a variety of elevations for azimuthal angles out to 100^{o} off nose-on. Those for the model without absorbing materials are reproduced here, as are a sequence of patterns indicating the reduction in cross section consequent upon the introduction of RAM at different locations within the ducts. It is shown that by the selective use of such materials the stipulated figure of 40 square meters out to 50^{o} off nose-on can be achieved. The conclusions reached as a result of the experimental investigations are summarized at the end of Section 4, and the overall recommendations given in Section 5.

The contract agreement with the NAA also provided that The University of Michigan would act as consultant on problems associated with the reduction in the scattering cross section of the B-70 antennas. This consulting service was provided in the form of a lecture given by Professor K. M. Siegel to NAA personnel in Los Angeles on 20 January 1960, and the problem is not therefore treated in this report.

2. BEAM ANALYSIS

The purpose of this section is to describe the calculations which have been carried out to determine the backscattering cross section of the B-70 aircraft for angles at and near to broadside. Calculations have also been made to show the effect of tilting the wings by as much as 20° above the horizontal or tilting the tail fins inwards by this amount, and all the relevant formulae, numerical results and cross sectional plots are given herein. It will be seen that a major reduction in the return at most broadside angles can be achieved in this manner, and ways are suggested by which the cross section can be still further reduced by structural modifications of this type. Other ways of reducing the effect of the broadside return are also proposed.

2.1. Preliminaries

From a study of the aircraft using diagrams and a model it is apparent that the major sources of the return for angles at and near to broadside are

(a) the tail fins
(b) the fuselage
(c) the vertical surface of the ducts. This surface can combine with the under surface of the wings to form one or more corner reflectors whose cross sections can then be appreciable (and, indeed, dominant) over a large range of angles.

The cross sections of (a), (b) and (c) have been computed at frequencies of 10,000, 3,000, 1,000 and 400 Mc, corresponding to wavelengths of 0.03, 0.10, 0.30 and 0.75 m respectively. At these frequencies the dimensions of

the contributing surfaces are all large compared with the wavelength and this allows the methods of physical and geometrical optics to be used in the calculations. At lower frequencies, however, these methods are no longer applicable (one or more of the dimensions being comparable with the wavelength), but the cross sections can be estimated at least in order of magnitude by other means and turn out to be much smaller than at the higher frequencies. In addition, the returns are not then dependent on the detailed structure of the aircraft, and for this reason the numerical work has been confined almost exclusively to the higher frequencies.

The coordinate system which has been used is shown in the following two diagrams. The angle θ measures the tilt of the wings above the horizontal and is allowed to range from 0° to 20° (see Fig. 1); β is the angle in the broadside plane between the direction of observation and the horizontal (the aircraft being assumed to be in level flight), and α is the angle out of the broadside plane, taken as positive when towards the nose of the aircraft (see Fig. 2). The calculations have been made for $0 \leqslant \alpha,\ \beta \leqslant 45^{\circ}$.

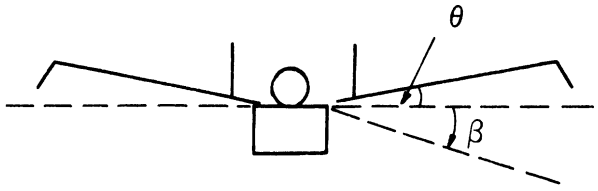

FIGURE 1

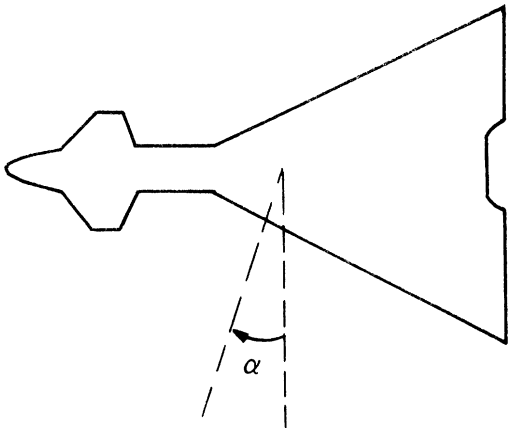

FIGURE 2

2.2. The Idealized Surfaces

In order to determine the cross sections of the tail fins, the fuselage, the duct side and the duct-wing combination, each of these structures is replaced by an equivalent surface or structure to which a mathematical analysis can be applied. Taking first the vertical side of the duct, it is felt that a good approximation to the original shape (as regards the radar return) can be obtained by taking 5 flat surfaces whose aspects are as shown below.

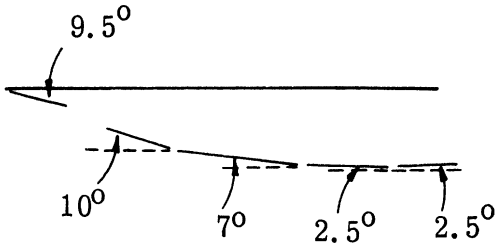

FIGURE 3

If these surfaces are numbered 1 through 5 starting from the left (duct-inlet end), the dimensions are as follows:

Surface	Slant Length	Depth
1	5.21 m. (205 in.)	1.65 m. (65 in.)
2	4.83 m. (190 in.)	1.65 m. (65 in.)
3	10.2 m. (400 in.)	1.45 m. (57 in.)
4	7.62 m. (300 in.)	1.27 m. (50 in.)
5	4.47 m. (176 in.)	0.76 m. (30 in.).

When $\beta = 0$, the cross section of any one of these plates is

$$\sigma = \frac{4\pi A^2}{\lambda^2} \left\{ \frac{\sin(k\ell \sin\alpha')}{k\ell \sin\alpha'} \right\}^2$$

where A is the area, ℓ is the slant length (i.e., actual length rather than projected length) and α' is the angle between the direction of observation and the direction of the peak return from the plate. The peak direction is, of course, normal to the plate surface, and the peak return is

$$\sigma = \frac{4\pi A^2}{\lambda^2},$$

as follows by putting $\alpha' = 0$ in the above. Because of the large values of $k\ell$ for each of the plates, $k\ell \sin\alpha'$ is large compared with unity for every value of α' (apart from $\alpha' \equiv 0$) which has to be considered. Accordingly, $\sin(k\ell \sin\alpha')$ has been replaced by unity in all calculations for non-zero α', so that the pattern factor employed is merely $(k\ell \sin\alpha')^{-2}$. This approximation is equivalent to following the peaks of the side lobes, and the resulting cross section for given α' is the largest that would be observed at angles in the immediate vicinity of α'.

When $\beta \neq 0$, each of the plates will combine with a portion of the adjacent wing surface to form a corner reflector. The selection of the portion to be associated with each plate is largely a matter of judgement, and from a study of the aircraft diagrams it was decided that the appropriate portions could be approximated by the following rectangular areas. In each case the length was chosen equal to that of the corresponding duct plate.

Wing Portion	Length	Breadth
1	5.21 m. (205 in.)	1.80 m. (71 in.)
2	4.83 m. (190 in.)	1.85 m. (73 in.)
3	10.2 m. (400 in.)	4.06 m. (160 in.)
4	7.62 m. (300 in.)	5.33 m. (210 in.)
5	4.47 m. (176 in.)	5.33 m. (210 in.)

The calculation of the cross section for each of these corners involves the consideration of a corner reflector whose arms are not equal and, in addition, whose angle may differ from 90° (as will be the case if $\theta \neq 0$). The appropriate formulae have been derived and are given in the Appendix as functions of β and θ for $\alpha' = 0$. The numerical values obtained for the 5 corners and the associated duct plates ($\beta = 0$) are given in Tables 1 through 5. In each table α' is taken to be zero, and consequently, in order to determine the total contribution of these corners at some chosen azimuth, the tabulated values must be multiplied by the appropriate pattern factors $(k\ell \sin \alpha')^{-2}$. The half and tenth power points of the corner reflector patterns in the azimuthal direction are given in the following table. From these values it is apparent that only with corner reflectors 1, 2 and

(at larger wavelengths) 3, is it possible to get two or more significant contributions to the total scattering cross section at any given azimuth angle.

	0.03m		0.10m		0.30m		0.75m	
CORNER	1/2	1/10	1/2	1/10	1/2	1/10	1/2	1/10
1	0.07^{o}	0.16^{o}	0.24^{o}	0.55^{o}	0.73^{o}	1.64^{o}	1.83^{o}	4.10^{o}
2	0.08^{o}	0.18^{o}	0.26^{o}	0.59^{o}	0.79^{o}	1.77^{o}	1.99^{o}	4.44^{o}
3	0.04^{o}	0.08^{o}	0.13^{o}	0.28^{o}	0.38^{o}	0.84^{o}	0.94^{o}	2.10^{o}
4	0.05^{o}	0.11^{o}	0.18^{o}	0.37^{o}	0.50^{o}	1.12^{o}	1.25^{o}	2.80^{o}
5	0.08^{o}	0.19^{o}	0.28^{o}	0.64^{o}	0.85^{o}	1.91^{o}	2.14^{o}	4.78^{o}

Turning now to the fuselage of the aircraft, the scattering cross section is estimated by considering an equivalent cylinder whose radius a and length ℓ are both large compared with the wavelength. The cross section of such a cylinder is

$$\sigma = k\ell^2 a \left\{ \frac{\sin(k\ell \sin\alpha)}{k\ell \sin\alpha} \right\}^2$$

which is, of course, independent of β. On the other hand, the presence of the wings to the aircraft produces a shielding effect which is a function[+] of β. The amount of shielding was estimated by eye and was taken into account by choosing ℓ differently for different β. For $\beta = 0$, the dimensions of the chosen cylinder were

$$a = 1.5\text{m.} \quad , \quad \ell = 30.5\text{m.}$$

[+] The shielding is also a function of α, but this effect can be ignored because of the restricted beamwidth in the azimuthal direction.

and the corresponding cross sections for $\alpha = \beta = 0$ are

λ	σ
0.03 m	2.22×10^5 m^2
0.10 m	6.67×10^4 m^2
0.30 m	2.22×10^4 m^2
0.75 m	8.89×10^3 m^2

In consequence, the fuselage only produces a significant contribution to the total cross section for azimuthal angles very near to zero (broadside).

For variations in the elevation angle β it is necessary to modify the length of the equivalent cylinder. The required length for each β is obtained by gauging the illuminated portion of the fuselage, and the resulting cross sections are as follows:

λ \ β	10^o	20^o	30^o	40^o	45^o
0.03	2.1×10^5	1.2×10^5	9.8×10^4	8.0×10^4	7.5×10^4
0.10	6.2×10^4	3.5×10^4	2.9×10^4	2.4×10^4	2.2×10^4
0.30	2.1×10^4	1.2×10^4	9.8×10^3	8.0×10^3	7.5×10^3
0.75	8.4×10^3	4.7×10^3	3.9×10^3	3.2×10^3	3.0×10^3

The only surfaces remaining to be considered are the tail fins, and for purposes of analysis these are replaced by equivalent rectangles. Let us first treat the case in which the fins are vertical.

In the broadside plane ($\alpha = 0$) only one fin is seen (the other being completely in shadow) and, in addition, some shadowing may be produced by the wing. In consequence, the dimensions of the chosen rectangle are dependent

on the value of β. When $\beta = 0$, the dimensions were chosen as 4.6m and 4.6m, and the cross sections for $\alpha = \beta = 0$ are then

λ	σ
0.03m	6.10×10^{6} m^2
0.10m	5.49×10^{5} m^2
0.30m	6.10×10^{4} m^2
0.75m	9.75×10^{3} m^2

As β increases the lower portion of the fin is obscured, leading to a reduction in the height of the equivalent rectangle, and by analyzing the degree of shadowing the following cross sections were obtained.

β	σ
10^{o}	1.7×10^{2} m^2
20^{o}	2.9×10^{1} m^2
30^{o}	8.0 m^2

For $\beta > 30^{o}$, a negligible portion of the fin remains unobscured. The fact that the above results are independent of wavelength is a consequence of the cancellation of the wavelength dependence of the flat plate cross section and the pattern factor.

For variations of α with $\beta = 0$, a shadowing of the nearer fin occurs, but now a portion of the second fin can become visible. Taking one fin alone, however, the half and tenth power points are

λ	1/2	1/10
0.03m	0.08^{o}	0.19^{o}
0.10m	0.28^{o}	0.62^{o}
0.30m	0.83^{o}	1.87^{o}
0.75m	2.10^{o}	4.64^{o}

and, in particular, for all but the largest wavelength the contribution from one fin has dropped to an insignificant level by the time α reaches 2.5^{o} (the angle at which the return from corner reflector 4 comes in). Since the contribution from the second fin will only produce a small percentage change in the above results, a calculation of the return from the unobscured portion of this fin is a trifle academic and will be ignored.

If the tail fins are not vertical, but instead are tilted inwards at an angle θ', the peak return is tilted up by twice this amount. The largest return from a fin in the elevation range $0 \leqslant \beta \leqslant 45^{o}$ then occurs at $\beta = 0$, and the cross sections for such a fin with $\alpha = \beta = 0$ are as follows.

θ'	σ
5^{o}	8.60×10^{2} m^2
10^{o}	2.17×10^{2} m^2
15^{o}	9.88×10^{1} m^2
20^{o}	5.59 m^2

These results are again wavelength independent and it will be observed that a tilt of as little as 5^{o} is sufficient to reduce the cross section to less than a tenth that of the fuselage at all frequencies. This will be true for all values of β.

2.3. The Cross Sectional Plots

In Figures 4 through 7 the cross sections are plotted as a function of β for $\alpha = 0$. Each figure is for one wavelength and the various curves are for

different inclinations θ of the wings to the horizontal, the fins being vertical. The cross sections are dominated by the returns from the fuselage and fins, and it is only at the lower frequencies that the returns from the duct-wing combinations become significant. In consequence, the tilting of the wings has little effect upon the patterns. The small oscillations present in the curves are produced by the shadowing effect of the wings on the fuselage and fins. Table 6 gives the numerical data on which Figures 4 - 7 are based.

Figures 8 through 11 differ from Figures 4 - 7 only in that the contribution of the fins has been removed, and apply, therefore, to the case in which the inclination of the fins to the vertical exceeds (about) 5°.

In Figures 12 through 15 the cross sections are plotted as a function of β for $\alpha = 2.5^{\circ}$, the azimuth at which corner reflector 4 produces its peak return. No other corner reflector nor the fuselage contributes, and the return from the tail fins (here assumed vertical) is only apparent at the longer wavelengths. The numerical data is given in Table 7. Figures 16 through 19 similarly show the cross section for $\alpha = 7.0^{\circ}$, and at this azimuth the corner reflector 3 is the sole contributor, (except for a small contribution from the corner reflectors 1 and 2 at $\beta = 0$ for the longest wavelength). The bulk of the data can therefore be taken directly from Table 3. Analogous plots for $\alpha = 9.5^{\circ}$ and 10° are given in Figures 20 - 23 and 24 - 27 respectively. For the first of these sets the corner reflector 1 is mainly responsible, though some contribution

does come from the adjacent reflector. The data is given in Table 8. In the second set the situations are reversed, and the relevant data is shown in Table 9.

In all of Figures 12 through 27 it is apparent that a major reduction in the return for all angles $\beta > 0$ can be achieved by tilting the wings. A more detailed discussion of this will be given in the next section.

The final set of curves (Figs. 28 through 31) show the cross section as functions of α for $\beta = 0$. The tilting of the wings here has no effect and the four figures are for the different wavelengths. The half beam width to one-tenth power is seen to vary from 10.5° to 12°, depending on the wavelength, and these are values which are entirely specified by the angular spread of the vertical surface of the duct. It is to be expected that this width will be much the same for all values of β, notwithstanding the fact that the structure of the beam is a function of elevation.

2.4. Further Remarks

All the results in this section have been obtained by physical and geometrical optics, and since these methods require that the wavelength be smaller (and preferably much smaller) that the dimensions of the contributing structures, the lowest frequency for which the methods can be rigorously justified (as regards the B-70 near broadside) is 400 Mc. At lower frequencies, however, it is expected that the cross section will be appreciably less than the cross sections which we have derived for 400 Mc. Moreover, as the frequency

decreases the cross section depends less and less on the detailed structure of the aircraft, and ultimately, when the wavelength becomes much greater than the overall dimensions of the aircraft, it is the volume of the aircraft which specifies the magnitude of the return. At frequencies greater than 400 Mc, however, the wavelength is small compared with all the important dimensions, and because of the formulae used the cross sections are polarization independent.

Let us now consider the effect of tilting various portions of the aircraft's surface. The portions which can be adjusted in this manner are the fins and duct sides (which can be tilted inwards or outwards) and the wings (which can be tilted up or down). Taking first the fins, if these are both tilted outwards by an amount θ'^{o}, the peak return will occur at $\beta = \theta'$ and will therefore appear in the lower quadrant. Away from the peak (specular) direction, the return falls off rapidly with increasing angle, and it is therefore clear that tilting outwards offers no advantages: indeed, such tilting produces a <u>greater</u> return in the lower quadrant. Tilting inwards, on the other hand, deflects the peak return into the upper quadrant where it is of no consequence, and we have seen that a tilt of as little as 5^{o} is sufficient to reduce the fin return to an insignificant level throughout the entire lower quadrant.

Considering now the wings, if these are tilted θ^{o} downwards, the angle of the corner reflectors will be reduced by this amount and it is then possible for a triple-bounce return to occur at some angle β in the lower quadrant. The

magnitude of this return will be comparable to that from a right angled corner, and will appear in the lower quadrant for any downward tilt of the wings. For this reason, a downward tilt is not recommended (a more complete discussion is given in the Appendix). Tilting the wings upwards, however, will reduce the return from every corner reflector for all $\beta > 0$, and this is clearly shown in the various cross sectional plots. When $\beta = 0$ the tilting of the wings has of course no effect, but apart from this elevation the reduction in the cross section is greater the more the wings are tilted. Nevertheless, the amount of reduction decreases with increasing θ and this suggests that a tilt of 5^{o} may be sufficient.

Throughout the above paragraph it has been assumed that the sides of the duct are vertical, but a major improvement will result from tilting these sides inwards[+]. If the tilt is ϕ^{o} and if the wings are also tilted upwards by $\theta^{o} + \phi^{o}$, the magnitude of the return in the lower quadrant can be determined from Figures 12 through 27 if the 'β' on these graphs is replaced by '$\beta - \phi$'. Excluding for the moment the plane $\alpha = 0$ (at broadside the fuselage return dominates), it can be seen that a tilt of, for example, 5^{o} in combination with a wing tilt of 10^{o} ($\theta = 5^{o}$ on the graphs) reduces the return to less than 2×10^{4} m^2 for all $\alpha \neq 0$ and all β; in combination with a wing tilt of 15^{o} ($\theta = 10^{o}$ on the graphs), the corresponding level is 5×10^{3} m^2.

[+] An outward tilt is detrimental for the reason given in the discussion of the fins.

It will be appreciated that such returns are less than the broadside returns ($\alpha = 0$) at the higher frequencies even when the fins are tilted. On the other hand, broadside returns are essentially due to the fuselage alone and it is not impossible that the use of an equivalent cylinder has given an unduly large return. Any fore-and-aft curvature which is present in the actual fuselage will reduce the return at $\alpha = 0$, whilst increasing the cross section at other values of α, and may bring down the broadside return to 10^4 m^2. In practice, therefore, it is felt that the overall cross section throughout the entire broadside beam in the lower quadrant can be reduced to 10^4 m^2 by tilting both the duct sides and the fin through 5^o, and by tilting the wing by (about) 10.0^o.

In passing, we note that with the unmodified aircraft the experimental results in Section 4.3.1 show a peak broadside cross section of 10^4 m^2 at a simulated frequency of 388 Mc (pattern A-1). For comparison with this we see from Figure 7 that the calculated peak return at 400 Mc is 1.9×10^4 m^2. Bearing in mind that the experimental value is a near-field measurement and is for a somewhat lower frequency (both of these would tend to reduce the cross section), the agreement between theory and experiment is extremely good.

Finally, it should be pointed out that the analysis has been based upon the aircraft shown in the diagrams supplied to us and in consequence no account has been taken of any radomes or antennas which may be subsequently added to the plane.

2.5. Summary Conclusions

To reduce the peak cross section of the broadside beam as observed in the elevation range $0 \leqslant \beta \leqslant 45^{\circ}$, the fins should be tilted upwards, the duct sides should be tilted inwards and the wings should be tilted upwards. A 5° tilt for the fins should be sufficient. With the same tilt for the ducts and a 10° tilt for the wings, the peak cross section will be reduced to approximately 10^{4} m^2. The azimuthal beam width is essentially determined by the curvature (fore-and-aft) of the ducts, and will not be affected to any marked extent by the above changes.

Alternatively, if the aim is to reduce the width of the broadside lobe at the expense of some increase in the peak return, this can be achieved by leaving the wings horizontal and the duct sides vertical, but straightening (fore-and-aft) the sides of the duct. If it is assumed that the tail fins are tilted as described above, the effect of this new modification will be to raise the peak return (at $\alpha = \beta = 0$) to approximately 8×10^{7} m^2 for $\lambda = 0.03$ m (4×10^{4} m^2 for $\lambda = 0.75$ m), but to reduce the half beam width (to one hundredth power point) to approximately 0.1° for $\lambda = 0.03$ m (2.4° for $\lambda = 0.75$ m). Although this appears to be an attractive proposition it may not be practically possible to straighten all the duct including, for example, portions 1 and 2 shown in Figure 3. Any curvature which is left in the duct will obviously increase the above (minimum) beamwidths.

Cross Section of Corner Reflector 1 ($\alpha = 9.5^{o}$)

β	λ	$\theta = 0^{o}$	$\theta = 5^{o}$	$\theta = 10^{o}$	$\theta = 15^{o}$	$\theta = 20^{o}$
0^{o}	0.03	1.03×10^{6}	independent of θ			
	0.10	9.29×10^{4}				
	0.30	1.03×10^{4}				
	0.75	1.65×10^{3}				
10^{o}	0.03	1.49×10^{5}	1.15×10^{3}	2.95×10^{2}	1.38×10^{2}	8.36×10^{1}
	0.10	1.34×10^{4}	1.12×10^{3}	2.95×10^{2}	1.38×10^{2}	8.35×10^{1}
	0.30	1.48×10^{3}	3.32×10^{2}	2.39×10^{2}	1.37×10^{2}	6.18×10^{1}
	0.75	2.37×10^{2}	5.85×10^{1}	5.54×10^{1}	5.12×10^{1}	4.66×10^{1}
20^{o}	0.03	5.77×10^{5}	4.58×10^{3}	2.95×10^{2}	1.38×10^{2}	8.35×10^{1}
	0.10	5.18×10^{4}	4.54×10^{3}	2.95×10^{2}	1.38×10^{2}	8.35×10^{1}
	0.30	5.75×10^{3}	2.37×10^{3}	1.91×10^{2}	1.38×10^{2}	8.36×10^{1}
	0.75	9.20×10^{2}	4.97×10^{2}	1.76×10^{2}	1.28×10^{2}	8.29×10^{1}
30^{o}	0.03	1.23×10^{6}	4.58×10^{3}	1.18×10^{3}	1.38×10^{2}	8.36×10^{1}
	0.10	1.11×10^{5}	4.58×10^{3}	1.18×10^{3}	1.38×10^{2}	8.35×10^{1}
	0.30	1.23×10^{4}	4.13×10^{3}	1.07×10^{3}	1.38×10^{2}	8.36×10^{1}
	0.75	1.97×10^{3}	1.24×10^{3}	5.74×10^{2}	1.25×10^{2}	3.60×10^{1}
40^{o}	0.03	2.04×10^{6}	4.58×10^{3}	1.18×10^{3}	5.52×10^{2}	8.36×10^{1}
	0.10	1.83×10^{5}	4.58×10^{3}	1.18×10^{3}	5.52×10^{2}	8.35×10^{1}
	0.30	2.03×10^{4}	3.95×10^{3}	9.60×10^{2}	5.51×10^{2}	8.36×10^{1}
	0.75	3.25×10^{3}	2.10×10^{3}	9.26×10^{2}	3.21×10^{2}	5.29×10^{1}
45^{o}	0.03	2.07×10^{6}	4.58×10^{3}	1.18×10^{3}	5.52×10^{2}	3.34×10^{2}
	0.10	1.86×10^{5}	4.58×10^{3}	1.18×10^{3}	5.52×10^{2}	3.34×10^{2}
	0.30	2.06×10^{4}	4.09×10^{3}	5.80×10^{2}	3.73×10^{2}	2.92×10^{2}
	0.75	3.30×10^{3}	2.18×10^{3}	1.03×10^{3}	4.56×10^{2}	1.55×10^{2}

TABLE 1

Cross Section of Corner Reflector 2 ($\alpha = 10^0$)

β	λ	$\theta = 0^0$	$\theta = 5^0$	$\theta = 10^0$	$\theta = 15^0$	$\theta = 20^0$
0^0	0.03	8.90×10^5	independent of θ			
	0.10	7.94×10^4				
	0.30	8.84×10^3				
	0.75	1.41×10^3				
10^0	0.03	1.35×10^5	9.83×10^2	2.54×10^2	1.19×10^2	7.18×10^1
	0.10	1.21×10^4	9.50×10^2	2.54×10^2	1.19×10^2	7.18×10^1
	0.30	1.35×10^3	3.00×10^2	2.12×10^2	1.17×10^2	4.92×10^1
	0.75	2.15×10^2	5.29×10^1	5.02×10^1	4.62×10^1	4.16×10^1
20^0	0.03	5.24×10^5	3.93×10^3	2.54×10^2	1.19×10^2	7.18×10^1
	0.10	4.70×10^4	3.87×10^3	2.54×10^2	1.19×10^2	7.18×10^1
	0.30	5.22×10^3	2.11×10^3	1.48×10^2	1.19×10^2	7.18×10^1
	0.75	8.36×10^2	4.50×10^2	1.58×10^2	1.12×10^2	7.05×10^1
30^0	0.03	1.12×10^6	3.93×10^3	1.01×10^3	1.19×10^2	7.18×10^1
	0.10	1.00×10^5	3.93×10^3	1.01×10^3	1.19×10^2	7.18×10^1
	0.30	1.12×10^4	3.58×10^3	9.28×10^2	1.19×10^2	7.18×10^1
	0.75	1.79×10^3	1.12×10^3	5.08×10^2	1.03×10^2	2.61×10^1
40^0	0.03	1.85×10^6	3.93×10^3	1.01×10^3	4.74×10^2	7.18×10^1
	0.10	1.66×10^5	3.93×10^3	1.01×10^3	4.74×10^2	7.18×10^1
	0.30	1.85×10^4	3.35×10^3	7.90×10^2	4.71×10^2	7.18×10^1
	0.75	2.95×10^3	1.86×10^3	8.09×10^2	2.82×10^2	4.55×10^1
45^0	0.03	1.78×10^6	3.93×10^3	1.01×10^3	4.74×10^2	2.87×10^2
	0.10	1.59×10^5	3.93×10^3	1.01×10^3	4.74×10^2	2.87×10^2
	0.30	1.77×10^4	3.45×10^3	4.49×10^2	3.00×10^2	2.55×10^2
	0.75	2.83×10^3	1.91×10^3	8.94×10^2	3.98×10^2	1.36×10^2

TABLE 2

Cross Section of Corner Reflector 3 ($\alpha = 7.0^{\circ}$)

β	λ	$\theta = 0^{\circ}$	$\theta = 5^{\circ}$	$\theta = 10^{\circ}$	$\theta = 15^{\circ}$	$\theta = 20^{\circ}$
0°	0.03	3.03×10^{6}	independent of θ			
	0.10	2.71×10^{5}				
	0.30	3.02×10^{4}				
	0.75	4.38×10^{3}				
10°	0.03	2.88×10^{6}	4.36×10^{3}	1.12×10^{3}	5.26×10^{2}	3.18×10^{2}
	0.10	2.58×10^{5}	4.36×10^{3}	1.12×10^{3}	5.26×10^{2}	3.18×10^{2}
	0.30	2.87×10^{4}	4.01×10^{3}	3.76×10^{2}	5.26×10^{2}	3.18×10^{2}
	0.75	4.59×10^{3}	1.05×10^{3}	8.06×10^{2}	5.21×10^{2}	2.85×10^{2}
20°	0.03	1.07×10^{7}	1.74×10^{4}	1.12×10^{3}	5.26×10^{2}	3.18×10^{2}
	0.10	9.59×10^{5}	1.74×10^{4}	1.12×10^{3}	5.26×10^{2}	3.18×10^{2}
	0.30	1.07×10^{5}	1.18×10^{4}	1.12×10^{3}	5.26×10^{2}	3.18×10^{2}
	0.75	1.71×10^{4}	7.44×10^{3}	1.07×10^{3}	1.97×10^{2}	7.83×10^{1}
30°	0.03	9.08×10^{6}	1.74×10^{4}	4.49×10^{3}	5.26×10^{2}	3.18×10^{2}
	0.10	8.15×10^{5}	1.74×10^{4}	4.49×10^{3}	5.26×10^{2}	3.18×10^{2}
	0.30	9.05×10^{4}	1.01×10^{4}	2.80×10^{3}	5.26×10^{2}	3.18×10^{2}
	0.75	1.45×10^{4}	1.08×10^{4}	3.83×10^{3}	3.72×10^{2}	1.13×10^{2}
40°	0.03	7.11×10^{6}	1.74×10^{4}	4.49×10^{3}	2.10×10^{3}	3.18×10^{2}
	0.10	6.37×10^{5}	1.74×10^{4}	4.50×10^{3}	2.10×10^{3}	3.18×10^{2}
	0.30	7.08×10^{4}	1.40×10^{4}	4.49×10^{3}	2.10×10^{3}	3.18×10^{2}
	0.75	1.13×10^{4}	8.99×10^{3}	4.26×10^{3}	2.06×10^{3}	2.75×10^{2}
45°	0.03	6.05×10^{6}	1.74×10^{4}	4.49×10^{3}	2.10×10^{3}	1.27×10^{3}
	0.10	5.43×10^{5}	1.74×10^{4}	4.50×10^{3}	2.10×10^{3}	1.27×10^{3}
	0.30	6.03×10^{4}	1.57×10^{4}	1.54×10^{3}	2.10×10^{3}	9.07×10^{2}
	0.75	9.65×10^{3}	7.91×10^{3}	4.14×10^{3}	1.72×10^{3}	1.05×10^{3}

TABLE 3

Cross Section of Corner Reflector 4 ($\alpha = 2.5^{\circ}$)

β	λ	$\theta = 0^{\circ}$	$\theta = 5^{\circ}$	$\theta = 10^{\circ}$	$\theta = 15^{\circ}$	$\theta = 20^{\circ}$
0°	0.03	1.31×10^{6}	independent of θ			
	0.10	1.18×10^{5}				
	0.30	1.31×10^{4}				
	0.75	2.09×10^{3}				
10°	0.03	2.79×10^{6}	2.45×10^{3}	6.32×10^{2}	2.96×10^{2}	1.79×10^{2}
	0.10	2.50×10^{5}	2.45×10^{3}	6.32×10^{2}	2.96×10^{2}	1.79×10^{2}
	0.30	2.78×10^{4}	2.42×10^{3}	6.32×10^{2}	2.96×10^{2}	1.79×10^{2}
	0.75	4.45×10^{3}	9.52×10^{2}	5.95×10^{2}	2.58×10^{2}	6.55×10^{1}
20°	0.03	4.63×10^{6}	9.81×10^{3}	6.32×10^{2}	2.96×10^{2}	1.79×10^{2}
	0.10	4.15×10^{5}	9.81×10^{3}	6.32×10^{2}	2.96×10^{2}	1.79×10^{2}
	0.30	4.61×10^{4}	8.49×10^{3}	6.32×10^{2}	2.96×10^{2}	1.79×10^{2}
	0.75	7.38×10^{3}	4.57×10^{3}	6.32×10^{2}	2.00×10^{2}	4.47×10^{1}
30°	0.03	3.93×10^{6}	9.81×10^{3}	2.53×10^{3}	2.96×10^{2}	1.79×10^{2}
	0.10	3.53×10^{5}	9.81×10^{3}	2.53×10^{3}	2.96×10^{2}	1.79×10^{2}
	0.30	3.92×10^{4}	8.09×10^{3}	2.53×10^{3}	2.96×10^{2}	3.92×10^{2}
	0.75	6.27×10^{3}	5.00×10^{3}	2.41×10^{3}	2.68×10^{2}	1.18×10^{2}
40°	0.03	3.08×10^{6}	9.81×10^{3}	2.53×10^{3}	1.18×10^{3}	1.79×10^{2}
	0.10	2.76×10^{5}	9.81×10^{3}	2.53×10^{3}	1.18×10^{3}	1.79×10^{2}
	0.30	3.07×10^{4}	9.30×10^{3}	9.37×10^{2}	1.18×10^{3}	1.79×10^{2}
	0.75	4.90×10^{3}	4.10×10^{3}	2.33×10^{3}	1.10×10^{3}	1.76×10^{3}
45°	0.03	2.62×10^{6}	9.81×10^{3}	2.53×10^{3}	1.18×10^{3}	7.16×10^{2}
	0.10	2.35×10^{5}	9.81×10^{3}	2.53×10^{3}	1.18×10^{3}	7.16×10^{2}
	0.30	2.61×10^{4}	9.58×10^{3}	1.44×10^{3}	1.18×10^{3}	1.84×10^{2}
	4.18	4.18×10^{3}	3.58×10^{3}	2.19×10^{3}	8.70×10^{2}	6.74×10^{2}

TABLE 4

Cross Section of Corner Reflector 5 ($\alpha = -2.5^{o}$)

β	λ	$\theta = 0^{o}$	$\theta = 5^{o}$	$\theta = 10^{o}$	$\theta = 15^{o}$	$\theta = 20^{o}$
0^{o}	0.03	1.62×10^{5}	independent of θ			
	0.10	1.46×10^{4}				
	0.30	1.62×10^{3}				
	0.75	2.59×10^{2}				
10^{o}	0.03	6.30×10^{5}	8.44×10^{2}	2.18×10^{2}	1.02×10^{2}	6.16×10^{1}
	0.10	5.65×10^{4}	8.44×10^{2}	2.18×10^{2}	1.02×10^{2}	6.16×10^{1}
	0.30	6.28×10^{3}	7.99×10^{2}	6.51×10^{1}	1.02×10^{2}	6.16×10^{1}
	0.75	1.00×10^{3}	2.19×10^{2}	1.59×10^{2}	1.00×10^{2}	5.90×10^{1}
20^{o}	0.03	5.73×10^{5}	3.38×10^{3}	2.18×10^{2}	1.02×10^{2}	6.16×10^{1}
	0.10	5.14×10^{4}	3.38×10^{3}	2.18×10^{2}	1.02×10^{2}	6.16×10^{1}
	0.30	5.71×10^{3}	3.12×10^{3}	1.08×10^{2}	1.02×10^{2}	6.16×10^{1}
	0.75	9.14×10^{2}	8.29×10^{2}	1.43×10^{2}	9.48×10^{1}	6.16×10^{1}
30^{o}	0.03	4.87×10^{5}	3.38×10^{3}	8.70×10^{2}	1.02×10^{2}	6.16×10^{1}
	0.10	4.37×10^{4}	3.38×10^{3}	8.70×10^{2}	1.02×10^{2}	6.16×10^{1}
	0.30	4.85×10^{3}	2.91×10^{3}	5.21×10^{2}	1.02×10^{1}	6.16×10^{1}
	0.75	7.77×10^{2}	7.14×10^{2}	5.55×10^{2}	8.31×10^{1}	5.77×10^{1}
40^{o}	0.03	3.81×10^{5}	3.38×10^{3}	8.70×10^{2}	4.07×10^{2}	6.16×10^{1}
	0.10	3.42×10^{4}	1.22×10^{3}	8.70×10^{2}	4.07×10^{2}	6.16×10^{1}
	0.30	3.80×10^{3}	2.54×10^{3}	6.18×10^{2}	3.13×10^{2}	1.84×10^{1}
	0.75	6.08×10^{2}	5.68×10^{2}	4.61×10^{2}	3.24×10^{2}	4.50×10^{1}
45^{o}	0.03	3.25×10^{5}	3.38×10^{3}	8.70×10^{2}	4.07×10^{2}	2.46×10^{2}
	0.10	2.91×10^{4}	1.79×10^{3}	8.70×10^{2}	4.07×10^{2}	2.46×10^{2}
	0.30	3.24×10^{3}	2.30×10^{3}	6.95×10^{2}	3.72×10^{2}	4.37×10^{1}
	0.75	5.18×10^{2}	4.87×10^{2}	4.06×10^{2}	2.93×10^{2}	1.80×10^{2}

TABLE 5

Total Cross Section at $\alpha = 0$ (fins vertical)

β	λ	$\theta = 0^\circ$	$\theta = 5^\circ$	$\theta = 10^\circ$	$\theta = 15^\circ$	$\theta = 20^\circ$
0°	0.03	6.3×10^6	independent of θ			
	0.10	6.2×10^5				
	0.30	8.3×10^4				
	0.75	1.9×10^4				
10°	0.03	2.1×10^5	2.1×10^5	2.1×10^5	2.1×10^5	2.1×10^5
	0.10	6.3×10^4	6.2×10^4	6.2×10^4	6.2×10^4	6.2×10^4
	0.30	2.2×10^4	2.1×10^4	2.1×10^4	2.1×10^4	2.1×10^4
	0.75	9.6×10^3	8.8×10^1	8.7×10^3	8.7×10^3	8.6×10^3
20°	0.03	1.2×10^5	1.2×10^5	1.2×10^5	1.2×10^5	1.2×10^5
	0.10	3.7×10^4	3.5×10^4	3.5×10^4	3.5×10^4	3.5×10^4
	0.30	1.3×10^4	1.2×10^4	1.2×10^4	1.2×10^4	1.2×10^4
	0.75	6.2×10^3	5.6×10^3	4.9×10^3	4.8×10^3	4.8×10^3
30°	0.03	9.9×10^4	9.8×10^4	9.8×10^4	9.8×10^4	9.8×10^4
	0.10	3.0×10^4	2.9×10^4	2.9×10^4	2.9×10^4	2.9×10^4
	0.30	1.1×10^4	1.0×10^4	9.9×10^3	9.8×10^3	9.8×10^3
	0.75	5.2×10^3	5.0×10^3	4.5×10^3	4.0×10^3	4.0×10^3
40°	0.03	8.1×10^4	8.0×10^4	8.0×10^4	8.0×10^4	8.0×10^4
	0.10	2.5×10^4	2.4×10^4	2.4×10^4	2.4×10^4	2.4×10^4
	0.30	9.1×10^3	8.4×10^3	8.0×10^3	8.0×10^3	8.0×10^3
	0.75	4.3×10^3	4.1×10^3	3.7×10^3	3.5×10^3	3.2×10^3
45°	0.03	7.6×10^4	7.5×10^4	7.5×10^4	7.5×10^4	7.5×10^4
	0.10	2.3×10^4	2.2×10^4	2.2×10^4	2.2×10^4	2.2×10^4
	0.30	8.4×10^3	7.9×10^3	7.6×10^3	7.6×10^3	7.5×10^3
	0.75	3.9×10^3	3.8×10^3	3.5×10^3	3.2×10^3	3.2×10^3

Total Cross Section at $\alpha = 2.5^{\circ}$

β	λ	$\theta = 0^{\circ}$	$\theta = 5^{\circ}$	$\theta = 10^{\circ}$	$\theta = 15^{\circ}$	$\theta = 20^{\circ}$
0°	0.03	1.31×10^{6}	independent of θ			
	0.10	1.21×10^{5}				
	0.30	1.66×10^{4}				
	0.75	5.55×10^{3}				
10°	0.03	2.79×10^{6}	2.45×10^{3}	6.32×10^{2}	2.96×10^{2}	1.79×10^{2}
	0.10	2.50×10^{5}	2.45×10^{3}	6.33×10^{2}	2.97×10^{2}	1.80×10^{2}
	0.30	2.78×10^{4}	2.43×10^{3}	6.42×10^{2}	3.06×10^{2}	1.89×10^{2}
	0.75	4.51×10^{3}	1.01×10^{3}	6.55×10^{2}	3.18×10^{2}	1.26×10^{2}
20°	0.03	4.63×10^{6}	9.81×10^{3}	6.32×10^{2}	2.96×10^{2}	1.79×10^{2}
	0.10	4.15×10^{5}	9.81×10^{3}	6.32×10^{2}	2.96×10^{2}	1.79×10^{2}
	0.30	4.61×10^{4}	8.49×10^{3}	6.34×10^{2}	2.98×10^{2}	1.81×10^{2}
	0.75	7.39×10^{3}	4.58×10^{3}	6.42×10^{2}	2.10×10^{2}	5.50×10^{1}
30°	0.03	3.93×10^{6}	9.81×10^{3}	2.53×10^{3}	2.96×10^{2}	1.79×10^{2}
	0.10	3.53×10^{5}	9.81×10^{3}	2.53×10^{3}	2.96×10^{2}	1.79×10^{2}
	0.30	3.92×10^{4}	8.09×10^{3}	2.53×10^{3}	2.96×10^{2}	3.92×10^{4}
	0.75	6.27×10^{3}	5.00×10^{3}	2.41×10^{3}	2.71×10^{2}	1.21×10^{2}
40°	0.03	3.08×10^{6}	9.81×10^{3}	2.53×10^{3}	1.18×10^{3}	1.79×10^{2}
	0.10	2.76×10^{5}	9.81×10^{3}	2.53×10^{3}	1.18×10^{3}	1.79×10^{2}
	0.30	3.07×10^{4}	9.30×10^{3}	9.37×10^{2}	1.18×10^{3}	1.79×10^{2}
	0.75	4.90×10^{3}	4.10×10^{3}	2.33×10^{3}	1.10×10^{3}	1.76×10^{3}
45°	0.03	2.62×10^{6}	9.81×10^{3}	2.53×10^{3}	1.18×10^{3}	7.16×10^{2}
	0.10	2.35×10^{5}	9.81×10^{3}	2.53×10^{3}	1.18×10^{3}	7.16×10^{2}
	0.30	2.61×10^{4}	9.58×10^{3}	1.44×10^{3}	1.18×10^{3}	1.84×10^{2}
	0.75	4.18×10^{3}	3.58×10^{3}	2.19×10^{3}	8.70×10^{2}	6.74×10^{2}

TABLE 7

Total Cross Section at $\alpha = 9.5^{\circ}$

β	λ	$\theta = 0^{\circ}$	$\theta = 5^{\circ}$	$\theta = 10^{\circ}$	$\theta = 15^{\circ}$	$\theta = 20^{\circ}$
0°	0.03	1.04×10^{6}	independent of θ			
	0.10	1.04×10^{5}				
	0.30	2.16×10^{4}				
	0.75	1.30×10^{4}				
10°	0.03	1.50×10^{5}	1.16×10^{3}	2.98×10^{2}	1.40×10^{2}	8.45×10^{1}
	0.10	1.51×10^{4}	1.26×10^{3}	3.31×10^{2}	1.55×10^{2}	9.38×10^{1}
	0.30	3.21×10^{3}	7.18×10^{2}	5.11×10^{2}	2.88×10^{2}	1.25×10^{2}
	0.75	1.97×10^{3}	4.84×10^{2}	4.59×10^{2}	4.23×10^{2}	3.81×10^{2}
20°	0.03	5.84×10^{5}	4.63×10^{3}	2.98×10^{2}	1.40×10^{2}	8.45×10^{1}
	0.10	5.85×10^{4}	5.09×10^{3}	3.31×10^{2}	1.55×10^{2}	9.38×10^{1}
	0.30	1.25×10^{4}	5.09×10^{3}	3.82×10^{2}	2.91×10^{2}	1.76×10^{2}
	0.75	7.64×10^{3}	4.12×10^{3}	1.44×10^{3}	1.03×10^{3}	6.49×10^{2}
30°	0.03	1.25×10^{6}	4.63×10^{3}	1.19×10^{3}	1.40×10^{2}	8.45×10^{1}
	0.10	1.25×10^{5}	5.14×10^{3}	1.33×10^{3}	1.55×10^{2}	9.38×10^{1}
	0.30	2.67×10^{4}	8.73×10^{3}	2.26×10^{3}	2.91×10^{2}	1.76×10^{2}
	0.75	1.63×10^{4}	1.03×10^{4}	4.66×10^{3}	9.54×10^{2}	2.46×10^{2}
40°	0.03	2.06×10^{6}	4.63×10^{3}	1.19×10^{3}	5.58×10^{2}	8.45×10^{1}
	0.10	2.07×10^{5}	5.14×10^{3}	1.33×10^{3}	6.20×10^{2}	9.38×10^{1}
	0.30	4.41×10^{4}	8.26×10^{3}	1.98×10^{3}	1.16×10^{3}	1.76×10^{2}
	0.75	2.70×10^{4}	1.70×10^{4}	7.43×10^{3}	2.59×10^{3}	4.18×10^{2}
45°	0.03	2.09×10^{6}	4.63×10^{3}	1.19×10^{3}	5.58×10^{2}	3.38×10^{2}
	0.10	2.08×10^{5}	5.14×10^{3}	1.33×10^{3}	6.20×10^{2}	3.75×10^{2}
	0.30	4.34×10^{4}	8.52×10^{3}	1.16×10^{3}	7.59×10^{2}	6.20×10^{2}
	0.75	2.61×10^{4}	1.76×10^{4}	8.21×10^{3}	3.65×10^{3}	1.25×10^{3}

TABLE 8

Total Cross Section at $\alpha = 10^{o}$

β	λ	$\theta = 0^{o}$	$\theta = 5^{o}$	$\theta = 10^{o}$	$\theta = 15^{o}$	$\theta = 20^{o}$
0^{o}	0.03	9.01×10^{5}	independent of θ			
	0.10	9.08×10^{4}				
	0.30	2.02×10^{4}				
	0.75	1.28×10^{4}				
10^{o}	0.03	1.37×10^{5}	9.96×10^{2}	2.57×10^{2}	1.20×10^{2}	7.27×10^{1}
	0.10	1.38×10^{4}	1.09×10^{3}	2.90×10^{2}	1.36×10^{2}	8.20×10^{1}
	0.30	2.98×10^{3}	6.67×10^{2}	4.76×10^{2}	2.69×10^{2}	1.18×10^{2}
	0.75	1.85×10^{3}	4.57×10^{2}	4.33×10^{2}	4.00×10^{2}	3.63×10^{2}
20^{o}	0.03	5.30×10^{5}	3.98×10^{3}	2.57×10^{2}	1.20×10^{2}	7.27×10^{1}
	0.10	5.34×10^{4}	4.42×10^{3}	2.90×10^{2}	1.36×10^{2}	8.20×10^{1}
	0.30	1.16×10^{4}	4.73×10^{3}	3.59×10^{2}	2.71×10^{2}	1.64×10^{2}
	0.75	7.19×10^{3}	3.89×10^{3}	1.37×10^{3}	9.92×10^{2}	6.43×10^{2}
30^{o}	0.03	1.13×10^{6}	3.98×10^{3}	1.03×10^{3}	1.20×10^{2}	7.27×10^{1}
	0.10	1.14×10^{5}	4.50×10^{3}	1.16×10^{3}	1.36×10^{2}	8.20×10^{1}
	0.30	2.47×10^{4}	8.13×10^{3}	2.10×10^{3}	2.71×10^{2}	1.64×10^{2}
	0.75	1.54×10^{4}	9.71×10^{3}	4.47×10^{3}	4.82×10^{3}	2.74×10^{2}
40^{o}	0.03	1.87×10^{6}	3.98×10^{3}	1.03×10^{3}	4.81×10^{2}	7.27×10^{1}
	0.10	1.88×10^{5}	4.50×10^{3}	1.16×10^{3}	5.42×10^{2}	8.20×10^{1}
	0.30	4.10×10^{4}	7.72×10^{3}	1.85×10^{3}	1.08×10^{3}	1.64×10^{2}
	0.75	2.54×10^{4}	1.64×10^{4}	7.20×10^{3}	2.50×10^{3}	4.11×10^{2}
45^{o}	0.03	1.80×10^{6}	3.98×10^{3}	1.03×10^{3}	4.81×10^{2}	2.91×10^{2}
	0.10	1.82×10^{5}	4.50×10^{3}	1.16×10^{3}	5.42×10^{2}	3.28×10^{2}
	0.30	4.05×10^{4}	7.96×10^{3}	1.09×10^{3}	7.12×10^{2}	5.78×10^{2}
	0.75	2.56×10^{4}	1.70×10^{4}	7.98×10^{3}	3.54×10^{3}	1.21×10^{3}

TABLE 9

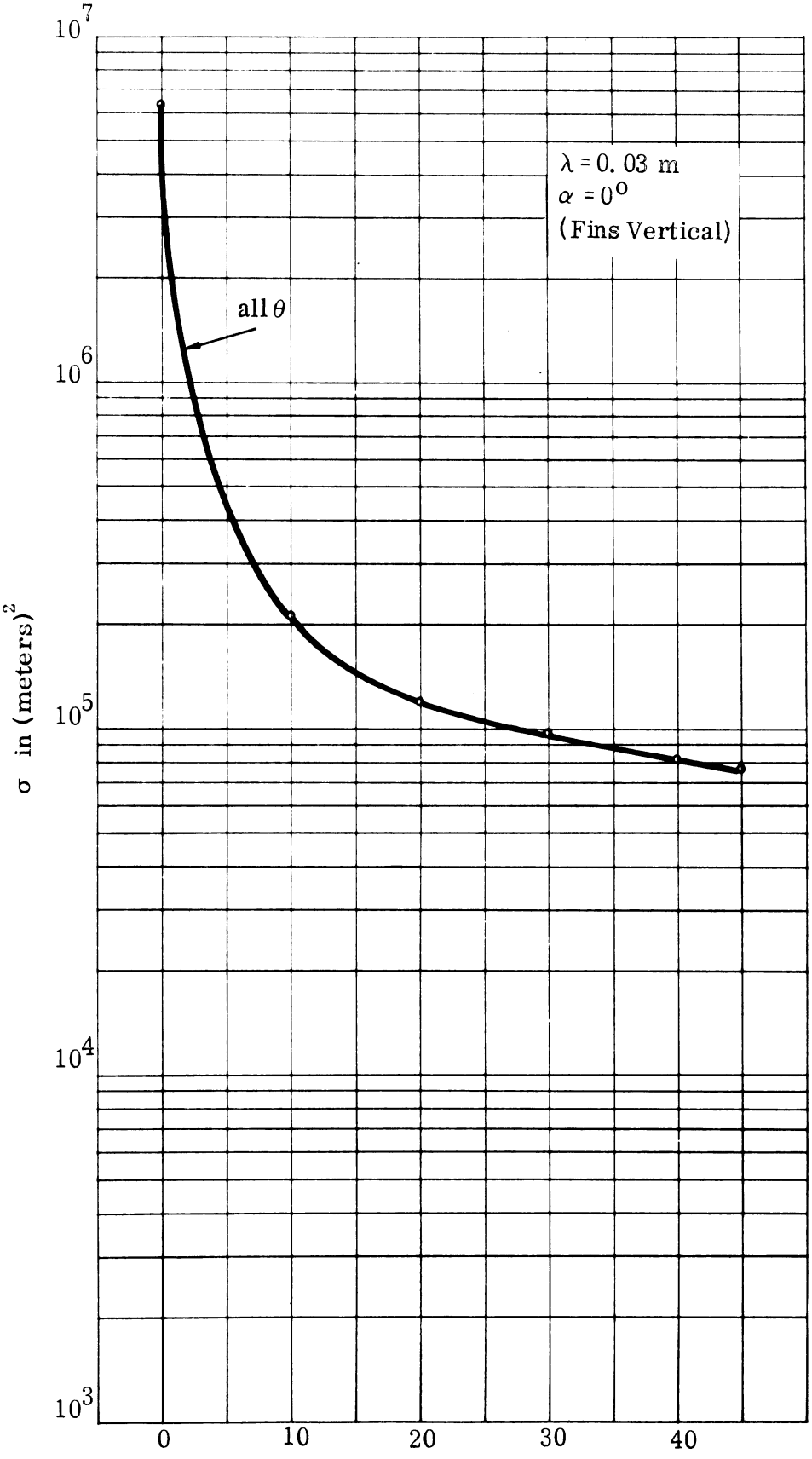
10^7
10^6
10^5
10^4
10^3
σ in (meters)^2
λ = 0.03 m
α = 0°
(Fins Vertical)
all θ
0
10
20
30
40
β in degrees

FIGURE 4

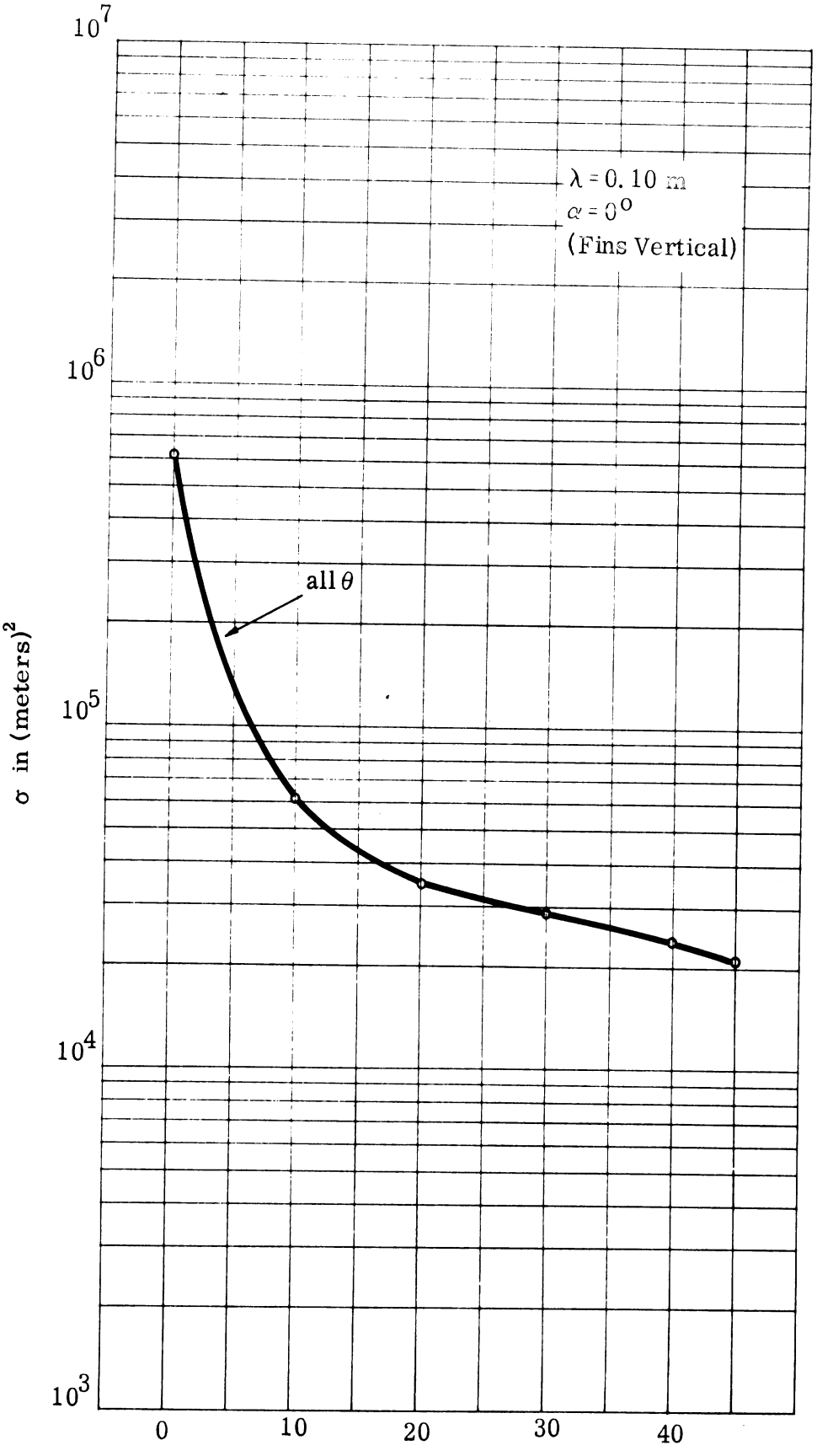
10^7
10^6
10^5
10^4
10^3
$\lambda = 0.10$ m
$\alpha = 0^o$
(Fins Vertical)
all θ
σ in (meters)^2
0
10
20
30
40
β in degrees

FIGURE 5

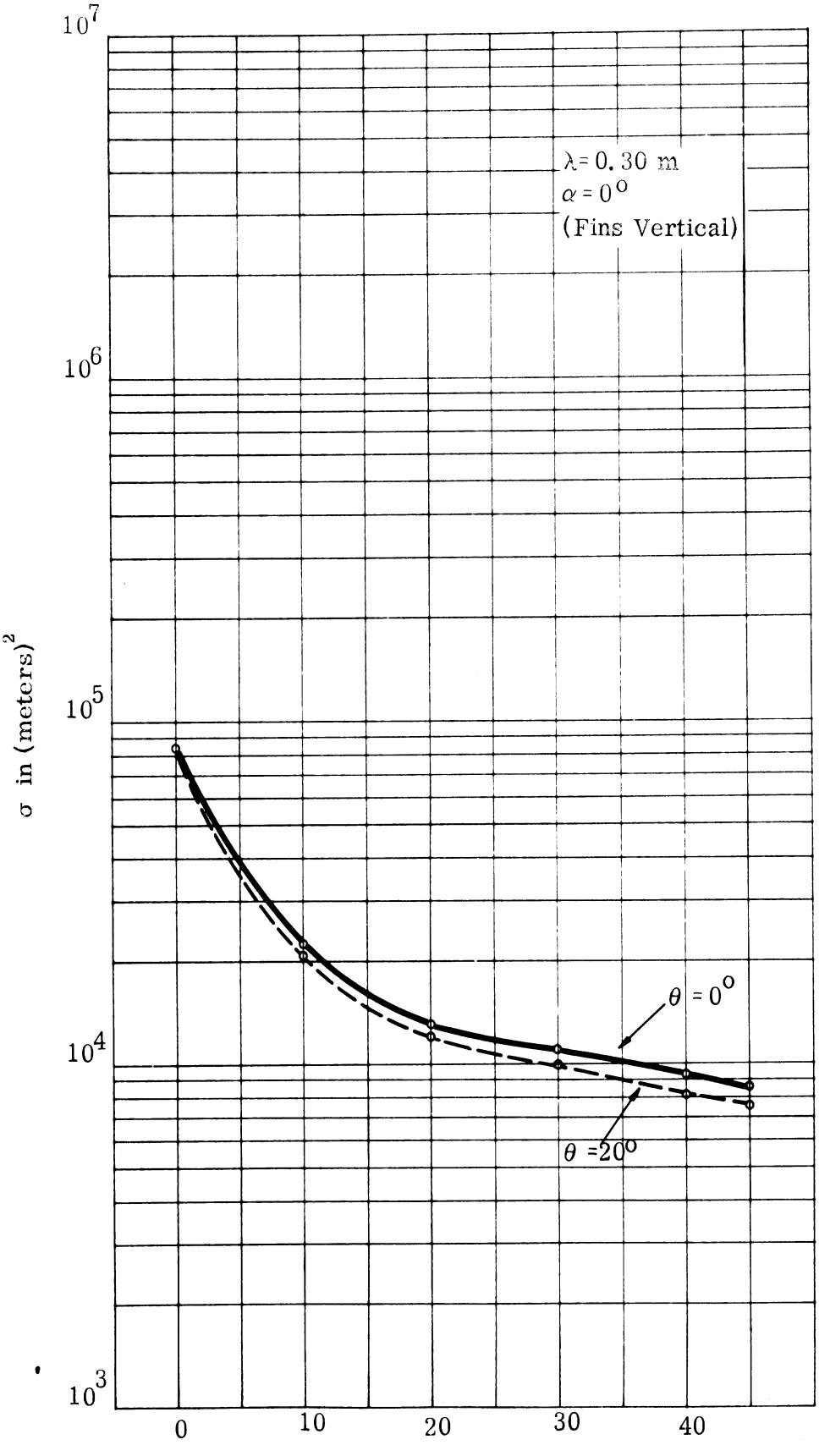
10^7
10^6
10^5
10^4
10^3
σ in (meters)^2
λ = 0.30 m
α = 0°
(Fins Vertical)
θ = 0°
θ = 20°
0
10
20
30
40
β in degrees

FIGURE 6

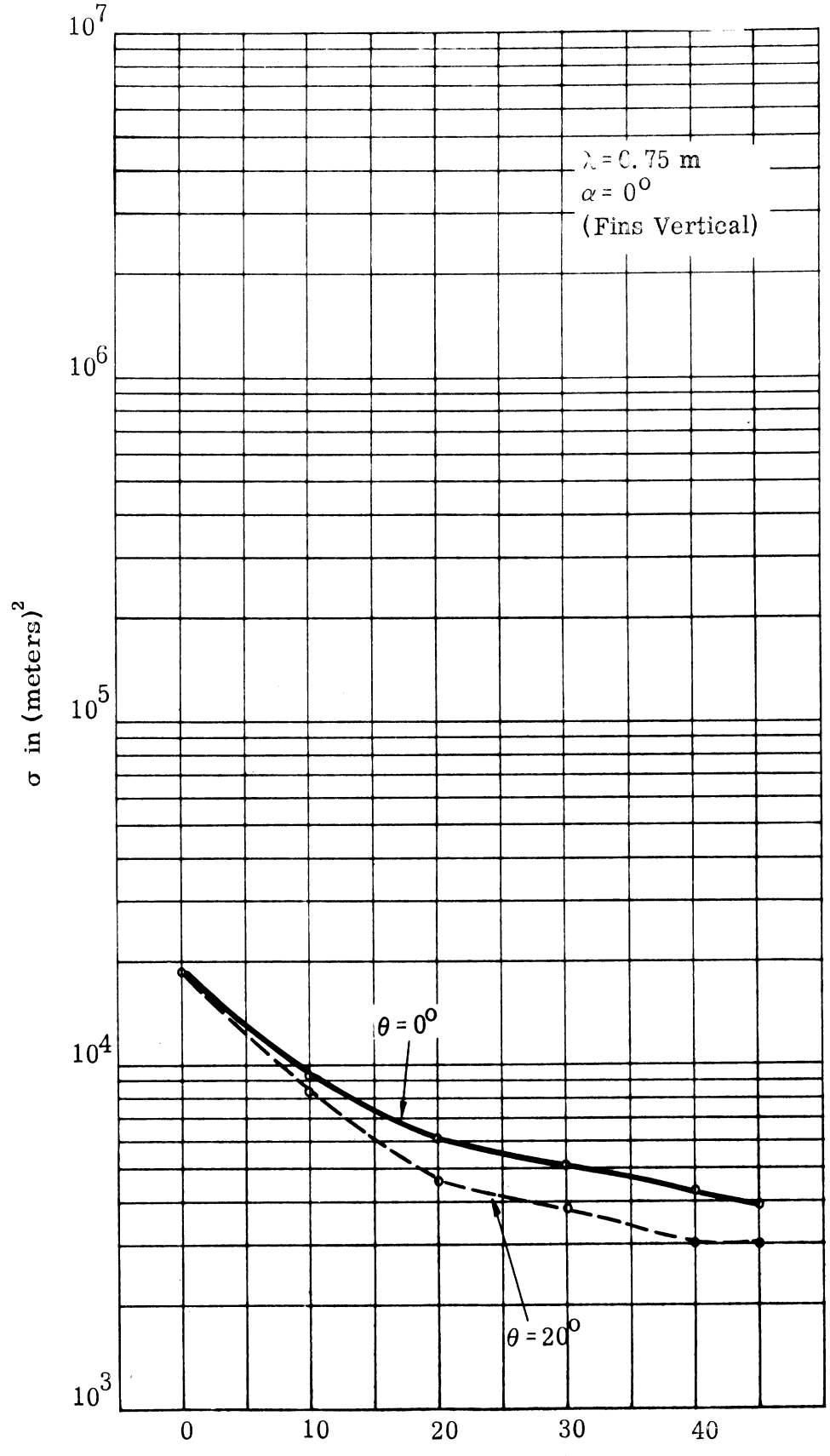
10^7
10^6
10^5
10^4
10^3
σ in (meters)^2
λ = 0.75 m
α = 0°
(Fins Vertical)
θ = 0°
θ = 20°
0
10
20
30
40
β in degrees

FIGURE 7

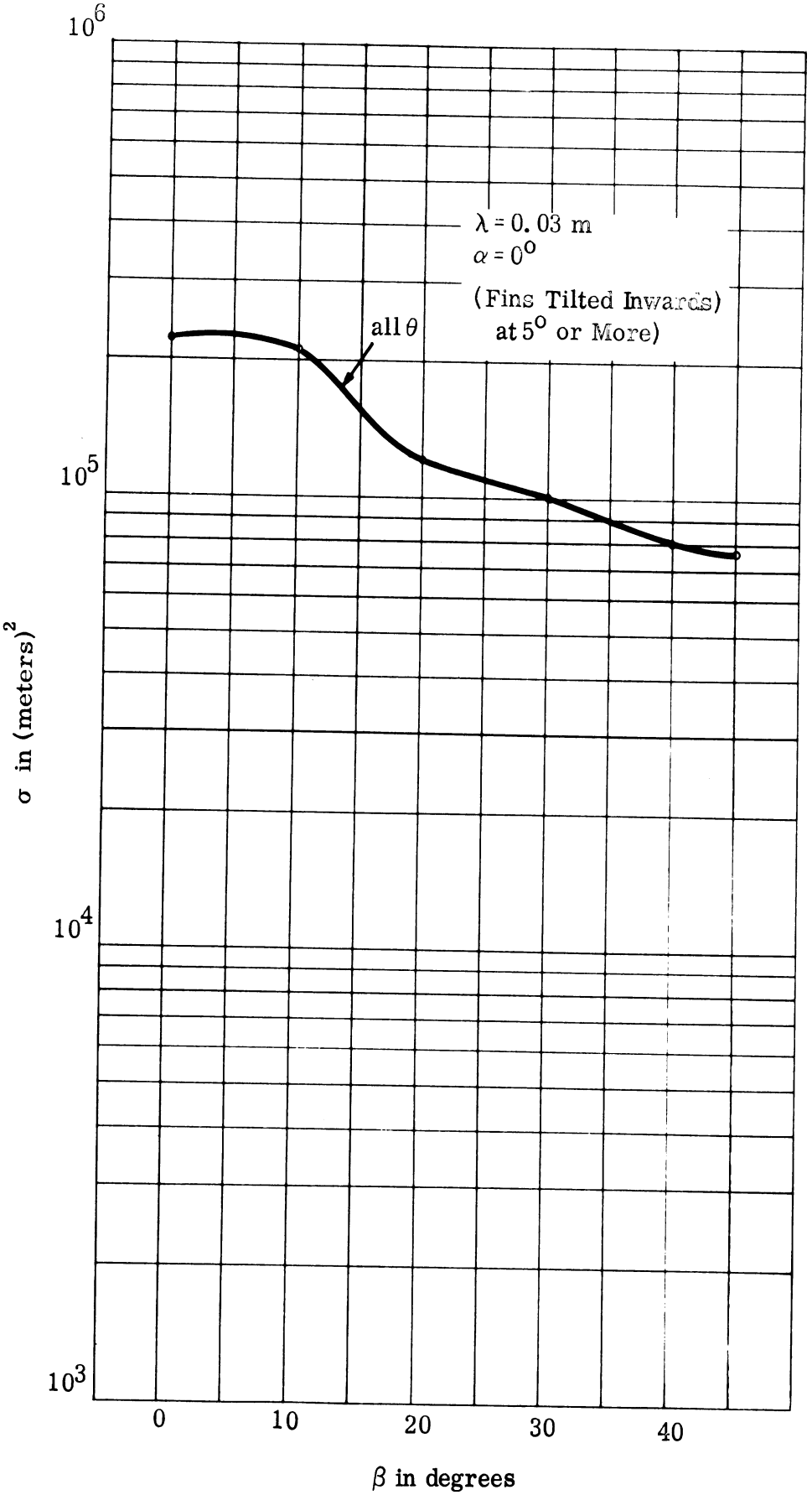
10^6
10^5
10^4
10^3
$\lambda = 0.03$ m
$\alpha = 0^o$
(Fins Tilted Inwards)
at 5^o or More)
all θ
σ in (meters)^2
0
10
20
30
40
β in degrees

FIGURE 8

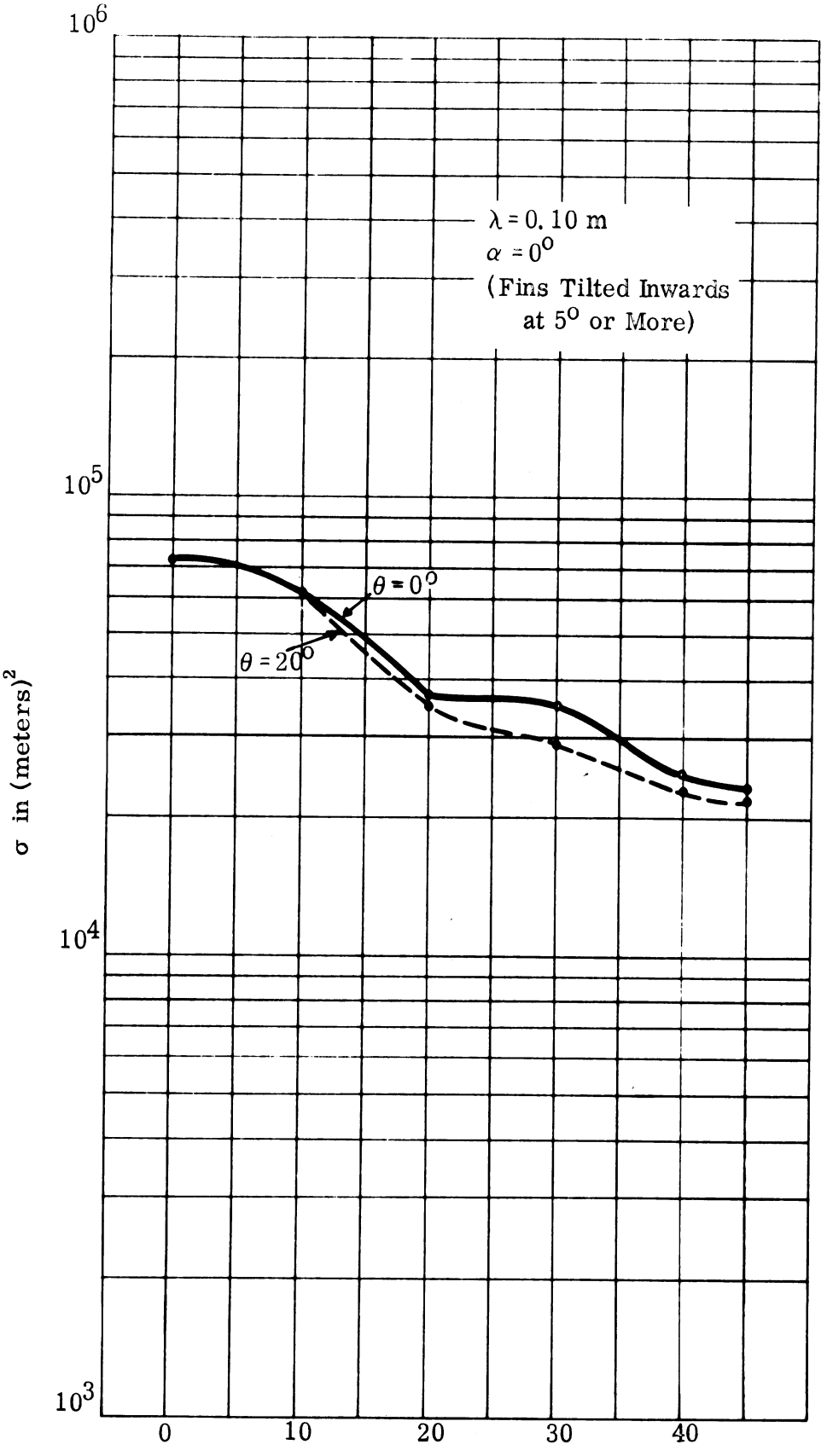
10^6
10^5
10^4
10^3
$\lambda = 0.10$ m
$\alpha = 0^o$
(Fins Tilted Inwards at 5^o or More)
$\theta = 0^o$
$\theta = 20^o$
σ in $(\text{meters})^2$
0
10
20
30
40
β in degrees

FIGURE 9

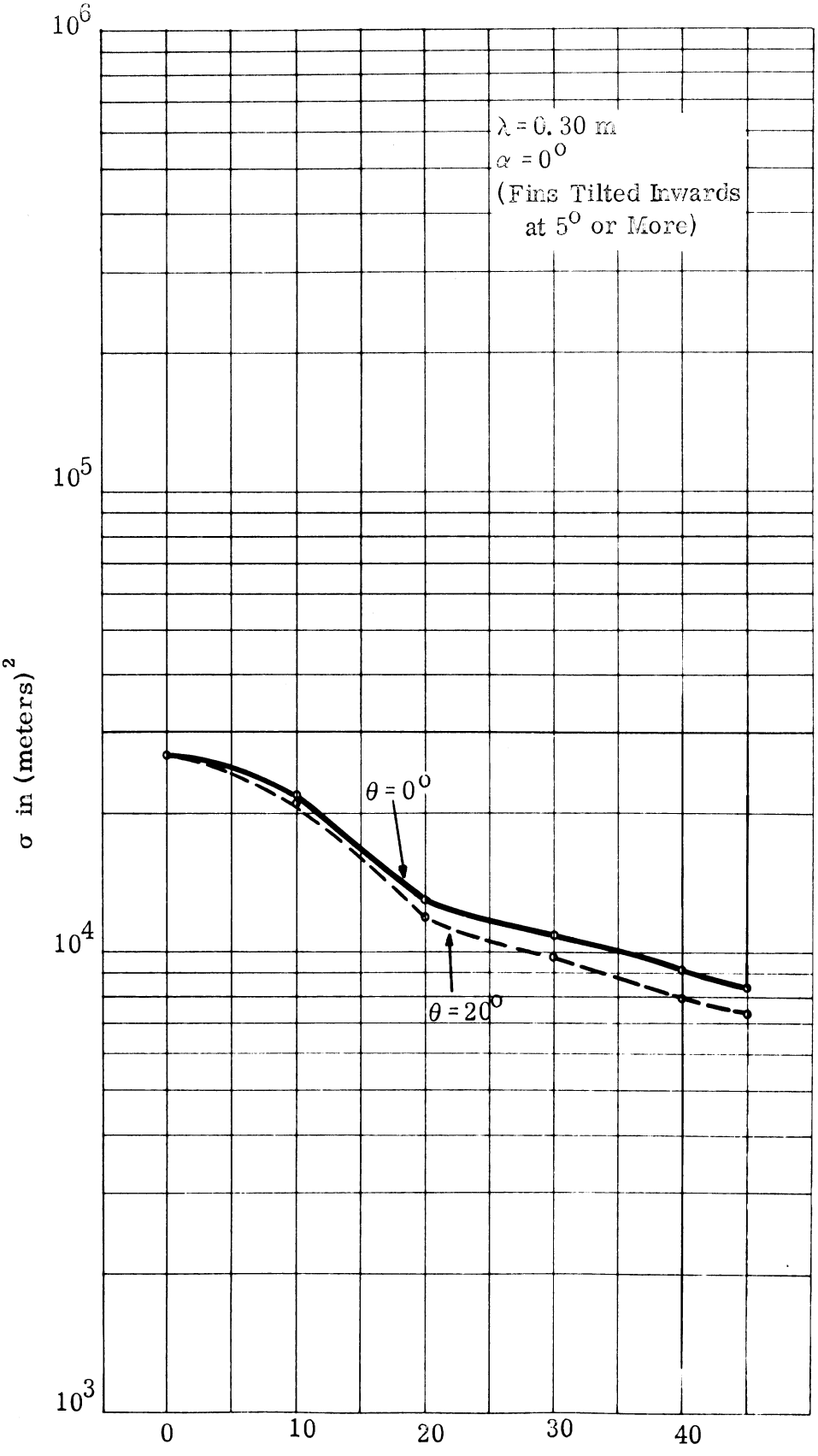
10^6
10^5
10^4
10^3
σ in (meters)^2
λ = 0.30 m
α = 0°
(Fins Tilted Inwards at 5° or More)
θ = 0°
θ = 20°
0
10
20
30
40
β in degrees

FIGURE 10

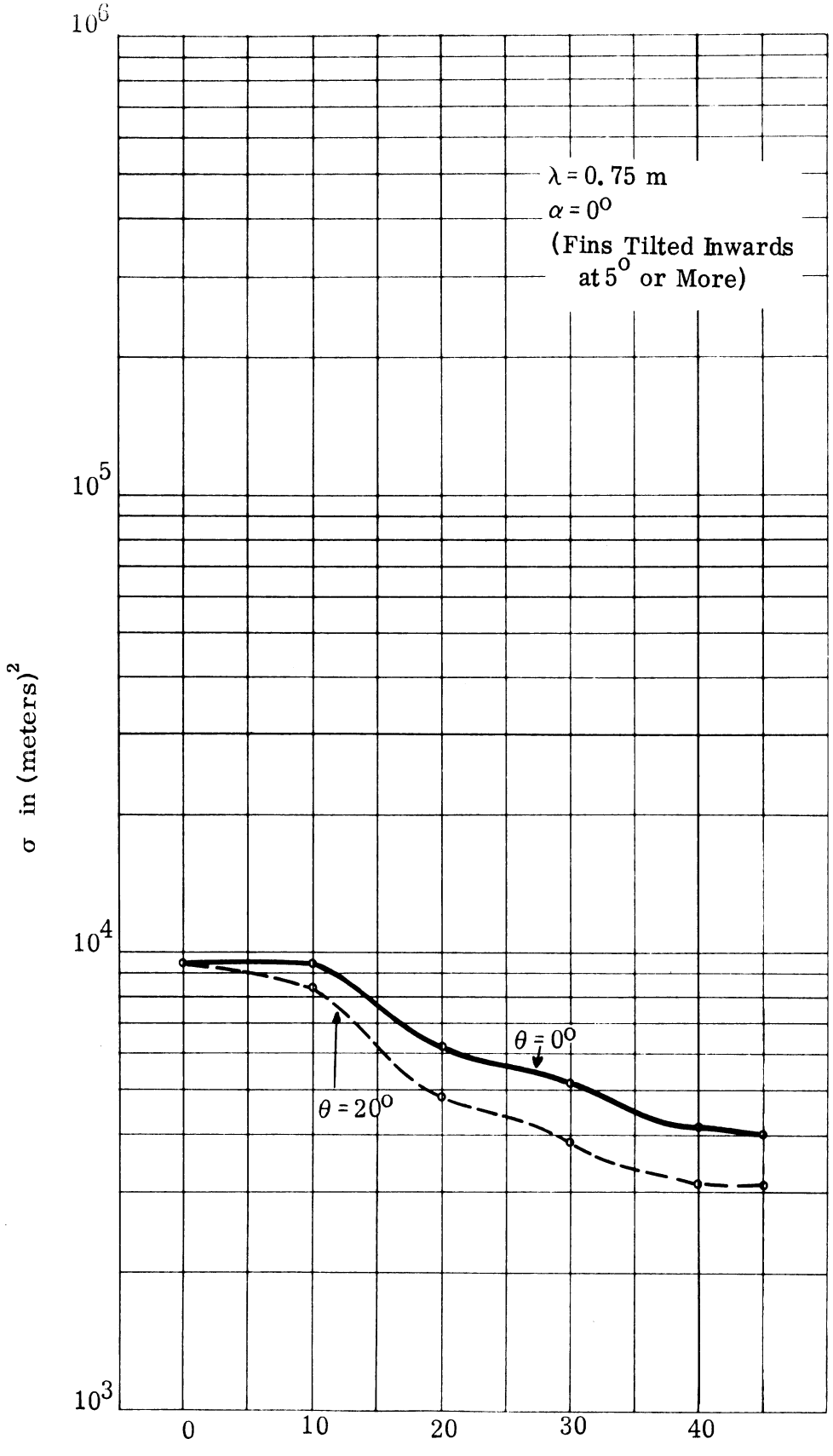
10^6
10^5
10^4
10^3
σ in (meters)^2
λ = 0.75 m
α = 0°
(Fins Tilted Inwards at 5° or More)
θ = 0°
θ = 20°
0
10
20
30
40
β in degrees

FIGURE 11

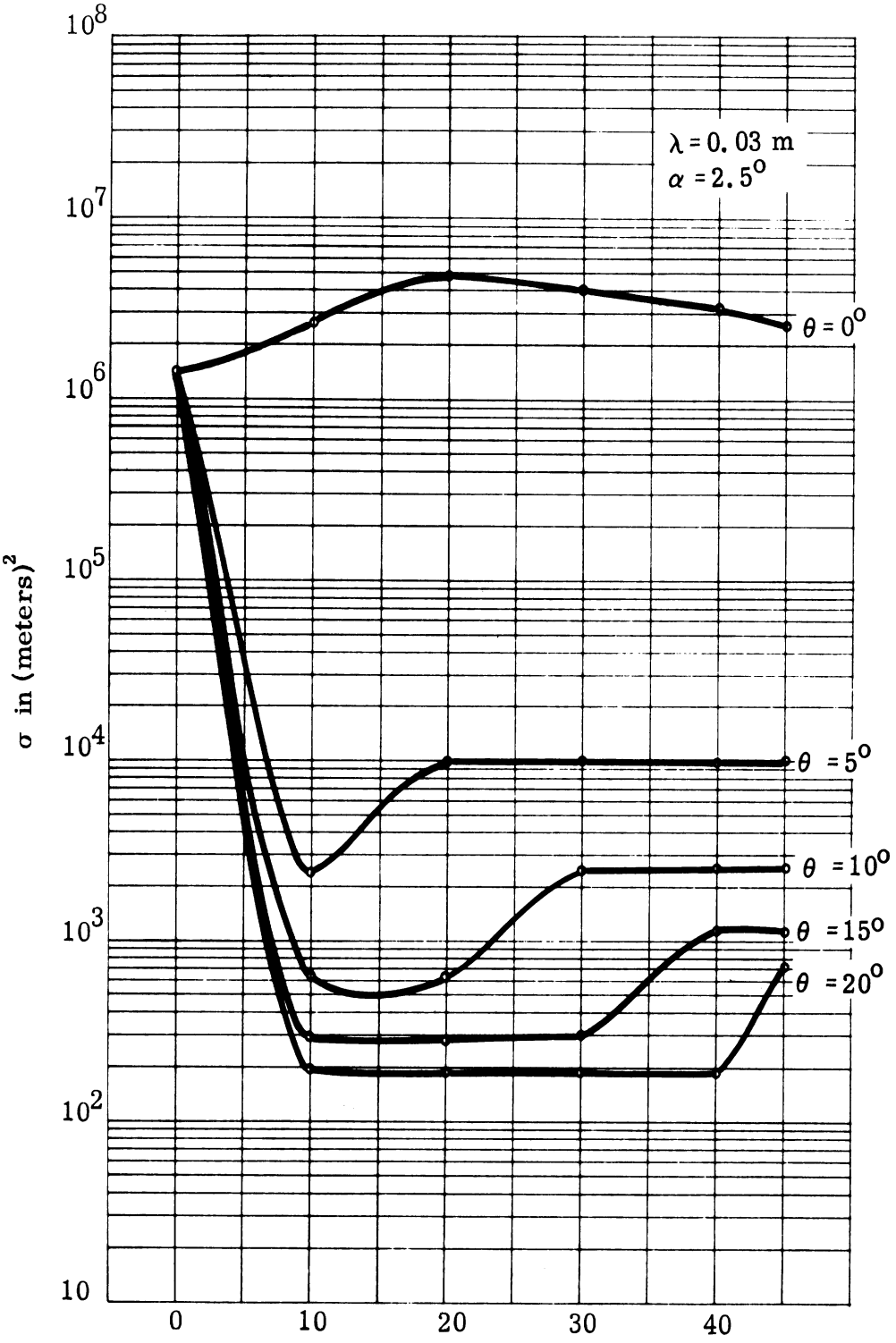
10^8
10^7
10^6
10^5
10^4
10^3
10^2
10
σ in (meters)²
λ = 0.03 m
α = 2.5°
θ = 0°
θ = 5°
θ = 10°
θ = 15°
θ = 20°
0
10
20
30
40
β in degrees

FIGURE 12

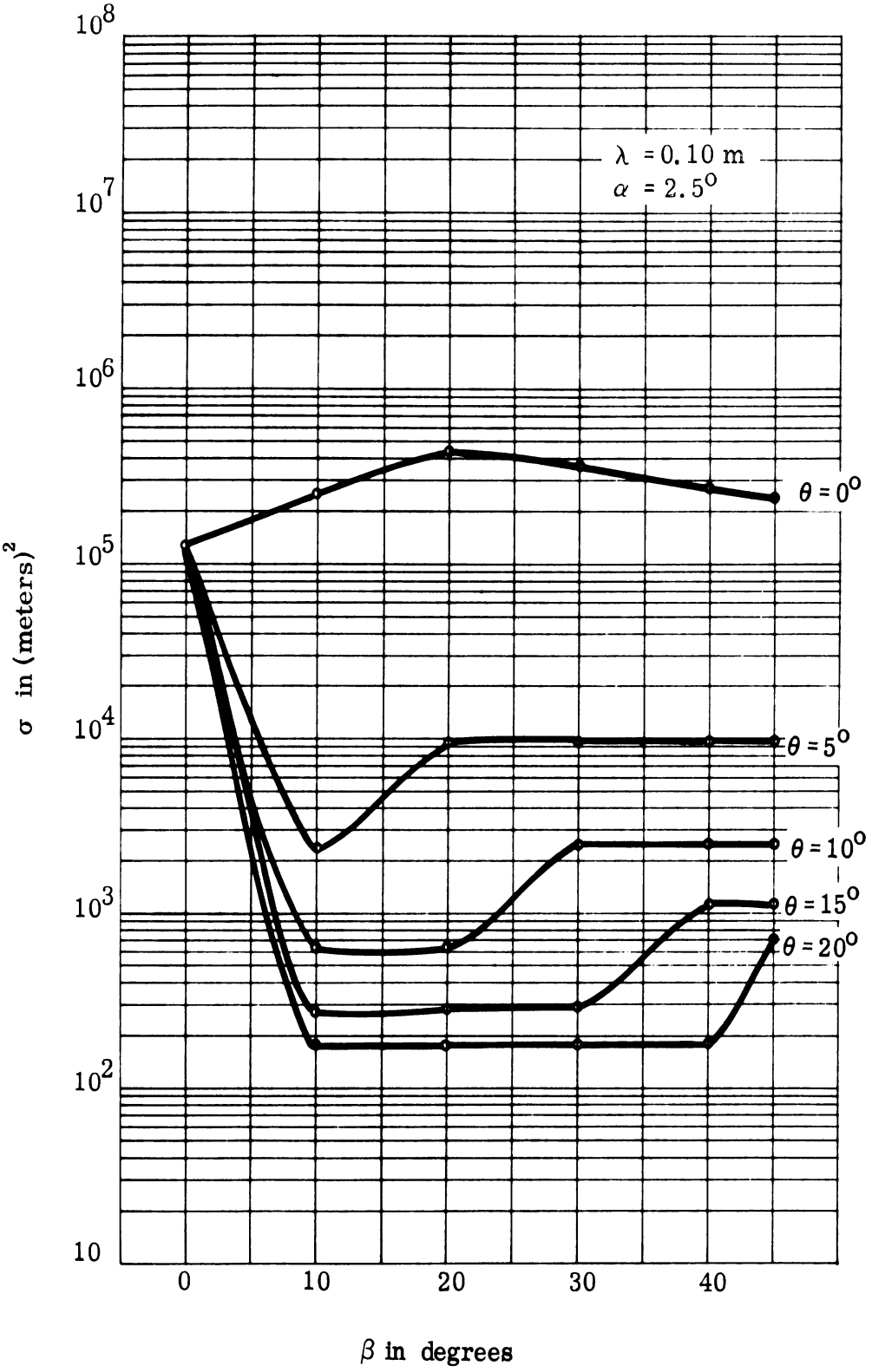
10^8
10^7
10^6
10^5
10^4
10^3
10^2
10
σ in (meters)^2
λ = 0.10 m
α = 2.5°
θ = 0°
θ = 5°
θ = 10°
θ = 15°
θ = 20°
0
10
20
30
40
β in degrees

FIGURE 13

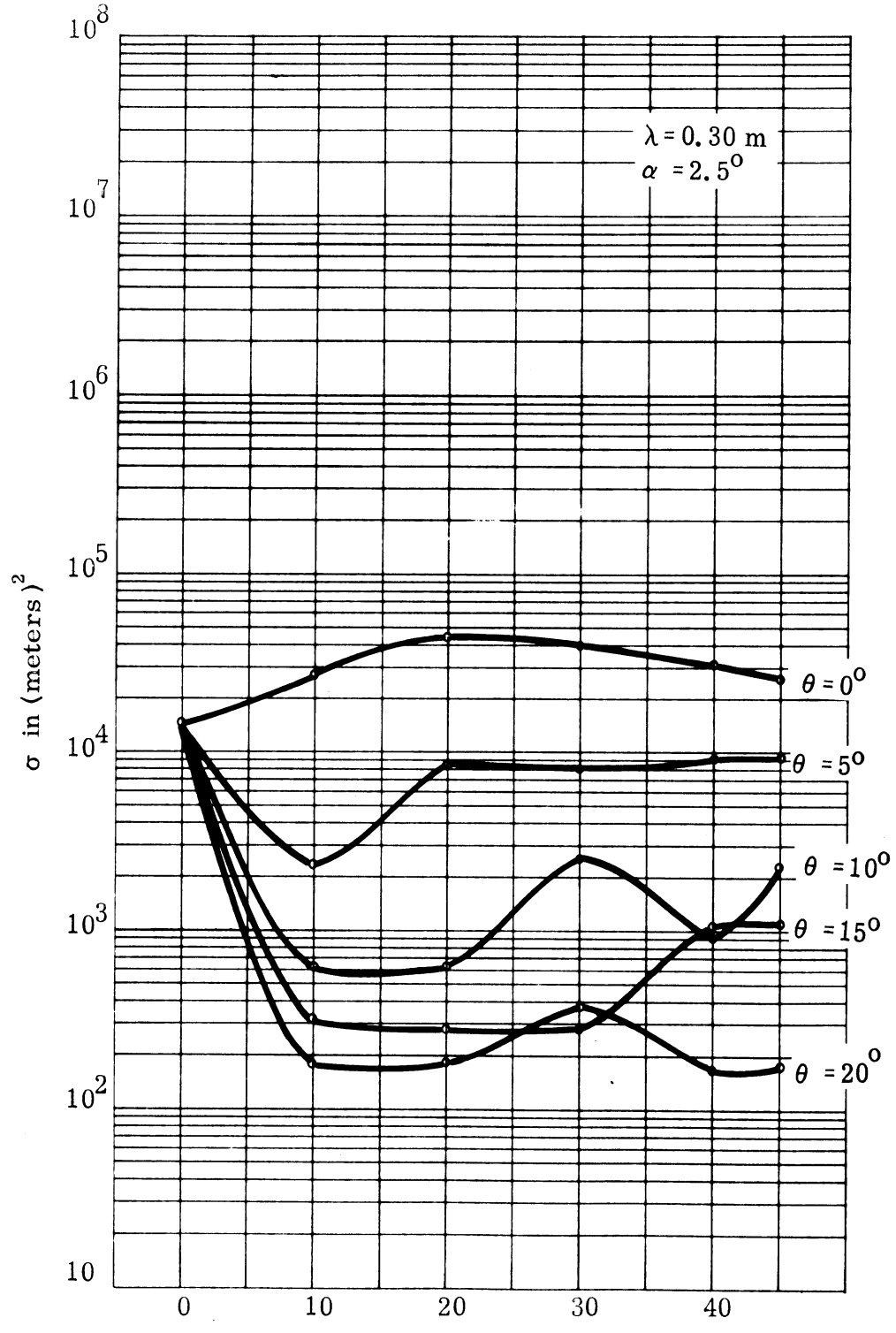
10^8
10^7
10^6
10^5
10^4
10^3
10^2
10
σ in (meters)^2
λ = 0.30 m
α = 2.5°
θ = 0°
θ = 5°
θ = 10°
θ = 15°
θ = 20°
0
10
20
30
40
β in degrees

FIGURE 14

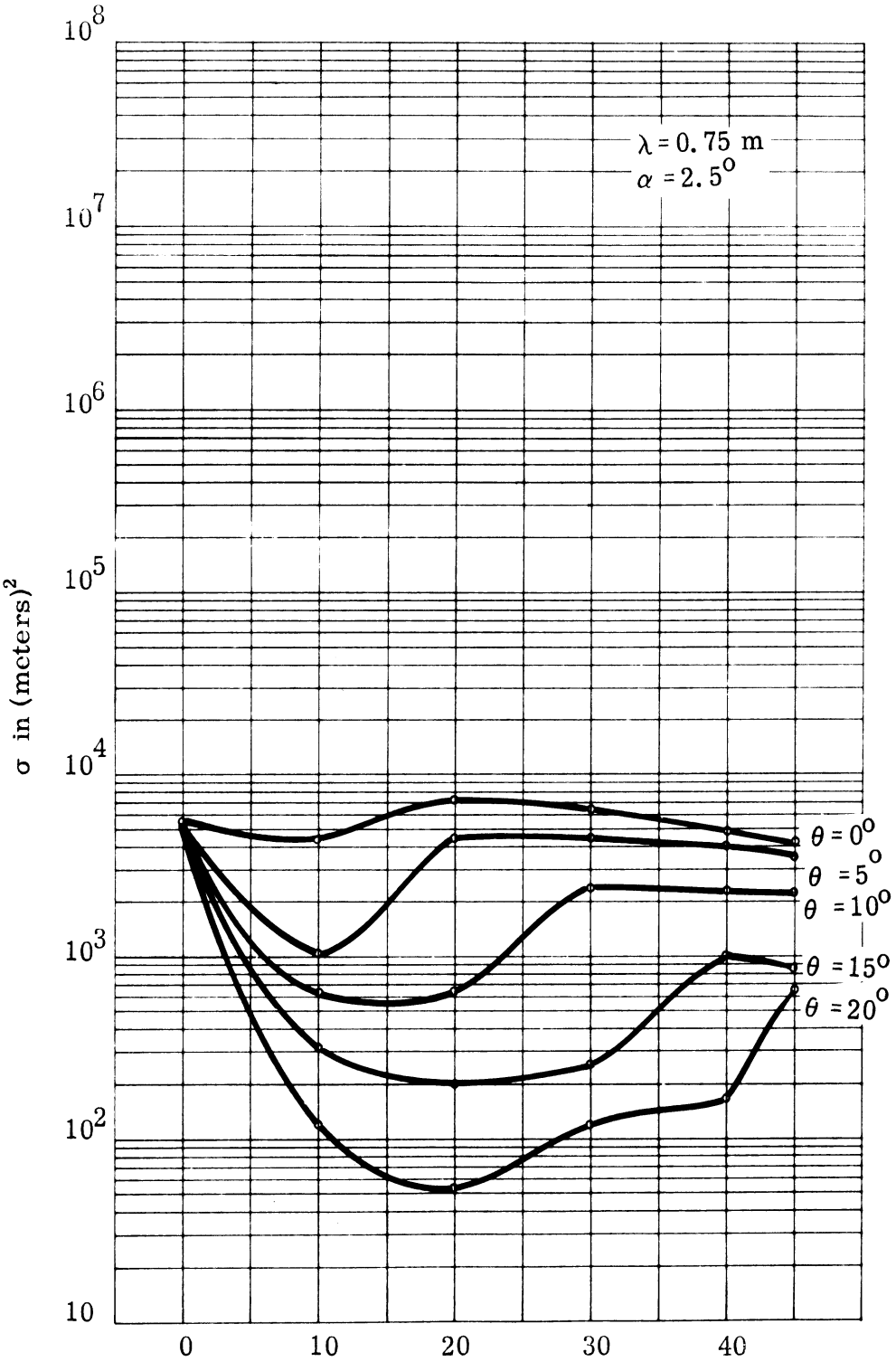
10^8
10^7
10^6
10^5
10^4
10^3
10^2
10
σ in (meters)²
λ = 0.75 m
α = 2.5°
θ = 0°
θ = 5°
θ = 10°
θ = 15°
θ = 20°
0
10
20
30
40
β in degrees

FIGURE 15

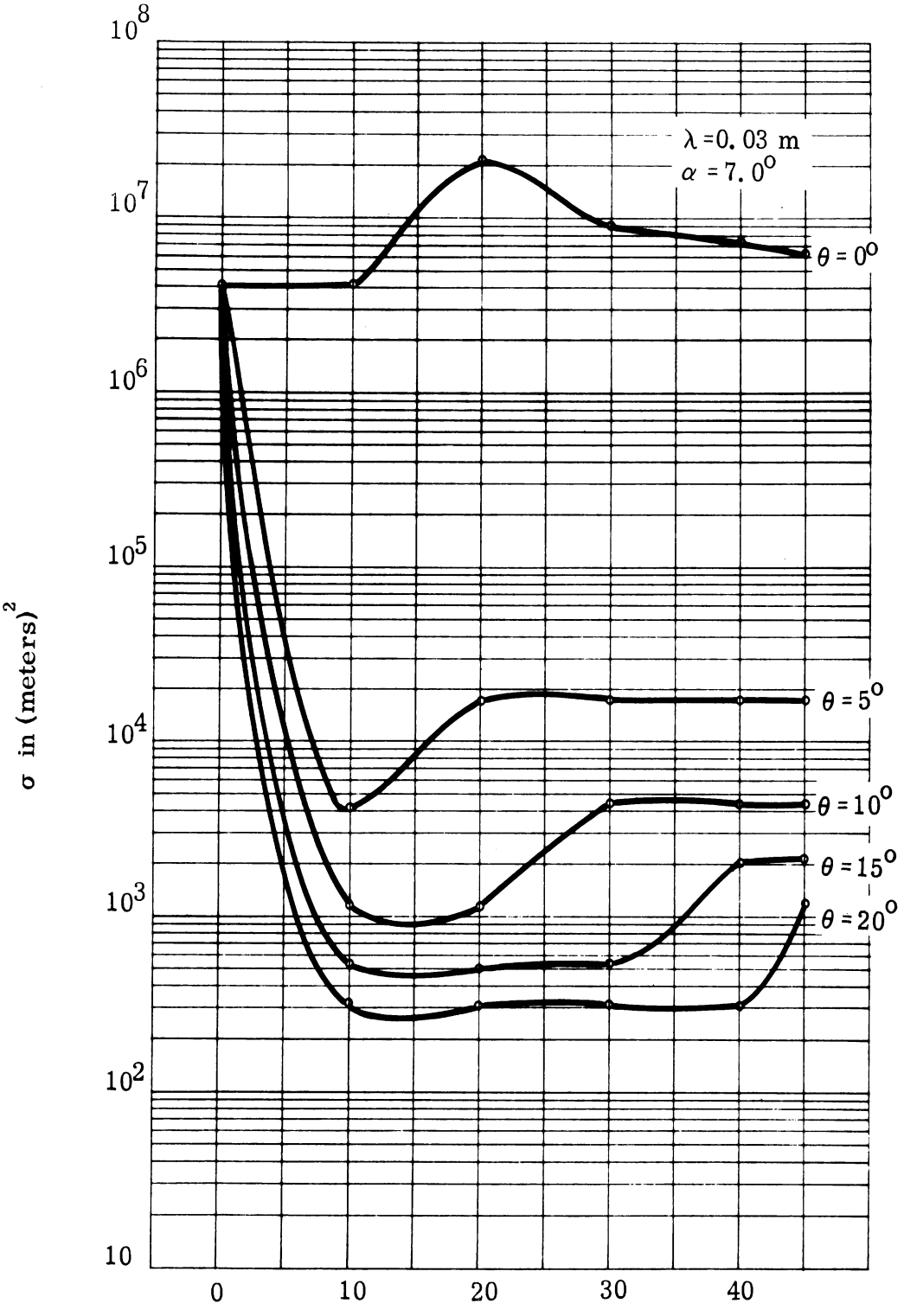
10^8
10^7
10^6
10^5
10^4
10^3
10^2
10
σ in (meters)^2
λ = 0.03 m
α = 7.0°
θ = 0°
θ = 5°
θ = 10°
θ = 15°
θ = 20°
0
10
20
30
40
β in degrees

FIGURE 16

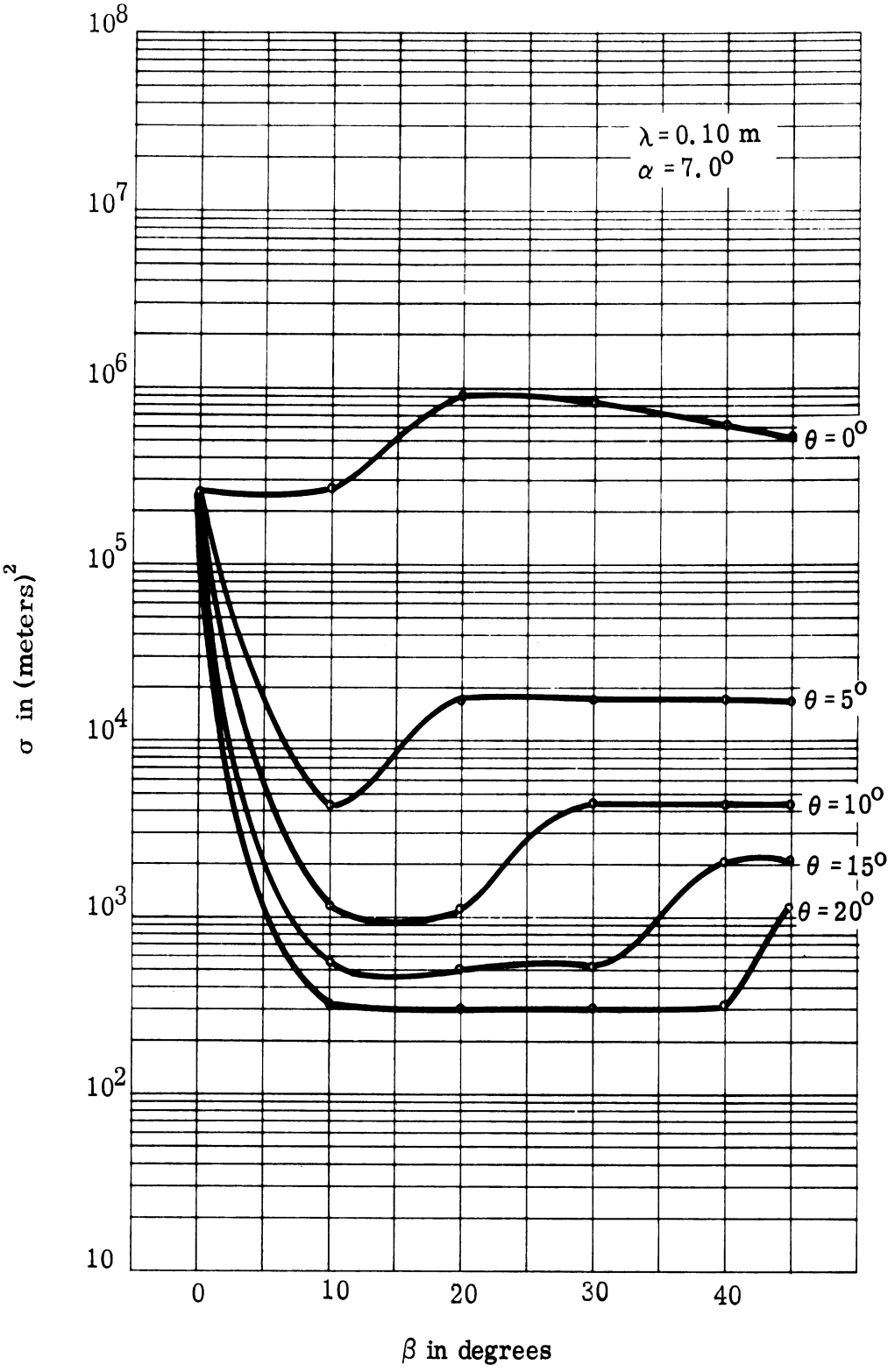
10^8
10^7
10^6
10^5
10^4
10^3
10^2
10
σ in (meters)^2
λ = 0.10 m
α = 7.0°
θ = 0°
θ = 5°
θ = 10°
θ = 15°
θ = 20°
0
10
20
30
40
β in degrees

FIGURE 17

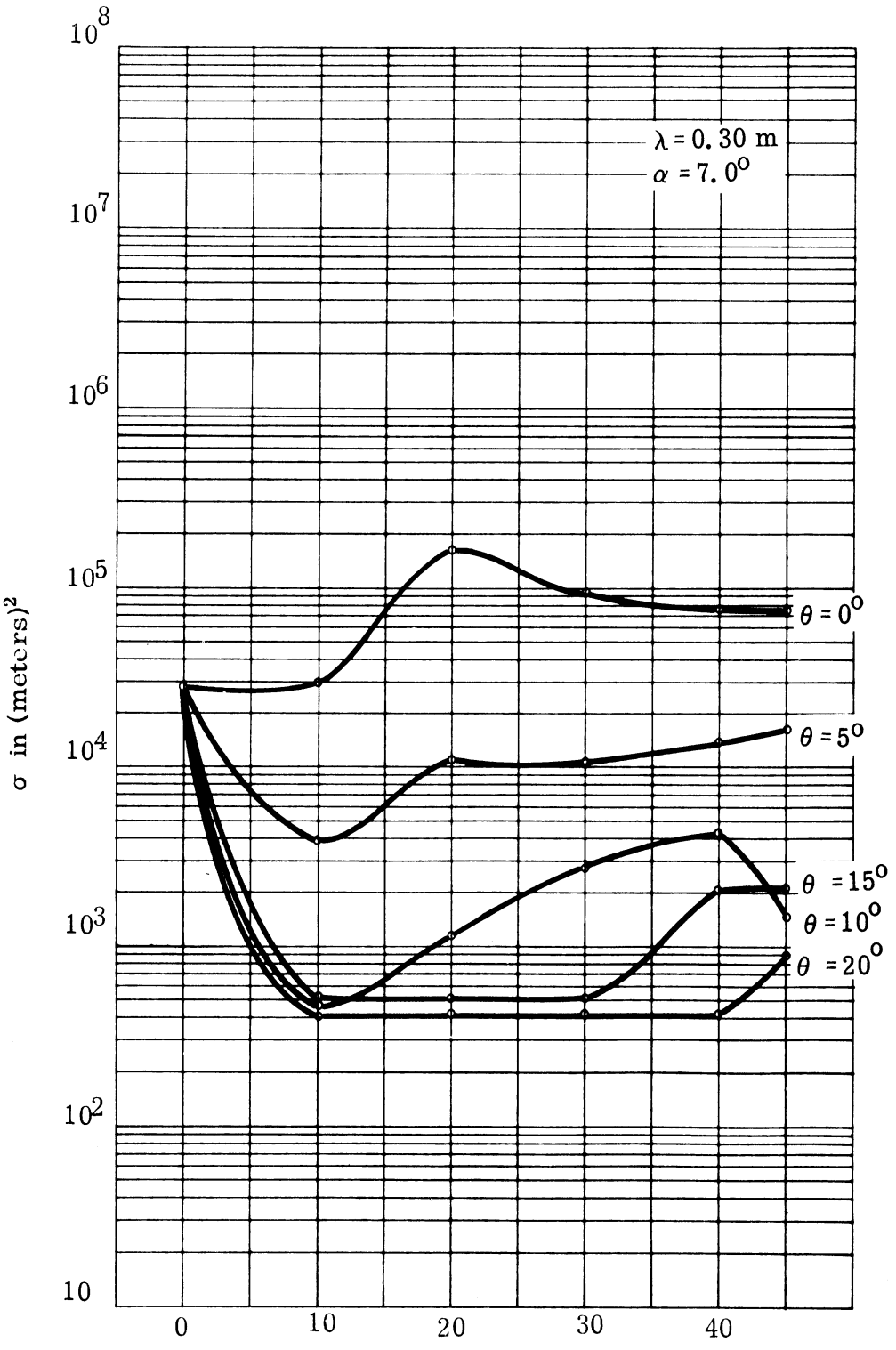
10^8
10^7
10^6
10^5
10^4
10^3
10^2
10
σ in (meters)²
λ = 0.30 m
α = 7.0°
θ = 0°
θ = 5°
θ = 15°
θ = 10°
θ = 20°
0
10
20
30
40
β in degrees

FIGURE 18

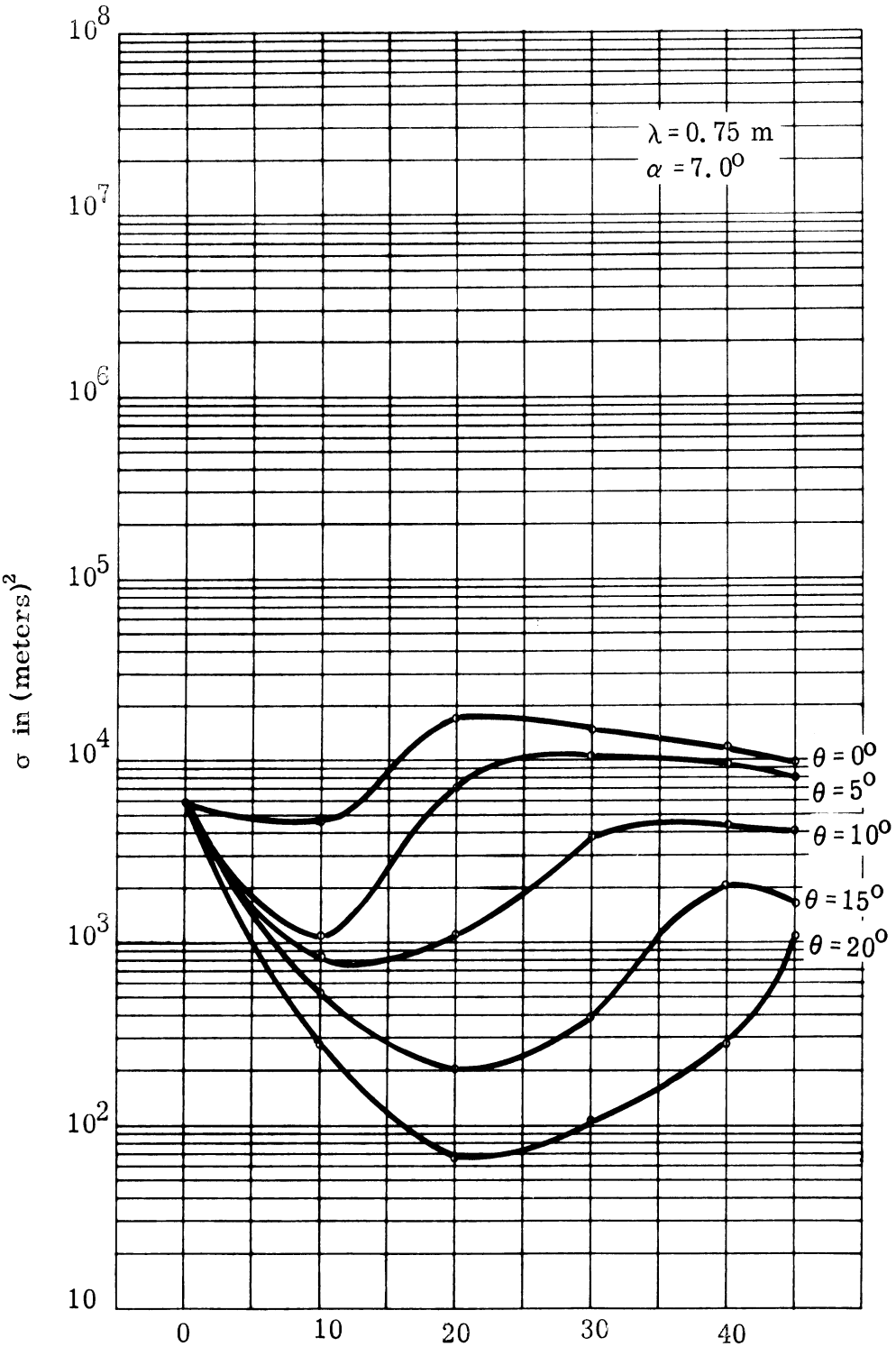
10^8
10^7
10^6
10^5
10^4
10^3
10^2
10
σ in (meters)²
λ = 0.75 m
α = 7.0°
θ = 0°
θ = 5°
θ = 10°
θ = 15°
θ = 20°
0
10
20
30
40
β in degrees

FIGURE 19

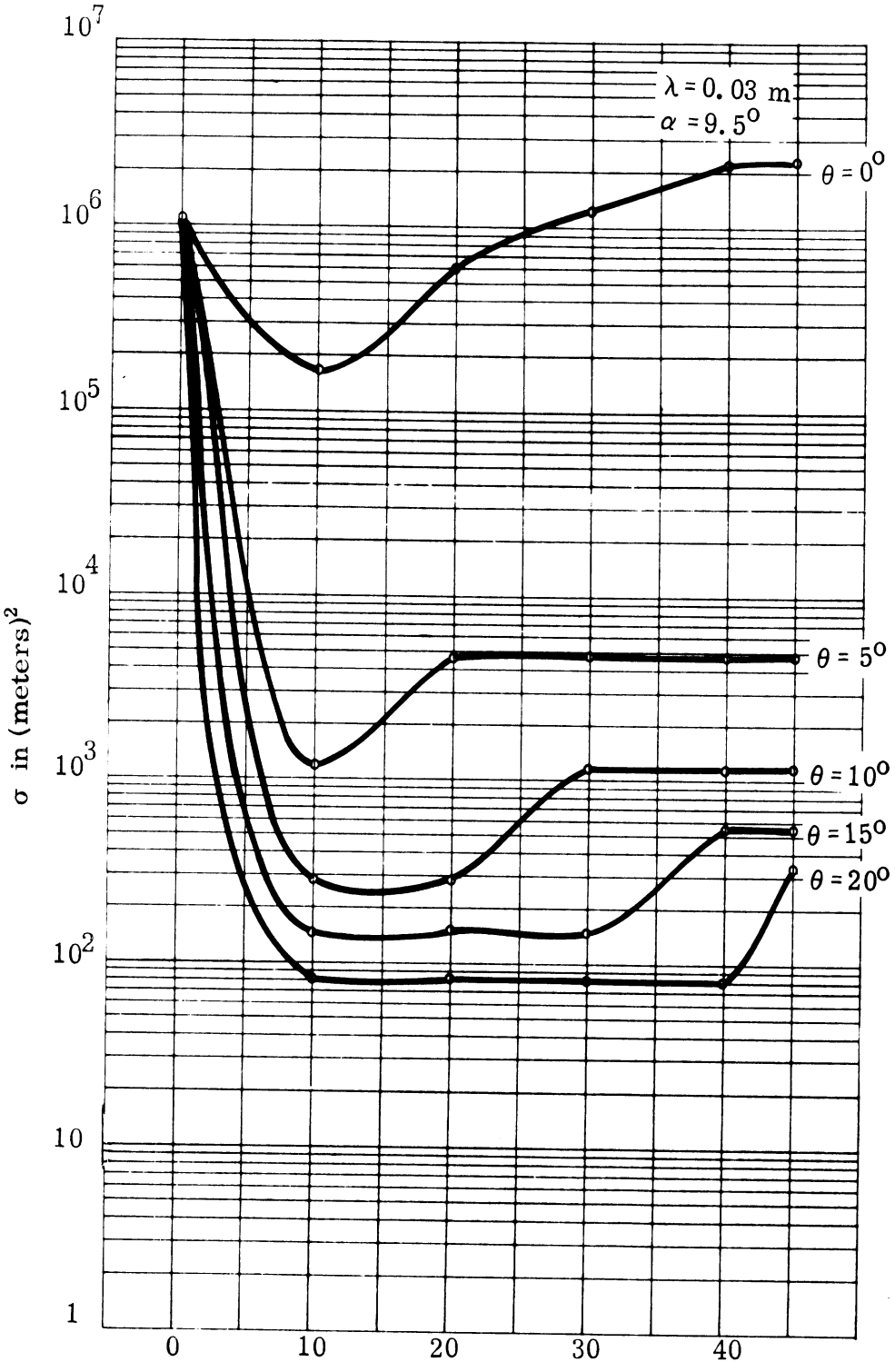
10^7
10^6
10^5
10^4
10^3
10^2
10
1
σ in (meters)²
λ = 0.03 m
α = 9.5°
θ = 0°
θ = 5°
θ = 10°
θ = 15°
θ = 20°
0
10
20
30
40
β in degrees

FIGURE 20

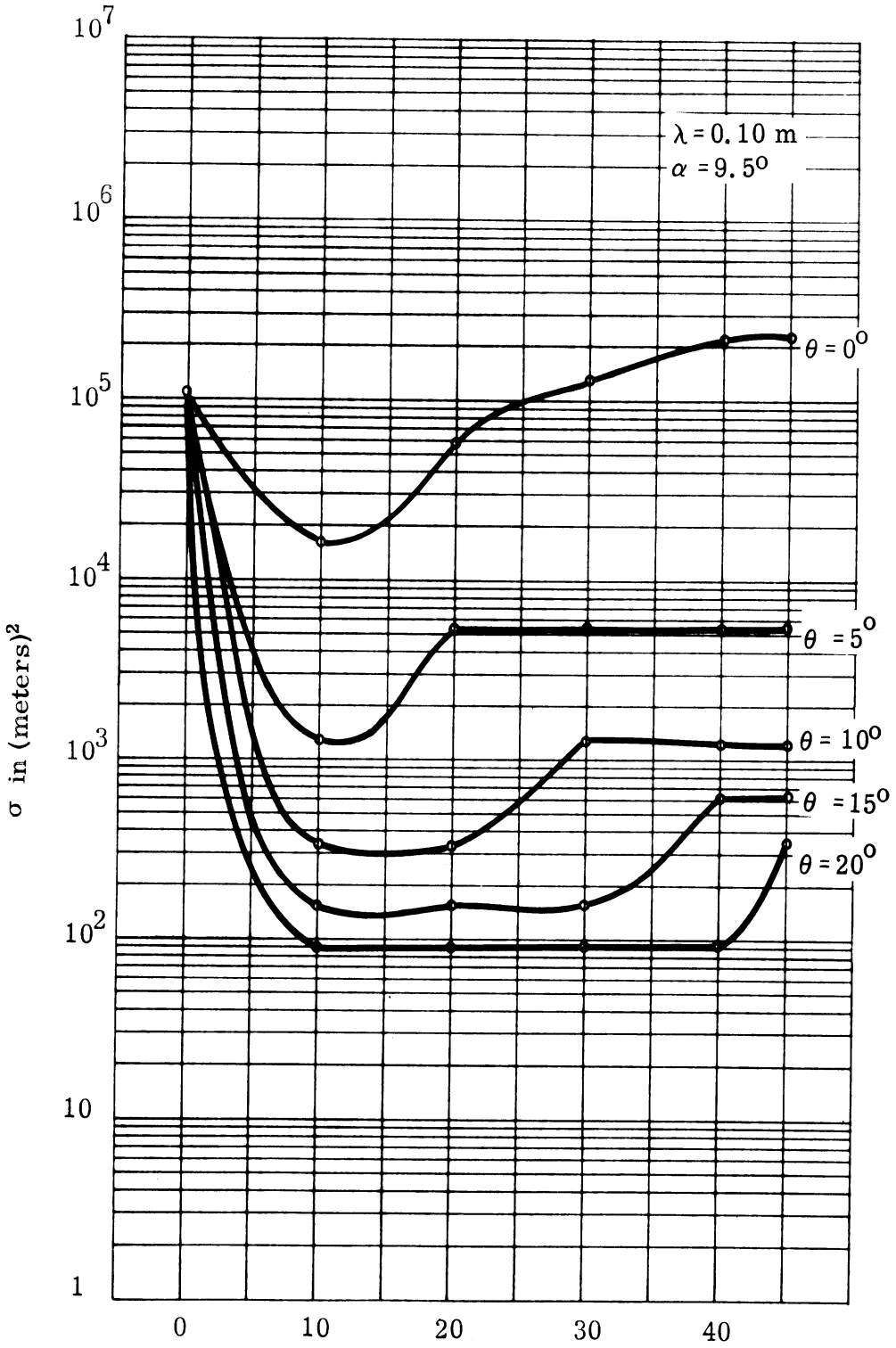
10^7
10^6
10^5
10^4
10^3
10^2
10
1
σ in (meters)²
λ = 0.10 m
α = 9.5°
θ = 0°
θ = 5°
θ = 10°
θ = 15°
θ = 20°
0
10
20
30
40
β in degrees

FIGURE 21

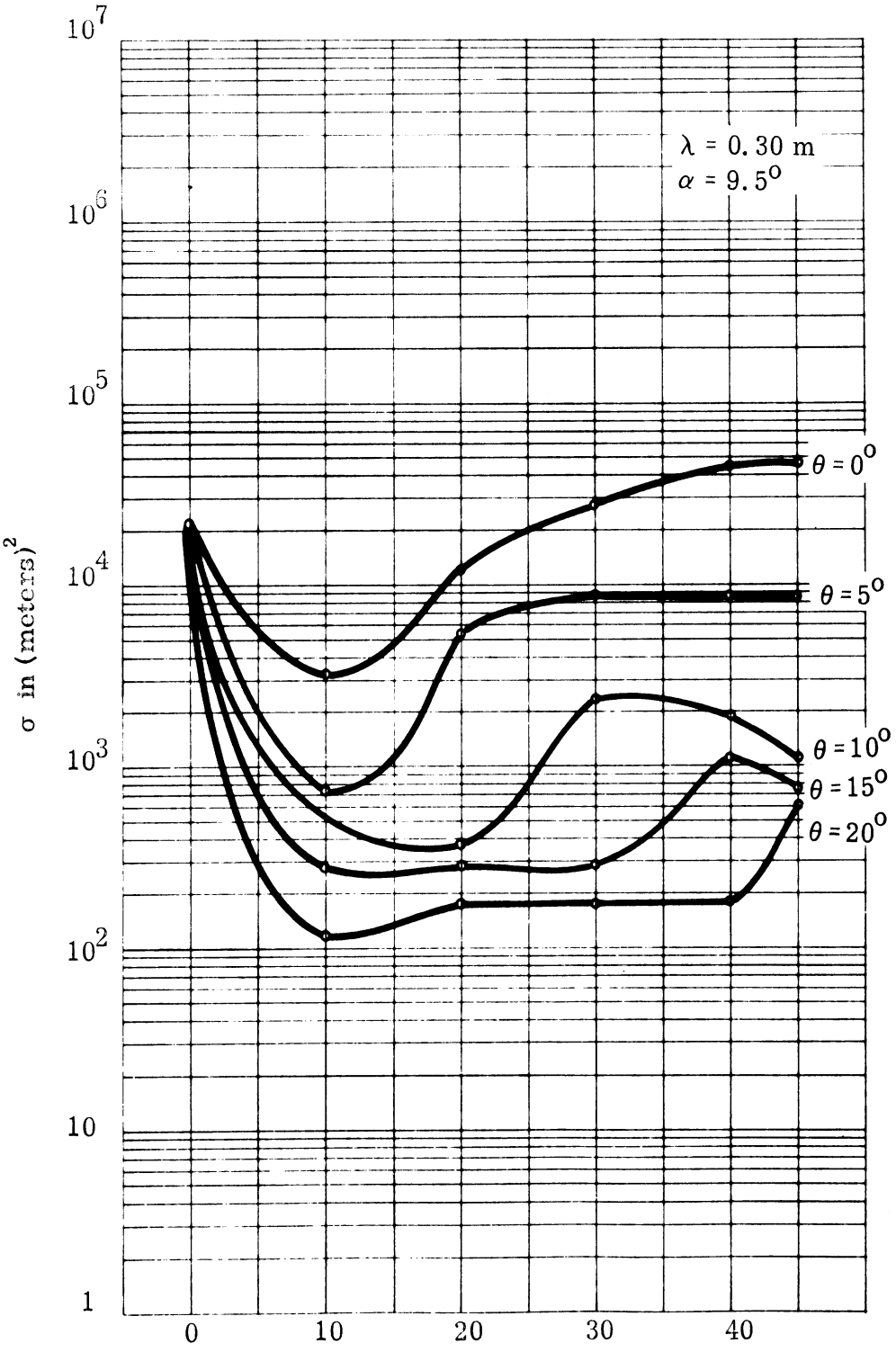
λ = 0.30 m
α = 9.5°
θ = 0°
θ = 5°
θ = 10°
θ = 15°
θ = 20°
σ in (meters)²
10⁷
10⁶
10⁵
10⁴
10³
10²
10
1
0
10
20
30
40
β in degrees

FIGURE 22

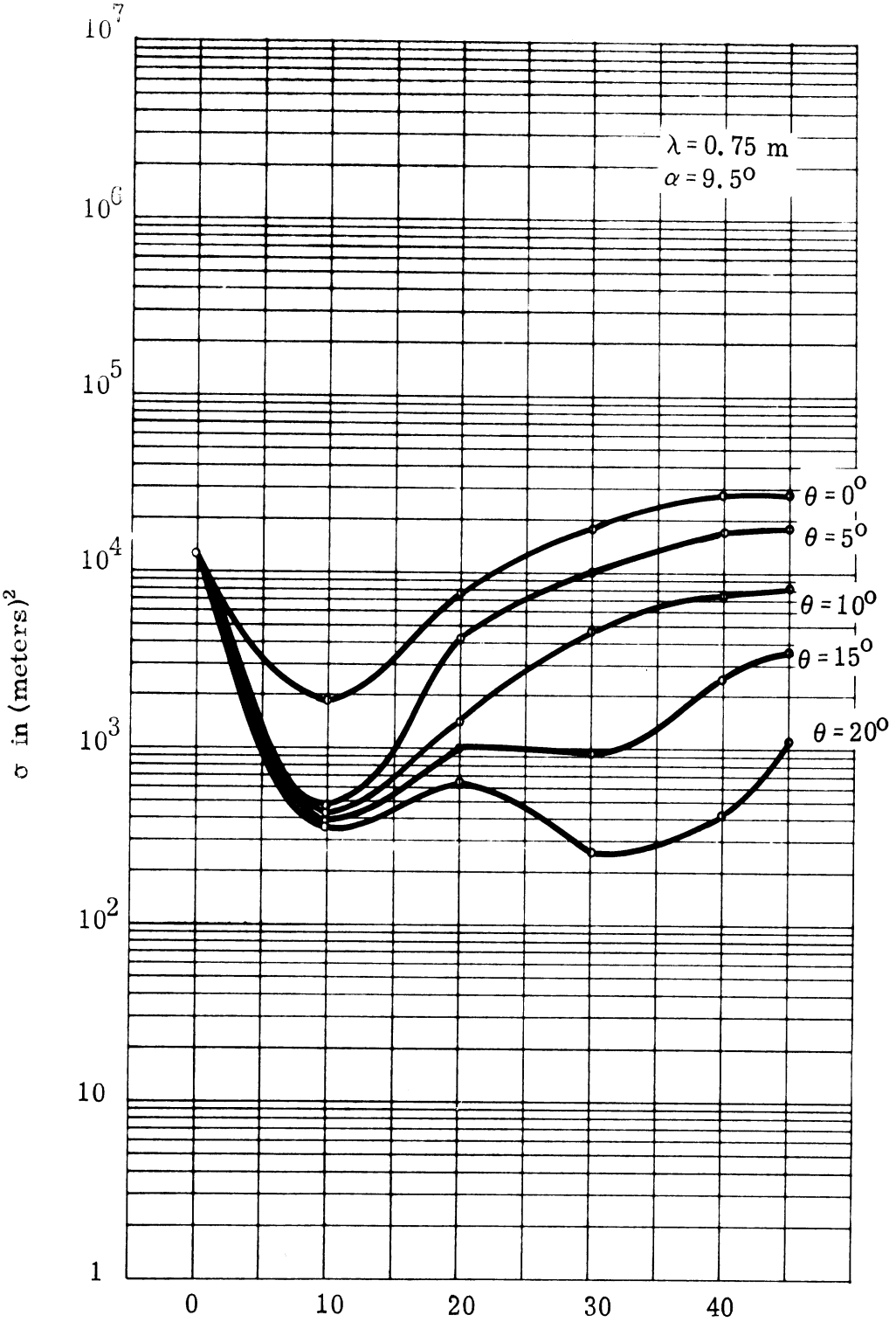
10^7
10^6
10^5
10^4
10^3
10^2
10
1
σ in (meters)²
λ = 0.75 m
α = 9.5°
θ = 0°
θ = 5°
θ = 10°
θ = 15°
θ = 20°
0
10
20
30
40
β in degrees

FIGURE 23

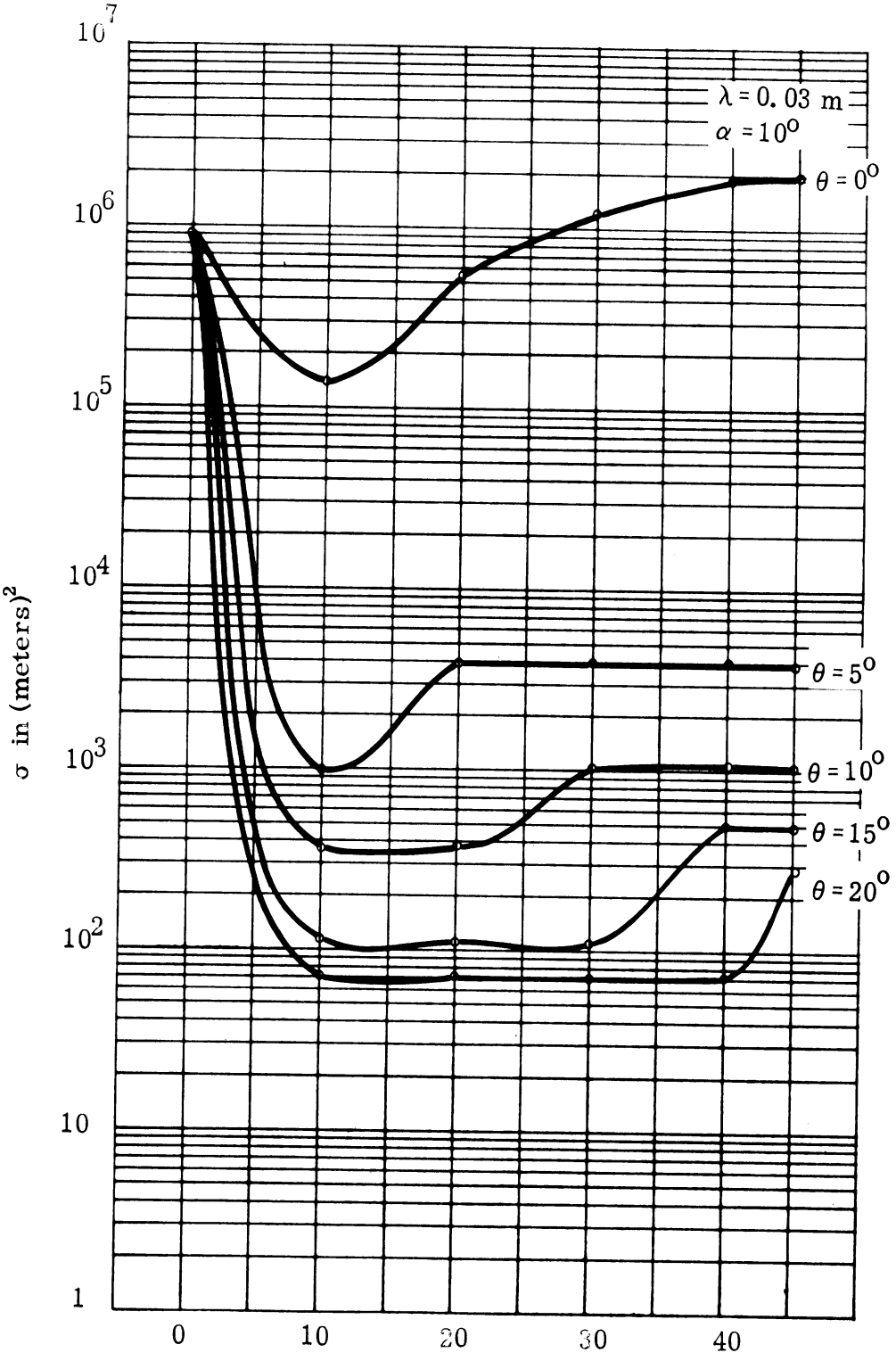
10^7
10^6
10^5
10^4
10^3
10^2
10
1
σ in (meters)^2
λ = 0.03 m
α = 10°
θ = 0°
θ = 5°
θ = 10°
θ = 15°
θ = 20°
0
10
20
30
40
β in degrees

FIGURE 24

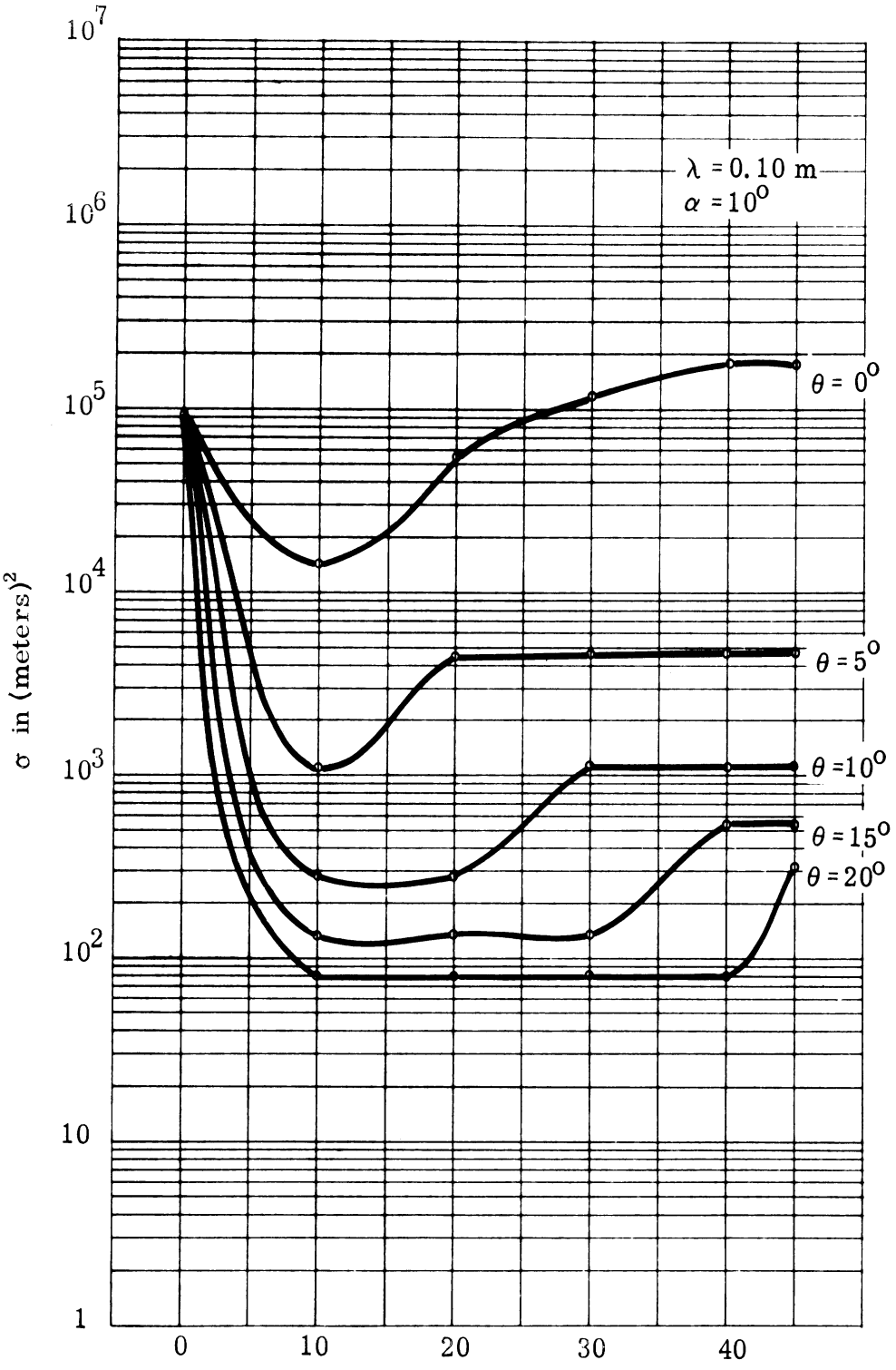
10^7
10^6
10^5
10^4
10^3
10^2
10
1
σ in (meters)^2
λ = 0.10 m
α = 10°
θ = 0°
θ = 5°
θ = 10°
θ = 15°
θ = 20°
0
10
20
30
40
β in degrees

FIGURE 25

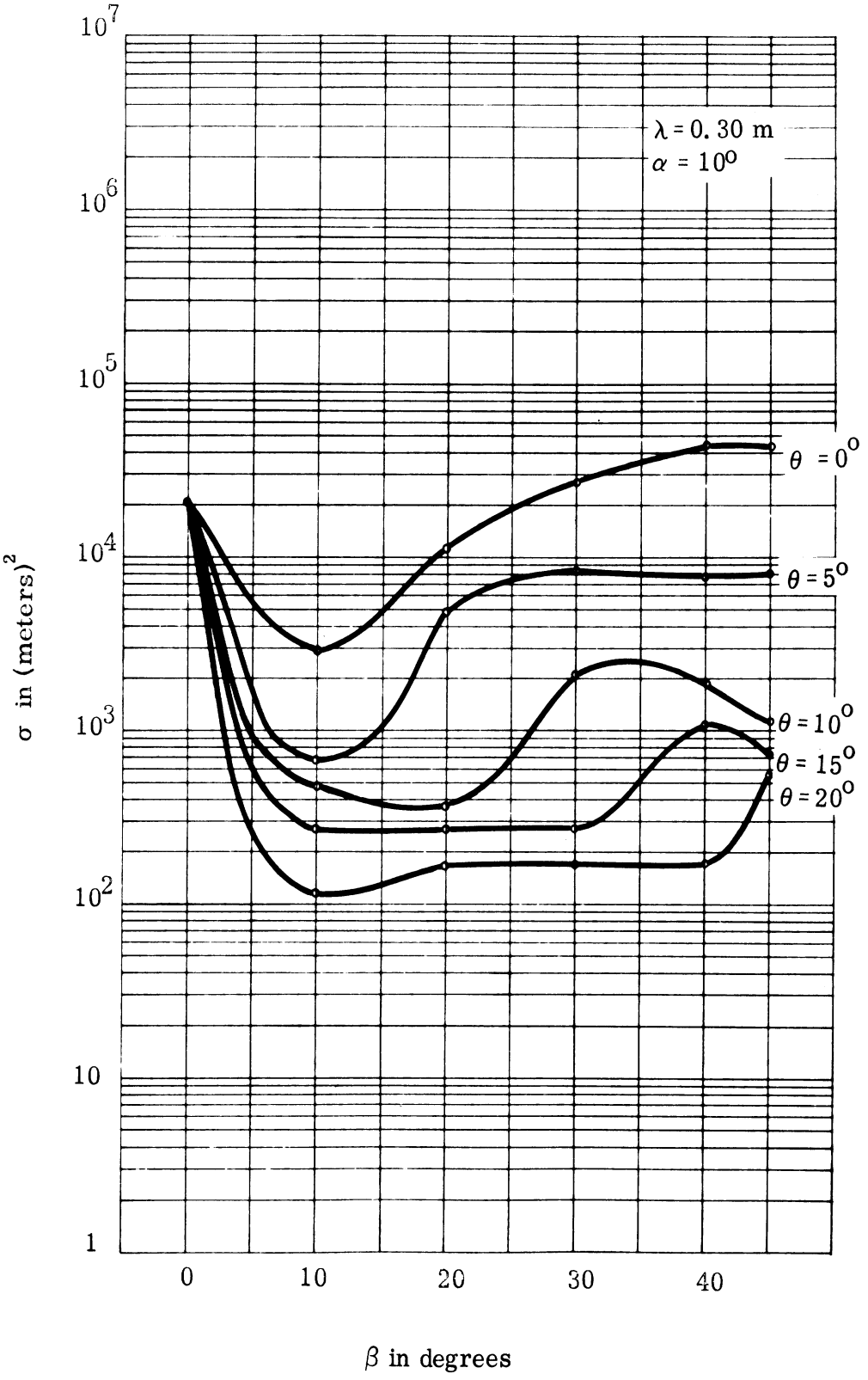
10^7
10^6
10^5
10^4
10^3
10^2
10
1
σ in (meters)^2
λ = 0.30 m
α = 10°
θ = 0°
θ = 5°
θ = 10°
θ = 15°
θ = 20°
0
10
20
30
40
β in degrees

FIGURE 26

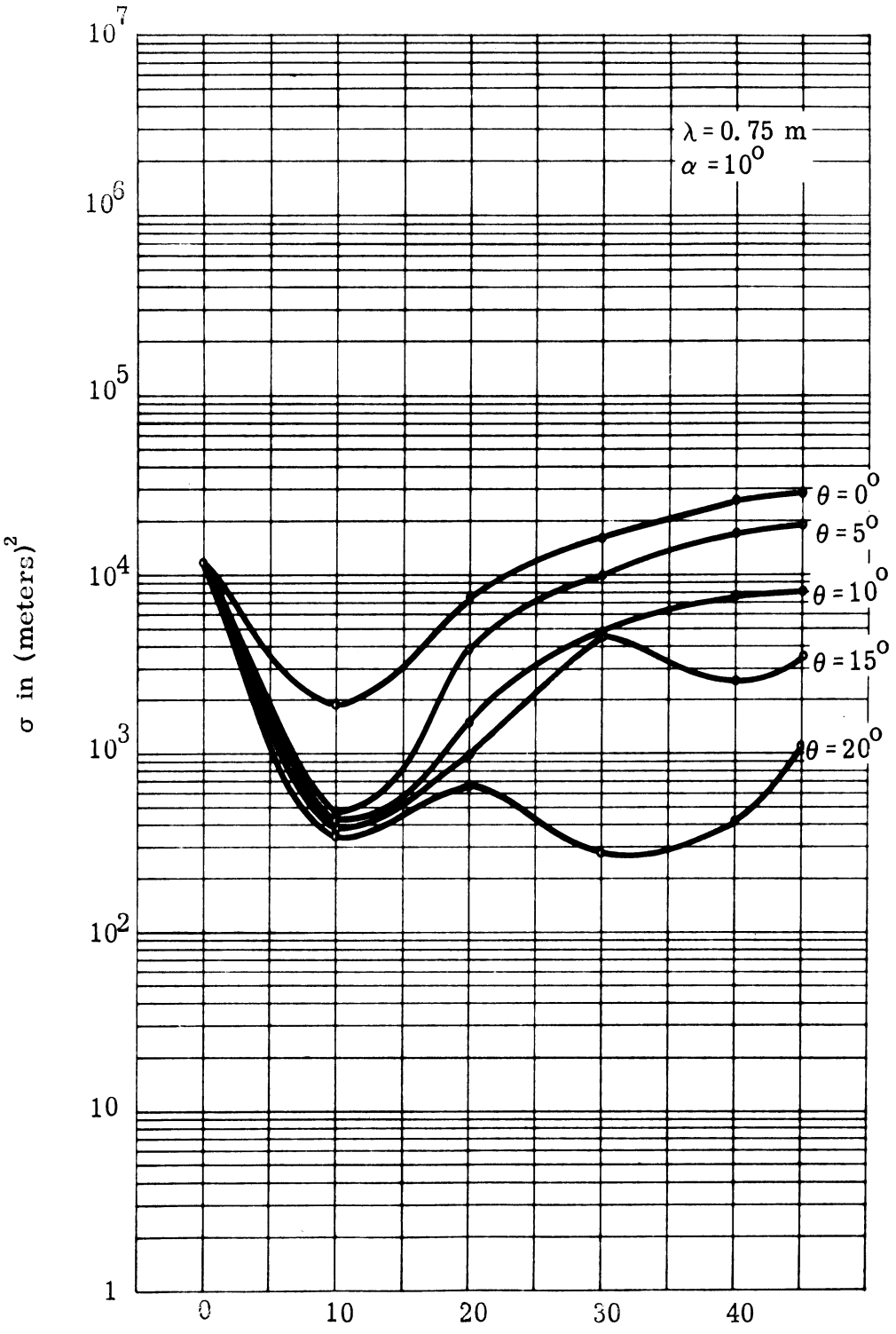
10^7
10^6
10^5
10^4
10^3
10^2
10
1
σ in (meters)^2
λ = 0.75 m
α = 10°
θ = 0°
θ = 5°
θ = 10°
θ = 15°
θ = 20°
0
10
20
30
40
β in degrees

FIGURE 27

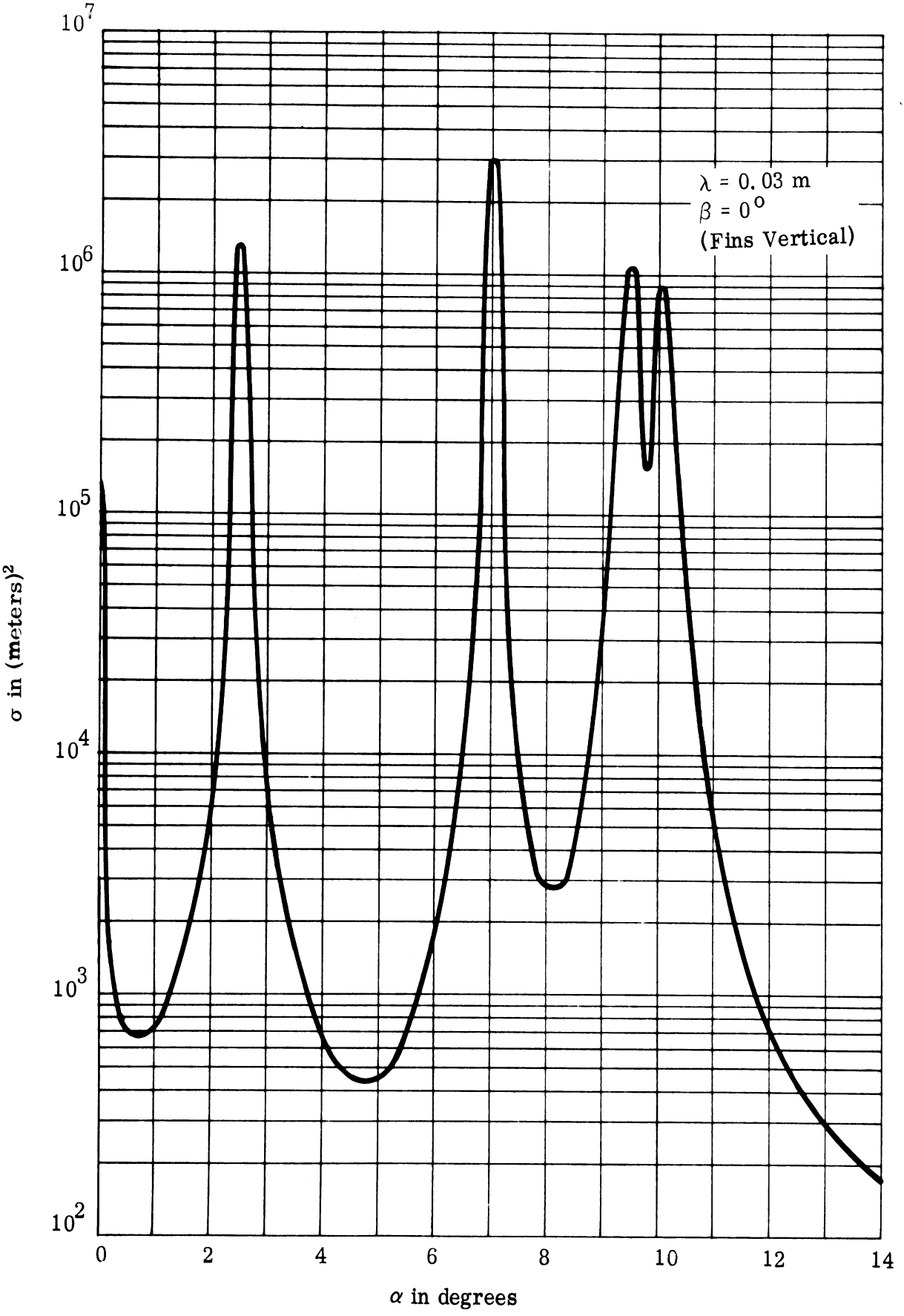
10^7
10^6
10^5
10^4
10^3
10^2
σ in (meters)²
λ = 0.03 m
β = 0°
(Fins Vertical)
0
2
4
6
8
10
12
14
α in degrees

FIGURE 28

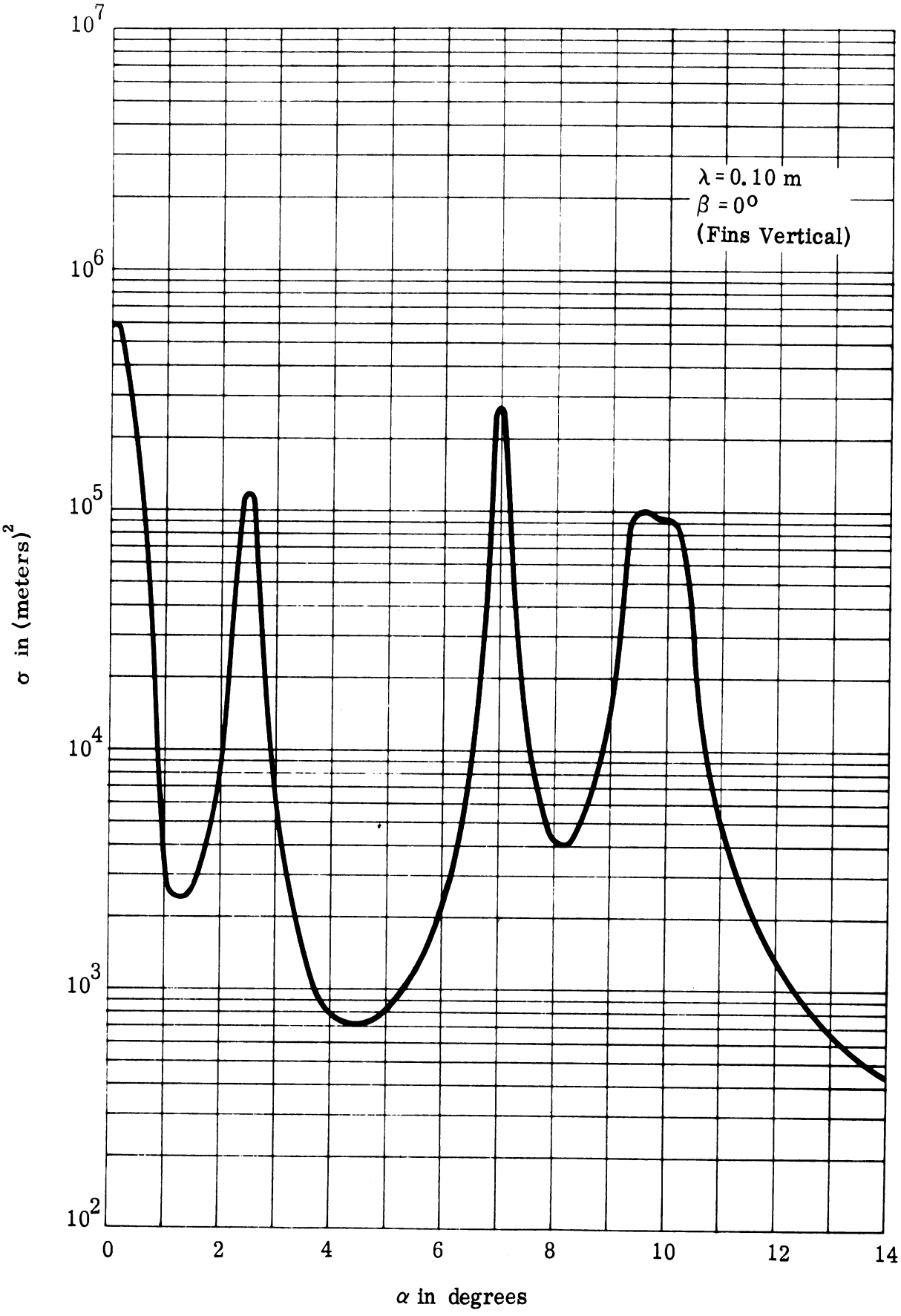
10^7
10^6
10^5
10^4
10^3
10^2
σ in (meters)^2
λ = 0.10 m
β = 0°
(Fins Vertical)
0
2
4
6
8
10
12
14
α in degrees

FIGURE 29

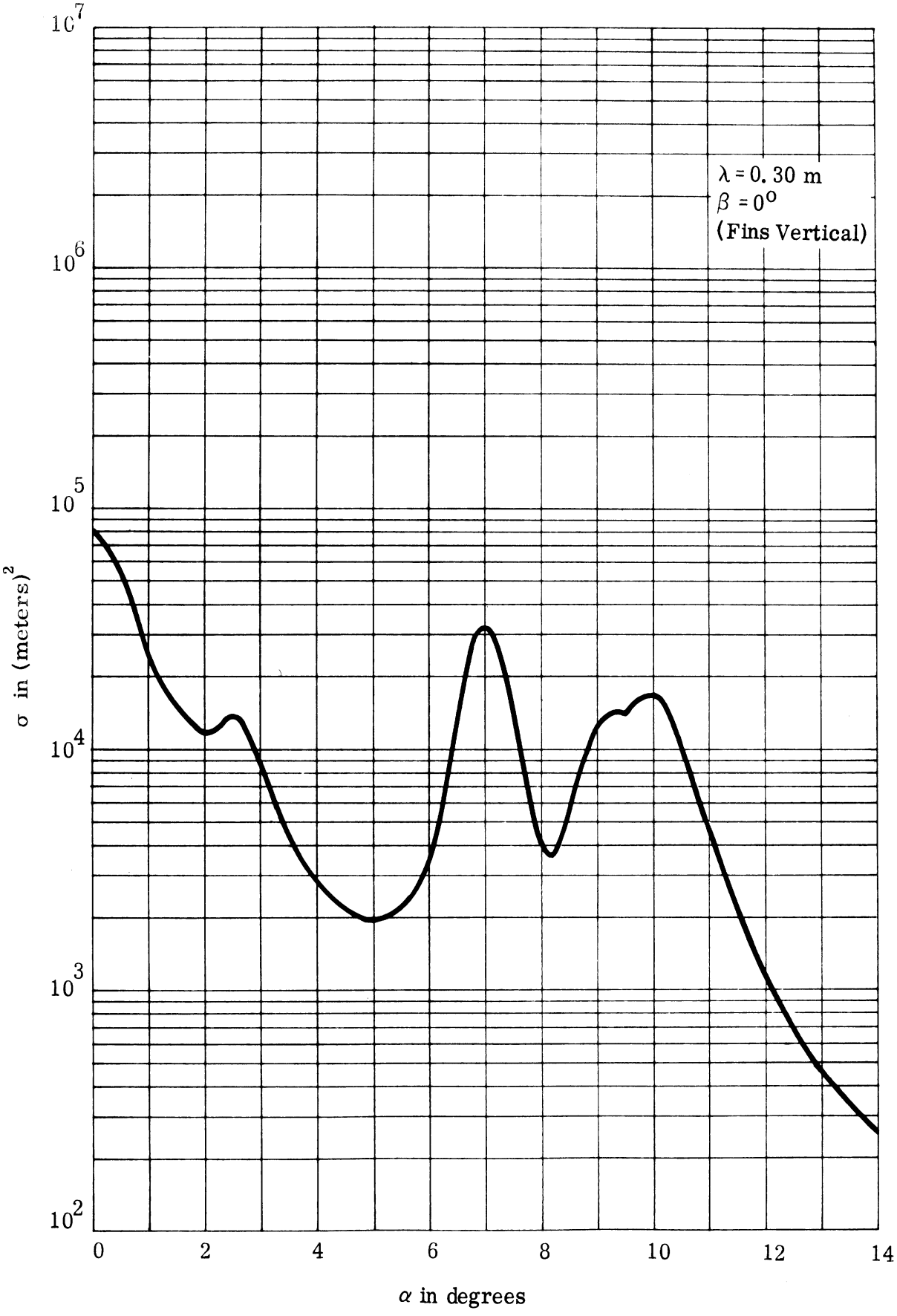
10^7
10^6
10^5
10^4
10^3
10^2
σ in (meters)^2
λ = 0.30 m
β = 0°
(Fins Vertical)
0
2
4
6
8
10
12
14
α in degrees

FIGURE 30

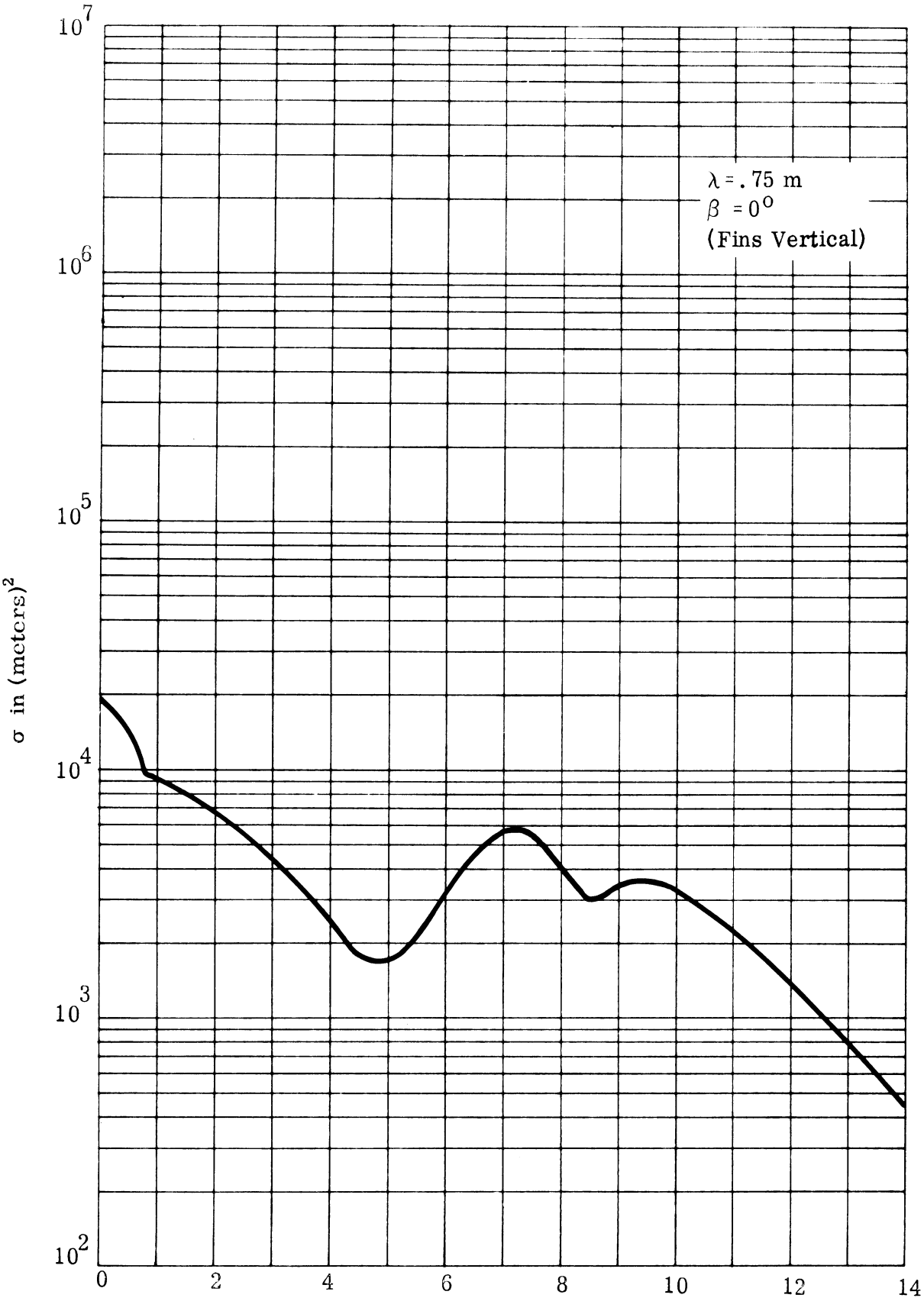
10^7
10^6
10^5
10^4
10^3
10^2
σ in (meters)^2
λ = .75 m
β = 0°
(Fins Vertical)
0
2
4
6
8
10
12
14
α in degrees

FIGURE 31

3. RADAR ABSORBING MATERIAL FOR THE B-70

The results of studies reported in Reference 1 as well as the work at NAA in Columbus have shown that the high cross section of the B-70 in the forward area is due to reflection from the air-intake ducts. An examination of photographs of the models (Fig. 32) would also lead one to this conclusion. One of the requirements in the present study was to determine the optimum method of minimizing this cross section by the addition of RAM along the duct walls. This work is described in Section 4. Another requirement called for a survey of RAM which might be suitable for lining the duct walls of the B-70 and the results of the survey are given in this section.

For a RAM to be satisfactory for use in the B-70 it must operate at temperatures up to 650^{o} F. Ideally its physical properties should also include toughness, resistence to shattering and the ability to be machined or moulded to fit the duct walls, or to be painted or sprayed on the duct walls. It should be able to absorb 90 % or more of the incident energy from 100 Mc to 10,000 Mc. The required thickness should be well under an inch and the weight per unit area of the layer should be a minimum.

Of the above requirements, the one which has received least attention among workers in the radar absorbing field is that concerning temperature. This requirement immediately rules out dielectric foams of plastic materials, hair flex and rubber absorbers. To the best of our knowledge, there are only

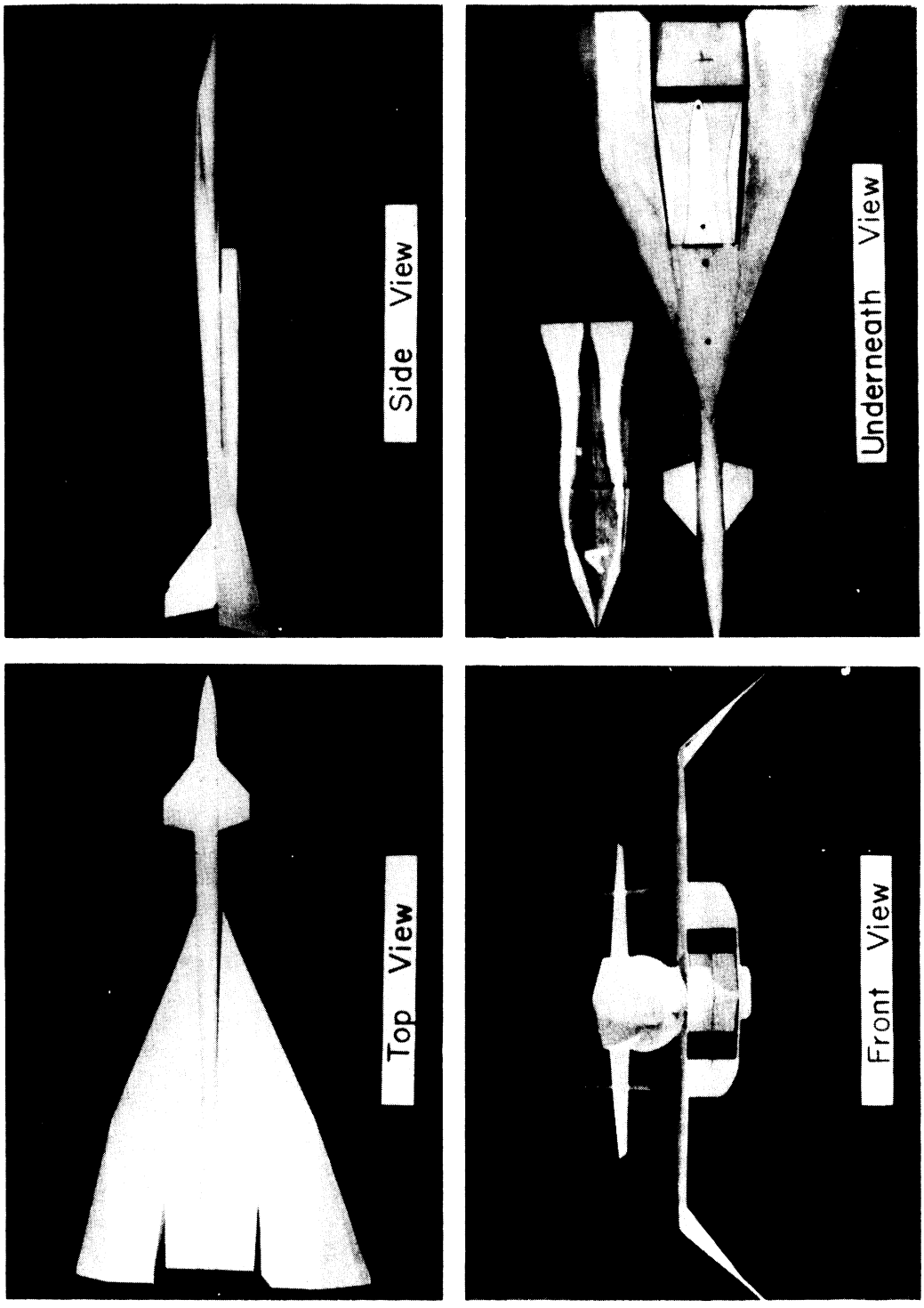

VIEWS OF THE B-70 MODEL

FIGURE 32

two organizations in this country that have been actively at work to develop a high-temperature RAM. The first, Rutgers University, has just started a program to produce a high-temperature RAM using ceramics (see Ref. 2), but it is much too early to capitalize on this effort. The second organization, Emerson and Cuming, Inc., has developed a high-temperature RAM, designated BNA-100 (Ref. 3), which consists of conductively-loaded foam materials. BNA-100 is a low-density material made of carbon-coated hollow microspheres, with the microspheres self-bonded in a hot press. A 2" thick layer of BNA-100 has a reflection coefficient of 3 to 5 % for frequencies higher than 1000 Mc. Such a layer weighs about 2.6 pounds per square foot.

At the present stage in the development BNA-100, it may be slightly marginal in respect to its ability to stand the 650° F temperature. It is believed, however, that this limitation will be overcome as the work continues. Further work on this material is needed to improve the particle-to-particle bonding, but it may be possible to solve the problem by enclosing the material within a silicon laminate. If the 2" thickness is maintained, the reflection coefficient will increase as the frequency decreases. It is doubtful, however, if the reflection coefficient would increase above 50 % at frequencies higher than 100 Mc.

The only other type of radar absorbing materials which would appear to come close to the physical and, in particular, the temperature requirements

for the B-70 application are the ferrite absorbers. These have been under development for a number of years (see, for example, reports on the work at the Naval Research Laboratories (Ref. 4), Battelle Memorial Institute (Ref. 5) and The University of Michigan (Ref. 6)), and it has been demonstrated that broad-band performance can be achieved. NRL reported on a material (Ref. 4) with a power reflection coefficient of 5 % or less from 100 to 10, 000 Mc. This material is pyramidal in form with a total thickness of 1" and uses a Ni-Mn-Zn ferrite. A flat piece 0.217" thick has a power reflection coefficient of less than 5 % from 100 to about 1400 Mc. Based on the NRL results with pyramidal absorbers, it would seem that one should be able to develop an absorber 0.5" thick with a power reflection coefficient of 10 % or less from 200 Mc to 10, 000 Mc. The maximum temperature for this material is about 150° C. It should be understood that the referenced NRL data represents their best results after a rather thorough study of low-temperature ferrites.

The University of Michigan (Ref. 6) has materials with a reflection coefficient of less than 5 % from 100 to 1000 Mc. To achieve this with a ZnY + 1 % sodium silicate, an estimated thickness of 2" to 3" would be required at 100 Mc. The required thickness decreases rapidly with wavelength and should be well under an inch for frequencies above 400 Mc. These estimates are based on curves appearing in Reference 6 which give depth of penetration for

an infinite sheet rather than the usual minimum thickness required for an absorber backed by a conductor. The Curie temperature of the lossy ferrite materials being developed at The University of Michigan extends to 300° C or better, but until now no particular effort had been made to work with the higher Curie temperature ferrites.

The military has been slow to use ferrite absorbers for airborne applications because of their weight. The weight per square foot of a 1" thick piece of the usual ferrite absorber is about 20 pounds. In the B-70 application, however, the advantages to be gained by the use of a relatively small amount of RAM suggests that more serious consideration should be given to the use of materials which might normally be regarded as too heavy or too thick. In this connection, the authors would like to press for the design of aircraft in which the requirement for low cross section is borne in mind at the initial design stage. Absorbing material would not then have to be added in order that an aircraft, whose design was already complete, might satisfy the requirement. Moreover, the presence of absorbing material on the aircraft may not increase the overall weight since the lower cross section enables the weight of the countermeasure package to be reduced.

In surveying the possible sources for a ferrite RAM it immediately becomes apparent that there has been little or no emphasis on the selection of ferrites with high Curie temperatures. At temperatures higher than the Curie temperature the permeability of ferrites decreases rapidly. To our knowledge, no ferrite RAM with Curie temperatures near 600° F has been

developed in this country, but the authors are aware of the successful work of the British on high-temperature lossy ferrites. The Royal Aircraft Establishment at Farnborough, Hants. has used an 0.060" layer of a Plessey P-type absorber as a cover on the forward half of a "bullet" in the jet exhaust of a Canberra bomber. It is believed that the use of such coatings is now standard on these aircraft. One of the materials used was reported to be a combination of aluminum oxide (95 %) and ferrite (5 %). The material acts as a lossy layer of so many ohms and not as a matched absorber. It was designed to be effective at S and X bands (10 cm and 3 cm) and for temperatures in excess of those used in the B-70 ducts. A reduction in cross section of the order of 10 db has been reported. The material is made by the Plessey Company of Ilford, Essex.

The energy that enters the B-70 ducts must propagate down the ducts as if it were a waveguide. The modes propagated will, of course, depend upon the frequency involved and the polarization of the incident wave, and it is of interest to consider methods of attenuating energy in a waveguide. Maximum attenuation occurs when a dielectric absorber is in a strong E field, which is in the center of the guide for the fundamental mode. On the other hand, absorbers having high magnetic loss will perform most efficiently when placed in strong H fields, that is, near the guide walls for most waveguide modes.

The similarity of the B-70 duct problem and the waveguide load problem became apparent in a discussion with R. W. Wright of NRL. Wright's group has recently developed a high-temperature waveguide load (Ref. 7) using a

ferrite as the lossy material. This load was made by lining the walls of standard L-band (1300 Mc) waveguide with Ferroxcube 105. The load was about 40" long, the large length being necessary to distribute the heat over a wide area. The thickness of the material varied from a few mills at the input end to about 0.2" at the far end. The extra thickness at the end was for the purpose of increasing the loss there to help distribute the heat over the entire load.

The load proved to operate quite satisfactorily at L band, and also performed well at 3000 Mc and in the 10,000 Mc range. The ferrite material used in this load has a Curie temperature of 465° C (869° F). The load has been operated up to 720° F apparently with good performance. It has successfully passed some shake-table tests and a humidity test cycle.

Detailed information has been given on this load because it is a good example of the use of a large slab of ferrite material as a lossy material at temperatures in excess of those expected in the B-70 ducts. In addition, the loss mechanism is not unlike that expected in the B-70 ducts.

Workers at Battelle, NRL and in the Solid State Group at The University of Michigan involved in the development of ferrite RAM, believed it was feasible to develop broad-band absorbers which would perform at temperatures well in excess of 630° F. There are, for example, the following commercial materials with high Curie temperatures:

Type	Curie Temp.
Ferroxcube 4C	600° F
Ferroxcube 4D	750° F
Ferroxcube 4E	930° F

These materials are cited only to show that ferrites with high Curie temperatures have been developed. Information on their loss characteristics in the frequency range of interest is not available.

To learn more about the properties of Ferroxcube 105, information on this and similar ferrites was requested from the Ferroxcube Corporation of America. Although two requests were made, including a request for quotation on a sample, very little information was obtained.

A request was then made to NRL for a sample of Ferroxcube 105. The only sample they were able to provide was a small one which had already been mixed with a silicone resin binder. The binder was Dow Corning number 993, and the Ferroxcube 105 made up 85 % by weight of the mixture. The material provided by NRL was given to Professor Grimes of the Electrical Engineering Department of The University of Michigan in order that it might be tested and analyzed in his Solid-State Laboratory. Part of the Ferroxcube 105 mixture was shaped to form a sample 0.2" thick for their coaxial sample holder and measurements were made of reflection coefficient versus frequency. The results obtained for power reflection coefficient are given in Table 10.

Following a procedure described in Reference 6 and using a sample 0.04" thick, the Solid-State Laboratory also made measurements to determine the permeability of Ferroxcube 105 versus frequency. The results are included in Table 10.

TABLE 10

Frequency (Mc)	Per Cent Power Reflection (Thickness = 0.2")	Permeability
500	52.6	4.10 - j 2.64
600	51.6	3.77 - j 2.40
700	48.1	3.58 - j 2.43
800	43.5	3.23 - j 2.43
900	39.2	3.15 - j 2.27
1000	35.8	2.80 - j 2.28
1100	30.2	2.75 - j 2.15
1200	29.3	2.48 - j 2.10
2600	4.9	1.78 - j 1.56
3000	0.5	1.66 - j 1.65
3500	1.2	1.41 - j 1.48
4000	0.8	1.41 - j 1.42

The remaining part of the sample provided by NRL was subjected to spectrographic and chemical analysis by the Detroit Testing Laboratory, Inc. Their report showed that iron, nickel, zinc and cobalt were the predominant metals contained in the sample. A copy of the complete analysis has been forwarded to NAA. Since there was some uncertainty in this analysis due to the small sample provided and due to the presence of the resin binder, another contact was made with Ferroxcube Corporation of America. As a result of this contact made near the end of the present study a sufficiently large sample

of Ferroxcube 105 powder will be obtained. Professor Grimes will continue his study of the material as part of his Air Force contract on ferrite absorbers.

The results of the search for an absorbing material which would be satisfactory for application in the B-70 ducts were somewhat disappointing in that so little information on high-temperature RAM was available. For this reason, undue attention may have been focussed on Ferroxcube 105. Based on the performance of this material as a waveguide load one would predict fairly good performance in the B-70 ducts. The limited information resulting from The University of Michigan tests on the NRL sample do not indicate outstanding characteristics.

It is hoped that an effort will be made to develop an optimum high-temperature RAM for the B-70, although Ferroxcube 105 may prove to be a satisfactory absorber in the interim.

4. EXPERIMENTAL PROCEDURES AND RESULTS

4.1. Introduction

Experimental measurements were made to determine the optimum method of reducing the cross section of the B-70 in the forward area to 40 m^2 or less. Most of the effort was restricted to cross section reduction by the addition of RAM to the interior of the ducts. By covering up the duct apertures with metal foil (see Patterns A-2 and B-2) it was shown that a significant reduction is achieved when the electromagnetic energy is prevented from entering the ducts. It seems feasible to use large mesh screens to lower the cross section in the 100 to 300 Mc range, but no work was done on this since the technique was being investigated at NAA, Columbus.

One other effort not concerned with the use of RAM was investigated, and will be discussed later. This study involved the effect of tilting the vertical duct walls to produce a non-rectangular duct cross section.

The investigation divides into two parts, with a RAM having dielectric loss being used in the first part, and a RAM having magnetic loss[+] in the second. Measurements were first carried out to determine the optimum locations for the RAM. Later measurements were made to determine the effectiveness of locating RAM at positions prescribed by NAA. In many instances the reduction achieved by using RAM at the prescribed locations was insufficient, in which case an effort was made to determine the minimum additional RAM necessary to achieve the 40 m^2 level.

[+] The magnetic RAM used has dielectric loss also, but the dielectric loss will be small since the E field is near zero in a thin absorber backed by a conductor.

In general, it can be said that the optimum locations appeared to be about the same regardless of the type of RAM used. Dielectric RAM from commercial suppliers was used in the first tests since it was readily available. As a result of the investigation to find a RAM suitable for the B-70, it appeared that a material with magnetic loss would more nearly meet the thickness and temperature specifications (see discussion in Section 3). Thereafter most of the measurements were made with a thin magnetic RAM made in our laboratory.

In the patterns which follow, the RAM used is denoted by a type number which can be identified from the following table.

TABLE 11

Type Number	Identification of RAM
1	McMillan Laboratory X-band resonant absorber Type T-XT-2 with a measured reflectivity+ of -19 db.
2	Emerson and Cuming X-band dielectric absorber Type Eccosorb AN-73; measured reflectivity about -20 db.
3	McMillan Laboratory K-band resonant absorber Type T-KQ-2; measured reflectivity about -20 db.
4	Emerson and Cuming K-band dielectric absorber Type Eccosorb AN-72; measured reflectivity better than -20 db.
5	Magnetic absorber, home-made according to formula supplied by R. W. Wright and W. H. Emerson of the Naval Research Laboratory. The absorber consists of 73 % J carbonyl iron powder in an epoxy resin. The epoxy resin is coil seal No. 11 made by the National Engineering Products Company of Washington D. C. The thickness is approximately 0.040". NRL recommends a thickness of about 0.72" for a resonant X-band absorber. The reflectivity of this material was measured to be -4 db at 9700 Mc and -9 db at 22.9 KMc.
6	Emerson and Cuming unmatched lossy dielectric Eccosorb Type LS-26; measured reflectivity at X band -6 db.
7	Magnetic material; similar to type 5 except that it is about 0.070" thick. The measured reflectivity at 23 KMc is -4 db.

+ A reflectivity of -n db means that for normal incidence the reflected power is ndb less from a flat piece of RAM than from a flat metal plate of the same size.

4.2. Experimental Facilities and Procedures

The measurements were made on an indoor scattering range using conventional cw equipment and techniques. The maximum range available was about 40 feet, which is considerably less than that required to be in the far field.

The range limitations and the residual reflections in the room limited the accuracy and the repeatability of the measurements. Scattering patterns were taken at slightly different ranges to evaluate the contributions due to the room reflections. The changes caused in the larger reflected signals were slight - usually less than one db. Changes in the level of the signal when the return is the order of the nose-on cross section ranged from one to four db for individual lobes. Any changes in the level averaged over several degrees were small.

The small asymmetries in the scattering pattern were found to be due to asymmetry in the model and in the measurement room.

Since the objective in these measurements was to determine the amount of cross section reduction that could be achieved, and since this involved the comparison of the scattering pattern of the same aircraft with and without RAM inserts, it is believed that inaccuracies due to range limitation, etc will generally cancel out. As a result, the value determined for the cross section reduction should be quite reliable.

A block diagram showing the equipment is given in Figure 33, and a photograph of the equipment and measurement room is shown in Figure 34.

At X band, frequency stabilization was achieved by the use of a reference cavity. At K band the oscillator frequency was phase-locked to an S-band crystal exciter. Background reflections and direct coupling between the transmitter and receiver through the hybrid tee were minimized by the proper adjustment of the RF tuners. The Scientific Atlanta receiver and recorder were used. Spheres and corner reflectors were employed as standard scatterers to calibrate the level of the return from the aircraft being studied.

Three aircraft models which were provided by NAA were available for this study. All were made of wood which had been metalized by The University of Michigan and the scales of the models were 0.01, 0.02 and 0.04. The corresponding lengths of the models were two feet, four feet and eight feet respectively. The scattering characteristics of all three were studied at X and K bands and the results are given in Reference 1. In the present study most of the work was carried out with the 0.04 scale model at simulated frequencies of 388 Mc and 918 Mc.

An explanation of the designations showing the amount and location of RAM used in the subsequent patterns is given in Figure 35. All positions along the duct walls are referred to in inches measured from the beginning of the outer duct wall, with points forward from the beginning of the duct taken

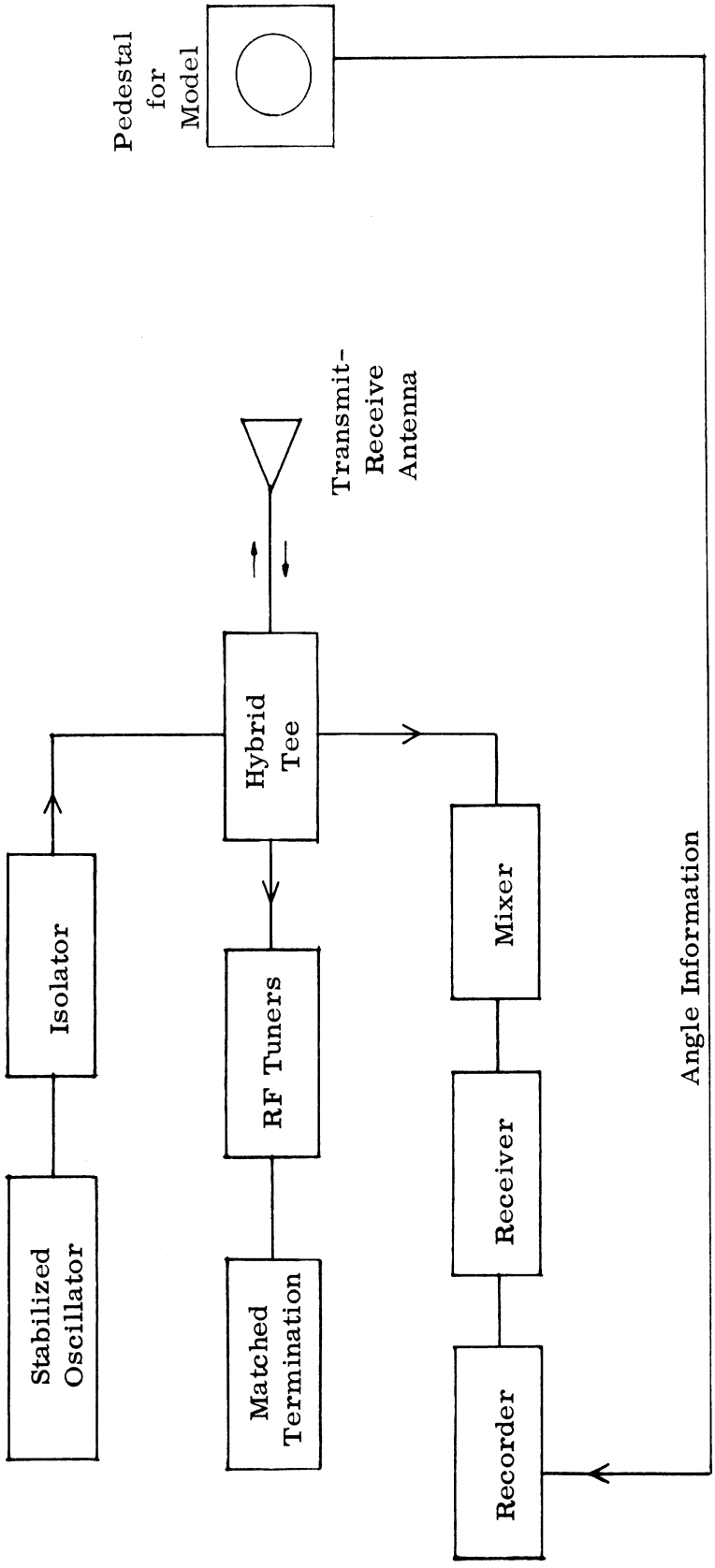
Pedestal for Model
Transmit-Receive Antenna
Hybrid Tee
Isolator
RF Tuners
Mixer
Stabilized Oscillator
Matched Termination
Receiver
Recorder
Angle Information

FIGURE 33

FIGURE 34

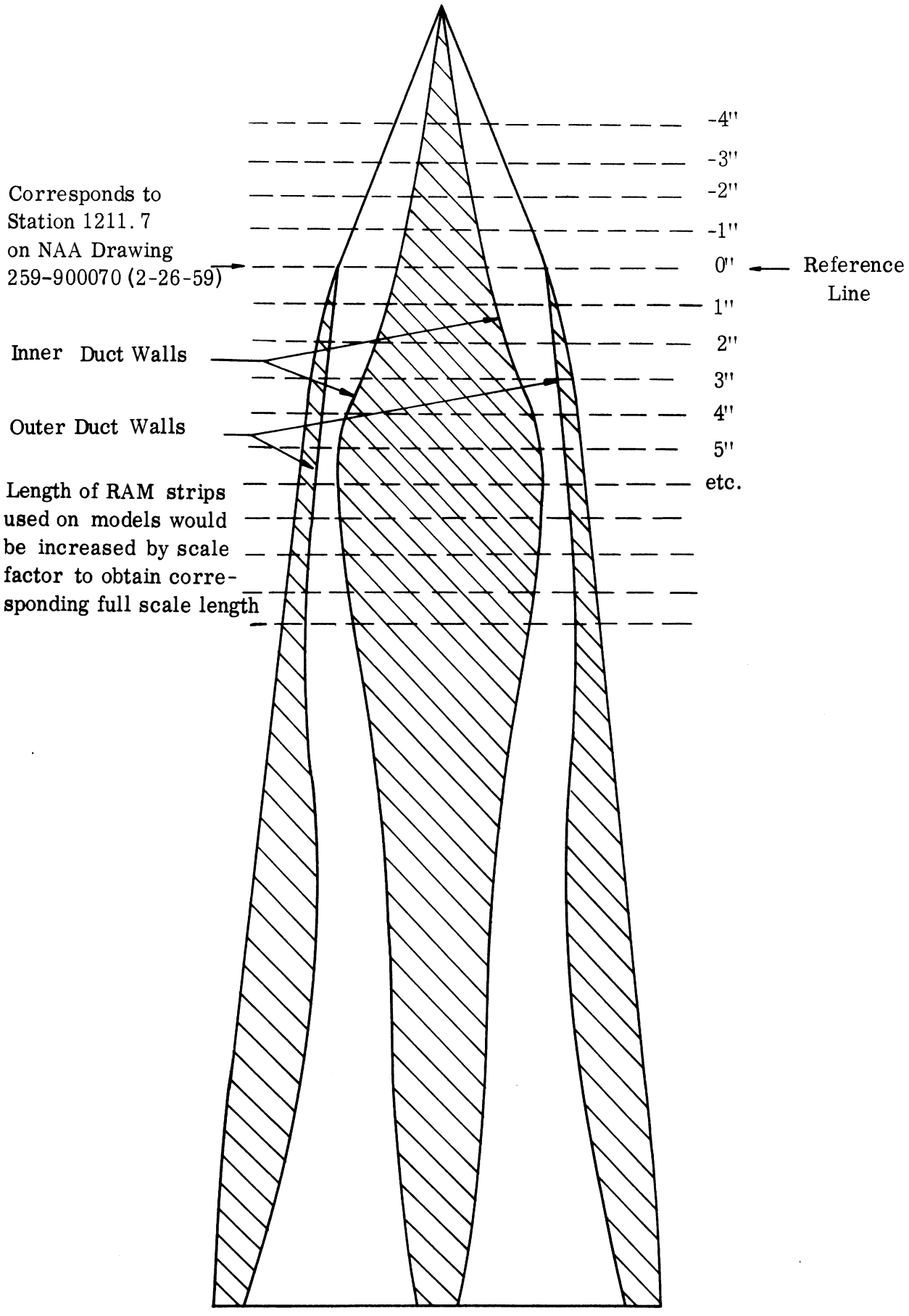

View of Duct System Showing Numbering Scheme for Location of RAM
FIGURE 35

to be negative. A 1" strip on the 0.04 model is equivalent to a 25" strip on the full-scale aircraft.

4.3. Results

4.3.1. Series A: Vertical Polarization, Dielectric RAM, 388 Mc

Fifteen patterns are presented in this group simulating results at 388 Mc with vertical polarization. Patterns taken in the horizontal plane of the model are denoted by a climb angle of 0^{o}. Other patterns are taken with the model at a climb angle of 10^{o} where the model is rotated about a vertical axis. Note that the plane of the observing radar intersects the plane of the model at an elevation angle of 10^{o}, but that the observing radar is at exactly -10^{o} in elevation for the nose-on aspect only. Since the objective is to lower the nose-on cross section to 40 m^2 or below, this level is shown on all patterns.

A comparison between the Standard Pattern A-1 and Pattern A-2 indicates the level of achievement one could expect if all the energy that entered the ducts were absorbed or reflected in another direction. Here the peaks have dropped by 14 db with a reduction in average level of about 8 db within $\pm 60^{o}$ from nose-on. The lobes at 65^{o} are due to the specular return from the sides of the foil "wedges" used to cover the duct apertures.

Patterns A-3, A-4 and A-5 show that most of the incident energy does not penetrate far into the ducts, and this agrees with ray tracing results reported by NAA.

From Patterns A-6 and A-7 it is seen that RAM is more effective when placed on the inner walls than it is on the outer. This was found to be true in other tests, and could have been predicted since the inner walls are favorably curved and are also more nearly in the direct view of an observing radar at angles 0^{o} to 50^{o} or so from nose-on. Patterns A-10, A-11 and A-12 show that little is to be achieved by adding RAM to the top and bottom of the ducts, and this too was found in other measurements, both with horizontal polarization and at the 10^{o} climb angle. Pattern A-12, the standard pattern for 10^{o} climb angle, shows little change as a result of the change in elevation angle. Patterns A-13 and A-14 show more favorable results at 10^{o} than for the corresponding condition at 0^{o} climb angle. This was consistently found throughout the tests.

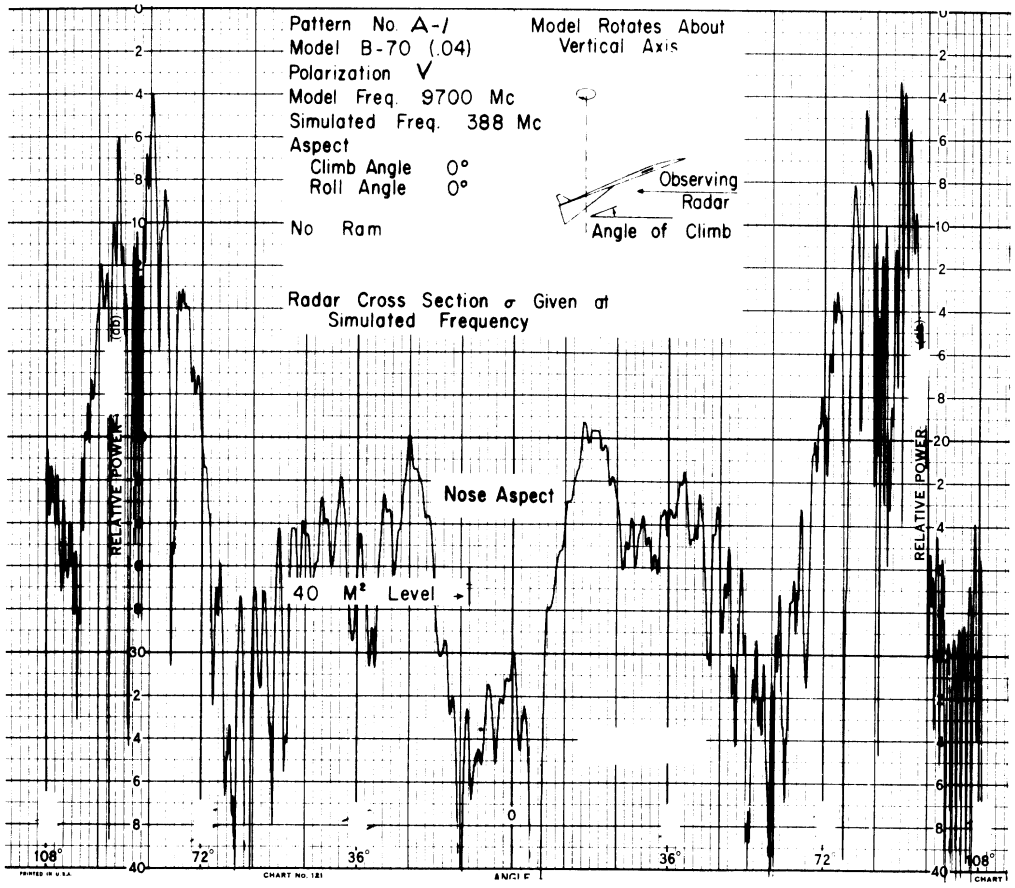
Pattern No. A-1
Model B-70 (.04)
Polarization V
Model Freq. 9700 Mc
Simulated Freq. 388 Mc
Aspect
Climb Angle 0°
Roll Angle 0°
No Ram
Model Rotates About Vertical Axis
Observing Radar
Angle of Climb
Radar Cross Section σ Given at Simulated Frequency
Nose Aspect
40 M² Level
RELATIVE POWER (db)
108°
72°
36°
0
36°
72
108°

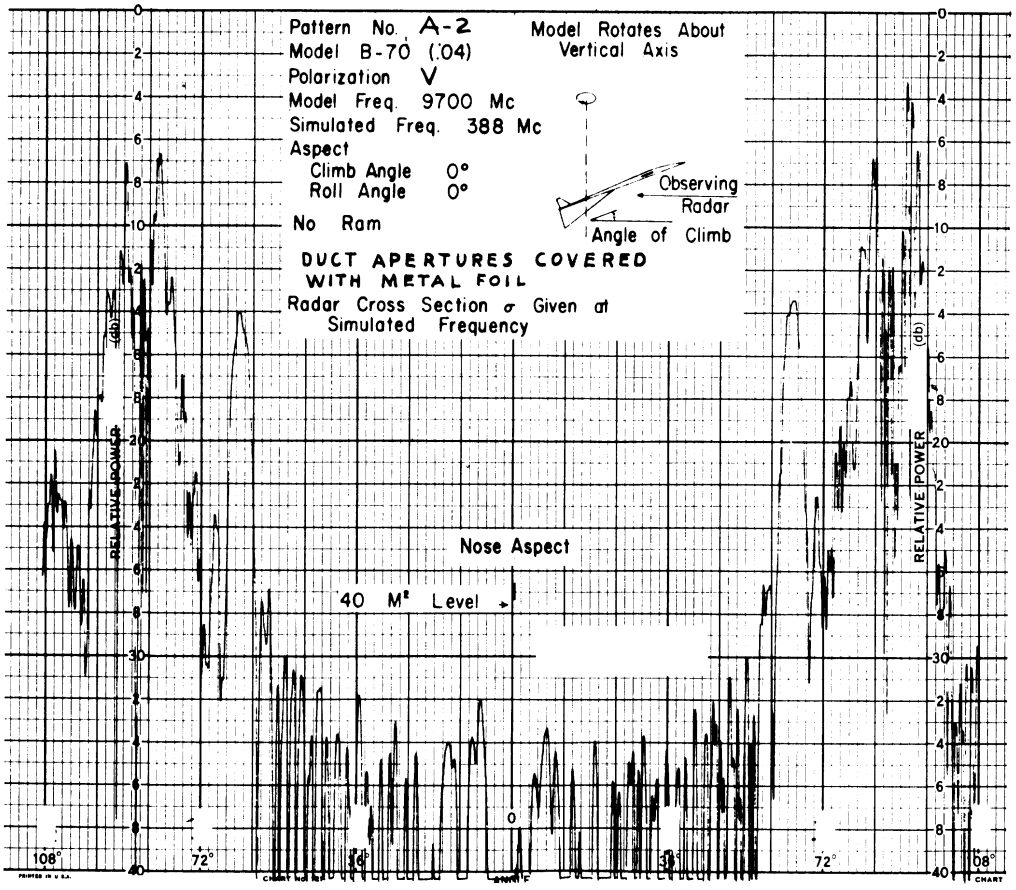
Pattern No. A-2
Model B-70 (.04)
Polarization V
Model Freq. 9700 Mc
Simulated Freq. 388 Mc
Aspect
Climb Angle 0°
Roll Angle 0°
No Ram
Model Rotates About Vertical Axis
Observing Radar
Angle of Climb
DUCT APERTURES COVERED WITH METAL FOIL
Radar Cross Section σ Given at Simulated Frequency
Nose Aspect
40 M² Level
RELATIVE POWER (db)
108°
72°
0
72°
108°

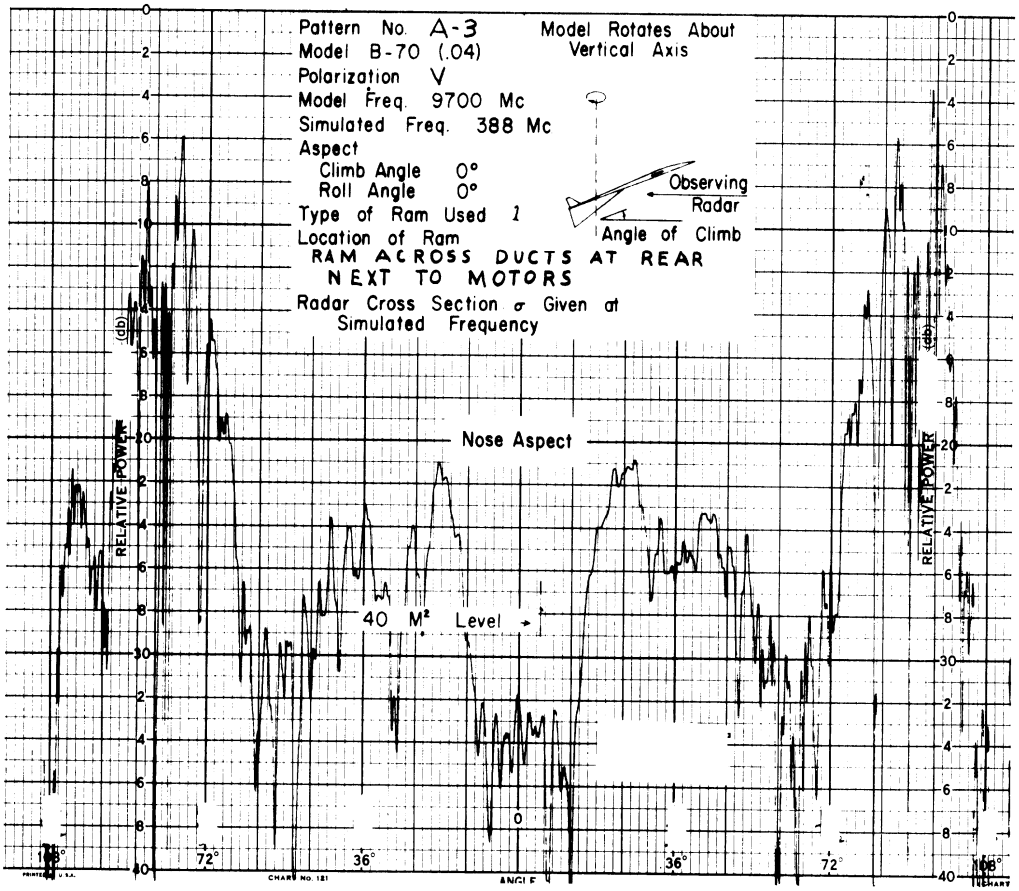
Pattern No. A-3
Model B-70 (.04)
Polarization V
Model Freq. 9700 Mc
Simulated Freq. 388 Mc
Aspect
Climb Angle 0°
Roll Angle 0°
Type of Ram Used 1
Location of Ram
RAM ACROSS DUCTS AT REAR NEXT TO MOTORS
Radar Cross Section σ Given at Simulated Frequency
Model Rotates About Vertical Axis
Observing Radar
Angle of Climb
Nose Aspect
40 M² Level
RELATIVE POWER (db)
108°
72°
36°
0
36°
72°
108°

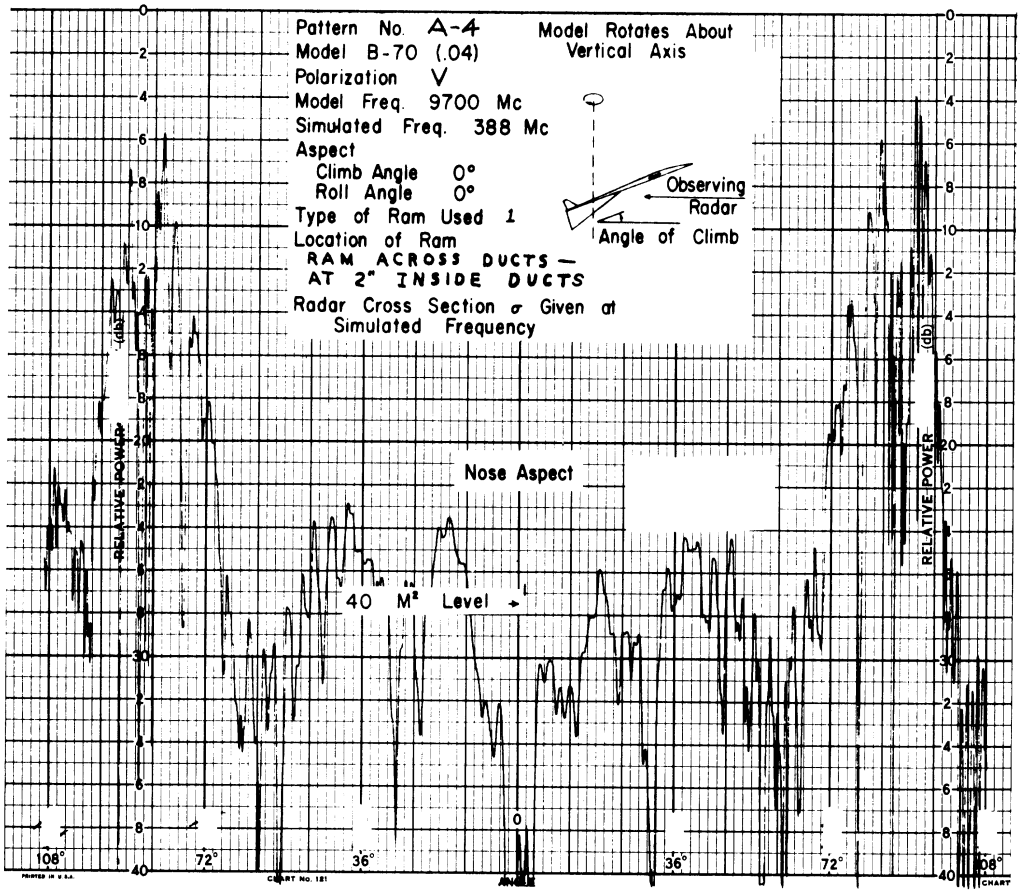
Pattern No. A-4
Model B-70 (.04)
Polarization V
Model Freq. 9700 Mc
Simulated Freq. 388 Mc
Aspect
Climb Angle 0°
Roll Angle 0°
Type of Ram Used 1
Location of Ram
RAM ACROSS DUCTS — AT 2" INSIDE DUCTS
Radar Cross Section σ Given at Simulated Frequency
Model Rotates About Vertical Axis
Observing Radar
Angle of Climb
Nose Aspect
40 M² Level
RELATIVE POWER (db)
108°
72°
36°
0
36°
72°
108°

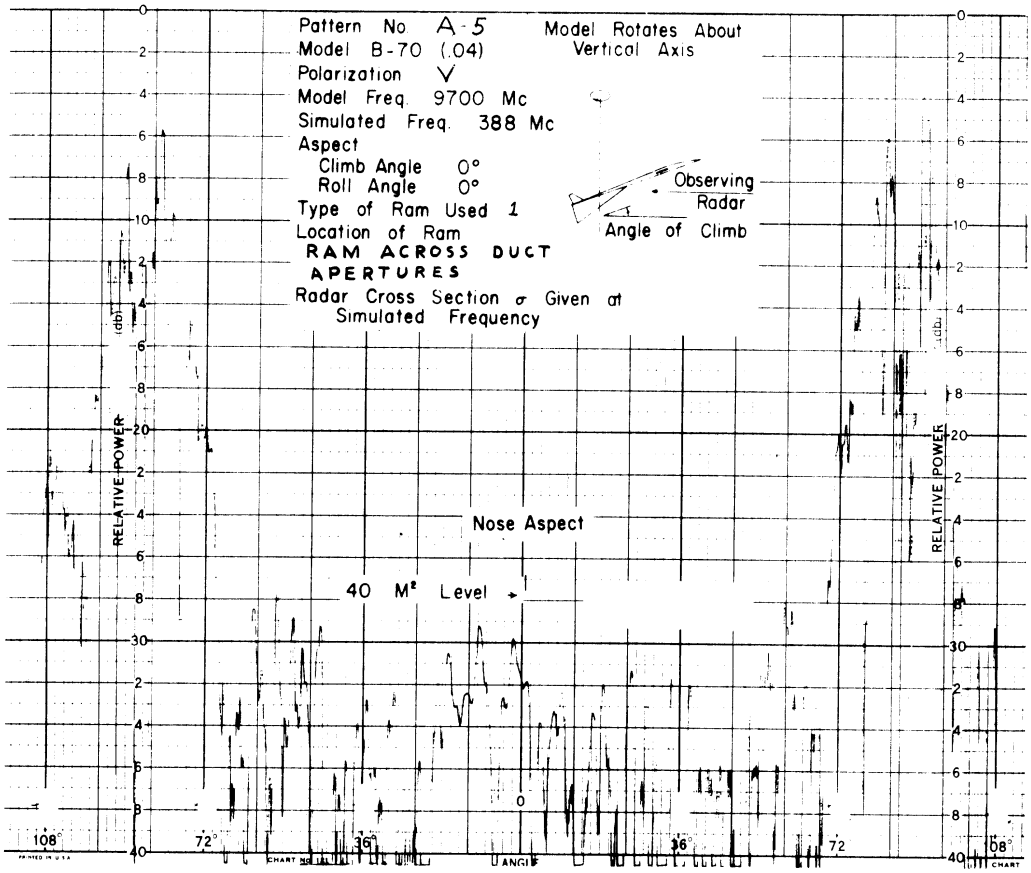
Pattern No. A-5
Model B-70 (.04)
Polarization V
Model Freq. 9700 Mc
Simulated Freq. 388 Mc
Aspect
Climb Angle 0°
Roll Angle 0°
Type of Ram Used 1
Location of Ram
RAM ACROSS DUCT APERTURES
Radar Cross Section σ Given at Simulated Frequency
Model Rotates About Vertical Axis
Observing Radar
Angle of Climb
Nose Aspect
40 M² Level
RELATIVE POWER (db)
ANGLE
108°
72°
36°
0
36°
72°
108°

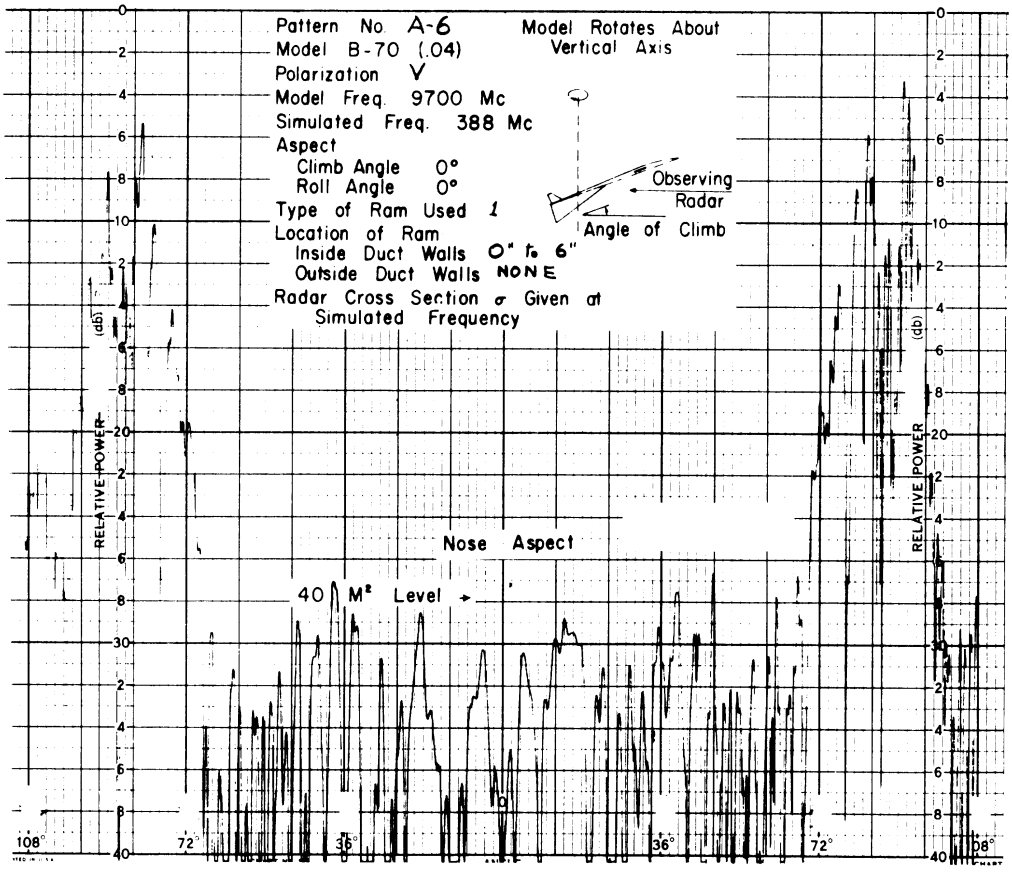
Pattern No. A-6
Model B-70 (.04)
Polarization V
Model Freq. 9700 Mc
Simulated Freq. 388 Mc
Aspect
Climb Angle 0°
Roll Angle 0°
Type of Ram Used 1
Location of Ram
Inside Duct Walls 0" to 6"
Outside Duct Walls NONE
Radar Cross Section σ Given at Simulated Frequency
Model Rotates About Vertical Axis
Observing Radar
Angle of Climb
Nose Aspect
40 M² Level
RELATIVE POWER (db)
108°
72°
36°
0
36°
72°
108°

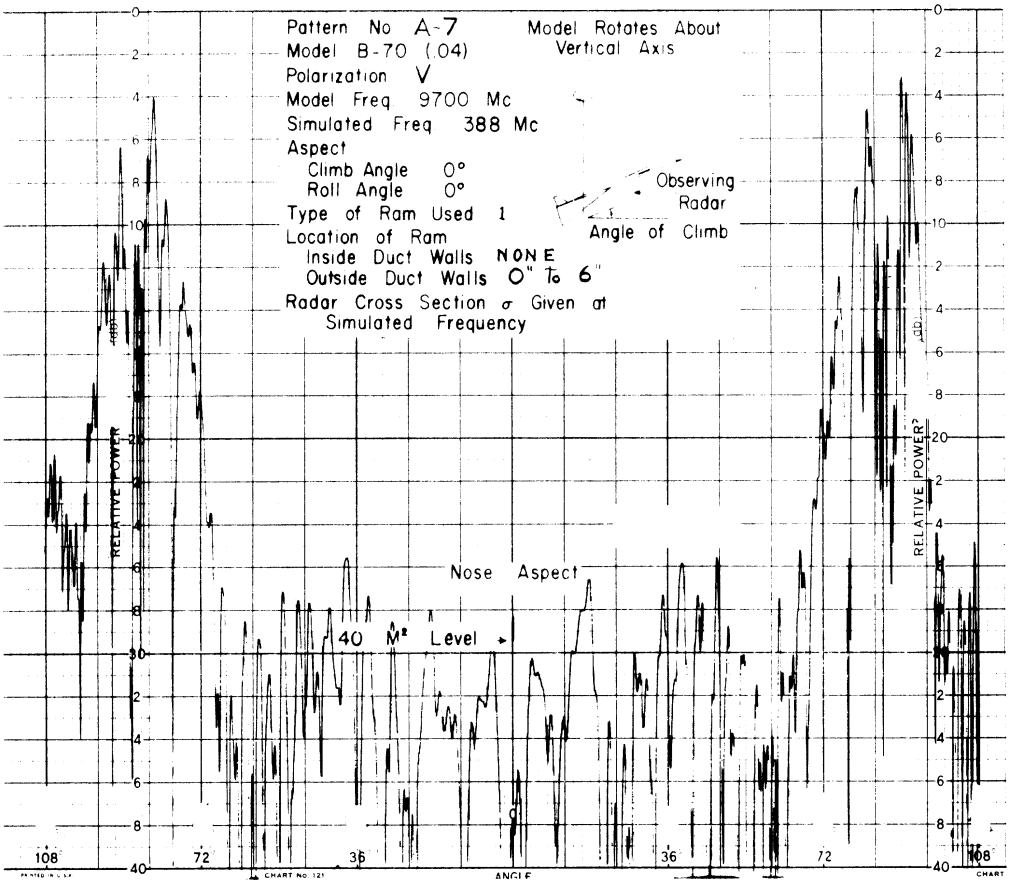
Pattern No A-7
Model B-70 (.04)
Polarization V
Model Freq 9700 Mc
Simulated Freq 388 Mc
Aspect
Climb Angle 0°
Roll Angle 0°
Type of Ram Used 1
Location of Ram
Inside Duct Walls NONE
Outside Duct Walls 0" To 6"
Radar Cross Section σ Given at
Simulated Frequency
Model Rotates About
Vertical Axis
Observing
Radar
Angle of Climb
Nose Aspect
40 M² Level
RELATIVE POWER
db
108
72
36
0
36
72
108
ANGLE
CHART

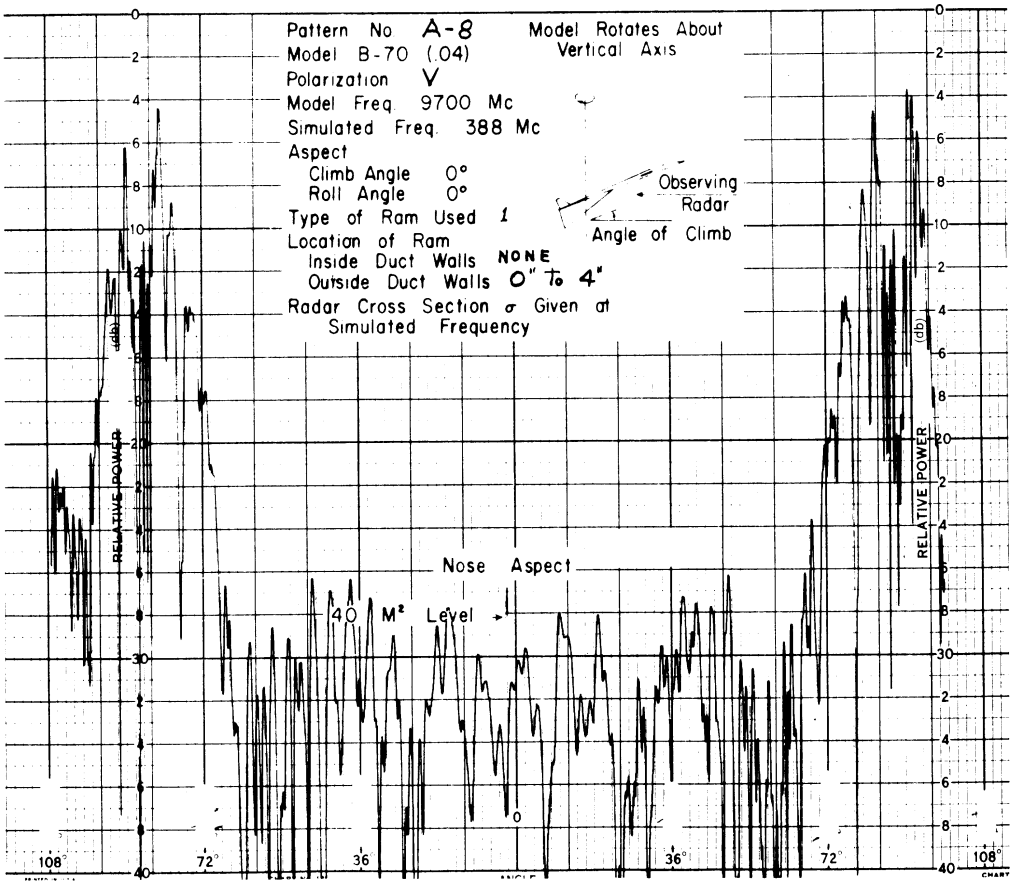
Pattern No A-8
Model B-70 (.04)
Polarization V
Model Freq 9700 Mc
Simulated Freq 388 Mc
Aspect
Climb Angle 0°
Roll Angle 0°
Type of Ram Used 1
Location of Ram
Inside Duct Walls NONE
Outside Duct Walls 0" To 4"
Radar Cross Section σ Given at
Simulated Frequency
Model Rotates About
Vertical Axis
Observing
Radar
Angle of Climb
Nose Aspect
40 M² Level
RELATIVE POWER
db
108°
72°
36
0
36°
72°
108°
ANGLE
CHART

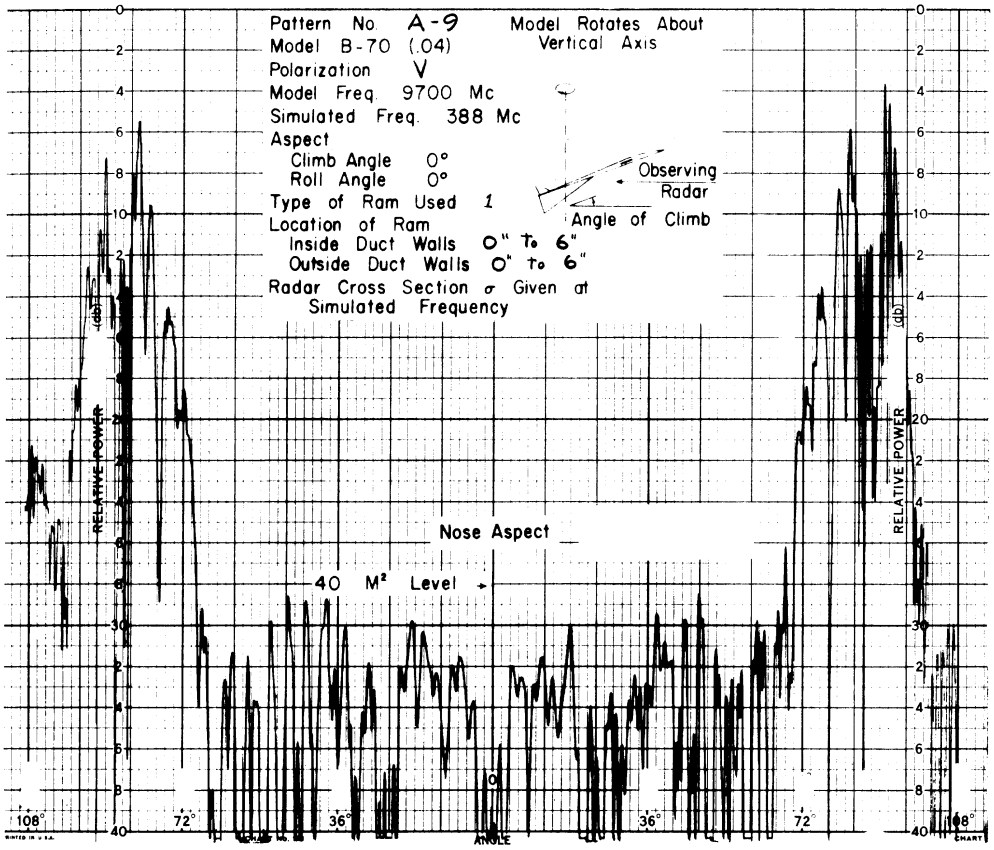
Pattern No. A-9
Model B-70 (.04)
Polarization V
Model Freq. 9700 Mc
Simulated Freq. 388 Mc
Aspect
Climb Angle 0°
Roll Angle 0°
Type of Ram Used 1
Location of Ram
Inside Duct Walls 0" To 6"
Outside Duct Walls 0" to 6"
Radar Cross Section σ Given at
Simulated Frequency
Model Rotates About
Vertical Axis
Observing
Radar
Angle of Climb
Nose Aspect
40 M² Level
RELATIVE POWER (db)
108°
72°
36°
0
ANGLE

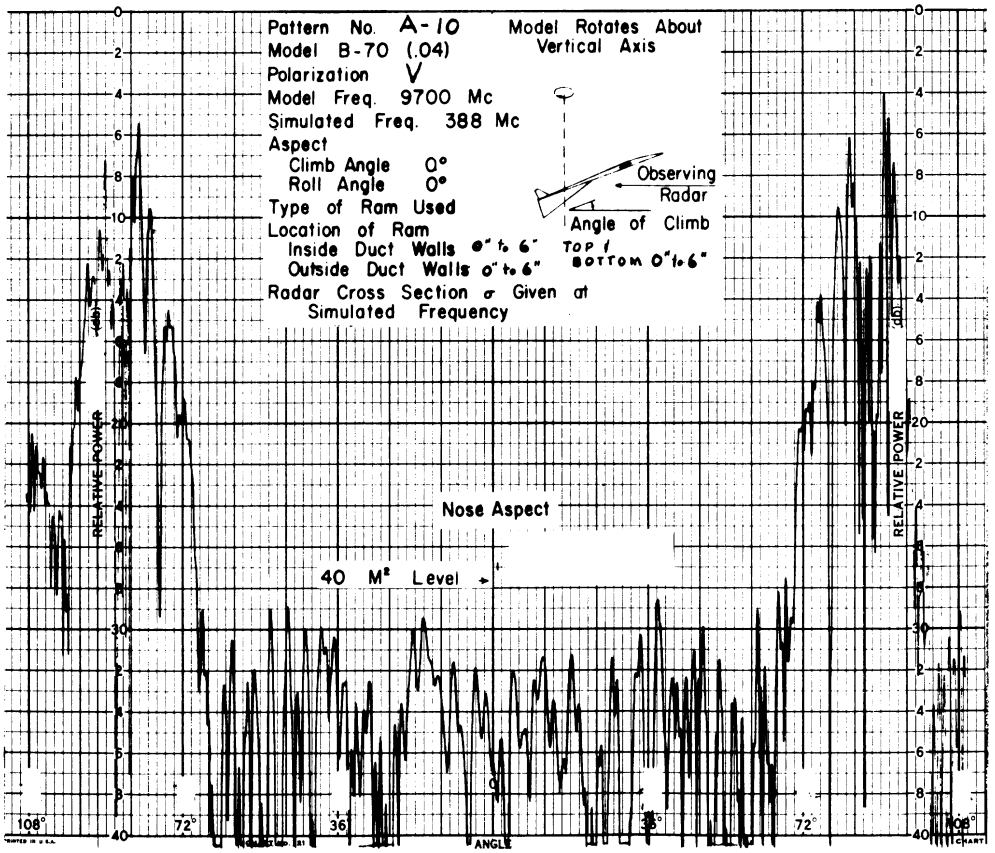
Pattern No. A-10
Model B-70 (.04)
Polarization V
Model Freq. 9700 Mc
Simulated Freq. 388 Mc
Aspect
Climb Angle 0°
Roll Angle 0°
Type of Ram Used
Location of Ram
Inside Duct Walls 0" to 6" TOP 1
Outside Duct Walls 0" to 6" BOTTOM 0" to 6"
Radar Cross Section σ Given at
Simulated Frequency
Model Rotates About
Vertical Axis
Observing
Radar
Angle of Climb
Nose Aspect
40 M² Level
RELATIVE POWER (db)
108°
72°
36°
0
ANGLE

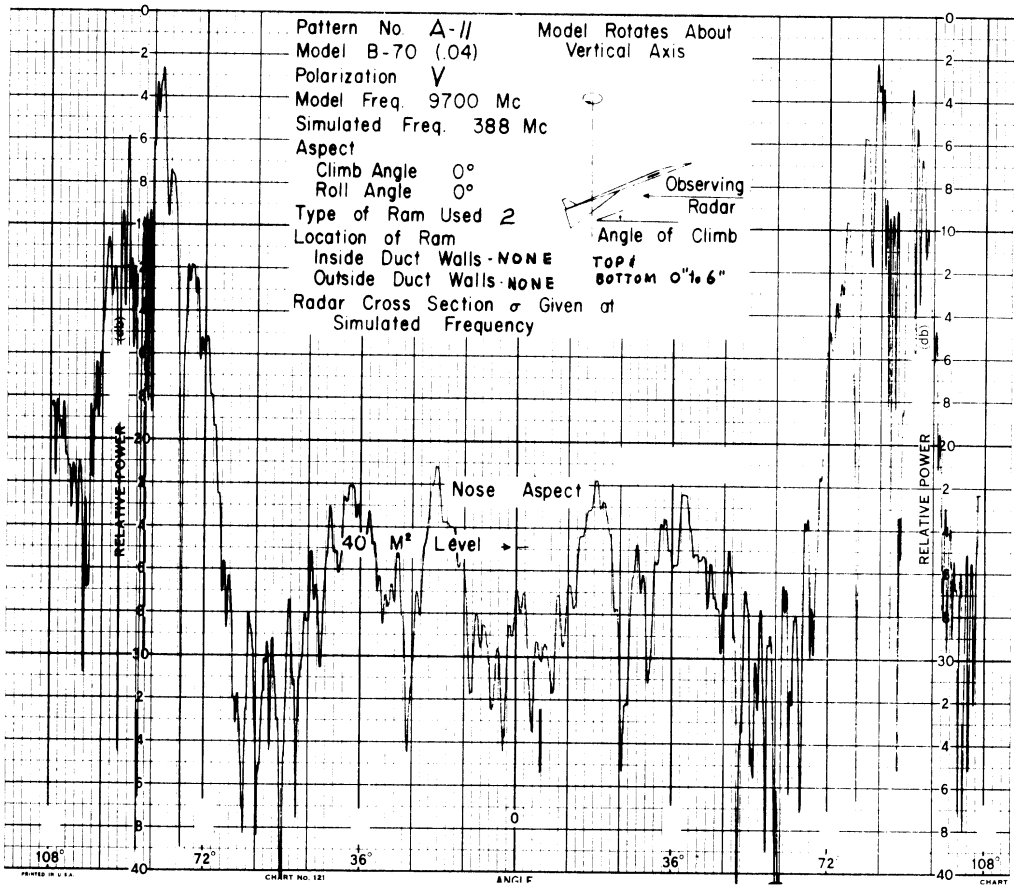
Pattern No. A-11
Model B-70 (.04)
Polarization V
Model Freq. 9700 Mc
Simulated Freq. 388 Mc
Aspect
Climb Angle 0°
Roll Angle 0°
Type of Ram Used 2
Location of Ram
Inside Duct Walls - NONE
Outside Duct Walls - NONE
Radar Cross Section σ Given at Simulated Frequency
Model Rotates About Vertical Axis
Observing Radar
Angle of Climb
TOP
BOTTOM 0"to 6"
Nose Aspect
40 M² Level
RELATIVE POWER (db)
108° 72° 36° 0 36° 72° 108°
ANGLE

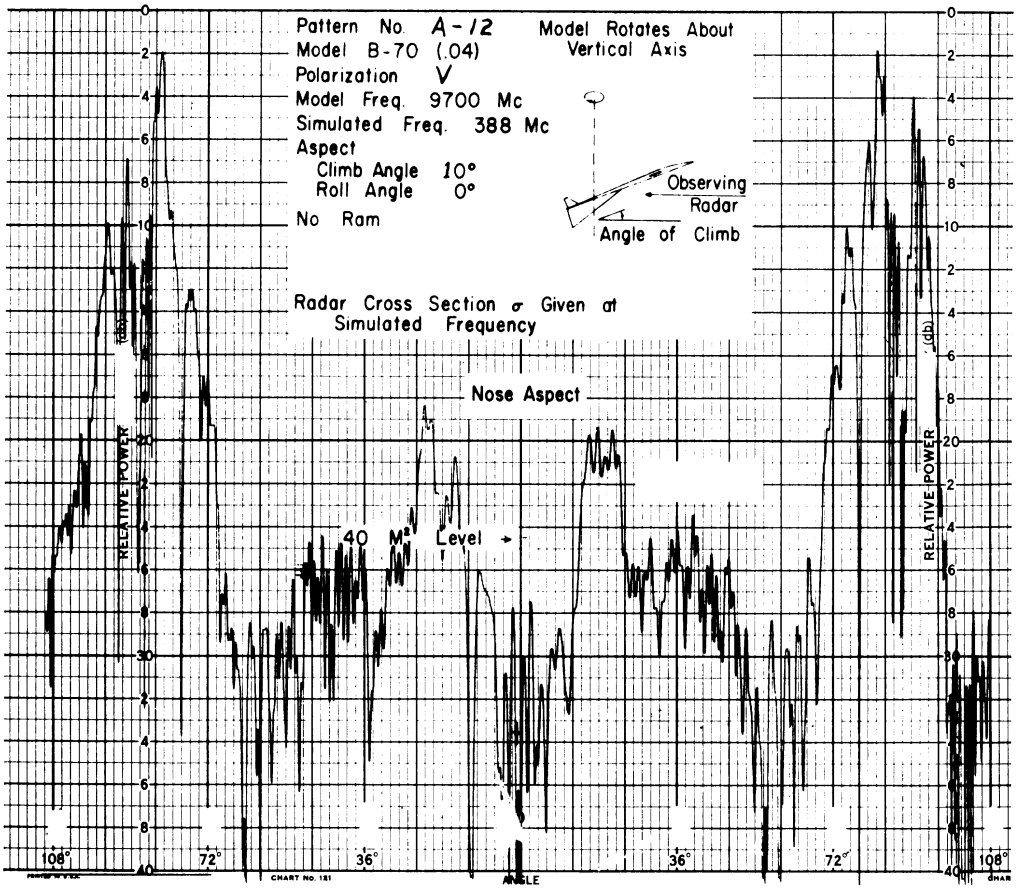
Pattern No. A-12
Model B-70 (.04)
Polarization V
Model Freq. 9700 Mc
Simulated Freq. 388 Mc
Aspect
Climb Angle 10°
Roll Angle 0°
No Ram
Radar Cross Section σ Given at Simulated Frequency
Model Rotates About Vertical Axis
Observing Radar
Angle of Climb
Nose Aspect
40 M² Level
RELATIVE POWER (db)
108° 72° 36° 0 36° 72° 108°
ANGLE

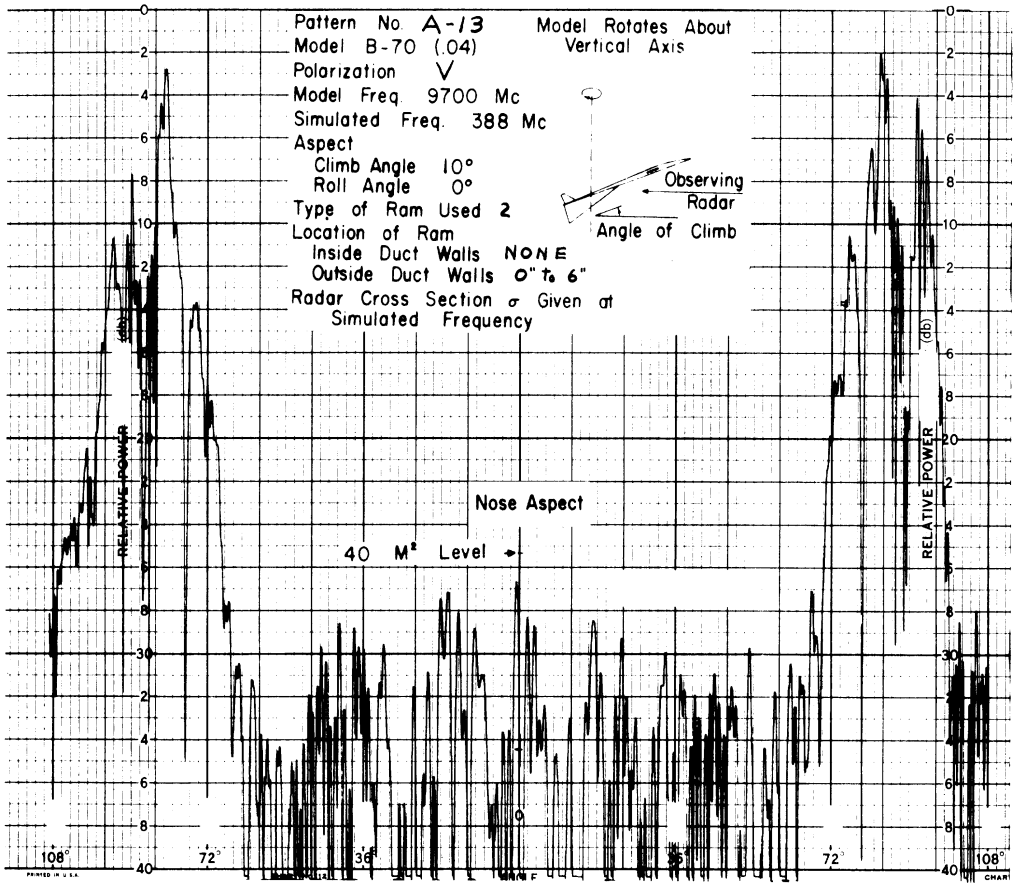
Pattern No. A-13
Model B-70 (.04)
Polarization V
Model Freq. 9700 Mc
Simulated Freq. 388 Mc
Aspect
Climb Angle 10°
Roll Angle 0°
Type of Ram Used 2
Location of Ram
Inside Duct Walls NONE
Outside Duct Walls 0" to 6"
Radar Cross Section σ Given at Simulated Frequency
Model Rotates About Vertical Axis
Observing Radar
Angle of Climb
Nose Aspect
40 M² Level
RELATIVE POWER (db)
108° 72° 36° 0 36° 72° 108°

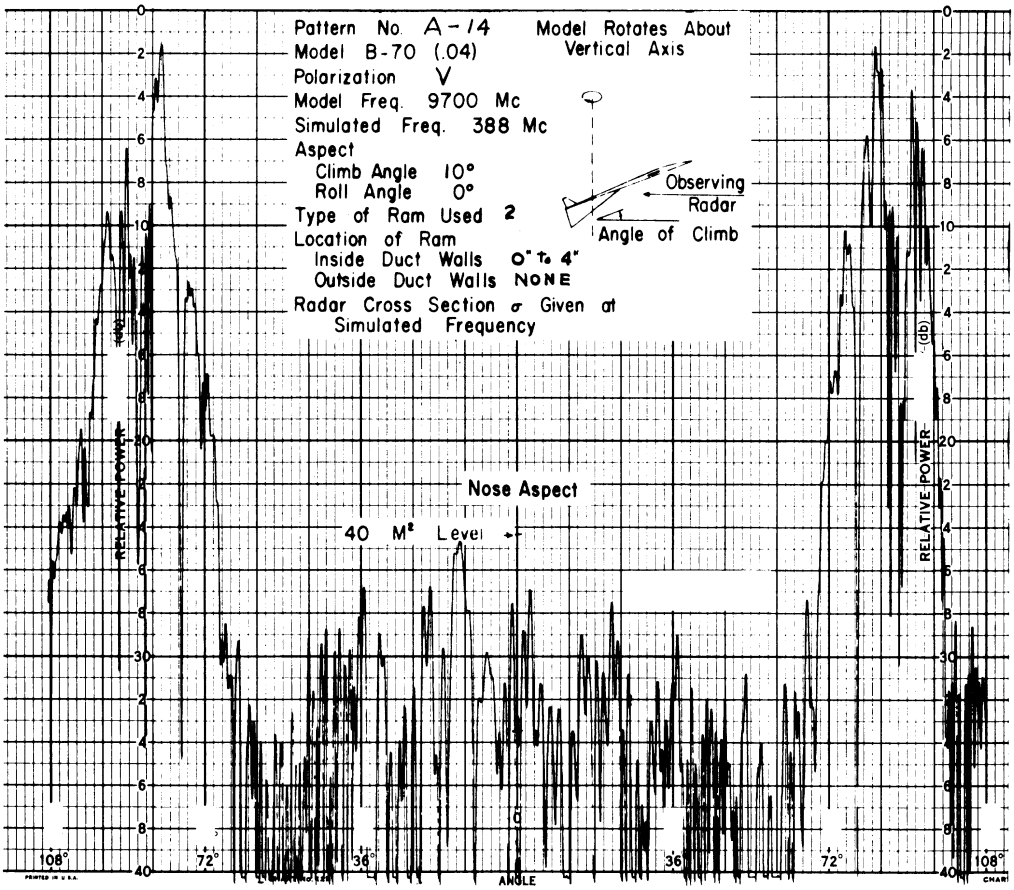
Pattern No. A-14
Model B-70 (.04)
Polarization V
Model Freq. 9700 Mc
Simulated Freq. 388 Mc
Aspect
Climb Angle 10°
Roll Angle 0°
Type of Ram Used 2
Location of Ram
Inside Duct Walls 0" to 4"
Outside Duct Walls NONE
Radar Cross Section σ Given at Simulated Frequency
Model Rotates About Vertical Axis
Observing Radar
Angle of Climb
Nose Aspect
40 M² Level
RELATIVE POWER (db)
108° 72° 36° 0 36° 72° 108°
ANGLE

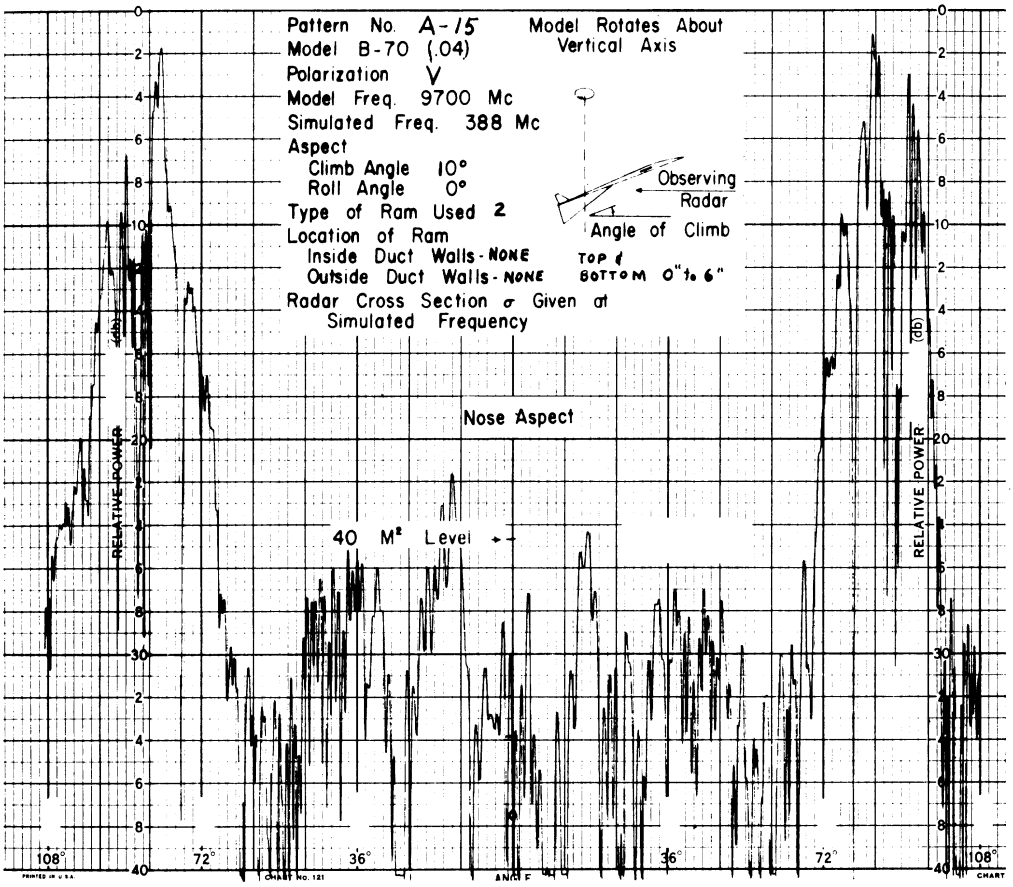
Pattern No. A-15
Model B-70 (.04)
Polarization V
Model Freq. 9700 Mc
Simulated Freq. 388 Mc
Aspect
Climb Angle 10°
Roll Angle 0°
Type of Ram Used 2
Location of Ram
Inside Duct Walls - NONE
Outside Duct Walls - NONE
Radar Cross Section σ Given at Simulated Frequency
Model Rotates About Vertical Axis
Observing Radar
Angle of Climb
TOP ¢
BOTTOM 0" to 6"
Nose Aspect
40 M² Level
RELATIVE POWER (db)
108°
72°
36°
36°
72°
108°

4.3.2. Series B: Horizontal Polarization, Dielectric RAM, 388 Mc

This group of patterns differs from the A series in that the plane of the E vector is parallel to the plane of the model. Generally the radar cross section is smaller with this polarization due to the smaller contribution from the several vertical edges that are seen at the forward aspects.

In Patterns B-1 and B-2 a considerable reduction in cross section is again evident when the ducts are covered with foil.

Patterns B-3 and B-4 show that a reduction over a wide range of forward angles cannot be achieved by working well within the ducts; this is consistent with results for vertical polarization.

Patterns B-6 through B-9 show that RAM along the inner duct wall is effective for this polarization and frequency, and that little improvement is to be gained by adding RAM to the other side wall or to the top and bottom, but that RAM on the top and bottom alone is not effective. The increased effectiveness of RAM on the vertical walls, as distinguished from RAM on the top and bottom,is believed to be due to (1) the curvature of the vertical walls and (2) the ratio of height to width. This ratio is more than 3 to 1 at the narrowest point, so that the area of RAM necessary to cover the side walls is much greater than that required to cover top and bottom. In addition, the field will be stronger in the narrower direction than in the wider direction.

In Patterns B-10 through B-12, the effect of moving a 6" strip of absorber progressively farther back on the inner wall is seen. The reduction in cross section is good when the strip starts 1" or 2" inside, but Pattern B-12 shows that little reduction is achieved with RAM 3" inside the ducts. In fact, other measurements (the patterns are not included here) showed that the decreased effectiveness was quite evident when the RAM started 2.5" inside the duct.

For Patterns B-13 and B-14, RAM with poor reflectivity was used. Type 4 was used in B-13. This is a good absorber for K band but at the X band frequency used, the reflectivity was measured as about -3 db. The type 6 material used in Pattern B-14 has a reflectivity of -6 db (see Table 11 for more information on the materials). These patterns show very effective cross section reduction, but it should not be concluded that a poor RAM will be sufficient for all conditions. This question is discussed further at the end of Section 4.

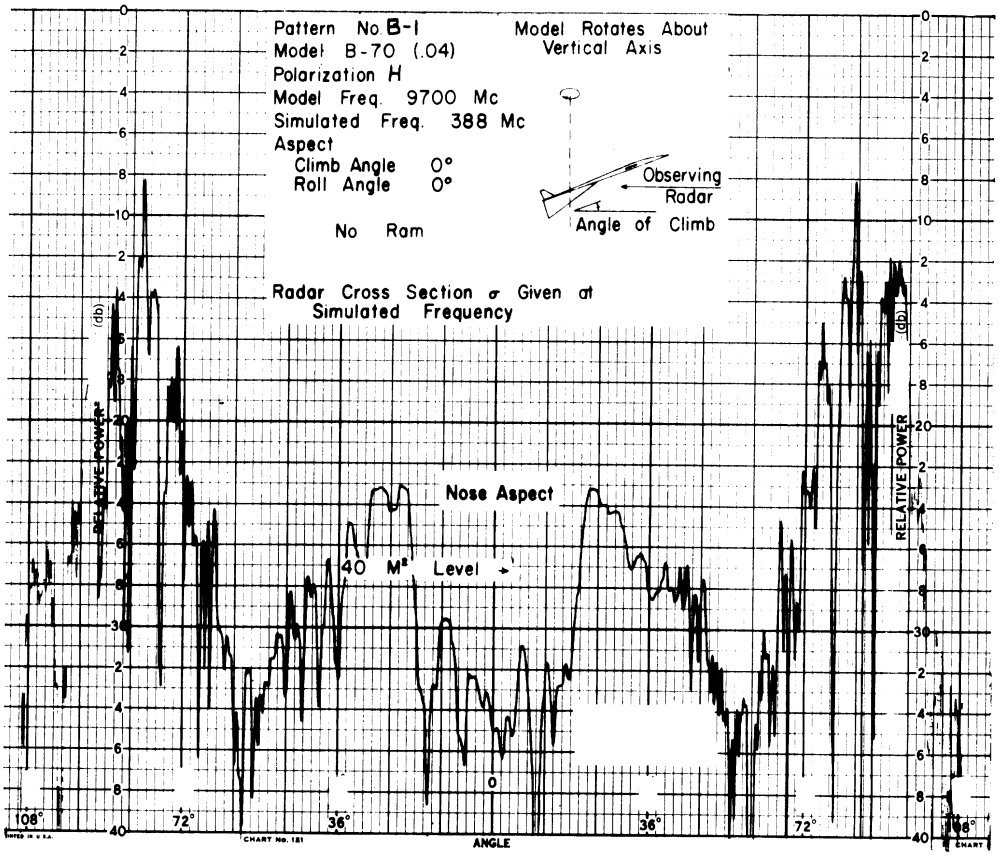
Pattern No. B-1
Model B-70 (.04)
Polarization H
Model Freq. 9700 Mc
Simulated Freq. 388 Mc
Aspect
Climb Angle 0°
Roll Angle 0°
No Ram
Radar Cross Section σ Given at Simulated Frequency
Model Rotates About Vertical Axis
Observing Radar
Angle of Climb
Nose Aspect
40 M² Level
RELATIVE POWER (db)
ANGLE
108°
72°
36°
0

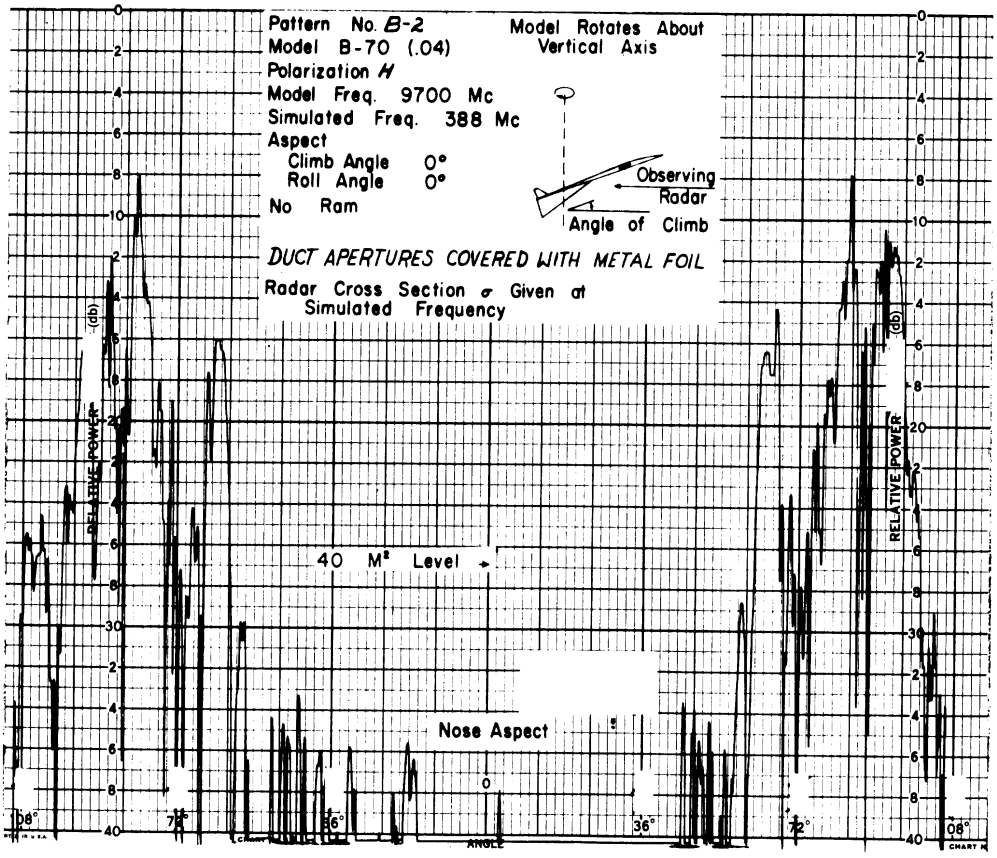
Pattern No. B-2
Model B-70 (.04)
Polarization H
Model Freq. 9700 Mc
Simulated Freq. 388 Mc
Aspect
Climb Angle 0°
Roll Angle 0°
No Ram
DUCT APERTURES COVERED WITH METAL FOIL
Radar Cross Section σ Given at Simulated Frequency
Model Rotates About Vertical Axis
Observing Radar
Angle of Climb
Nose Aspect
40 M² Level
RELATIVE POWER (db)
ANGLE
108°
72°
36°
0

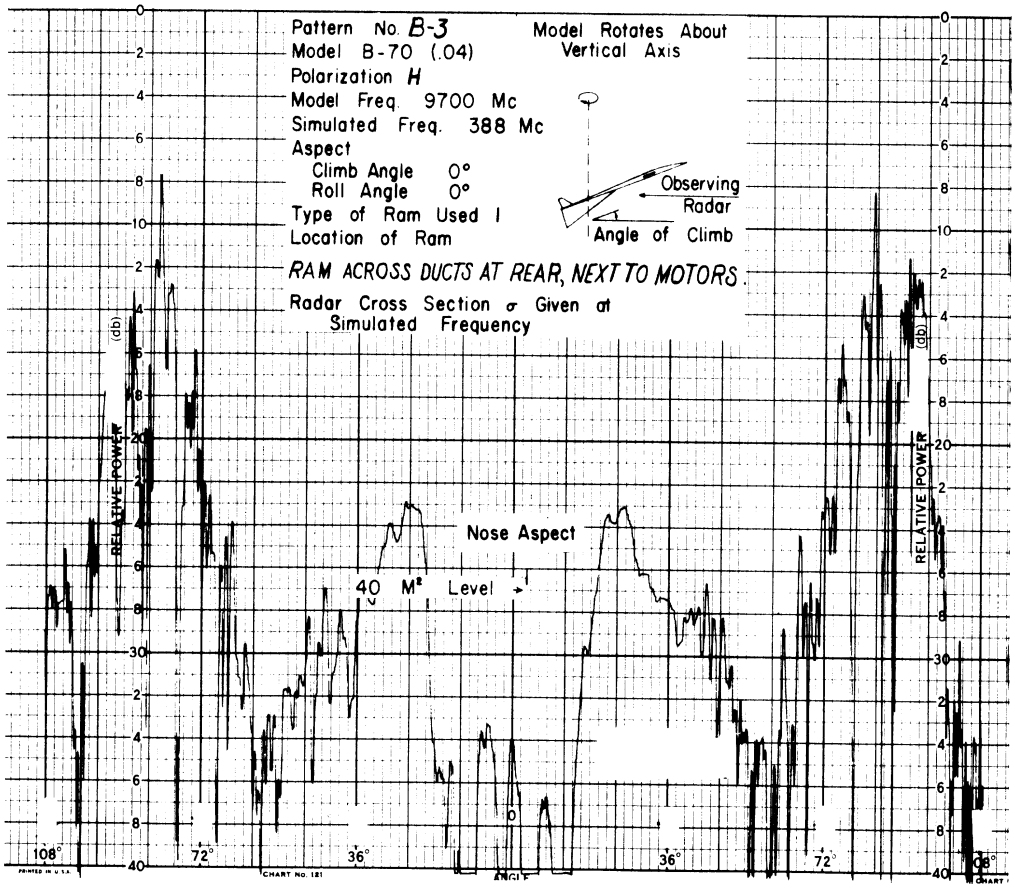
Pattern No. B-3
Model B-70 (.04)
Polarization H
Model Freq. 9700 Mc
Simulated Freq. 388 Mc
Aspect
Climb Angle 0°
Roll Angle 0°
Type of Ram Used I
Location of Ram
RAM ACROSS DUCTS AT REAR, NEXT TO MOTORS
Radar Cross Section σ Given at Simulated Frequency
Model Rotates About Vertical Axis
Observing Radar
Angle of Climb
Nose Aspect
40 M² Level
RELATIVE POWER (db)
108°
72°
36°
0
ANGLE
CHART No. 121

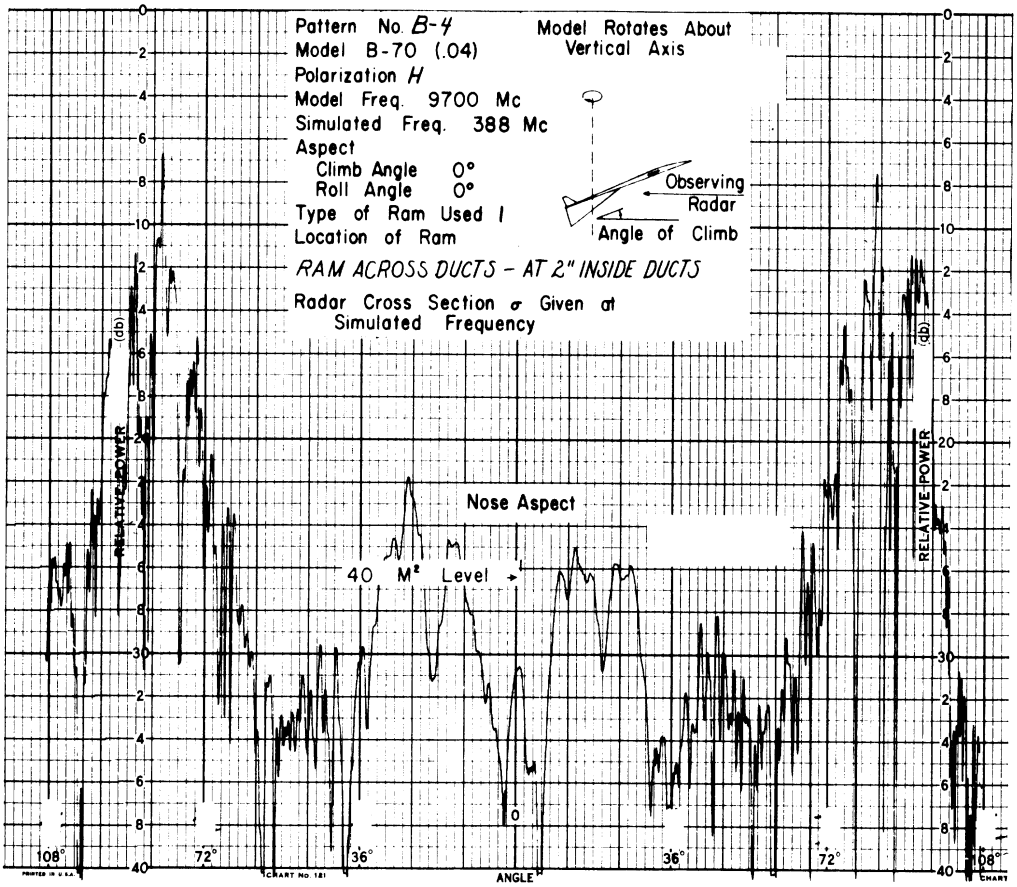
Pattern No. B-4
Model B-70 (.04)
Polarization H
Model Freq. 9700 Mc
Simulated Freq. 388 Mc
Aspect
Climb Angle 0°
Roll Angle 0°
Type of Ram Used I
Location of Ram
RAM ACROSS DUCTS - AT 2" INSIDE DUCTS
Radar Cross Section σ Given at Simulated Frequency
Model Rotates About Vertical Axis
Observing Radar
Angle of Climb
Nose Aspect
40 M² Level
RELATIVE POWER (db)
108°
72°
36°
0
ANGLE
CHART No. 121

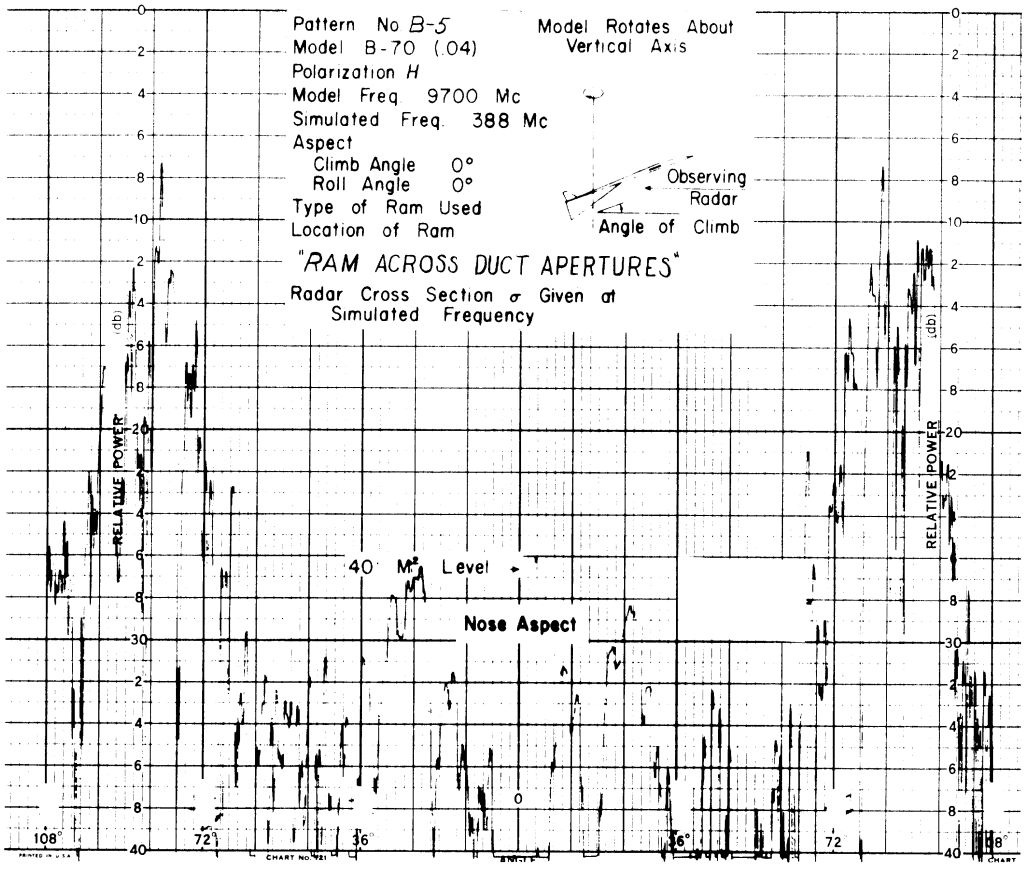
Pattern No B-5
Model B-70 (.04)
Polarization H
Model Freq 9700 Mc
Simulated Freq. 388 Mc
Aspect
Climb Angle 0°
Roll Angle 0°
Type of Ram Used
Location of Ram
"RAM ACROSS DUCT APERTURES"
Radar Cross Section σ Given at Simulated Frequency
Model Rotates About Vertical Axis
Observing Radar
Angle of Climb
RELATIVE POWER (db)
40 M² Level
Nose Aspect
108° 72° 36° 0 36° 72° 108°
CHART NO. 921
ANGLE
CHART

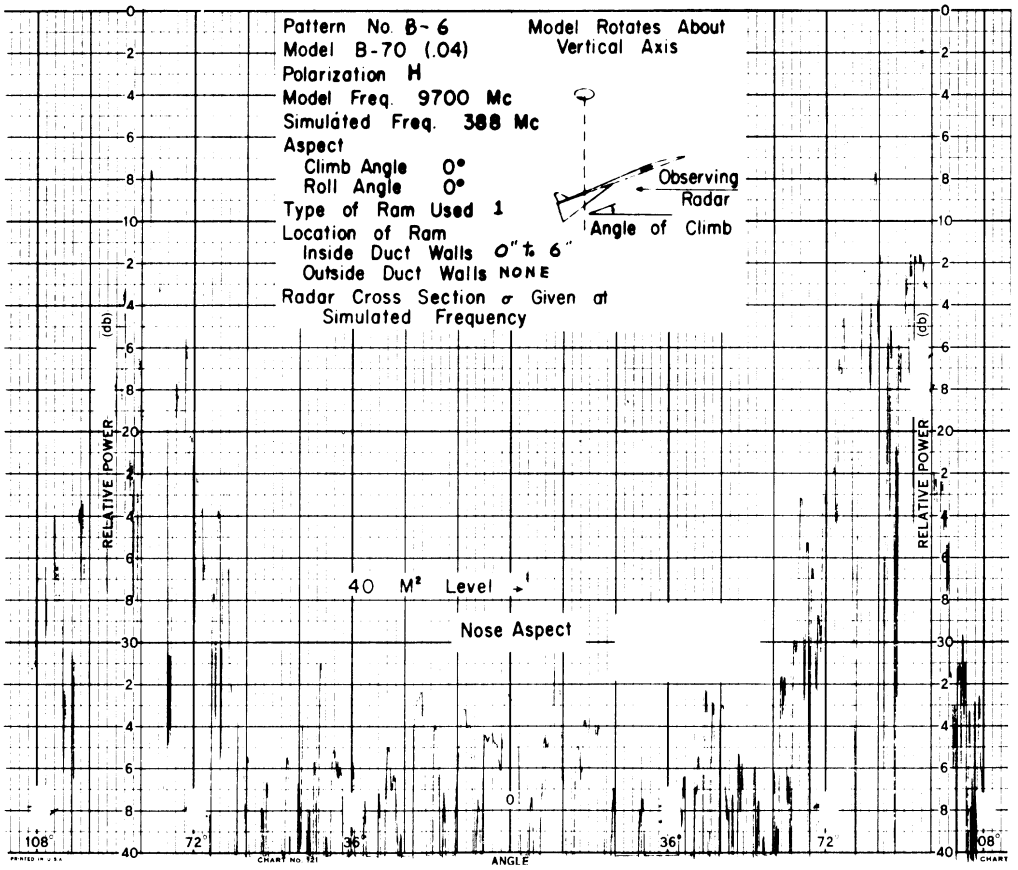
Pattern No. B-6
Model B-70 (.04)
Polarization H
Model Freq. 9700 Mc
Simulated Freq. 388 Mc
Aspect
Climb Angle 0°
Roll Angle 0°
Type of Ram Used 1
Location of Ram
Inside Duct Walls 0" to 6"
Outside Duct Walls NONE
Radar Cross Section σ Given at Simulated Frequency
Model Rotates About Vertical Axis
Observing Radar
Angle of Climb
RELATIVE POWER (db)
40 M² Level
Nose Aspect
108° 72° 36° 0 36° 72° 108°
CHART NO. 921
ANGLE
CHART

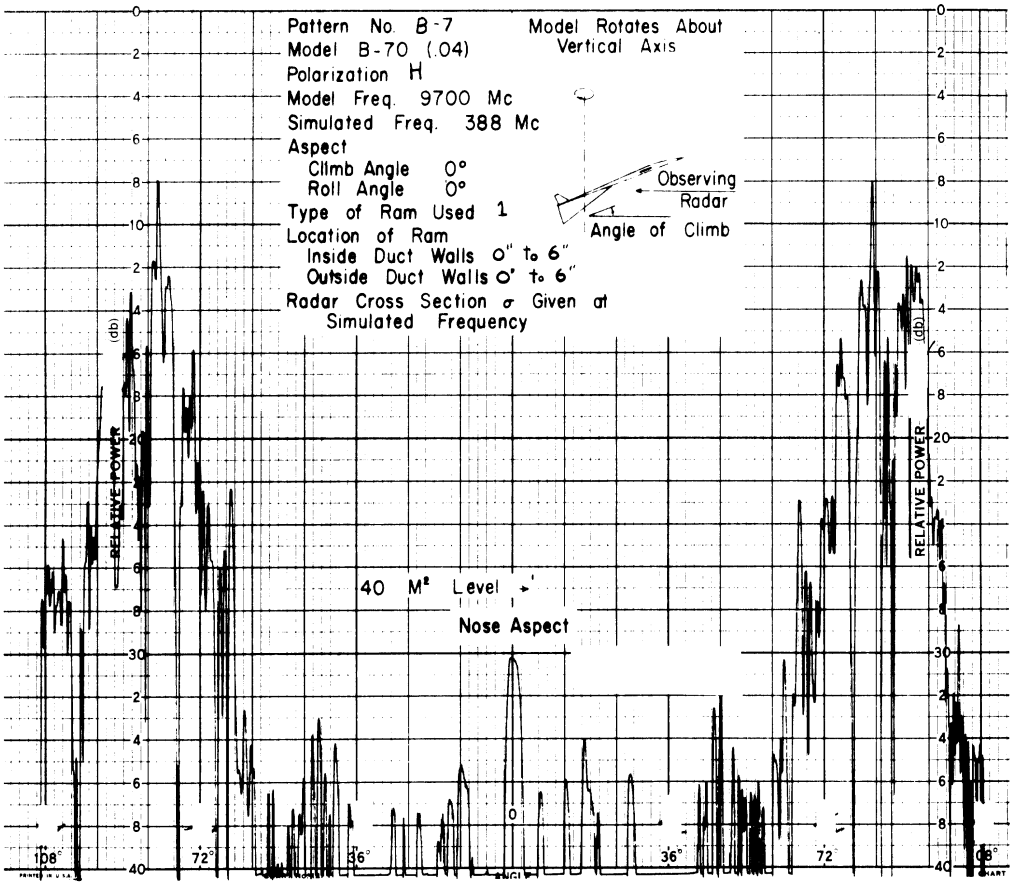
Pattern No. B-7
Model B-70 (.04)
Polarization H
Model Freq. 9700 Mc
Simulated Freq. 388 Mc
Aspect
Climb Angle 0°
Roll Angle 0°
Type of Ram Used 1
Location of Ram
Inside Duct Walls 0" to 6"
Outside Duct Walls 0" to 6"
Radar Cross Section σ Given at
Simulated Frequency
Model Rotates About
Vertical Axis
Observing
Radar
Angle of Climb
RELATIVE POWER (db)
40 M² Level
Nose Aspect
108°
72°
36°
0
36°
72°
108°

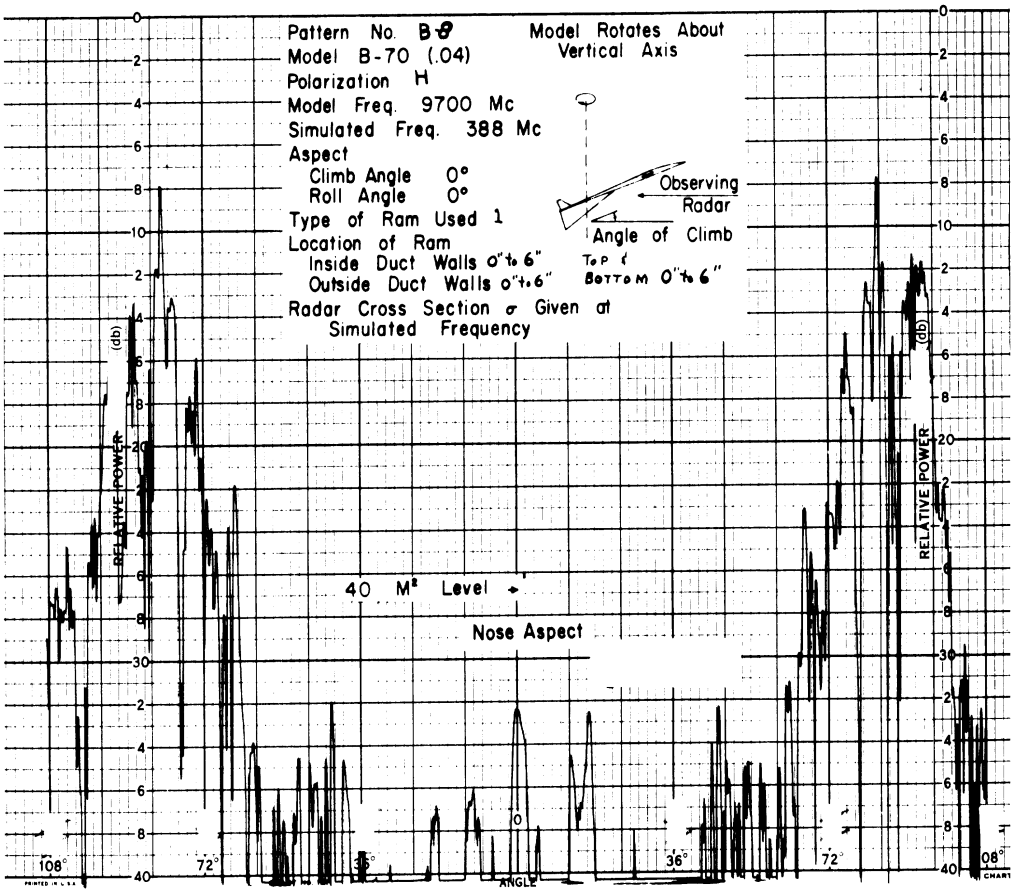
Pattern No. B-8
Model B-70 (.04)
Polarization H
Model Freq. 9700 Mc
Simulated Freq. 388 Mc
Aspect
Climb Angle 0°
Roll Angle 0°
Type of Ram Used 1
Location of Ram
Inside Duct Walls 0" to 6"
Outside Duct Walls 0" to 6"
Top &
Bottom 0" to 6"
Radar Cross Section σ Given at
Simulated Frequency
Model Rotates About
Vertical Axis
Observing
Radar
Angle of Climb
RELATIVE POWER (db)
40 M² Level
Nose Aspect
108°
72°
36°
0
36°
72°
108°
ANGLE

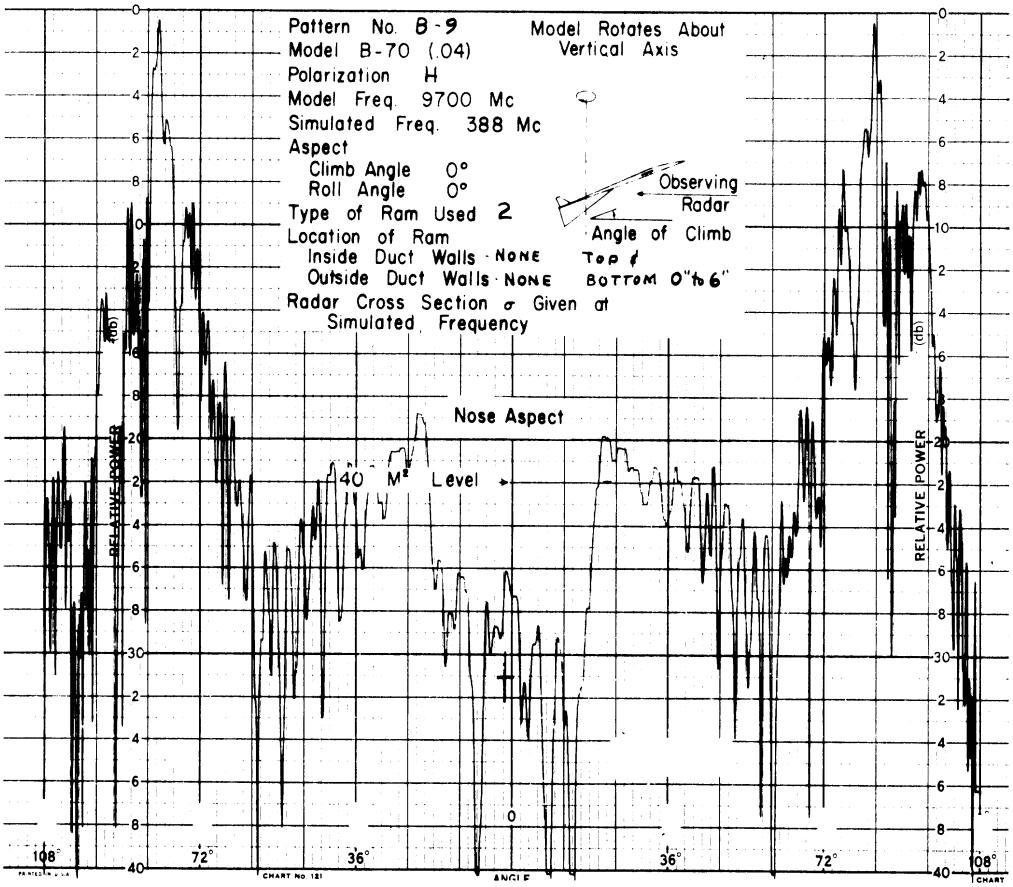
Pattern No. B-9
Model B-70 (.04)
Polarization H
Model Freq. 9700 Mc
Simulated Freq. 388 Mc
Aspect
Climb Angle 0°
Roll Angle 0°
Type of Ram Used 2
Location of Ram
Inside Duct Walls NONE
Outside Duct Walls NONE
Radar Cross Section σ Given at Simulated Frequency
Model Rotates About Vertical Axis
Observing Radar
Angle of Climb
Top 1
Bottom 0" to 6"
Nose Aspect
40 M² Level
RELATIVE POWER (db)
ANGLE
108° 72° 36° 0 36° 72° 108°

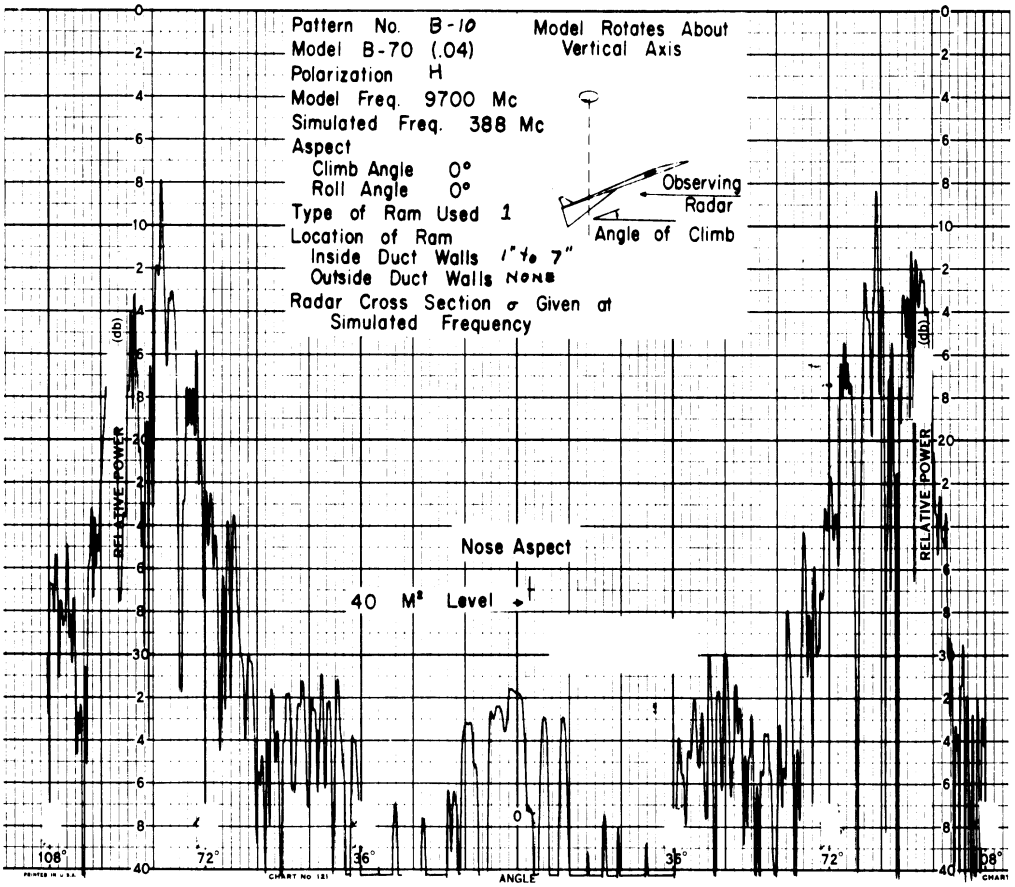
Pattern No. B-10
Model B-70 (.04)
Polarization H
Model Freq. 9700 Mc
Simulated Freq. 388 Mc
Aspect
Climb Angle 0°
Roll Angle 0°
Type of Ram Used 1
Location of Ram
Inside Duct Walls 1" to 7"
Outside Duct Walls NONE
Radar Cross Section σ Given at Simulated Frequency
Model Rotates About Vertical Axis
Observing Radar
Angle of Climb
Nose Aspect
40 M² Level
RELATIVE POWER (db)
ANGLE
108° 72° 36° 0 36° 72° 108°

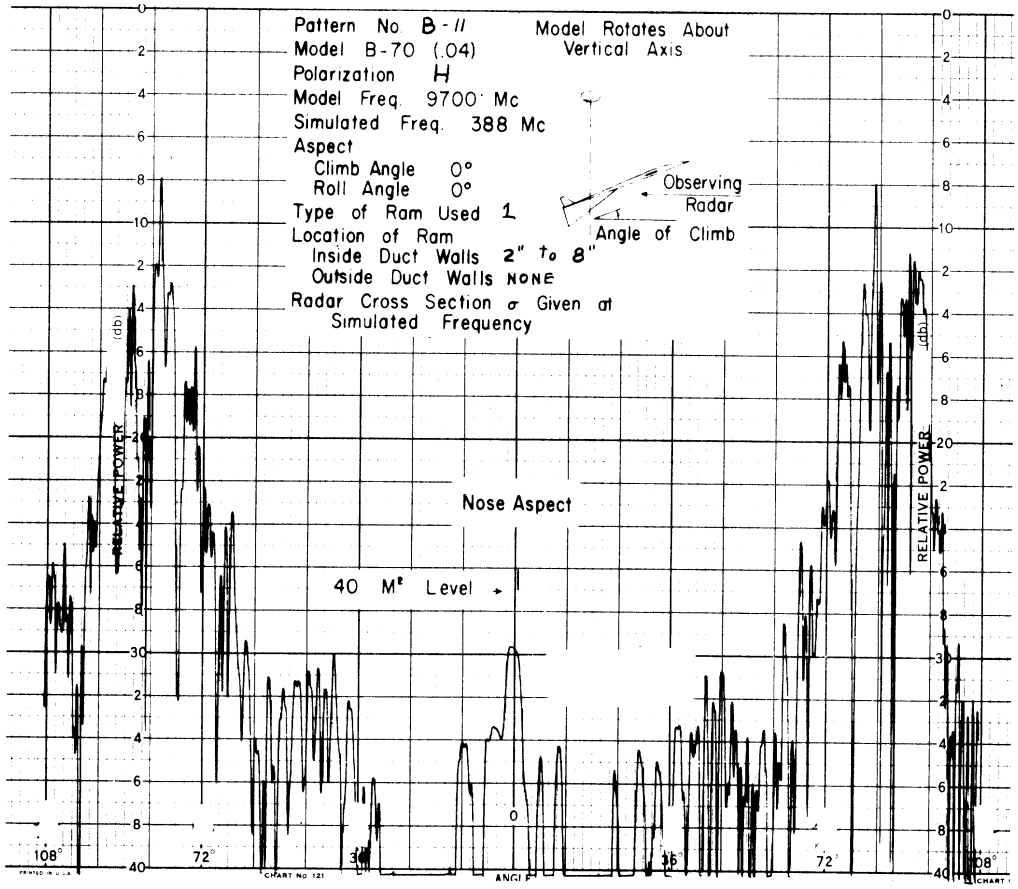
Pattern No. B-11
Model B-70 (.04)
Polarization H
Model Freq. 9700 Mc
Simulated Freq. 388 Mc
Aspect
Climb Angle 0°
Roll Angle 0°
Type of Ram Used 1
Location of Ram
Inside Duct Walls 2" to 8"
Outside Duct Walls NONE
Radar Cross Section σ Given at
Simulated Frequency
Model Rotates About
Vertical Axis
Observing
Radar
Angle of Climb
Nose Aspect
40 M² Level
RELATIVE POWER (db)
108°
72°
36°
0
36°
72°
108°
ANGLE

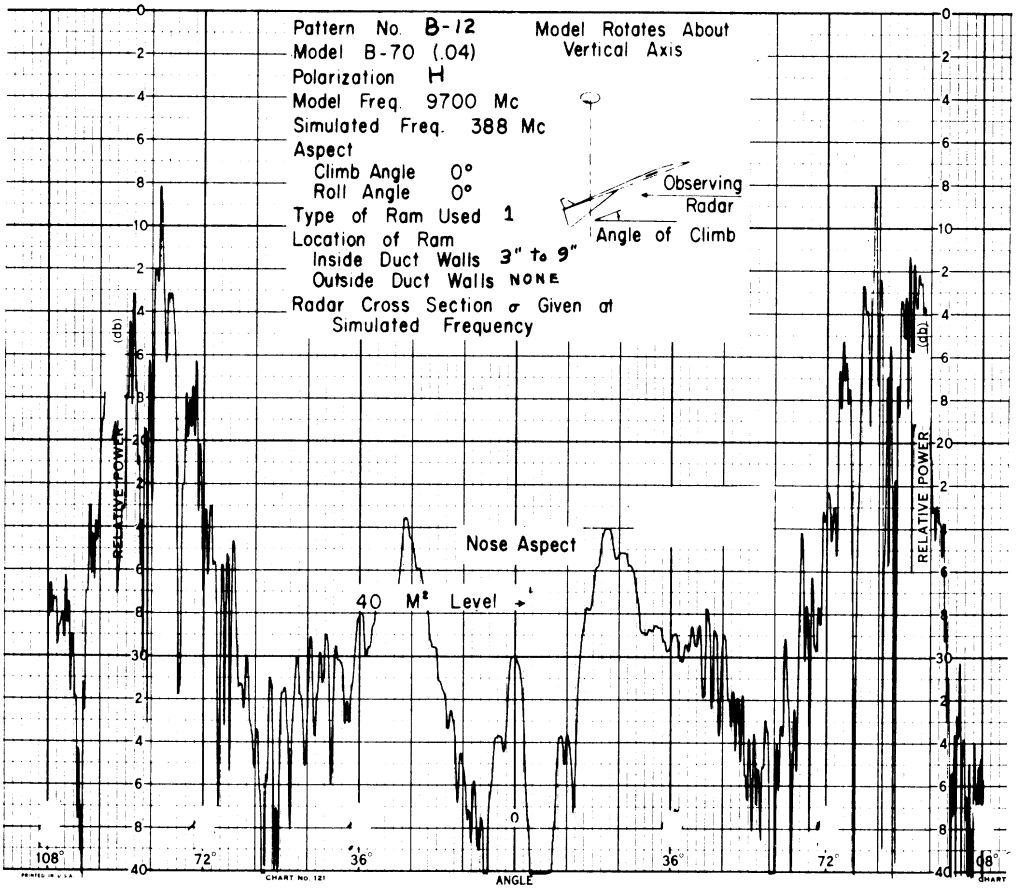
Pattern No. B-12
Model B-70 (.04)
Polarization H
Model Freq. 9700 Mc
Simulated Freq. 388 Mc
Aspect
Climb Angle 0°
Roll Angle 0°
Type of Ram Used 1
Location of Ram
Inside Duct Walls 3" to 9"
Outside Duct Walls NONE
Radar Cross Section σ Given at
Simulated Frequency
Model Rotates About
Vertical Axis
Observing
Radar
Angle of Climb
Nose Aspect
40 M² Level
RELATIVE POWER (db)
108°
72°
36°
0
36°
72°
108°
ANGLE

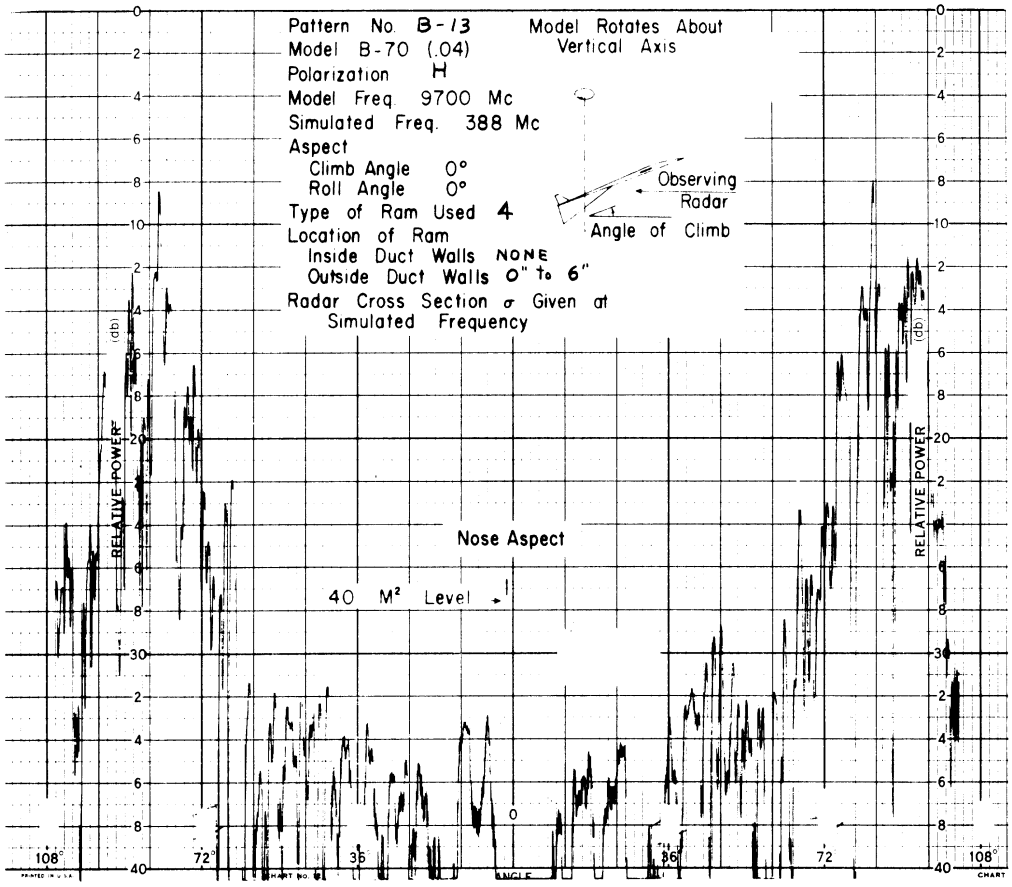
Pattern No. B-13
Model B-70 (.04)
Polarization H
Model Freq. 9700 Mc
Simulated Freq. 388 Mc
Aspect
Climb Angle 0°
Roll Angle 0°
Type of Ram Used 4
Location of Ram
Inside Duct Walls NONE
Outside Duct Walls 0" to 6"
Radar Cross Section σ Given at
Simulated Frequency
Model Rotates About
Vertical Axis
Observing
Radar
Angle of Climb
RELATIVE POWER (db)
Nose Aspect
40 M² Level
108° 72° 36° 0 36° 72° 108°
ANGLE

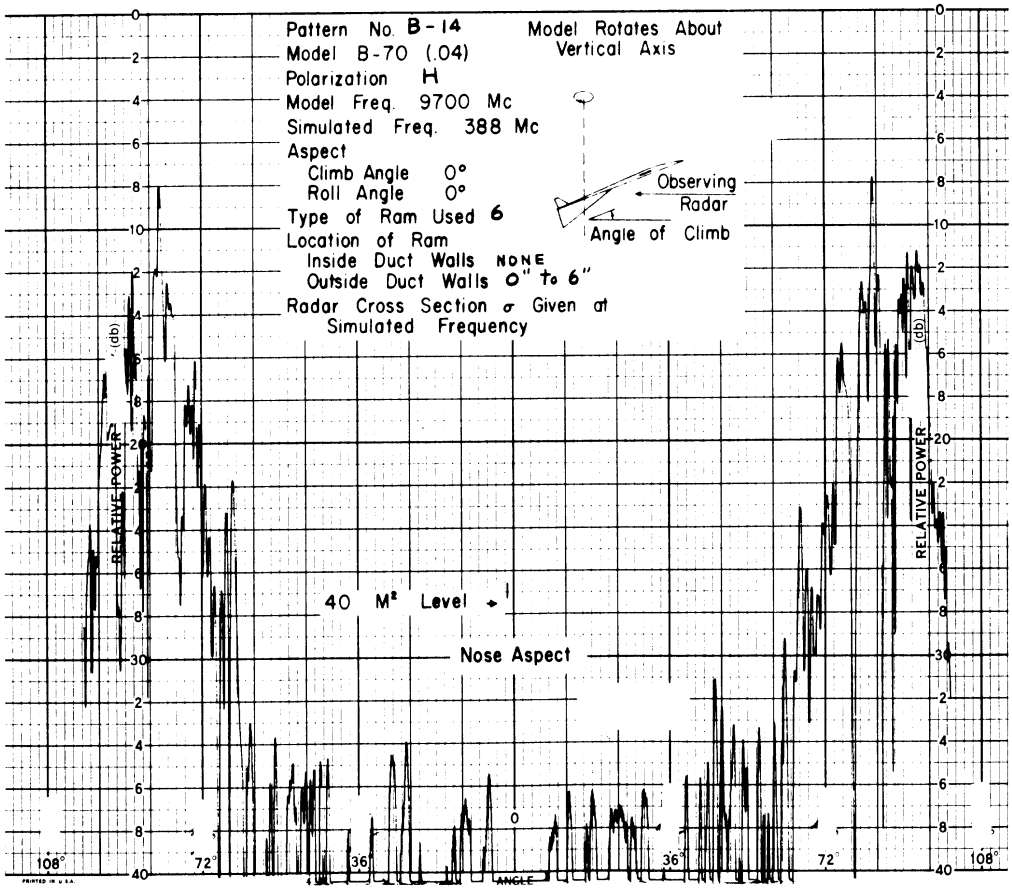
Pattern No. B-14
Model B-70 (.04)
Polarization H
Model Freq. 9700 Mc
Simulated Freq. 388 Mc
Aspect
Climb Angle 0°
Roll Angle 0°
Type of Ram Used 6
Location of Ram
Inside Duct Walls NONE
Outside Duct Walls 0" to 6"
Radar Cross Section σ Given at
Simulated Frequency
Model Rotates About
Vertical Axis
Observing
Radar
Angle of Climb
RELATIVE POWER (db)
40 M² Level
Nose Aspect
108° 72° 36° 0 36° 72° 108°
ANGLE

4.3.3. Series C: Vertical Polarization, Magnetic RAM, 388 Mc

This group is comparable to the A group in that the frequency (X band) and the polarization (vertical) are the same. In group A, however, the RAM was a well-matched commercial absorber with dielectric loss, but in the Series C patterns an absorber of type 5 with magnetic loss was employed and, in addition, no effort was made to achieve a good match. The intent was to have a magnetic absorber with nominal loss that might more nearly match the properties of a ferrite RAM on the full-scale aircraft. The measured reflectivity at the X-band frequency was -4 db.

In this series, a particular effort was made to check the effectiveness of the three locations for RAM inserts which were most acceptable to NAA on the basis of aerodynamic considerations. The station numbers for these locations in order of preference are given below, with the approximate dimensions in inches appropriate to the 0.04 model (see Figure 35 for an explanation of the notation). For the outer wall a 4", rather than a 3.75", piece was used for the second and third NAA locations.

Location	Station Numbers		Position on .04 Model	
	Inner Wall	Outer Wall	Inner Wall	Outer Wall
1	none	1275 to 1325	none	2.5" to 4.5"
2	none	1230 to 1325	none	.75" to 4.5"
3	1276 to 1321	1230 to 1325	2.5" to 4.5"	.75" to 4.5"

Patterns C-1, C-2 and C-3 show results for the three NAA locations described above. It is seen that little benefit is obtained from the 2.5" to 4.5" location on the outer wall; that .75" to 4.75" is better, and that the addition of a strip on the inner wall 2.5" back was not very effective. Pattern C-4 shows the importance of having RAM on the first 2" of the inner duct wall. This fact was demonstrated many times. In Patterns C-5 through C-10 RAM is used from .75" to 4.75" on the outer wall, and the effectiveness of adding RAM on the inner duct wall, forward to the duct aperture as well as inside the duct, is shown. As may be seen, there are several combinations that lower the cross section to 40 m^2. A 2" strip is sufficient if properly located as shown in Pattern C-7.

In Patterns C-11 to C-13 the 10^o climb angle is studied. It is again demonstrated that it is easier to achieve the desired 40 m^2 level at a 10^o climb angle than at the 0^o elevation aspect. The RAM locations used in these three patterns are the three NAA preferred locations.

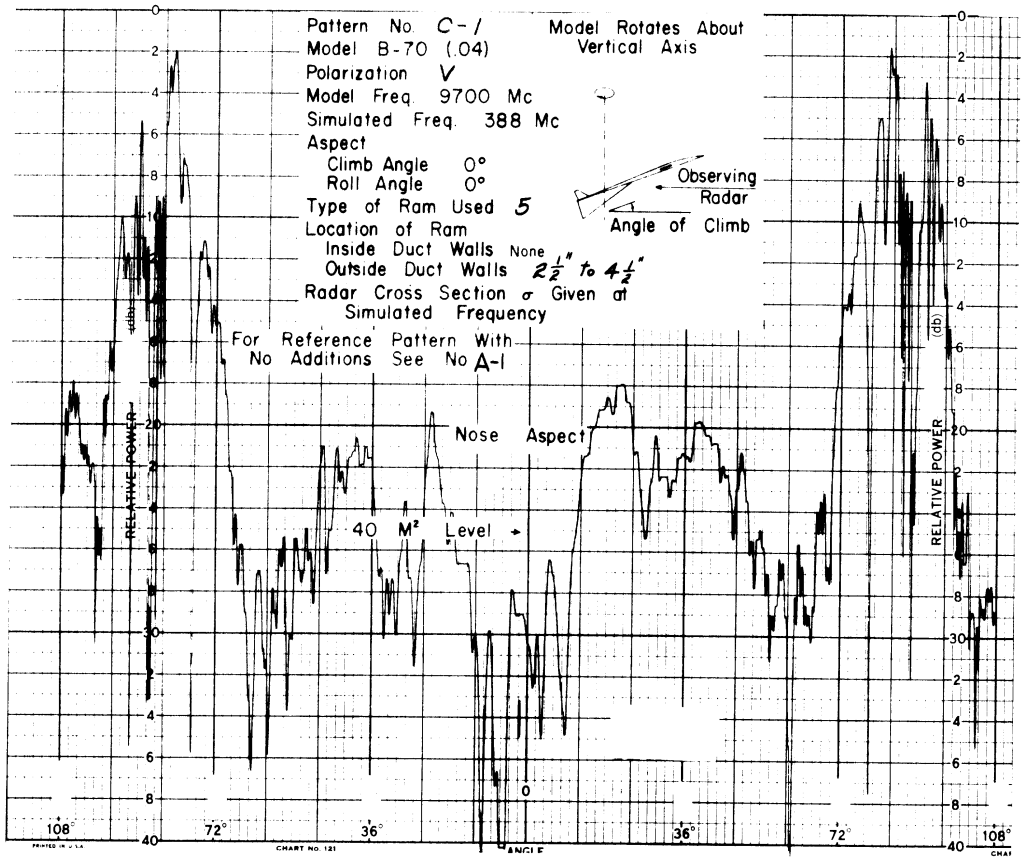
Pattern No. C-1
Model B-70 (.04)
Polarization V
Model Freq. 9700 Mc
Simulated Freq. 388 Mc
Aspect
Climb Angle 0°
Roll Angle 0°
Type of Ram Used 5
Location of Ram
Inside Duct Walls None
Outside Duct Walls 2½" to 4½"
Radar Cross Section σ Given at Simulated Frequency
For Reference Pattern With No Additions See No A-1
Model Rotates About Vertical Axis
Observing Radar
Angle of Climb
Nose Aspect
40 M² Level
RELATIVE POWER (db)
ANGLE
108° 72° 36° 0 36° 72° 108°

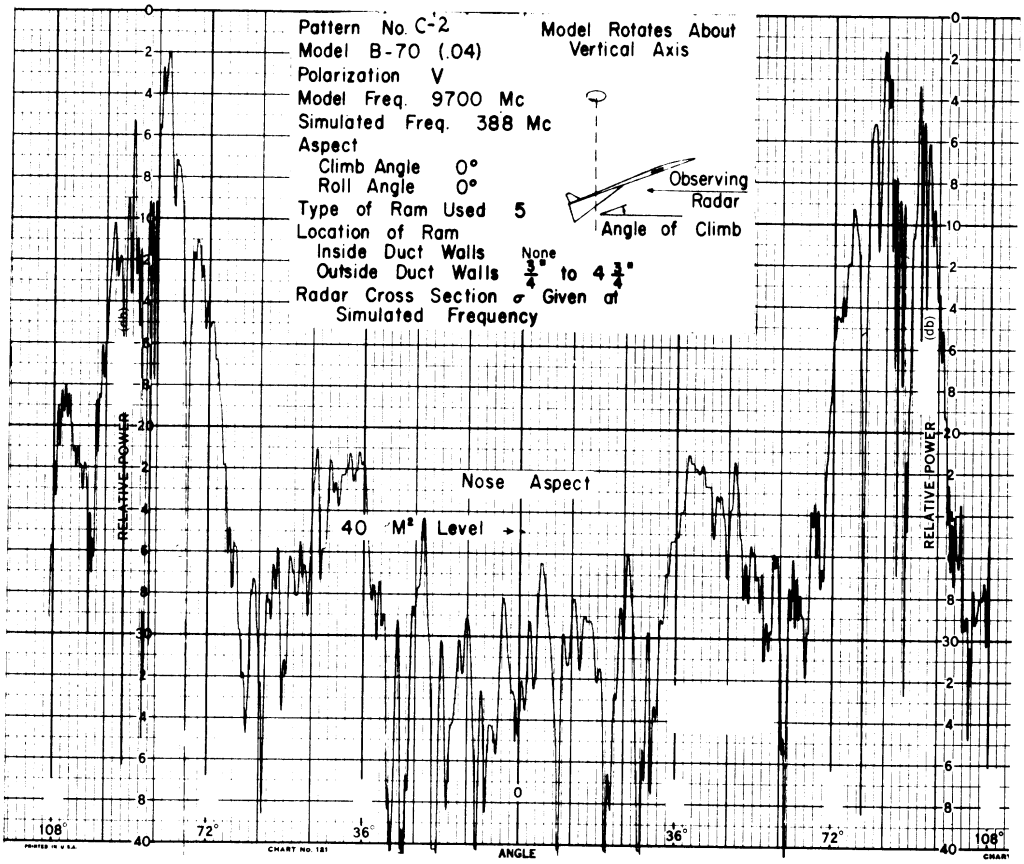
Pattern No. C-2
Model B-70 (.04)
Polarization V
Model Freq. 9700 Mc
Simulated Freq. 388 Mc
Aspect
Climb Angle 0°
Roll Angle 0°
Type of Ram Used 5
Location of Ram
Inside Duct Walls None
Outside Duct Walls ¾" to 4¾"
Radar Cross Section σ Given at Simulated Frequency
Model Rotates About Vertical Axis
Observing Radar
Angle of Climb
Nose Aspect
40 M² Level
RELATIVE POWER (db)
ANGLE
108° 72° 36° 0 36° 72° 108°

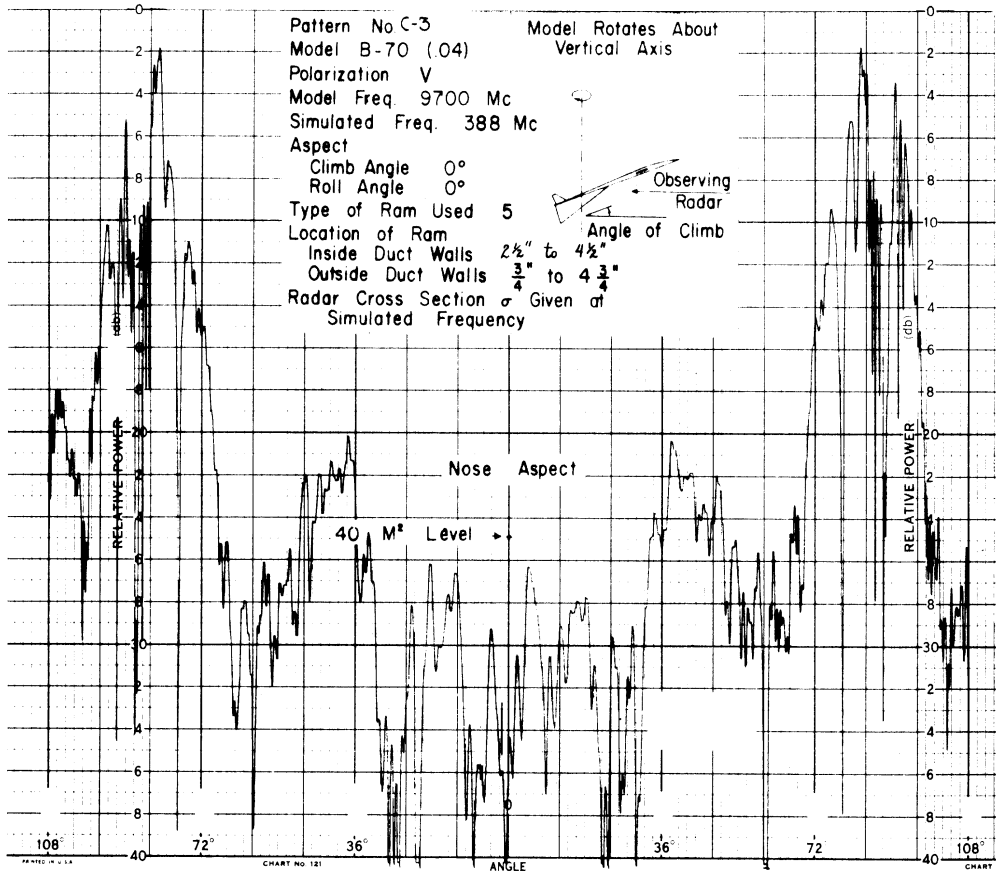
Pattern No C-3
Model B-70 (.04)
Polarization V
Model Freq. 9700 Mc
Simulated Freq. 388 Mc
Aspect
Climb Angle 0°
Roll Angle 0°
Type of Ram Used 5
Location of Ram
Inside Duct Walls 2½" to 4½"
Outside Duct Walls ¾" to 4¾"
Radar Cross Section σ Given at
Simulated Frequency
Model Rotates About
Vertical Axis
Observing
Radar
Angle of Climb
Nose Aspect
40 M² Level
RELATIVE POWER (db)
108° 72° 36° 0 36° 72° 108°
ANGLE
CHART NO. 121

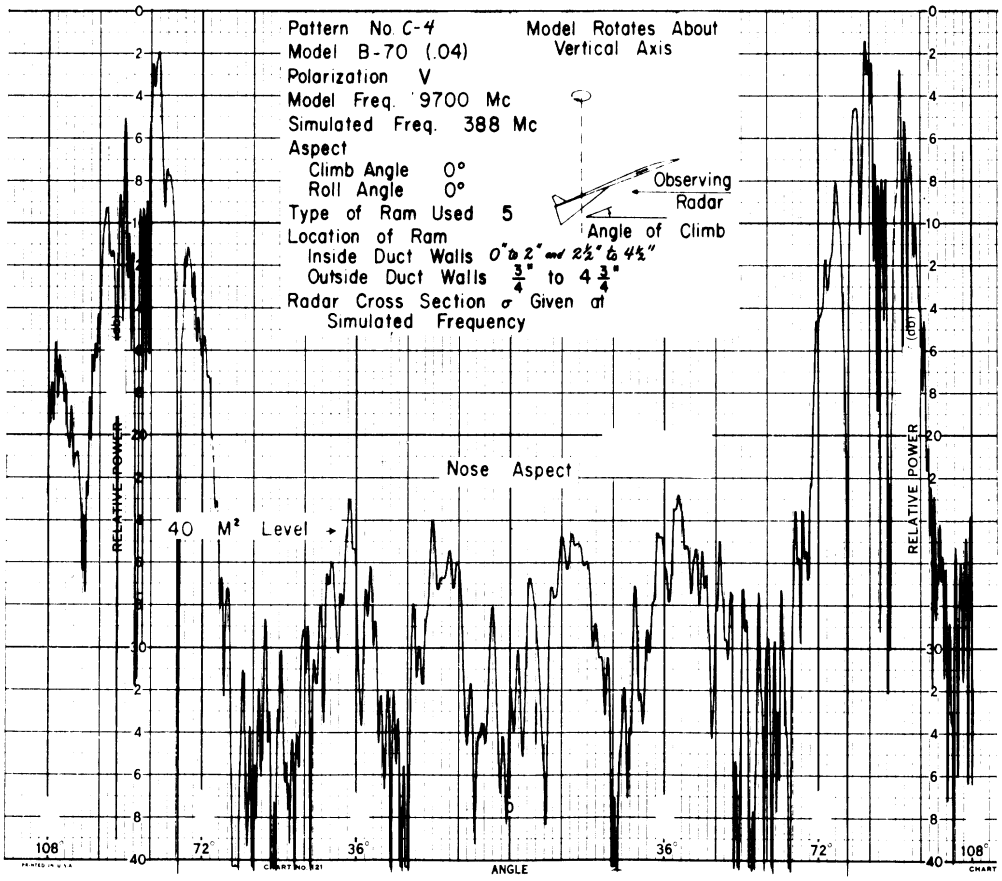
Pattern No C-4
Model B-70 (.04)
Polarization V
Model Freq. 9700 Mc
Simulated Freq. 388 Mc
Aspect
Climb Angle 0°
Roll Angle 0°
Type of Ram Used 5
Location of Ram
Inside Duct Walls 0" to 2" and 2½" to 4½"
Outside Duct Walls ¾" to 4¾"
Radar Cross Section σ Given at
Simulated Frequency
Model Rotates About
Vertical Axis
Observing
Radar
Angle of Climb
Nose Aspect
40 M² Level
RELATIVE POWER (db)
108° 72° 36° 0 36° 72° 108°
ANGLE

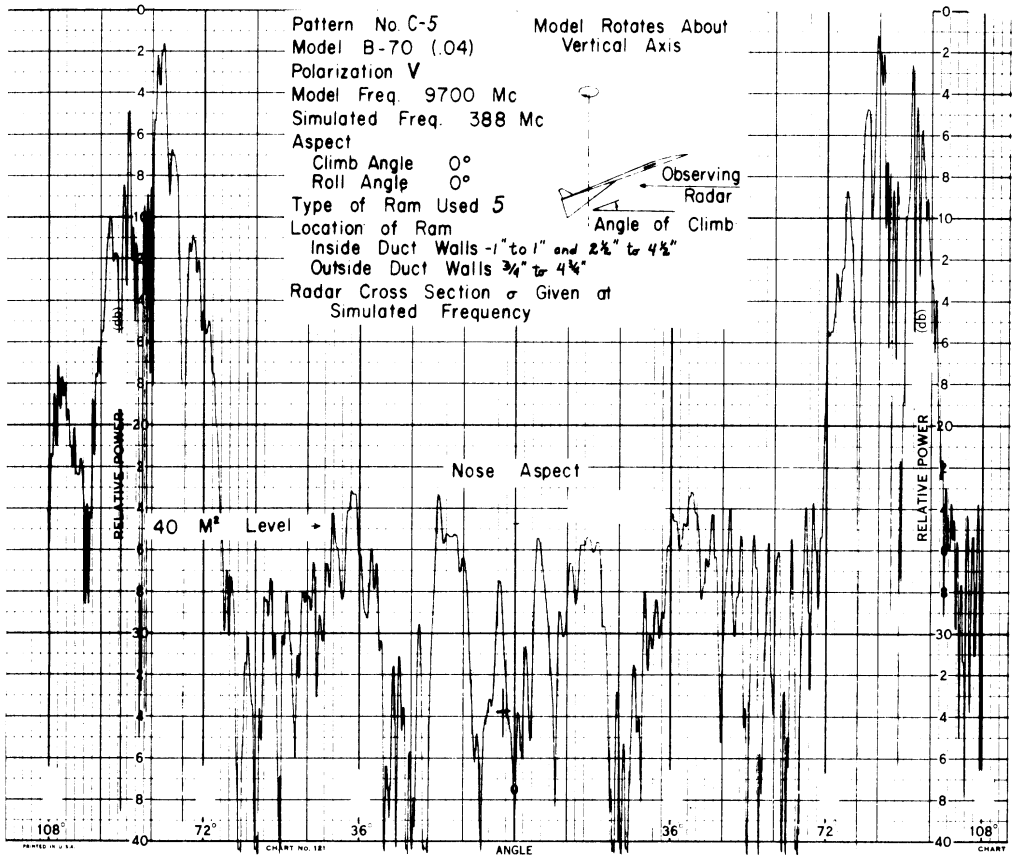
Pattern No. C-5
Model B-70 (.04)
Polarization V
Model Freq. 9700 Mc
Simulated Freq. 388 Mc
Aspect
Climb Angle 0°
Roll Angle 0°
Type of Ram Used 5
Location of Ram
Inside Duct Walls -1" to 1" and 2¾" to 4½"
Outside Duct Walls ¾" to 4¾"
Radar Cross Section σ Given at Simulated Frequency
Model Rotates About Vertical Axis
Observing Radar
Angle of Climb
Nose Aspect
40 M² Level
RELATIVE POWER (db)
ANGLE
108° 72° 36° 36° 72° 108°

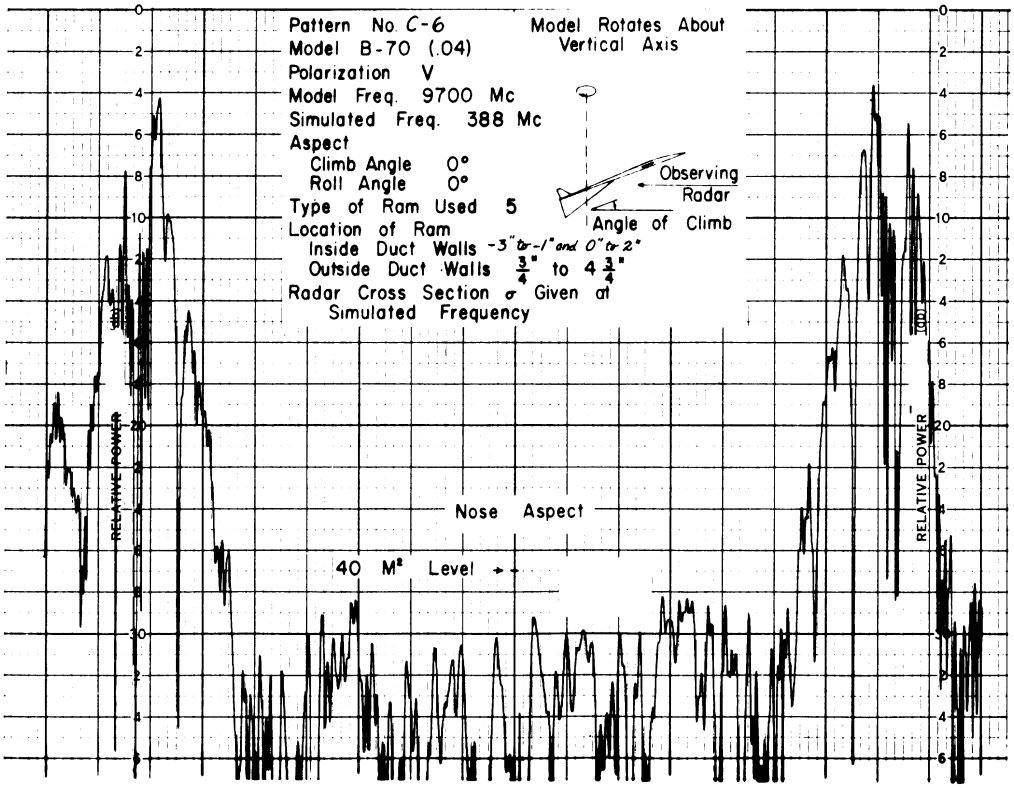
Pattern No. C-6
Model B-70 (.04)
Polarization V
Model Freq. 9700 Mc
Simulated Freq. 388 Mc
Aspect
Climb Angle 0°
Roll Angle 0°
Type of Ram Used 5
Location of Ram
Inside Duct Walls -3" to -1" and 0" to 2"
Outside Duct Walls ¾" to 4¾"
Radar Cross Section σ Given at Simulated Frequency
Model Rotates About Vertical Axis
Observing Radar
Angle of Climb
Nose Aspect
40 M² Level
RELATIVE POWER (db)

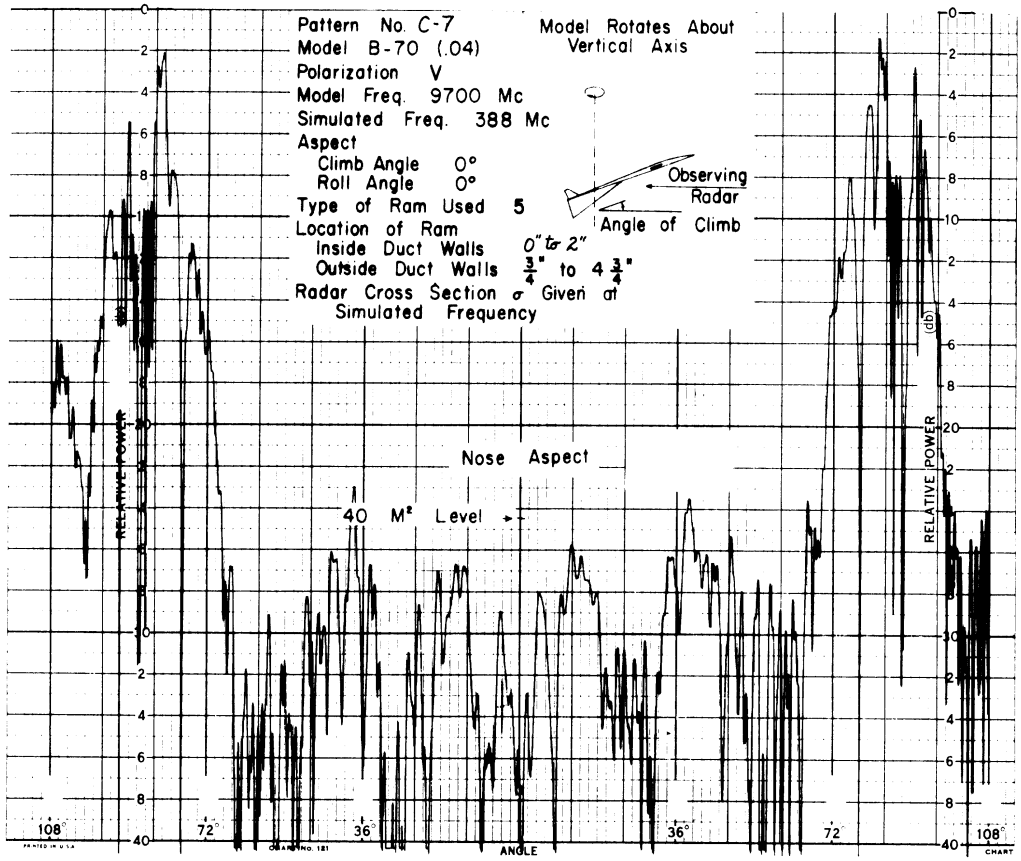
Pattern No. C-7
Model B-70 (.04)
Polarization V
Model Freq. 9700 Mc
Simulated Freq. 388 Mc
Aspect
Climb Angle 0°
Roll Angle 0°
Type of Ram Used 5
Location of Ram
Inside Duct Walls 0" to 2"
Outside Duct Walls ¾" to 4¾"
Radar Cross Section σ Given at
Simulated Frequency
Model Rotates About
Vertical Axis
Observing
Radar
Angle of Climb
Nose Aspect
40 M² Level
RELATIVE POWER
(db)
108°
72°
36°
ANGLE
CHART No. 121

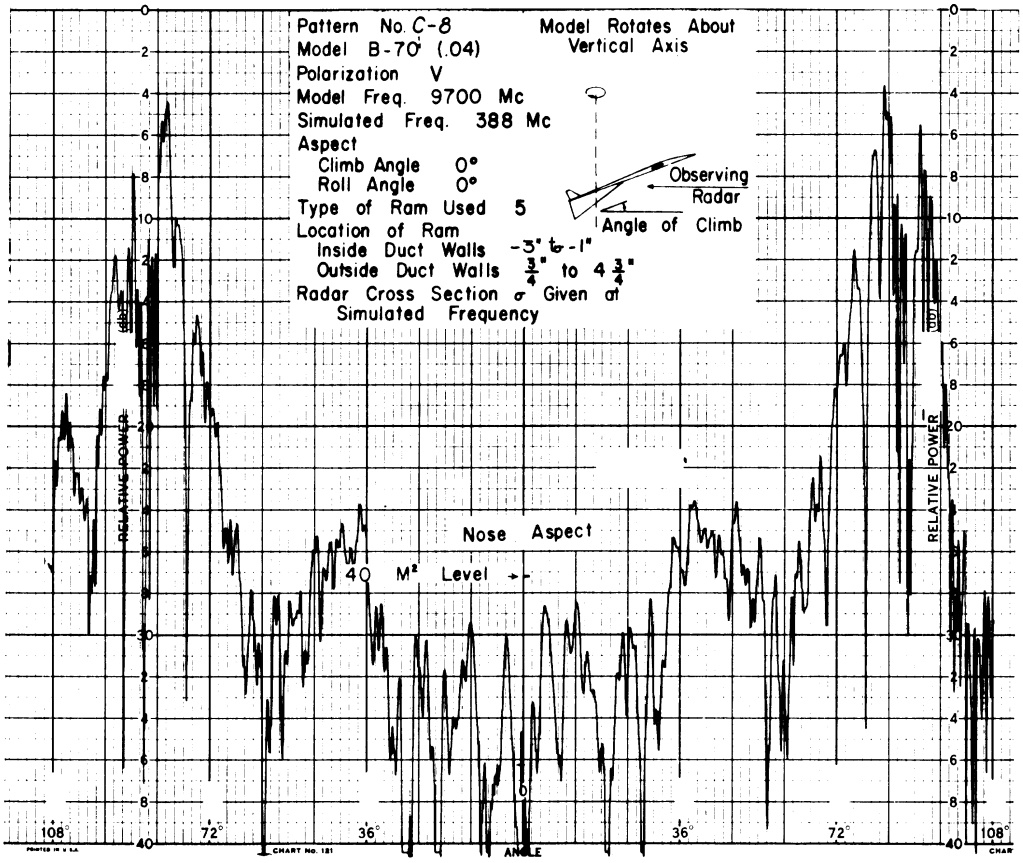
Pattern No. C-8
Model B-70 (.04)
Polarization V
Model Freq. 9700 Mc
Simulated Freq. 388 Mc
Aspect
Climb Angle 0°
Roll Angle 0°
Type of Ram Used 5
Location of Ram
Inside Duct Walls -3" to -1"
Outside Duct Walls ¾" to 4¾"
Radar Cross Section σ Given at
Simulated Frequency
Model Rotates About
Vertical Axis
Observing
Radar
Angle of Climb
Nose Aspect
40 M² Level
RELATIVE POWER
(db)
108°
72°
36°
ANGLE
CHART No. 121

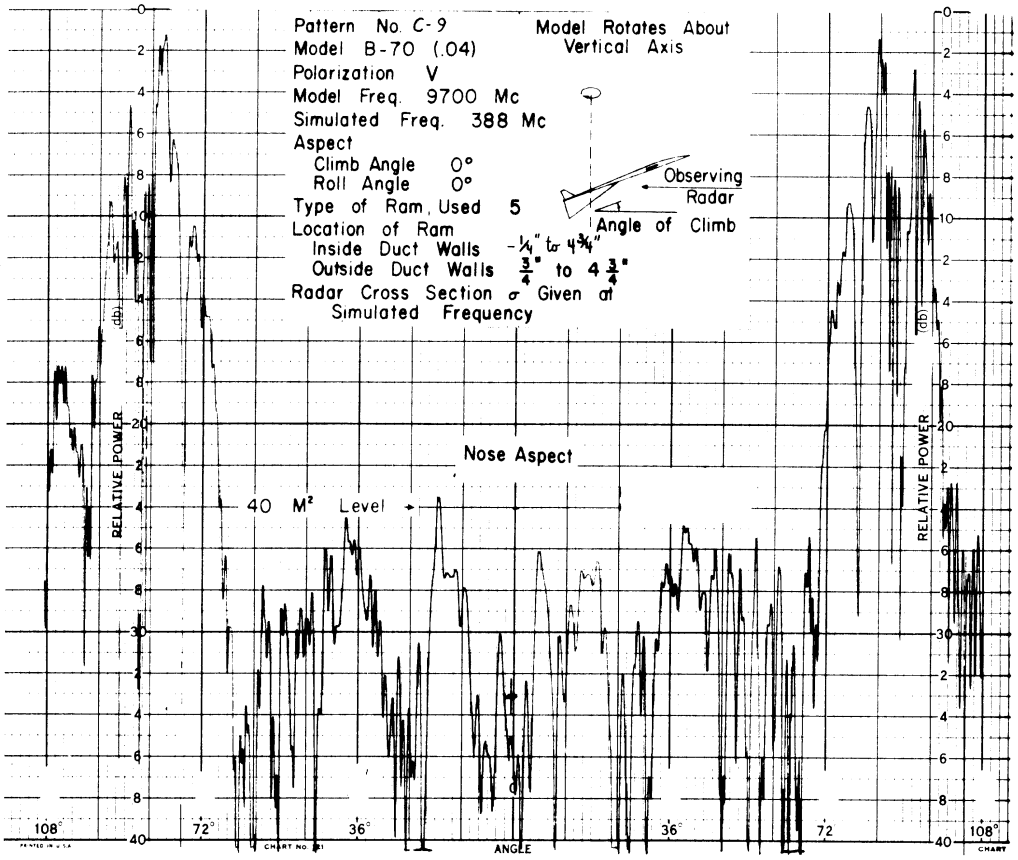
Pattern No. C-9
Model B-70 (.04)
Polarization V
Model Freq. 9700 Mc
Simulated Freq. 388 Mc
Aspect
Climb Angle 0°
Roll Angle 0°
Type of Ram, Used 5
Location of Ram
Inside Duct Walls -¼" to 4¾"
Outside Duct Walls ¾" to 4¾"
Radar Cross Section σ Given at
Simulated Frequency
Model Rotates About
Vertical Axis
Observing
Radar
Angle of Climb
Nose Aspect
40 M² Level
RELATIVE POWER
(db)
108°
72°
36°
ANGLE
36°
72°
108°

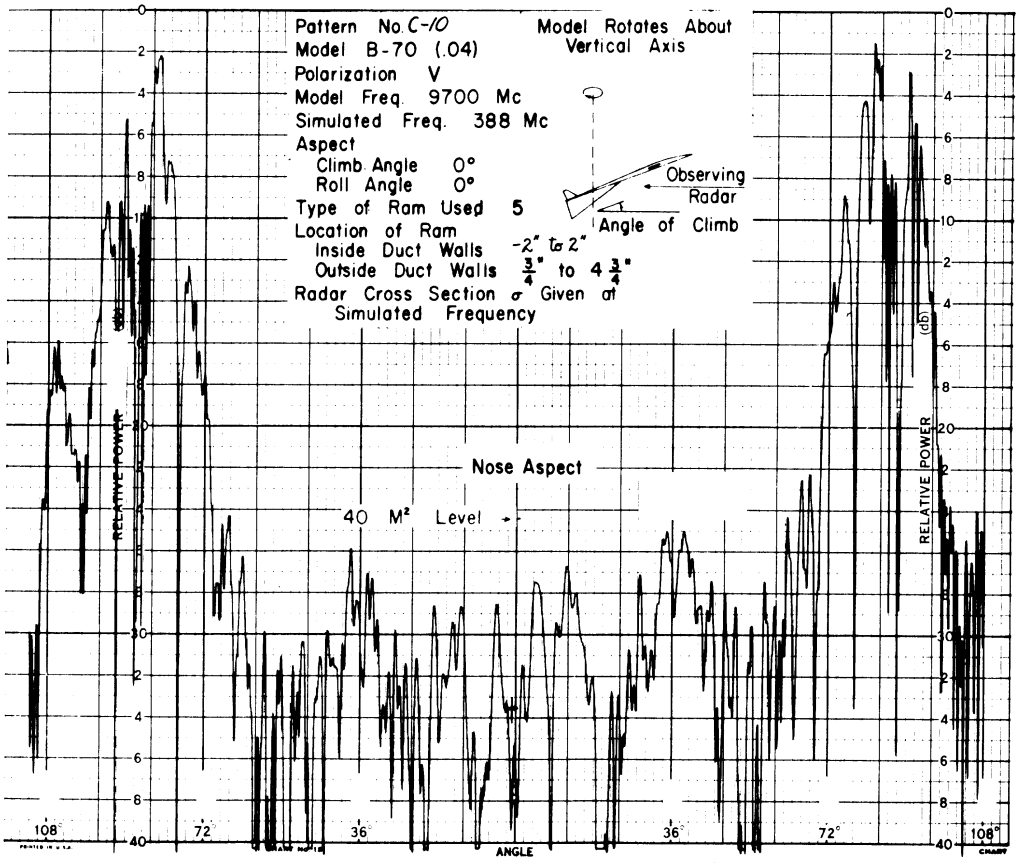
Pattern No. C-10
Model B-70 (.04)
Polarization V
Model Freq. 9700 Mc
Simulated Freq. 388 Mc
Aspect
Climb Angle 0°
Roll Angle 0°
Type of Ram Used 5
Location of Ram
Inside Duct Walls -2" to 2"
Outside Duct Walls ¾" to 4¾"
Radar Cross Section σ Given at
Simulated Frequency
Model Rotates About
Vertical Axis
Observing
Radar
Angle of Climb
Nose Aspect
40 M² Level
RELATIVE POWER
(db)
108°
72°
36°
ANGLE
36°
72°
108°

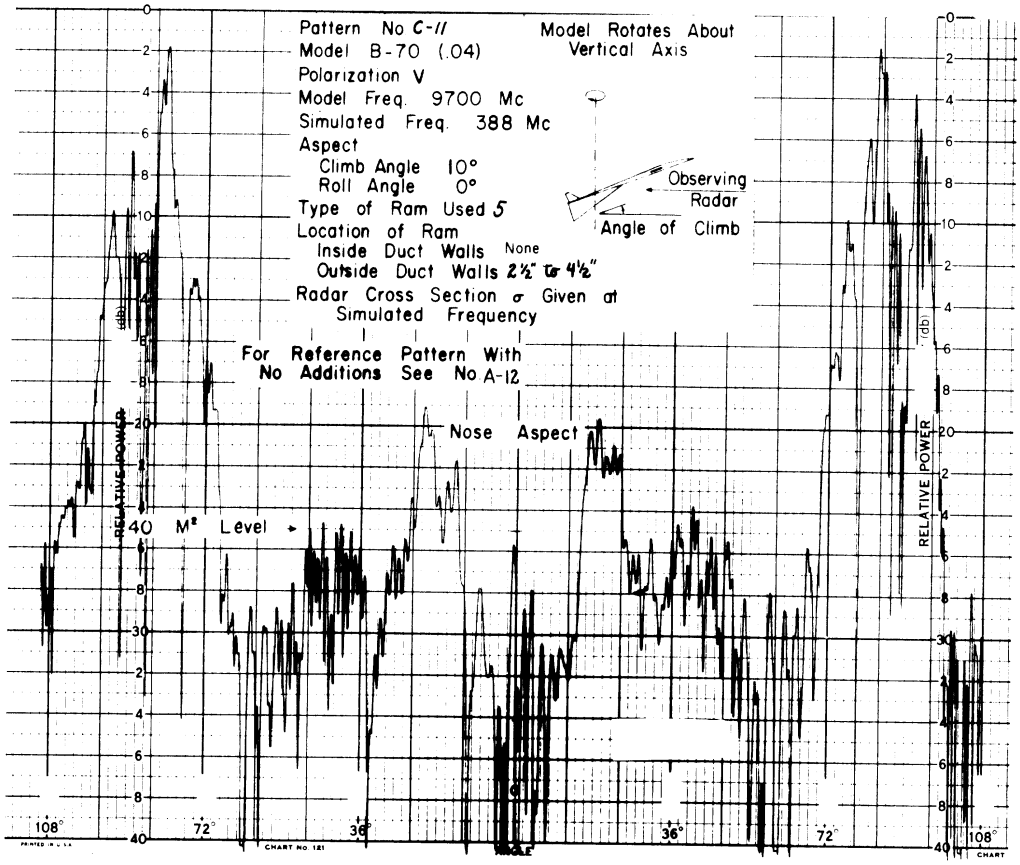
Pattern No C-11
Model B-70 (.04)
Polarization V
Model Freq. 9700 Mc
Simulated Freq. 388 Mc
Aspect
Climb Angle 10°
Roll Angle 0°
Type of Ram Used 5
Location of Ram
Inside Duct Walls None
Outside Duct Walls 2½" to 4½"
Radar Cross Section σ Given at Simulated Frequency
For Reference Pattern With No Additions See No A-12
Model Rotates About Vertical Axis
Observing Radar
Angle of Climb
Nose Aspect
40 M² Level
RELATIVE POWER
(db)
108°
72°
36°
CHART NO. 121
ANGLE
CHART

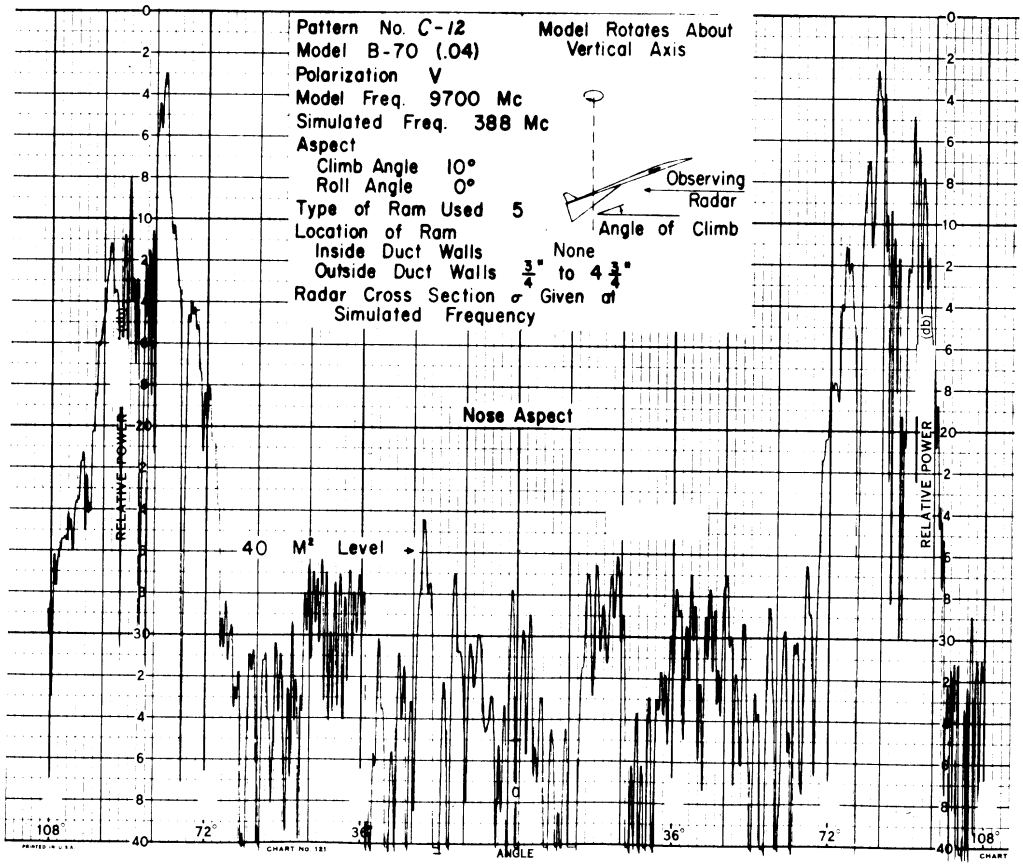
Pattern No. C-12
Model B-70 (.04)
Polarization V
Model Freq. 9700 Mc
Simulated Freq. 388 Mc
Aspect
Climb Angle 10°
Roll Angle 0°
Type of Ram Used 5
Location of Ram
Inside Duct Walls None
Outside Duct Walls ¾" to 4¾"
Radar Cross Section σ Given at Simulated Frequency
Model Rotates About Vertical Axis
Observing Radar
Angle of Climb
Nose Aspect
40 M² Level
RELATIVE POWER
(db)
108°
72°
36°
CHART NO. 121
ANGLE
CHART

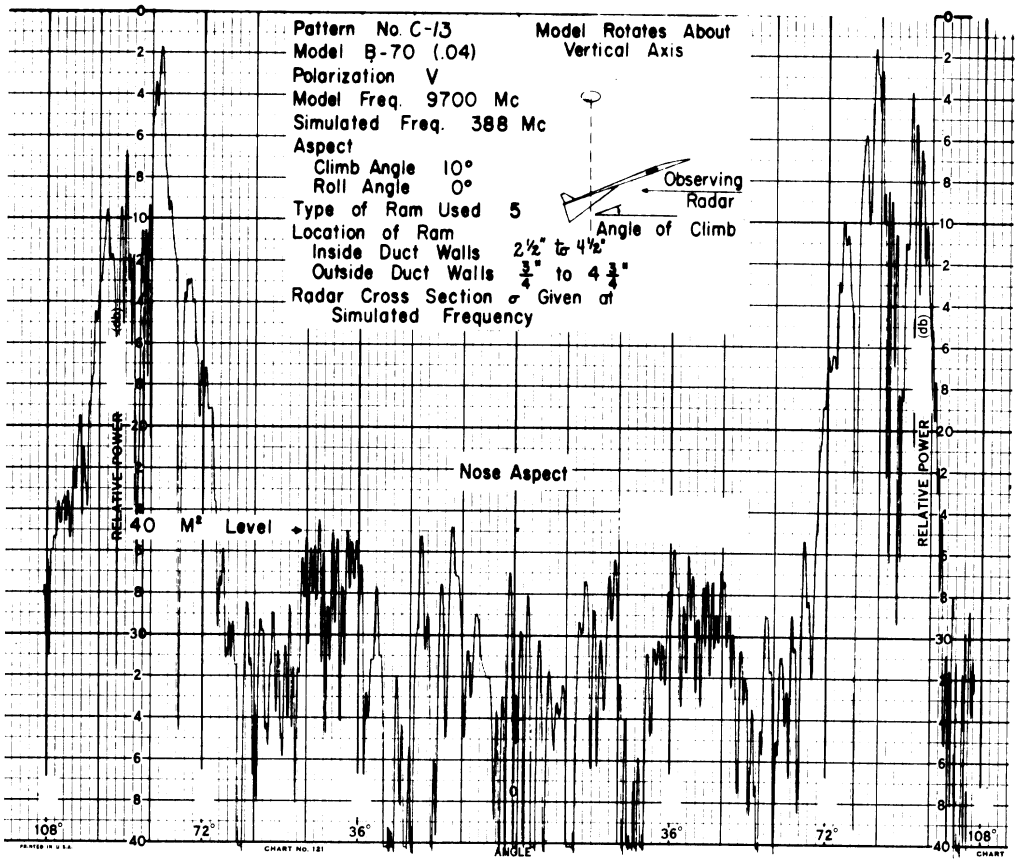
Pattern No. C-13
Model B-70 (.04)
Polarization V
Model Freq. 9700 Mc
Simulated Freq. 388 Mc
Aspect
Climb Angle 10°
Roll Angle 0°
Type of Ram Used 5
Location of Ram
Inside Duct Walls 2½" to 4½"
Outside Duct Walls ¾" to 4¾"
Radar Cross Section σ Given at Simulated Frequency
Model Rotates About Vertical Axis
Observing Radar
Angle of Climb
Nose Aspect
40 M² Level
RELATIVE POWER (db)
ANGLE
108°
72°
36°
0
CHART No. 121

4.3.4. Series D: Horizontal Polarization, Magnetic RAM, 388 Mc

Most of the discussion that proceeds the C series applies here except that horizontal polarization is now used. The polarization and the frequency are the same as in series B. The RAM is of type 5 (magnetic loss) and has a reflectivity of -4 db.

This series shows that it is much easier to achieve the 40 m^2 objective with horizontal polarization than with vertical polarization. In Patterns D-1 to D-3 and D-5 to D-7 results are shown for the three NAA preferred locations with 0^o and 10^o climb. The 40 m^2 objective is obtained for both the second and third location at both climb angles. Pattern D-4 is shown as a standard pattern with no RAM for the 10^o climb angle.

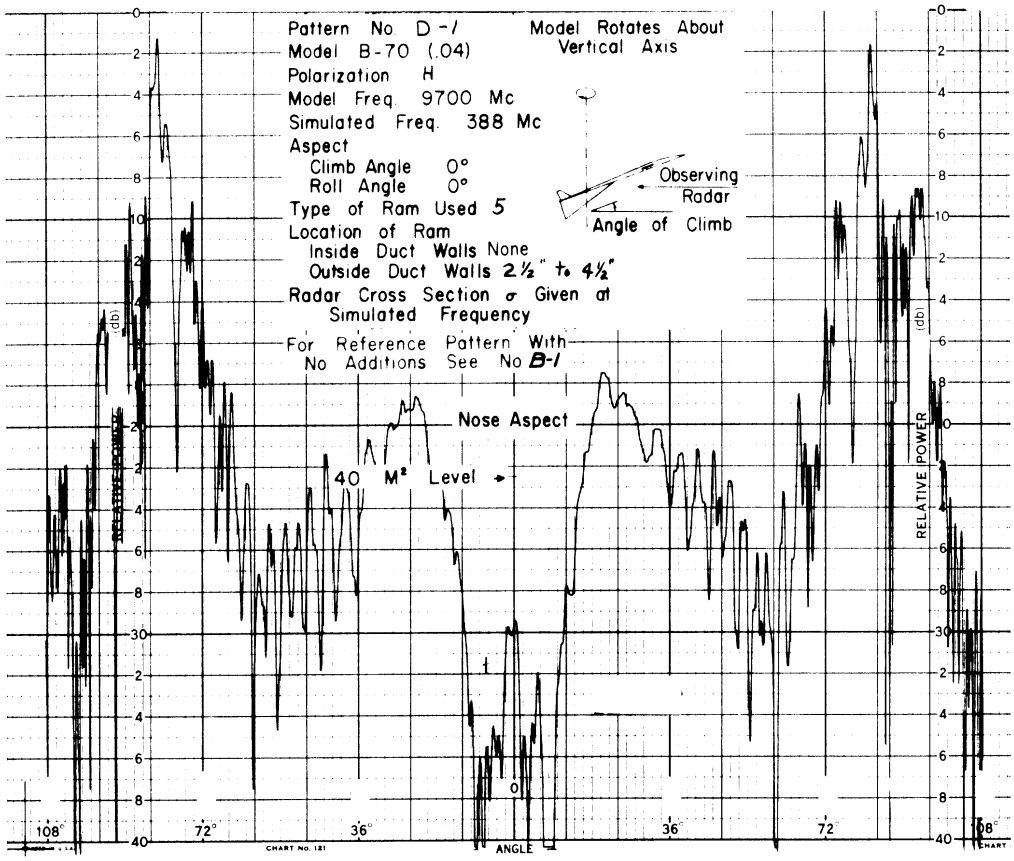
Pattern No. D-1
Model B-70 (.04)
Polarization H
Model Freq. 9700 Mc
Simulated Freq. 388 Mc
Aspect
Climb Angle 0°
Roll Angle 0°
Type of Ram Used 5
Location of Ram
Inside Duct Walls None
Outside Duct Walls 2½" to 4½"
Radar Cross Section σ Given at Simulated Frequency
For Reference Pattern With No Additions See No B-1
Model Rotates About Vertical Axis
Observing Radar
Angle of Climb
Nose Aspect
40 M² Level
RELATIVE POWER (db)
ANGLE
108° 72° 36° 36° 72° 108°

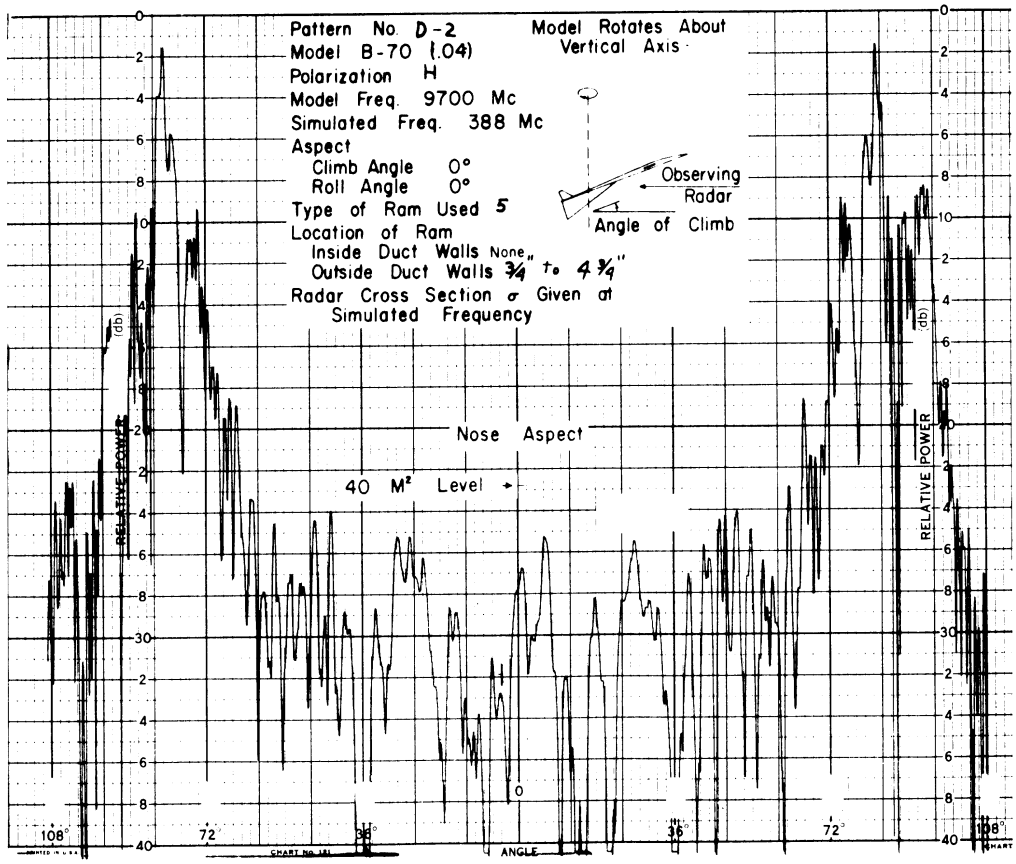
Pattern No. D-2
Model B-70 (.04)
Polarization H
Model Freq. 9700 Mc
Simulated Freq. 388 Mc
Aspect
Climb Angle 0°
Roll Angle 0°
Type of Ram Used 5
Location of Ram
Inside Duct Walls None
Outside Duct Walls ¾" to 4¾"
Radar Cross Section σ Given at Simulated Frequency
Model Rotates About Vertical Axis
Observing Radar
Angle of Climb
Nose Aspect
40 M² Level
RELATIVE POWER (db)
ANGLE
108° 72° 36° 36° 72° 108°

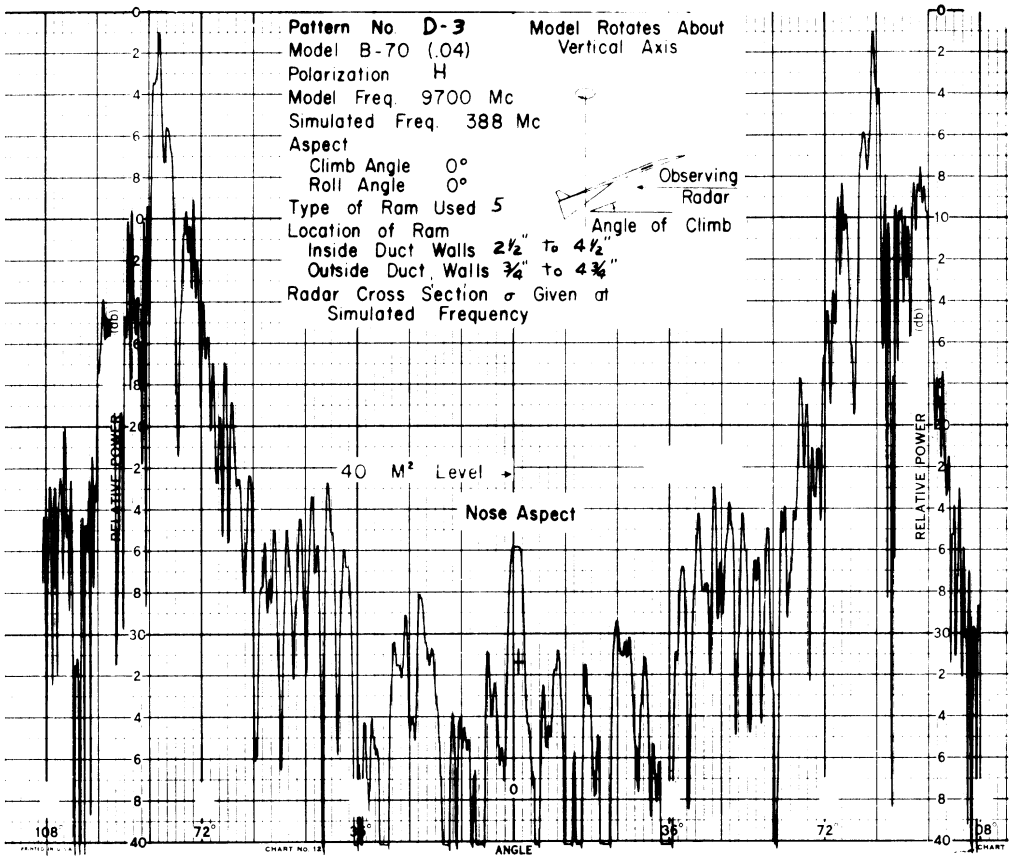
Pattern No. D-3
Model B-70 (.04)
Polarization H
Model Freq. 9700 Mc
Simulated Freq. 388 Mc
Aspect
Climb Angle 0°
Roll Angle 0°
Type of Ram Used 5
Location of Ram
Inside Duct Walls 2½" to 4½"
Outside Duct Walls ¾" to 4¾"
Radar Cross Section σ Given at Simulated Frequency
Model Rotates About Vertical Axis
Observing Radar
Angle of Climb
40 M² Level
Nose Aspect
RELATIVE POWER (db)
ANGLE
108°
72°
36°
0
36°
72°
108°

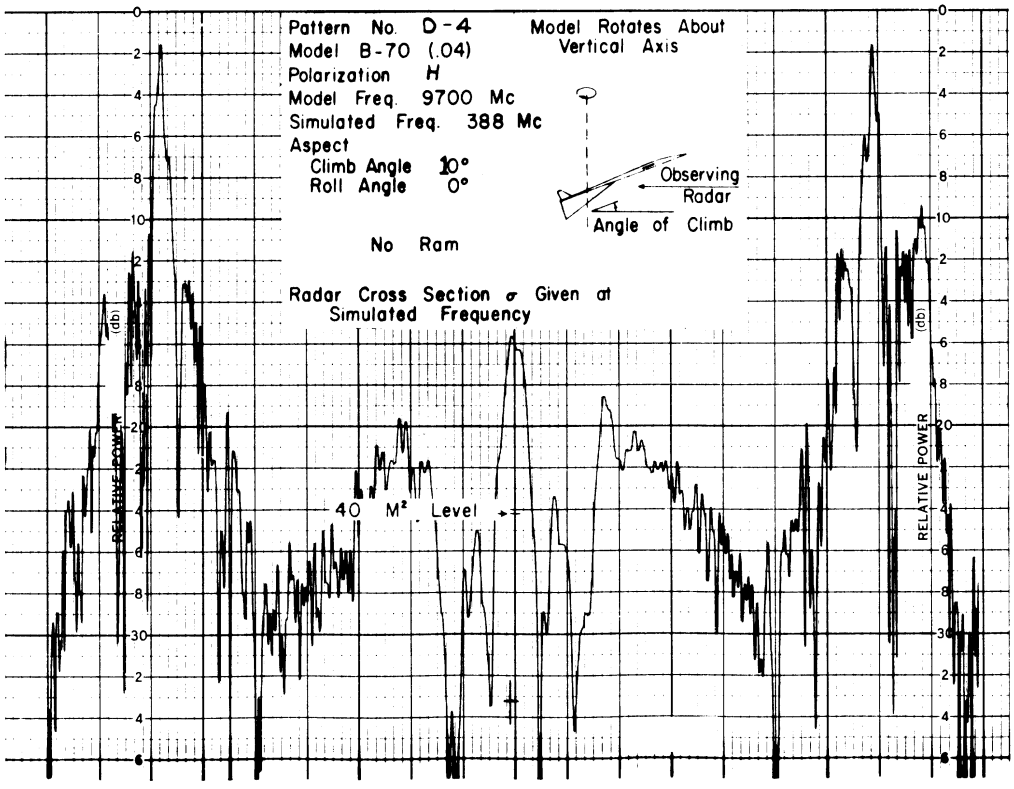
Pattern No. D-4
Model B-70 (.04)
Polarization H
Model Freq. 9700 Mc
Simulated Freq. 388 Mc
Aspect
Climb Angle 10°
Roll Angle 0°
No Ram
Radar Cross Section σ Given at Simulated Frequency
Model Rotates About Vertical Axis
Observing Radar
Angle of Climb
40 M² Level
RELATIVE POWER (db)

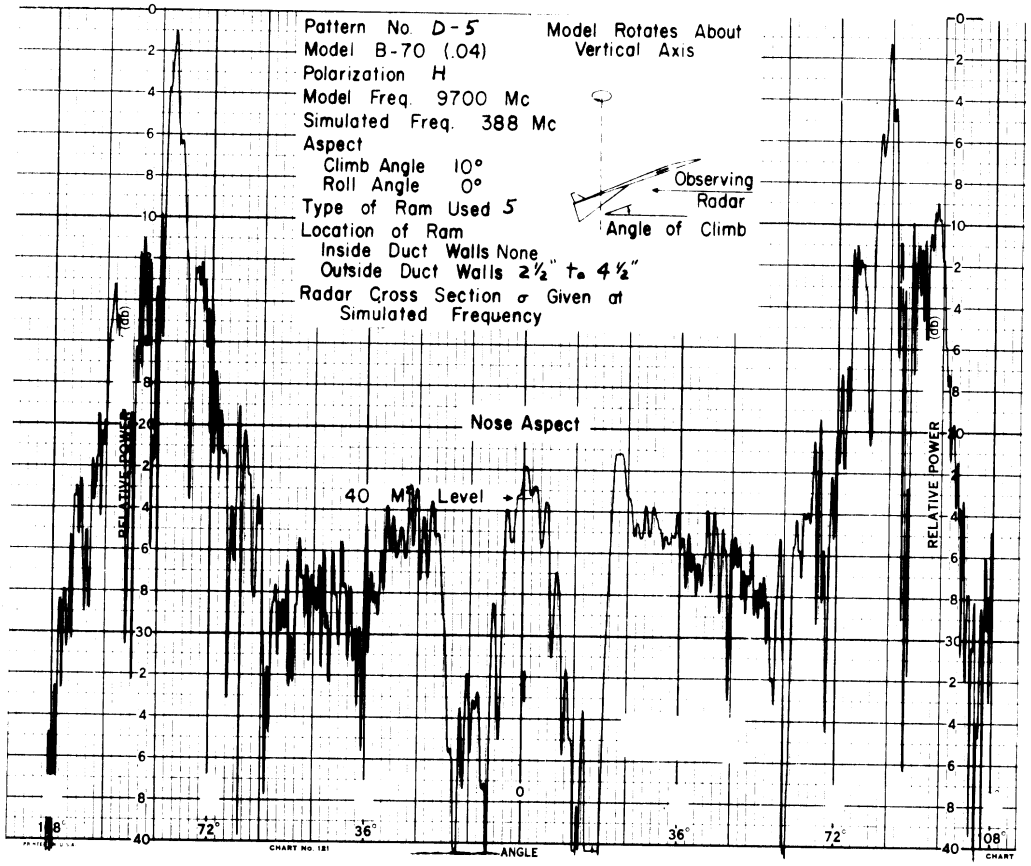
Pattern No. D-5
Model B-70 (.04)
Polarization H
Model Freq. 9700 Mc
Simulated Freq. 388 Mc
Aspect
Climb Angle 10°
Roll Angle 0°
Type of Ram Used 5
Location of Ram
Inside Duct Walls None
Outside Duct Walls 2½" to 4½"
Radar Cross Section σ Given at
Simulated Frequency
Model Rotates About
Vertical Axis
Observing
Radar
Angle of Climb
Nose Aspect
40 M² Level
RELATIVE POWER (db)
ANGLE
72°
36°
0
CHART

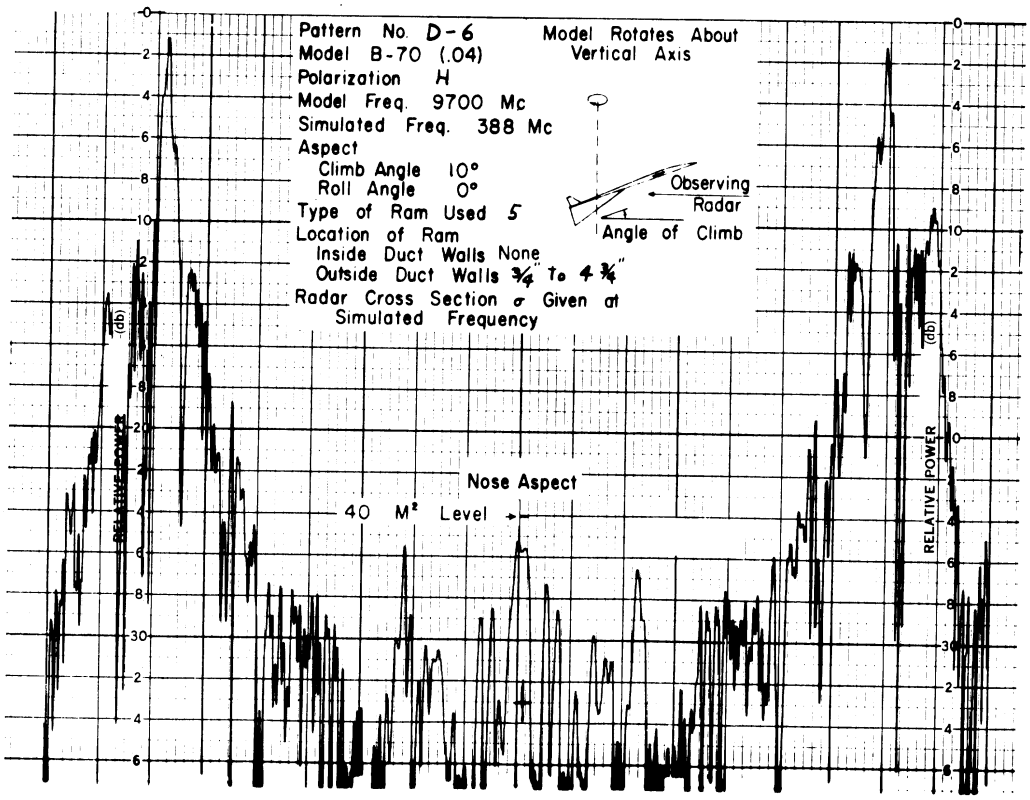
Pattern No. D-6
Model B-70 (.04)
Polarization H
Model Freq. 9700 Mc
Simulated Freq. 388 Mc
Aspect
Climb Angle 10°
Roll Angle 0°
Type of Ram Used 5
Location of Ram
Inside Duct Walls None
Outside Duct Walls ¾" to 4¾"
Radar Cross Section σ Given at
Simulated Frequency
Model Rotates About
Vertical Axis
Observing
Radar
Angle of Climb
Nose Aspect
40 M² Level
RELATIVE POWER (db)

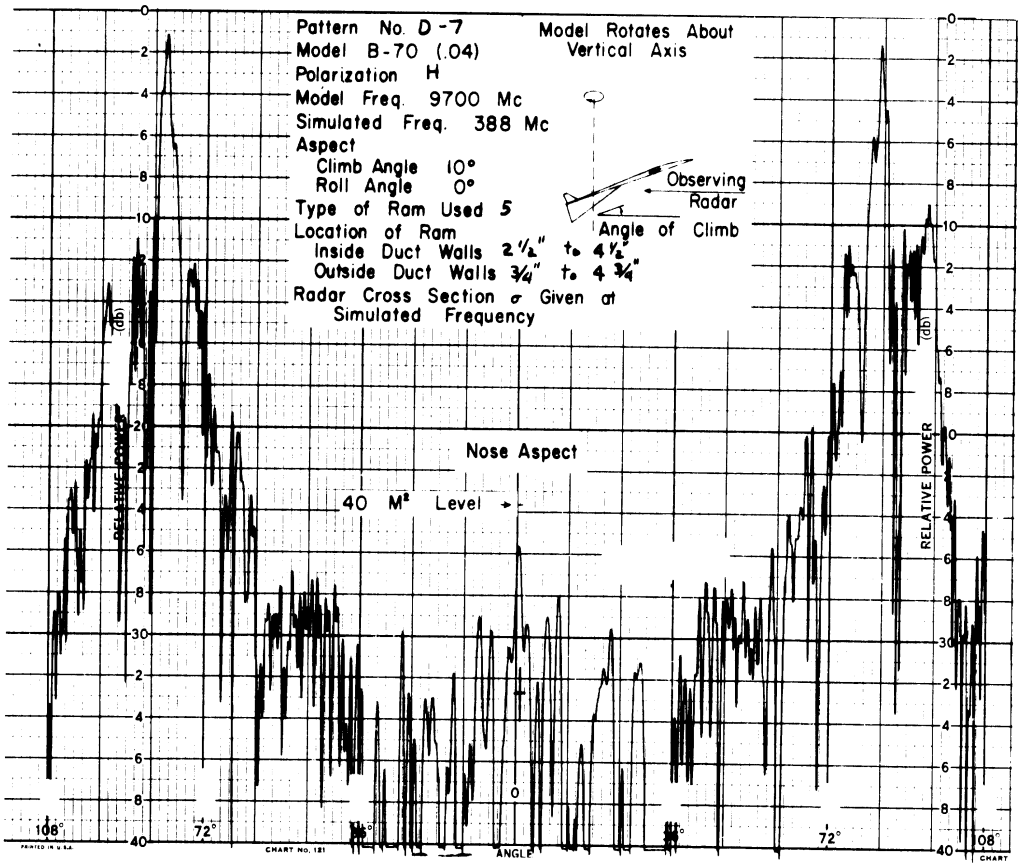
Pattern No. D-7
Model B-70 (.04)
Polarization H
Model Freq. 9700 Mc
Simulated Freq. 388 Mc
Aspect
Climb Angle 10°
Roll Angle 0°
Type of Ram Used 5
Location of Ram
Inside Duct Walls 2 1/2" to 4 1/2"
Outside Duct Walls 3/4" to 4 3/4"
Radar Cross Section σ Given at Simulated Frequency
Model Rotates About Vertical Axis
Observing Radar
Angle of Climb
Nose Aspect
40 M² Level
RELATIVE POWER (db)
ANGLE
CHART

4.3.5. Series E: Dielectric RAM, 918 Mc

In the next three groups (E, F and G), results for the K band model measurements are shown. The model frequency was 22.96 KMc corresponding to a simulated frequency of 918 Mc. The Series E measurements were made with both vertical and horizontal polarization using the Emerson and Cuming dielectric absorber.

Patterns E-1 through E-6 show results for vertical polarization at 0^{o} climb. Pattern E-2 shows that the 40 m^2 level is not obtained with good RAM at the third preferred NAA location, but succeeding patterns show that this level can be reached by adding more RAM on the inner wall. Pattern E-6 is presented to show the significant contribution which comes from the vertical edges that form the beginning of the outer duct wall and from the wedge that forms the beginning of the inner duct walls. A comparison with E-5 shows that an average reduction of about 2 db is obtained when the vertical edges are broken by the addition of a metallic, serrated edge. The serrations are of the order of a wavelength in depth.

Patterns E-7 through E-9 are for the 10^{o} climb angle with vertical polarization. These patterns show that the cross section level is 2 or 3 db lower than for similar conditions at 0^{o} and indicate that any acceptable choice of RAM for the 0^{o} climb angle will be quite satisfactory for the 10^{o} climb angle.

Patterns E-10 through E-13 are for horizontal polarization. Patterns E-10 and E-12 show that this RAM at the third preferred NAA location is hardly sufficient at 0^{o}, but is quite adequate for 10^{o} climb. Patterns E-11 and E-13 show that a 4" strip of RAM on the inner wall centered at the point where the duct starts, plus the usual strip on the outer wall, is more than adequate for both climb angles.

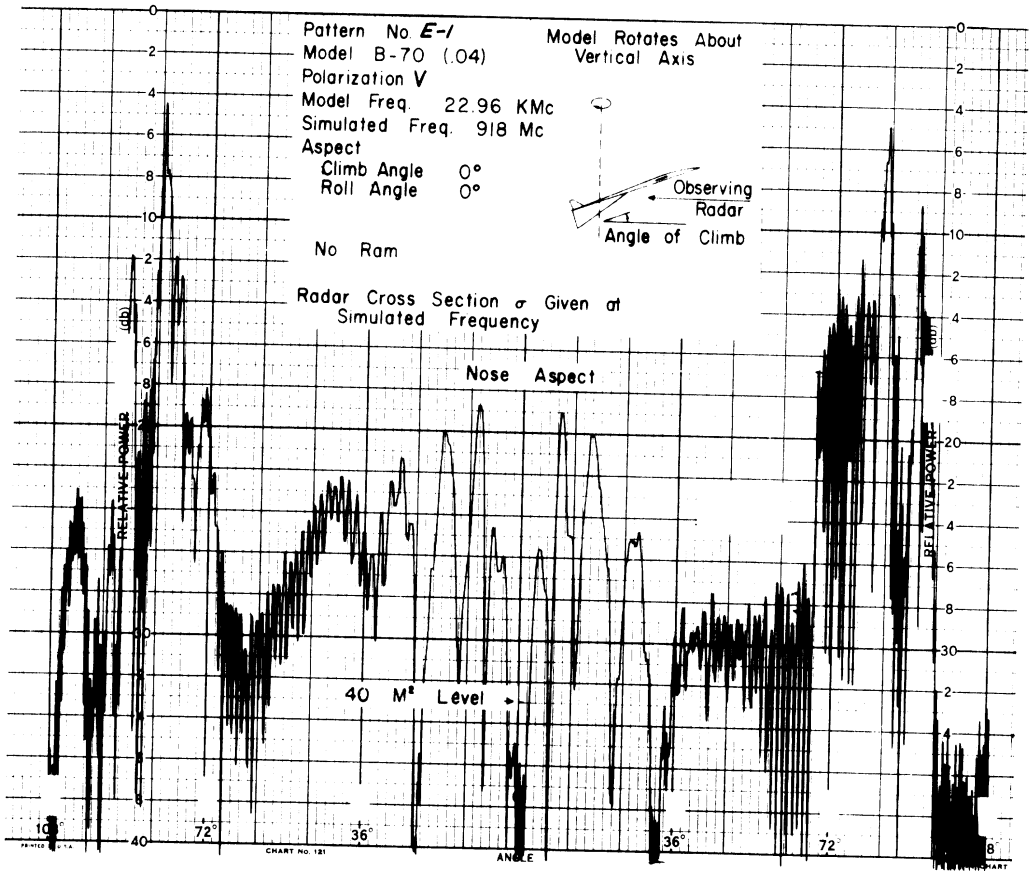
Pattern No. E-1
Model B-70 (.04)
Polarization V
Model Freq. 22.96 KMc
Simulated Freq. 918 Mc
Aspect
Climb Angle 0°
Roll Angle 0°
No Ram
Radar Cross Section σ Given at Simulated Frequency
Model Rotates About Vertical Axis
Observing Radar
Angle of Climb
Nose Aspect
40 M² Level
RELATIVE POWER (db)
ANGLE
72°
36°

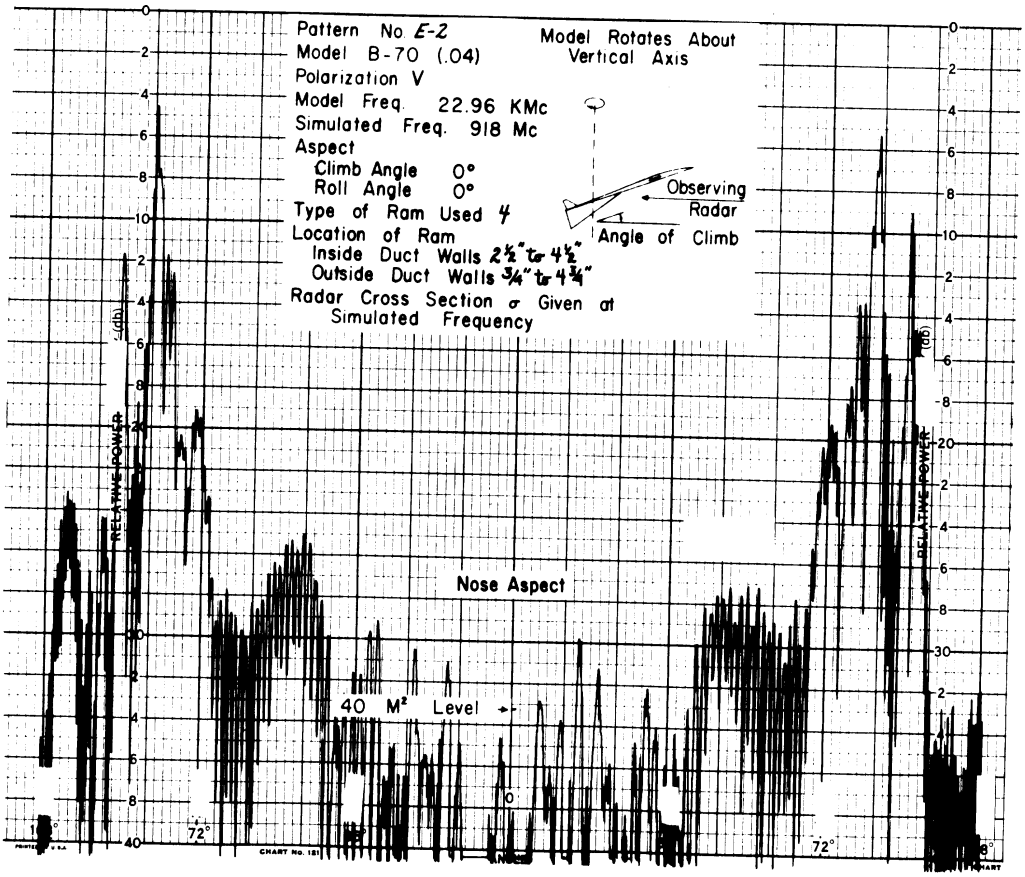
Pattern No. E-2
Model B-70 (.04)
Polarization V
Model Freq. 22.96 KMc
Simulated Freq. 918 Mc
Aspect
Climb Angle 0°
Roll Angle 0°
Type of Ram Used 4
Location of Ram
Inside Duct Walls 2½" to 4½"
Outside Duct Walls ¾" to 4¾"
Radar Cross Section σ Given at Simulated Frequency
Model Rotates About Vertical Axis
Observing Radar
Angle of Climb
Nose Aspect
40 M² Level
RELATIVE POWER (db)
72°

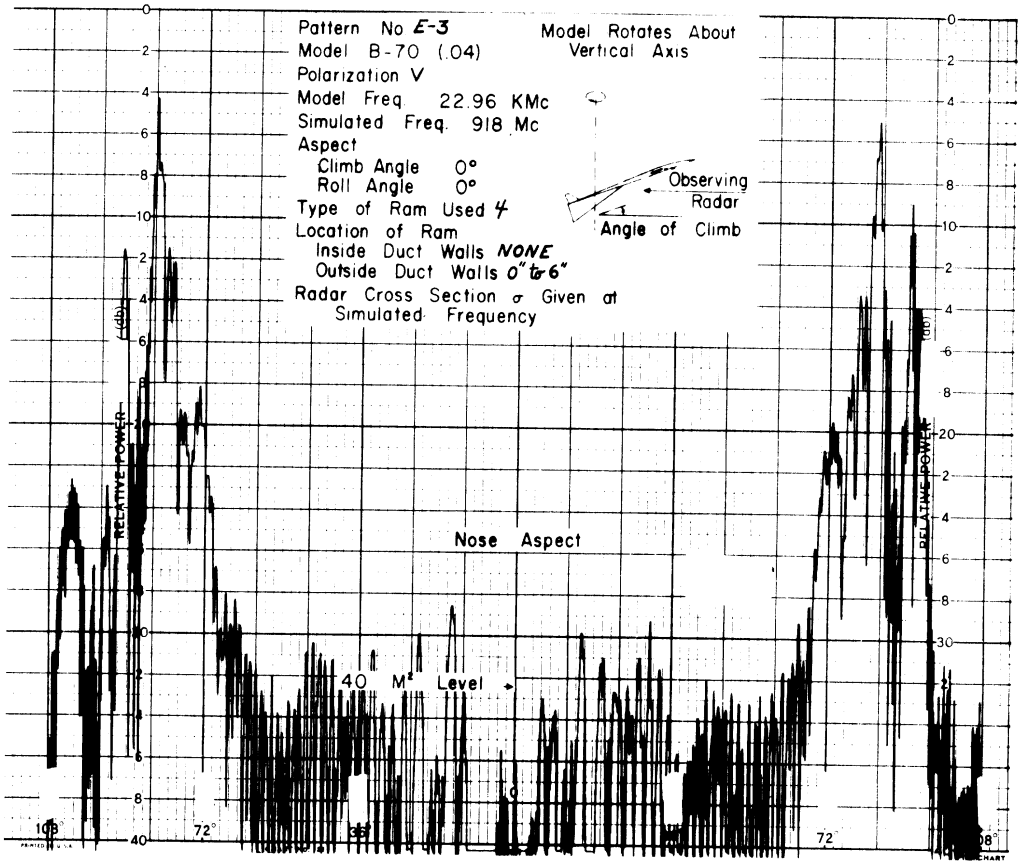
Pattern No E-3
Model B-70 (.04)
Polarization V
Model Freq. 22.96 KMc
Simulated Freq. 918 Mc
Aspect
Climb Angle 0°
Roll Angle 0°
Type of Ram Used 4
Location of Ram
Inside Duct Walls NONE
Outside Duct Walls 0" to 6"
Radar Cross Section σ Given at
Simulated Frequency
Model Rotates About
Vertical Axis
Observing
Radar
Angle of Climb
Nose Aspect
40 M² Level
RELATIVE POWER (db)
72°

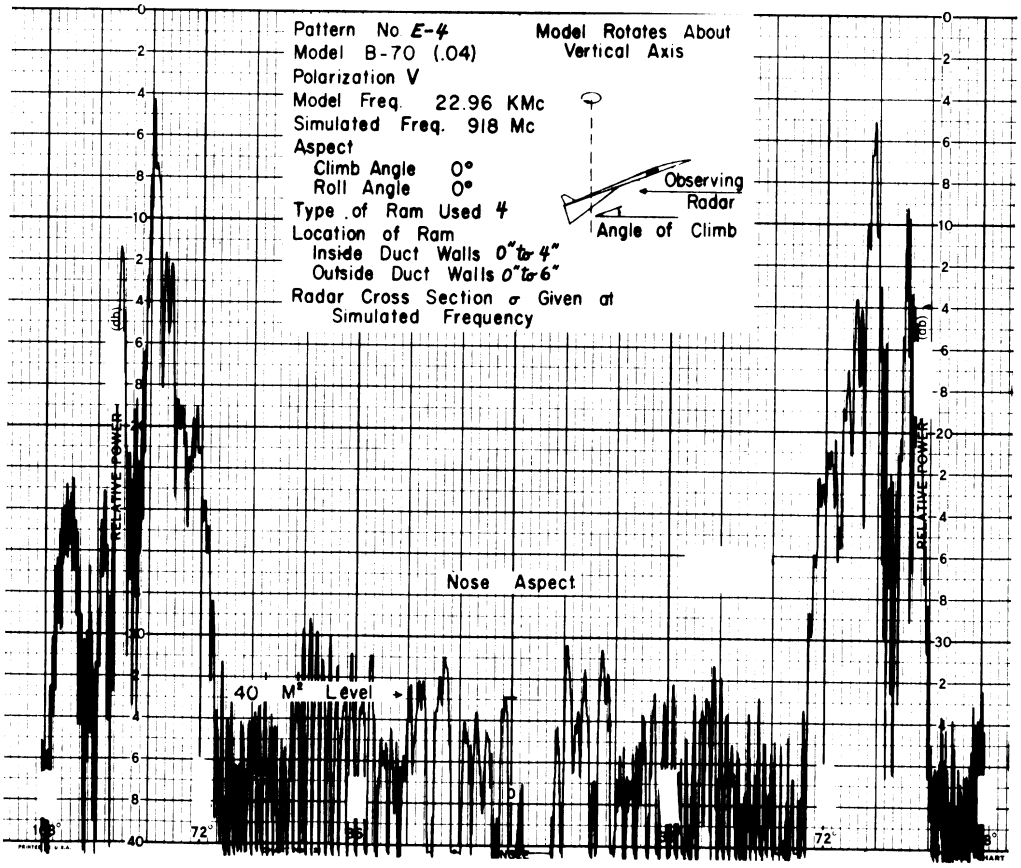
Pattern No E-4
Model B-70 (.04)
Polarization V
Model Freq. 22.96 KMc
Simulated Freq. 918 Mc
Aspect
Climb Angle 0°
Roll Angle 0°
Type of Ram Used 4
Location of Ram
Inside Duct Walls 0" to 4"
Outside Duct Walls 0" to 6"
Radar Cross Section σ Given at
Simulated Frequency
Model Rotates About
Vertical Axis
Observing
Radar
Angle of Climb
Nose Aspect
40 M² Level
RELATIVE POWER (db)
72°

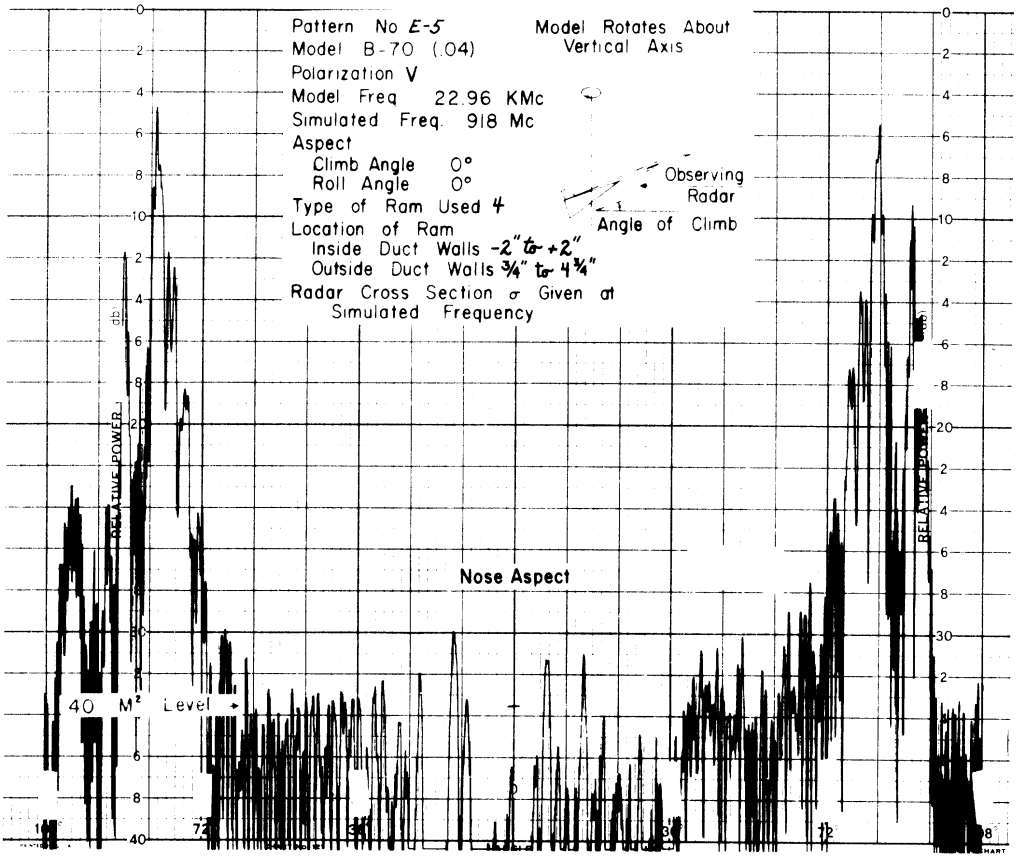
Pattern No E-5
Model B-70 (.04)
Polarization V
Model Freq 22.96 KMc
Simulated Freq. 918 Mc
Aspect
Climb Angle 0°
Roll Angle 0°
Type of Ram Used 4
Location of Ram
Inside Duct Walls -2" to +2"
Outside Duct Walls 3/4" to 4 3/4"
Radar Cross Section σ Given at Simulated Frequency
Model Rotates About Vertical Axis
Observing Radar
Angle of Climb
Nose Aspect
40 M² Level
RELATIVE POWER (db)

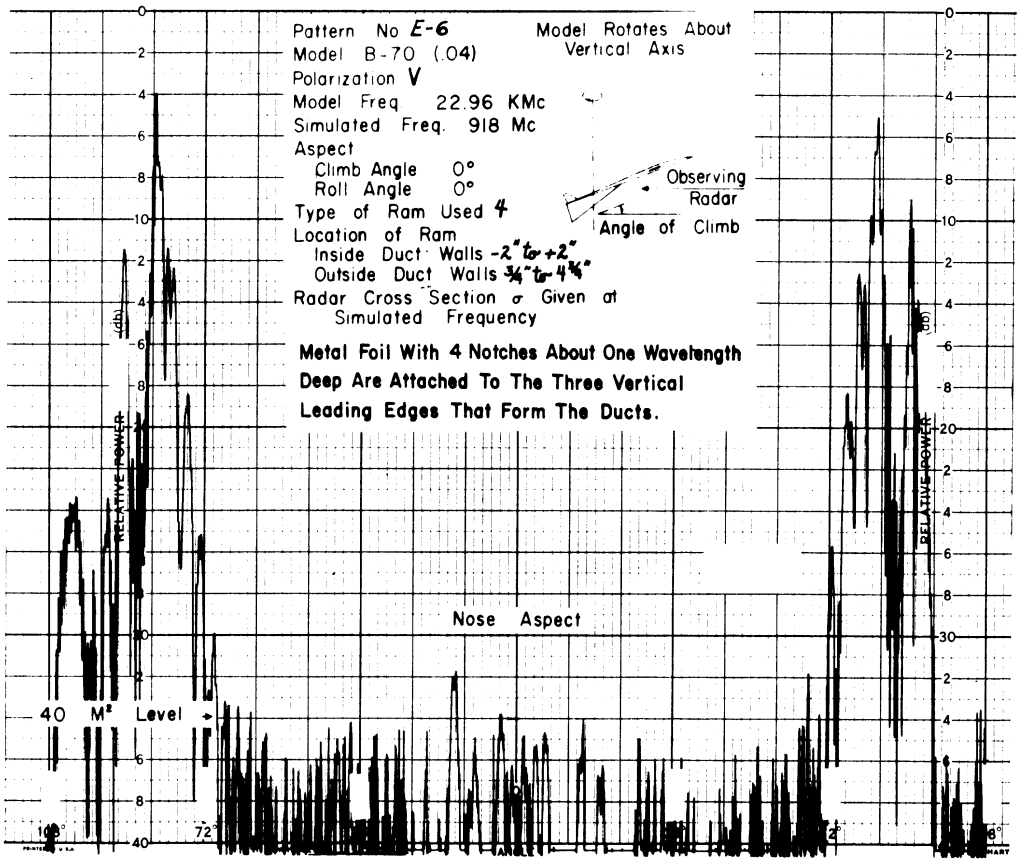
Pattern No E-6
Model B-70 (.04)
Polarization V
Model Freq 22.96 KMc
Simulated Freq. 918 Mc
Aspect
Climb Angle 0°
Roll Angle 0°
Type of Ram Used 4
Location of Ram
Inside Duct Walls -2" to +2"
Outside Duct Walls 3/4" to 4 3/4"
Radar Cross Section σ Given at Simulated Frequency
Model Rotates About Vertical Axis
Observing Radar
Angle of Climb
Metal Foil With 4 Notches About One Wavelength Deep Are Attached To The Three Vertical Leading Edges That Form The Ducts.
Nose Aspect
40 M² Level
RELATIVE POWER (db)

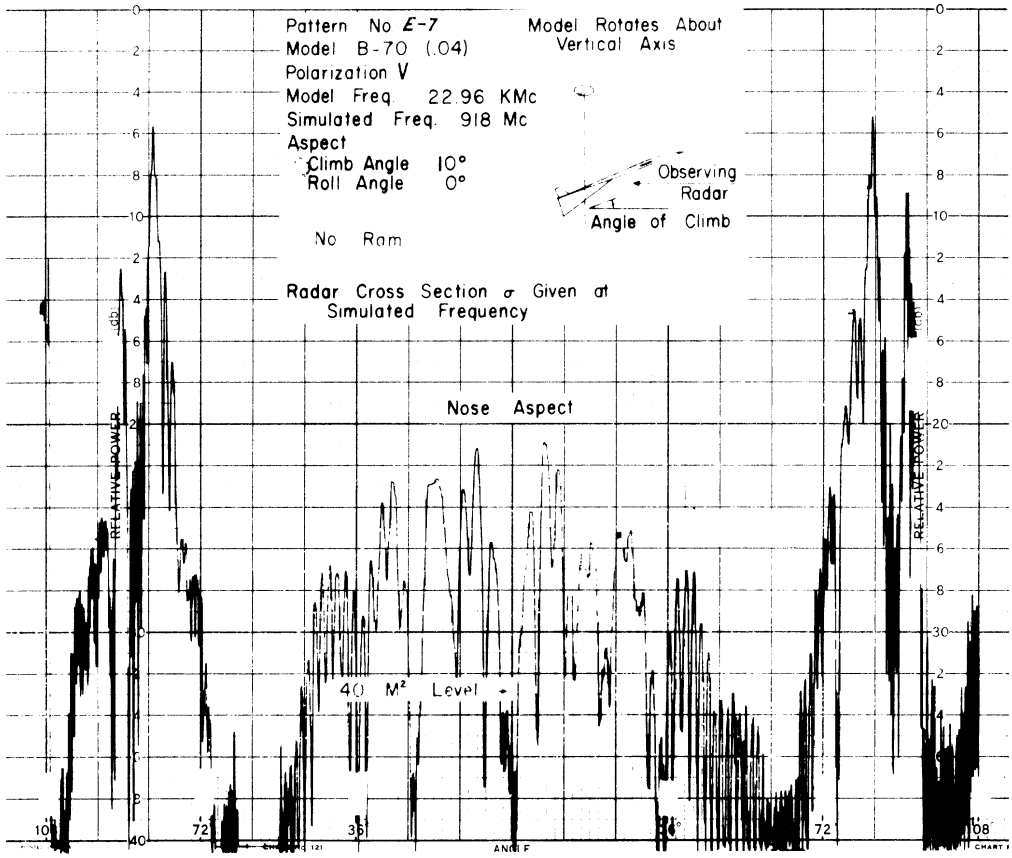
Pattern No E-7
Model B-70 (.04)
Polarization V
Model Freq. 22.96 KMc
Simulated Freq. 918 Mc
Aspect
Climb Angle 10°
Roll Angle 0°
No Ram
Radar Cross Section σ Given at Simulated Frequency
Model Rotates About Vertical Axis
Observing Radar
Angle of Climb
Nose Aspect
40 M² Level
RELATIVE POWER (db)
RELATIVE POWER (dbr)
72
72
108°

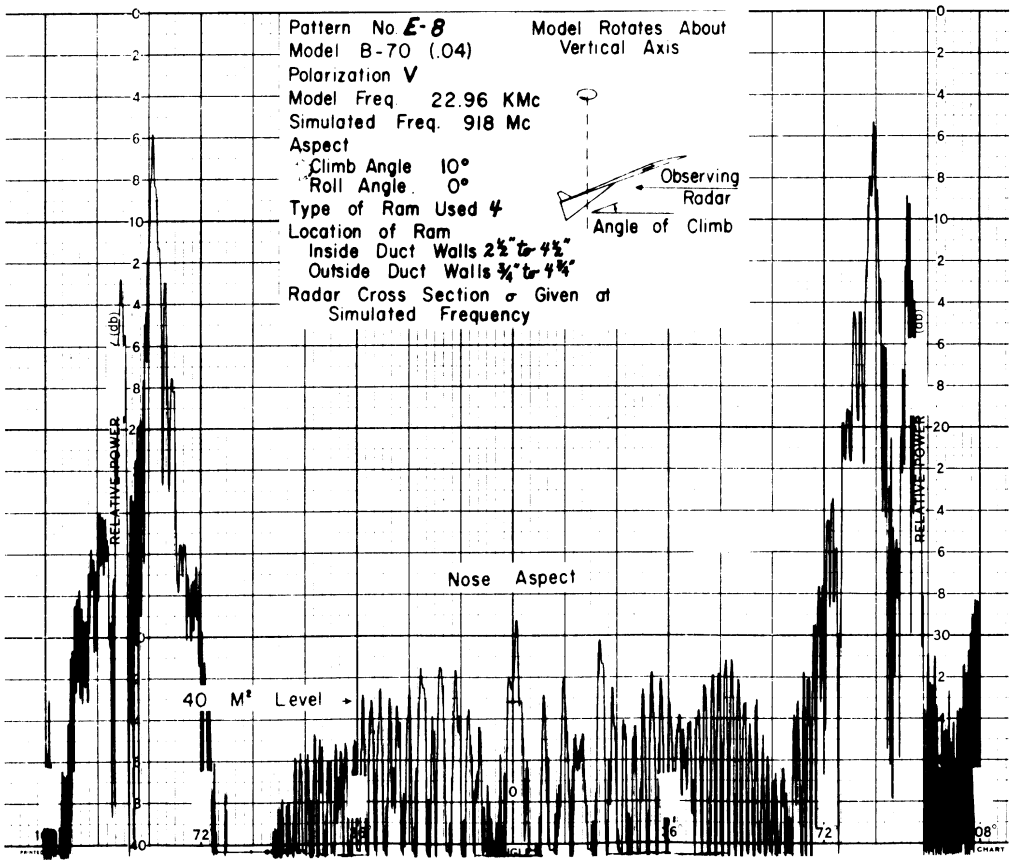
Pattern No E-8
Model B-70 (.04)
Polarization V
Model Freq. 22.96 KMc
Simulated Freq. 918 Mc
Aspect
Climb Angle 10°
Roll Angle 0°
Type of Ram Used 4
Location of Ram
Inside Duct Walls 2½" to 4½"
Outside Duct Walls ¾" to 4¾"
Radar Cross Section σ Given at Simulated Frequency
Model Rotates About Vertical Axis
Observing Radar
Angle of Climb
Nose Aspect
40 M² Level
RELATIVE POWER (db)
RELATIVE POWER (dbr)
72
72
108°

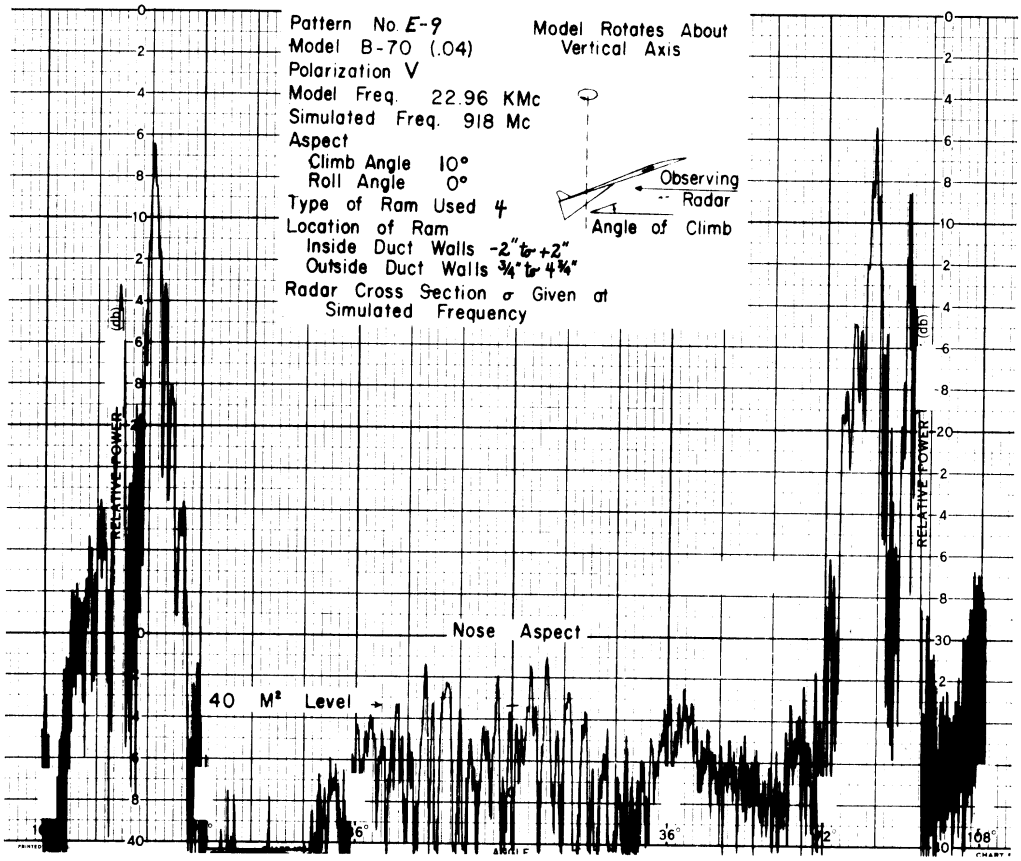
Pattern No. E-9
Model B-70 (.04)
Polarization V
Model Freq. 22.96 KMc
Simulated Freq. 918 Mc
Aspect
Climb Angle 10°
Roll Angle 0°
Type of Ram Used 4
Location of Ram
Inside Duct Walls -2" to +2"
Outside Duct Walls ¾" to 4¾"
Radar Cross Section σ Given at Simulated Frequency
Model Rotates About Vertical Axis
Observing Radar
Angle of Climb
Nose Aspect
40 M² Level
RELATIVE POWER (db)
ANGLE

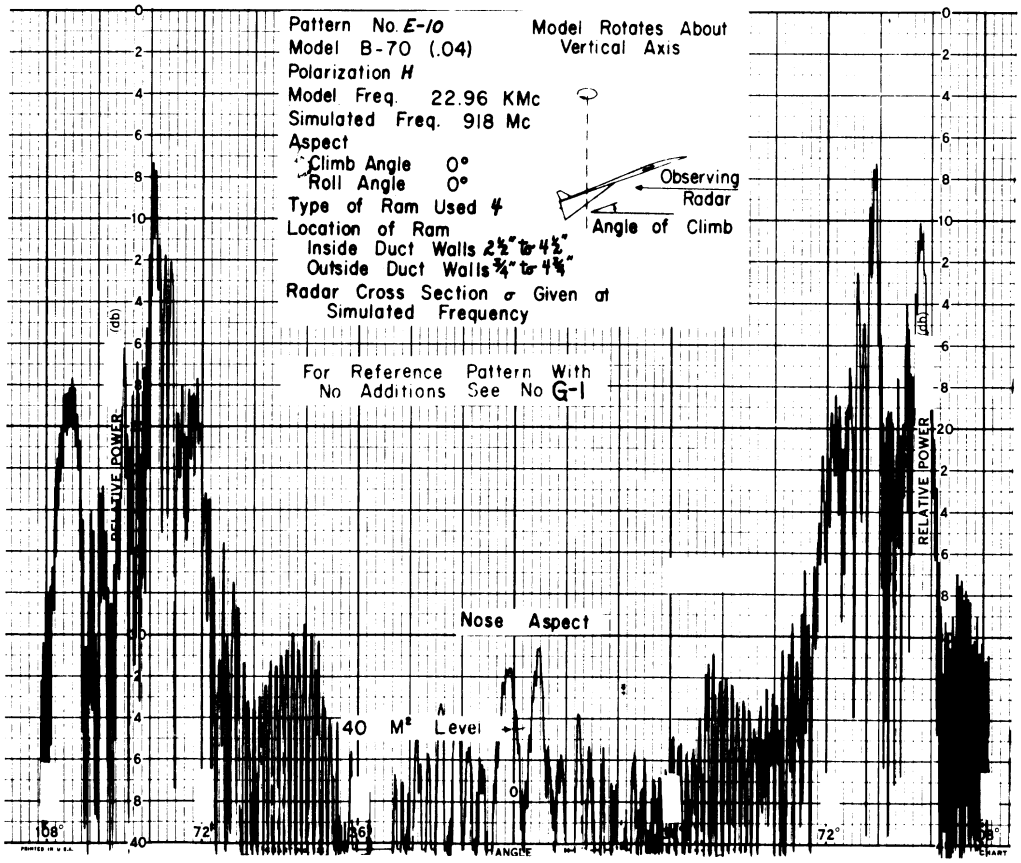
Pattern No. E-10
Model B-70 (.04)
Polarization H
Model Freq. 22.96 KMc
Simulated Freq. 918 Mc
Aspect
Climb Angle 0°
Roll Angle 0°
Type of Ram Used 4
Location of Ram
Inside Duct Walls 2½" to 4½"
Outside Duct Walls ¾" to 4¾"
Radar Cross Section σ Given at Simulated Frequency
Model Rotates About Vertical Axis
Observing Radar
Angle of Climb
For Reference Pattern With No Additions See No G-1
Nose Aspect
40 M² Level
RELATIVE POWER (db)
ANGLE

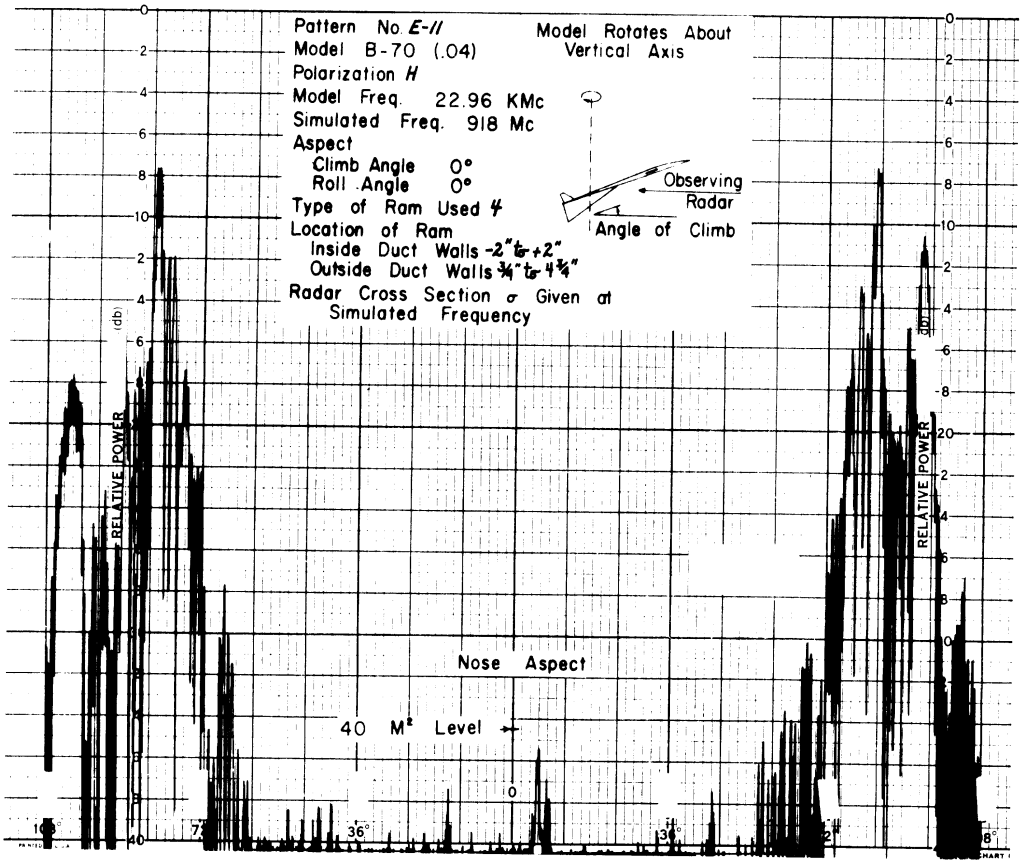
Pattern No. E-11
Model B-70 (.04)
Polarization H
Model Freq. 22.96 KMc
Simulated Freq. 918 Mc
Aspect
Climb Angle 0°
Roll Angle 0°
Type of Ram Used 4
Location of Ram
Inside Duct Walls -2" to +2"
Outside Duct Walls 3/4" to 4 3/4"
Radar Cross Section σ Given at Simulated Frequency
Model Rotates About Vertical Axis
Observing Radar
Angle of Climb
RELATIVE POWER (db)
Nose Aspect
40 M² Level
ANGLE
CHART

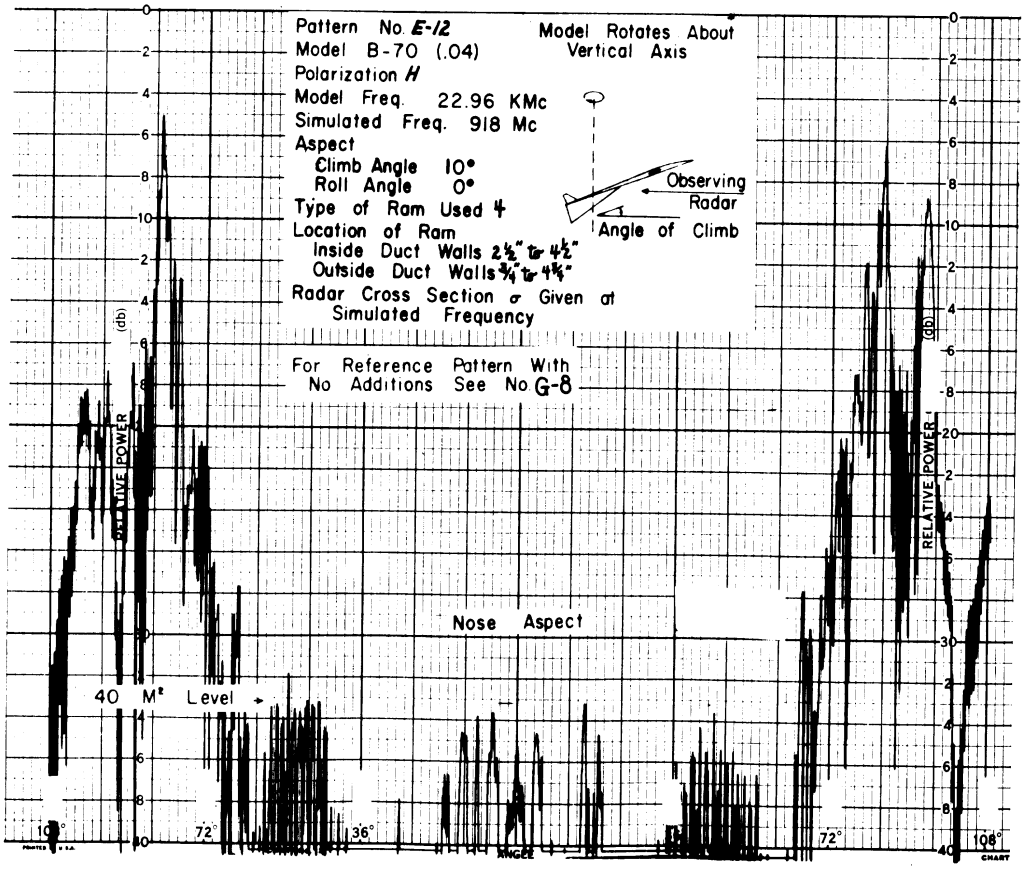
Pattern No. E-12
Model B-70 (.04)
Polarization H
Model Freq. 22.96 KMc
Simulated Freq. 918 Mc
Aspect
Climb Angle 10°
Roll Angle 0°
Type of Ram Used 4
Location of Ram
Inside Duct Walls 2½" to 4½"
Outside Duct Walls 3/4" to 4 3/4"
Radar Cross Section σ Given at Simulated Frequency
Model Rotates About Vertical Axis
Observing Radar
Angle of Climb
For Reference Pattern With No Additions See No G-8
RELATIVE POWER (db)
Nose Aspect
40 M² Level
ANGLE
CHART

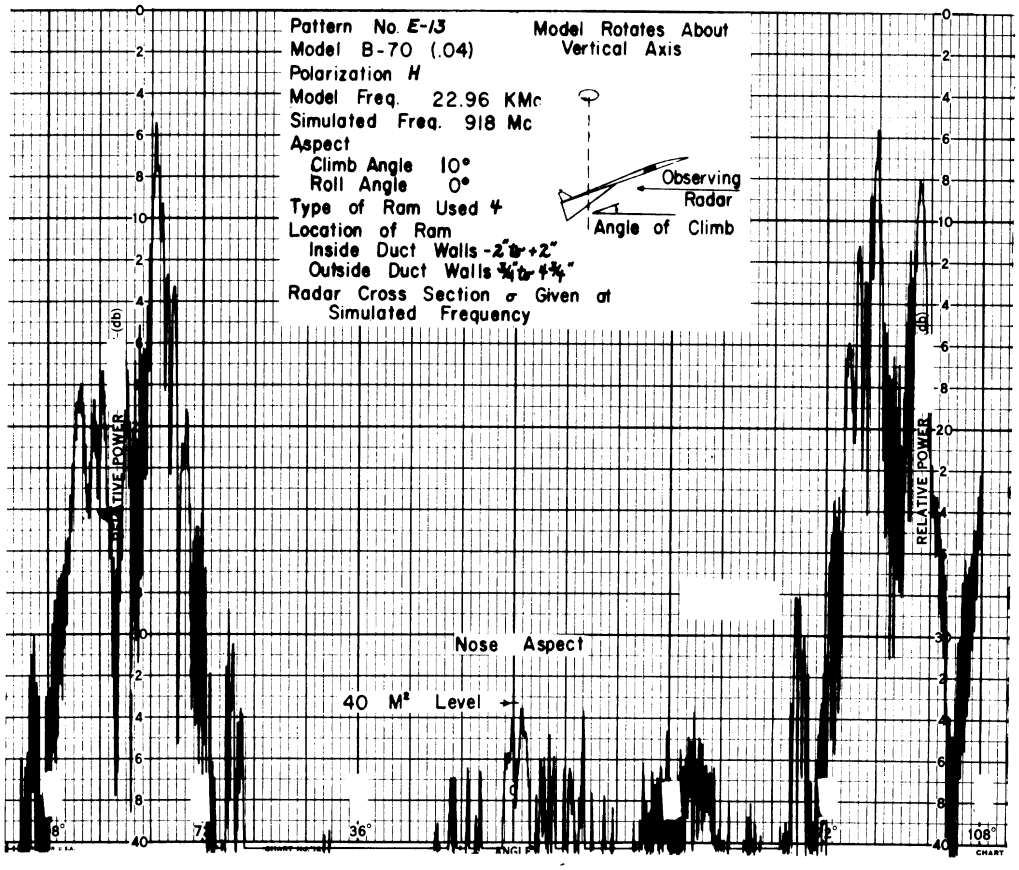
Pattern No. E-13
Model B-70 (.04)
Polarization H
Model Freq. 22.96 KMc
Simulated Freq. 918 Mc
Aspect
Climb Angle 10°
Roll Angle 0°
Type of Ram Used 4
Location of Ram
Inside Duct Walls -2" to +2"
Outside Duct Walls ¾" to 1¾"
Radar Cross Section σ Given at Simulated Frequency
Model Rotates About Vertical Axis
Observing Radar
Angle of Climb
RELATIVE POWER (db)
Nose Aspect
40 M² Level
36°
108°

4.3.6. Series F: Vertical Polarization, Magnetic RAM, 918 Mc

This is a continuation of the E series with the chief difference that a magnetic RAM was used in all patterns except F-17. For Patterns F-1 through F-14, the reflectivity of the RAM was -9 db. In Patterns F-15 and F-16 a magnetic RAM with a reflectivity of -4 db was used, while in Pattern F-17 a dielectric RAM with a reflectivity of -20 db was employed. All patterns are for vertical polarization.

Patterns F-1, F-2 and F-3 are for the three NAA locations, and it is obvious that more RAM (or a better RAM) is required. With RAM from 0" to 4" on the outer wall the general level is well down except for a large return near nose-on. In the interest of locating the source of this return, RAM was placed across the ducts (but well inside), and the resulting Pattern F-5 shows that the original return near nose-on return was due to energy entering and being reradiated from the ducts.

In Patterns F-6 through F-11, additional RAM was added as shown on the patterns in order to find the most effective method for reducing the cross section to 40 m^2. With RAM as shown in F-10, the results obtained are almost acceptable. It is doubtful if more can be achieved by additional RAM, although better RAM would, of course, give some improvement. As shown in Pattern F-9 and F-11, the return can be decreased considerably by minimizing the effect of the contribution from the vertical edges.

In Patterns F-12, F-13 and F-14 results are given for the three preferred NAA locations with the 10^{o} climb angle. The average return in F-14 is below 40 m^2. With the use of RAM similar to that required for the 0^{o} climb angle (as in Pattern F-10), the return at the 10^{o} climb angle would be well below 40 m^2.

In order to relate the radar scattering pattern to the quality of the RAM, three more patterns are presented. Pattern F-15 used a magnetic RAM (made in the laboratory) with a measured reflectivity of -4 db. It was presumed that the amount of cross section reduction achieved would be inferior to that obtained with a -9 db material. A comparison of F-15 with F-3 shows that there is, in fact, very little difference. The RAM locations for these two patterns are the same as in Pattern E-2, where the -20 db dielectric absorber was used. E-2 is seen to be better than both F-3 and F-15.

In Patterns F-16 and F-17 this study is continued. In these two patterns the RAM locations are the same as in F-6. The RAM used is as follows:

Pattern	Type	Reflectivity
F-6	5	-9 db
F-16	7	-4 db
F-17	4	-20 db

There is little difference between Patterns F-6 and F-16, but Pattern F-17 shows definite improvement over the other two patterns. The amount of the improvement averages about 2 or 3 db.

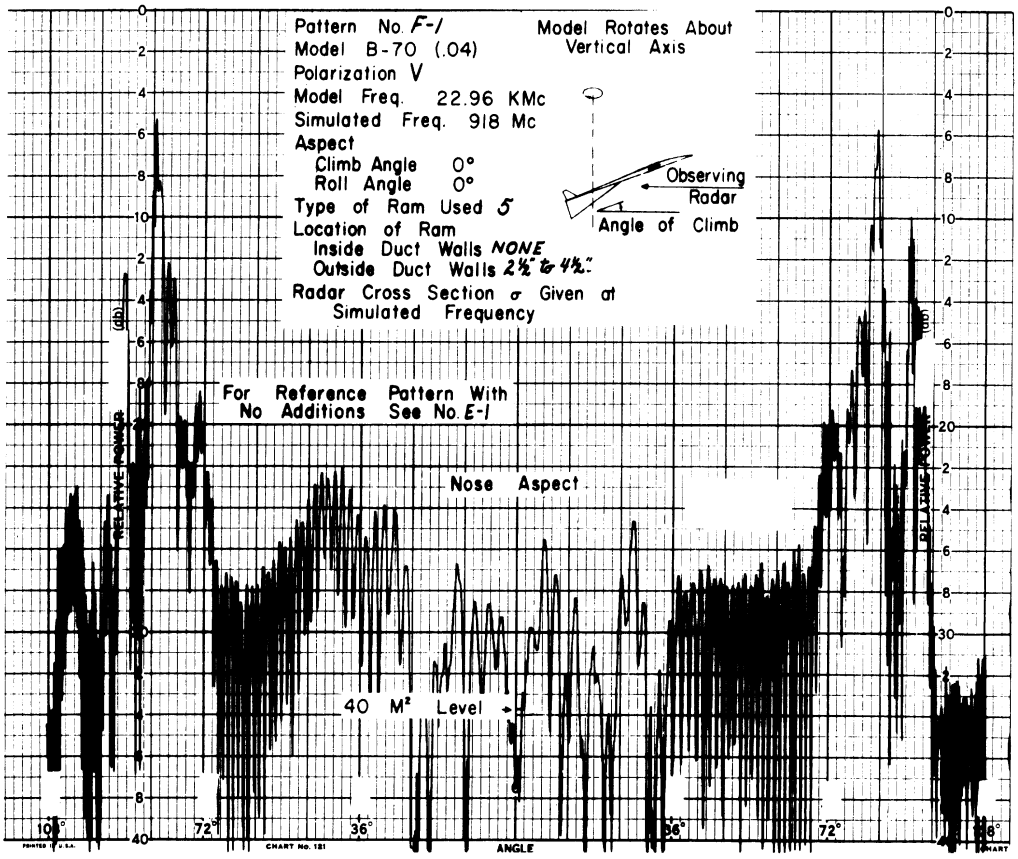
Pattern No. F-1
Model B-70 (.04)
Polarization V
Model Freq. 22.96 KMc
Simulated Freq. 918 Mc
Aspect
Climb Angle 0°
Roll Angle 0°
Type of Ram Used 5
Location of Ram
Inside Duct Walls NONE
Outside Duct Walls 2½" to 4½"
Radar Cross Section σ Given at
Simulated Frequency
Model Rotates About
Vertical Axis
Observing
Radar
Angle of Climb
For Reference Pattern With
No Additions See No. E-1
Nose Aspect
40 M² Level
RELATIVE POWER (db)
ANGLE
CHART No. 121

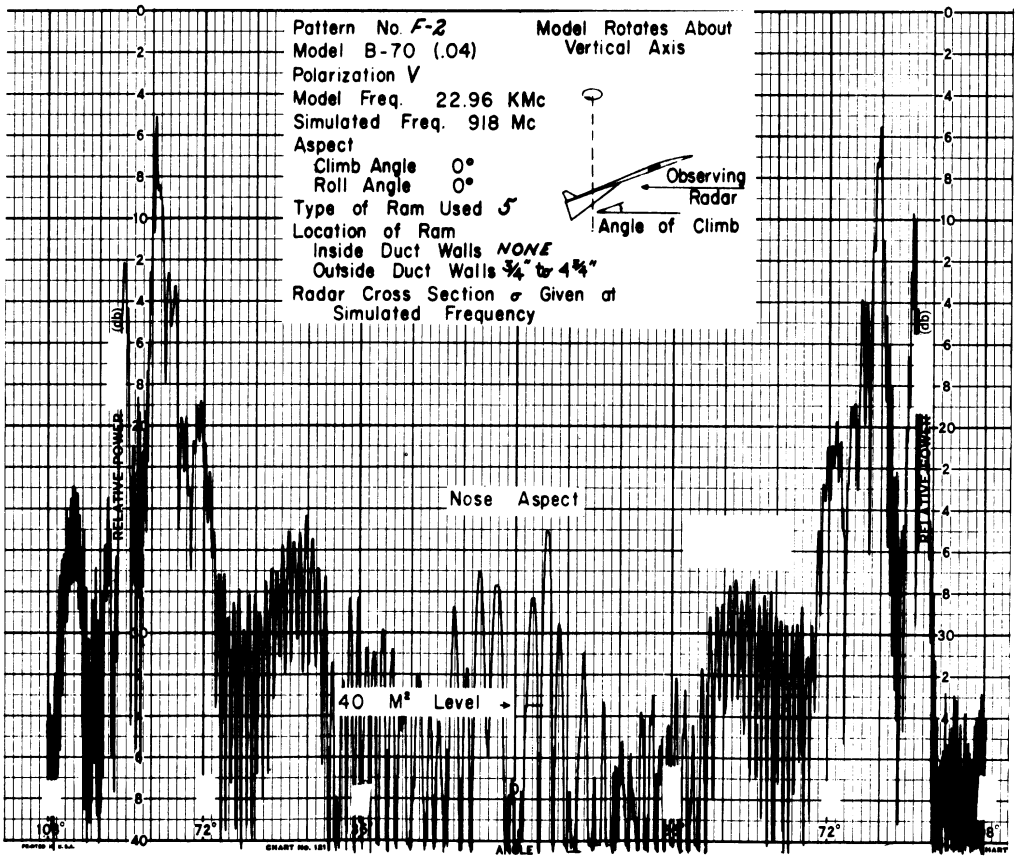
Pattern No. F-2
Model B-70 (.04)
Polarization V
Model Freq. 22.96 KMc
Simulated Freq. 918 Mc
Aspect
Climb Angle 0°
Roll Angle 0°
Type of Ram Used 5
Location of Ram
Inside Duct Walls NONE
Outside Duct Walls ¾" to 4¾"
Radar Cross Section σ Given at
Simulated Frequency
Model Rotates About
Vertical Axis
Observing
Radar
Angle of Climb
Nose Aspect
40 M² Level
RELATIVE POWER (db)
ANGLE
CHART No. 121

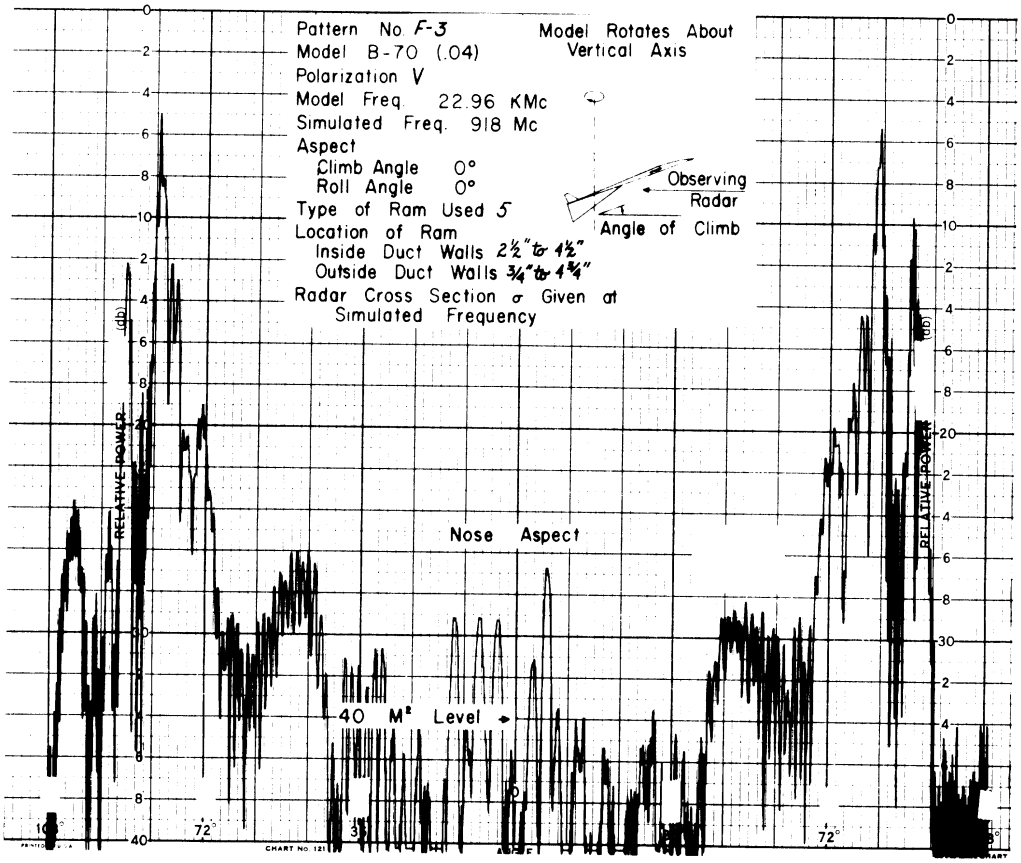
Pattern No. F-3
Model B-70 (.04)
Polarization V
Model Freq. 22.96 KMc
Simulated Freq. 918 Mc
Aspect
Climb Angle 0°
Roll Angle 0°
Type of Ram Used 5
Location of Ram
Inside Duct Walls 2½" to 1½"
Outside Duct Walls ¾" to 1¾"
Radar Cross Section σ Given at Simulated Frequency
Model Rotates About Vertical Axis
Observing Radar
Angle of Climb
Nose Aspect
40 M² Level
RELATIVE POWER (db)
ANGLE

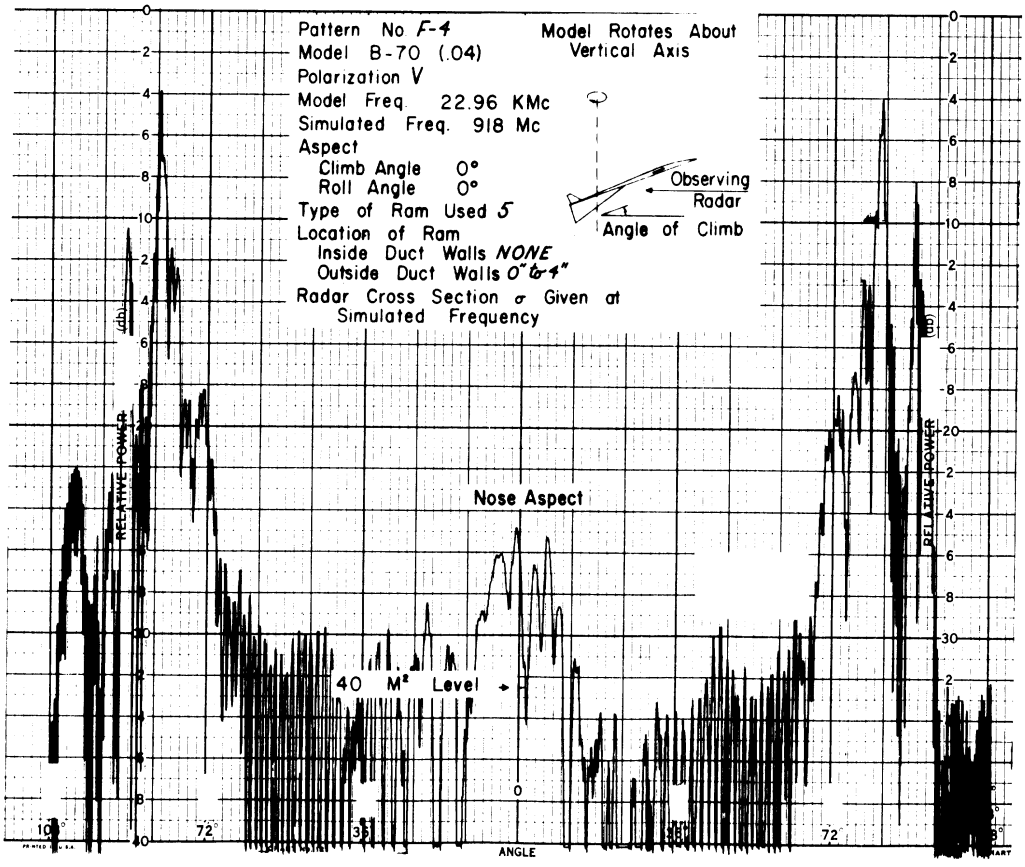
Pattern No. F-4
Model B-70 (.04)
Polarization V
Model Freq. 22.96 KMc
Simulated Freq. 918 Mc
Aspect
Climb Angle 0°
Roll Angle 0°
Type of Ram Used 5
Location of Ram
Inside Duct Walls NONE
Outside Duct Walls 0" to 4"
Radar Cross Section σ Given at Simulated Frequency
Model Rotates About Vertical Axis
Observing Radar
Angle of Climb
Nose Aspect
40 M² Level
RELATIVE POWER (db)
ANGLE

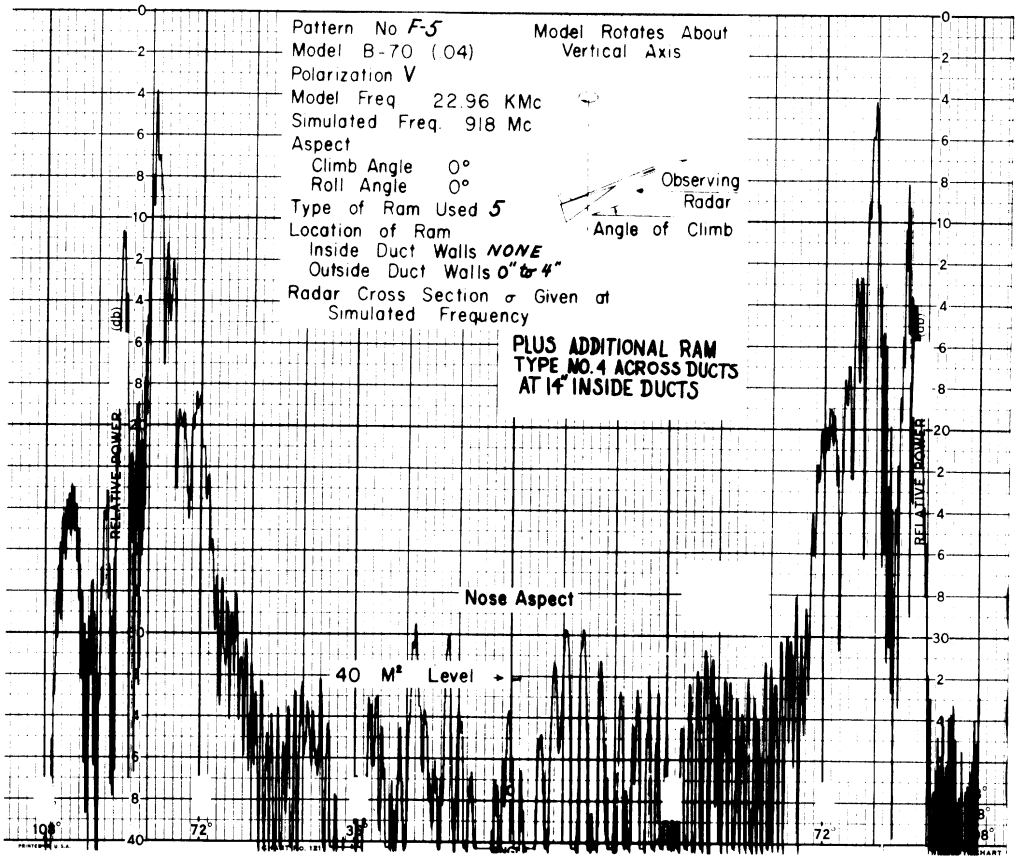
Pattern No. F-5
Model B-70 (04)
Polarization V
Model Freq. 22.96 KMc
Simulated Freq. 918 Mc
Aspect
Climb Angle 0°
Roll Angle 0°
Type of Ram Used 5
Location of Ram
Inside Duct Walls NONE
Outside Duct Walls 0" to 4"
Radar Cross Section σ Given at
Simulated Frequency
Model Rotates About
Vertical Axis
Observing
Radar
Angle of Climb
PLUS ADDITIONAL RAM
TYPE NO. 4 ACROSS DUCTS
AT 14" INSIDE DUCTS
RELATIVE POWER (db)
Nose Aspect
40 M² Level
72°
72°

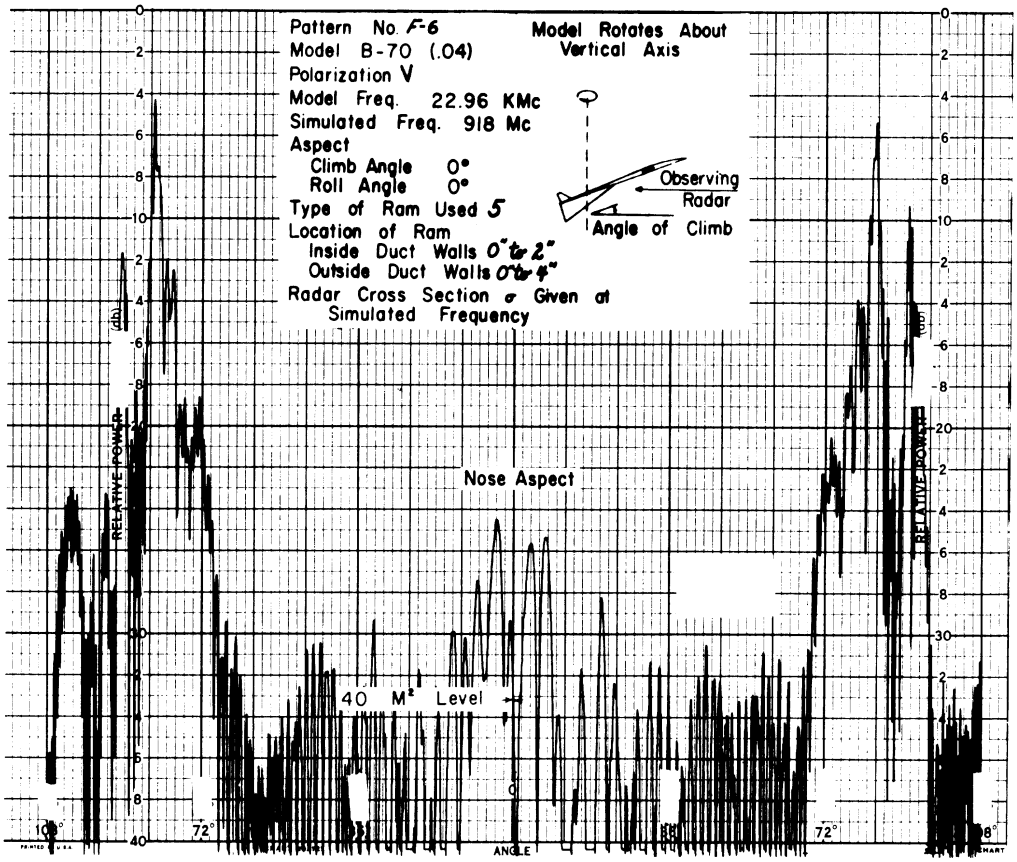
Pattern No. F-6
Model B-70 (.04)
Polarization V
Model Freq. 22.96 KMc
Simulated Freq. 918 Mc
Aspect
Climb Angle 0°
Roll Angle 0°
Type of Ram Used 5
Location of Ram
Inside Duct Walls 0" to 2"
Outside Duct Walls 0" to 4"
Radar Cross Section σ Given at
Simulated Frequency
Model Rotates About
Vertical Axis
Observing
Radar
Angle of Climb
RELATIVE POWER (db)
Nose Aspect
40 M² Level
72°
72°
ANGLE

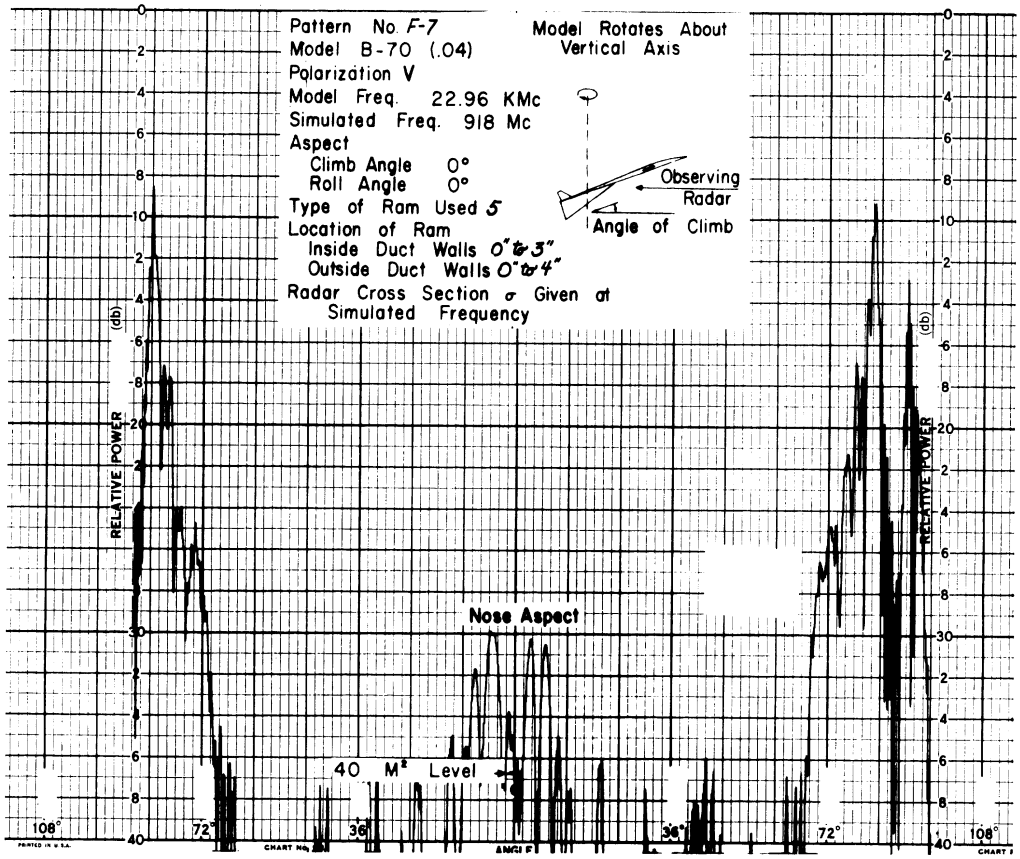
Pattern No. F-7
Model B-70 (.04)
Polarization V
Model Freq. 22.96 KMc
Simulated Freq. 918 Mc
Aspect
Climb Angle 0°
Roll Angle 0°
Type of Ram Used 5
Location of Ram
Inside Duct Walls 0" to 3"
Outside Duct Walls 0" to 4"
Radar Cross Section σ Given at Simulated Frequency
Model Rotates About Vertical Axis
Observing Radar
Angle of Climb
RELATIVE POWER (db)
Nose Aspect
40 M² Level
108°
72°
36°

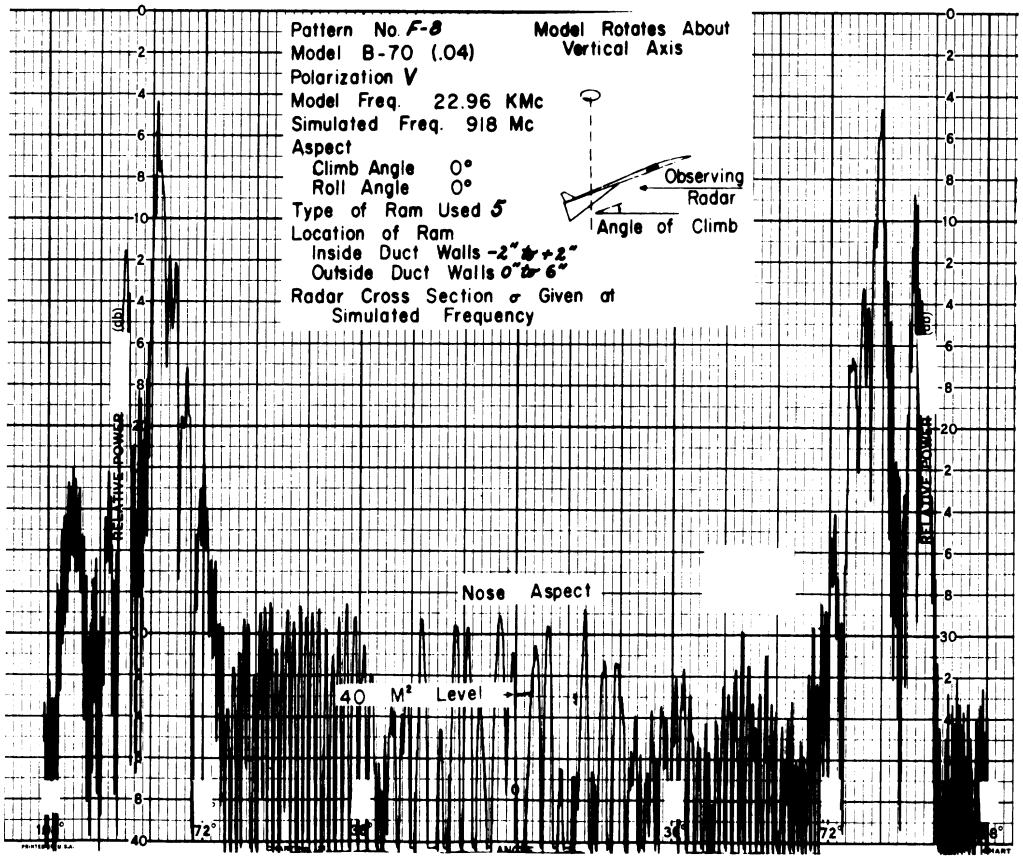
Pattern No. F-8
Model B-70 (.04)
Polarization V
Model Freq. 22.96 KMc
Simulated Freq. 918 Mc
Aspect
Climb Angle 0°
Roll Angle 0°
Type of Ram Used 5
Location of Ram
Inside Duct Walls -2" to +2"
Outside Duct Walls 0" to 6"
Radar Cross Section σ Given at Simulated Frequency
Model Rotates About Vertical Axis
Observing Radar
Angle of Climb
RELATIVE POWER (db)
Nose Aspect
40 M² Level
72°
36°

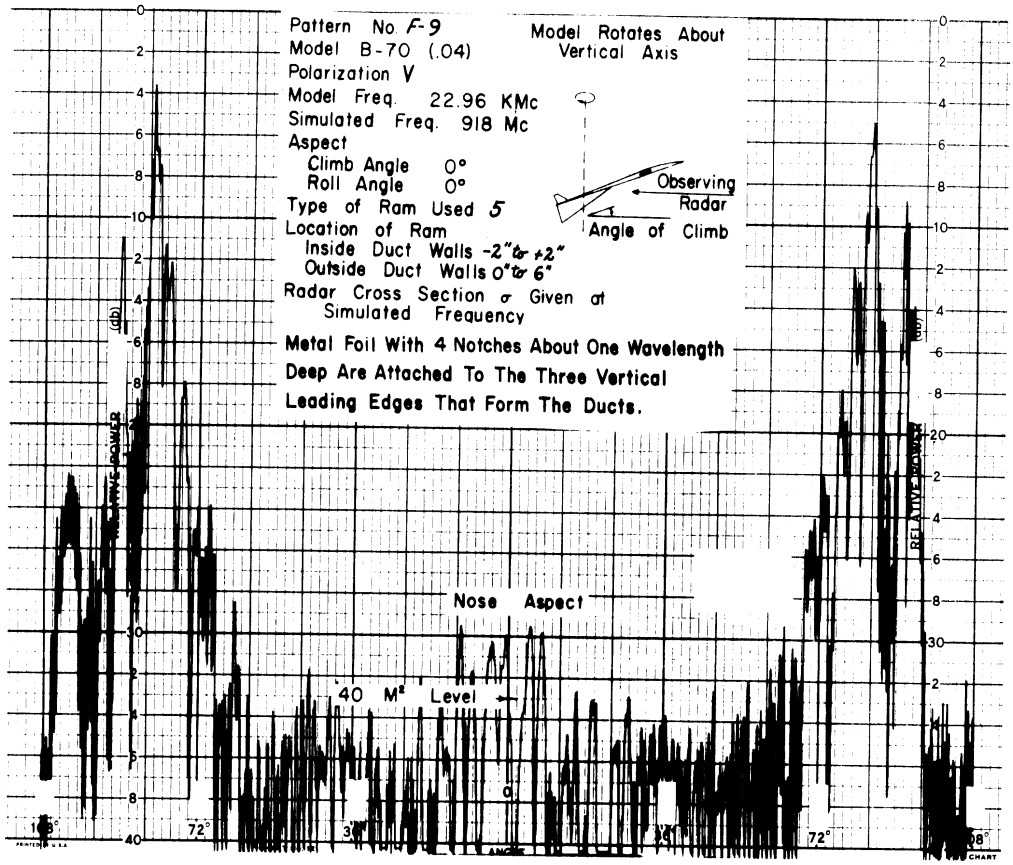
Pattern No. F-9
Model B-70 (.04)
Polarization V
Model Freq. 22.96 KMc
Simulated Freq. 918 Mc
Aspect
Climb Angle 0°
Roll Angle 0°
Type of Ram Used 5
Location of Ram
Inside Duct Walls -2" to +2"
Outside Duct Walls 0" to 6"
Radar Cross Section σ Given at Simulated Frequency
Metal Foil With 4 Notches About One Wavelength Deep Are Attached To The Three Vertical Leading Edges That Form The Ducts.
Model Rotates About Vertical Axis
Observing Radar
Angle of Climb
Nose Aspect
40 M² Level
RELATIVE POWER (db)
ANGLE

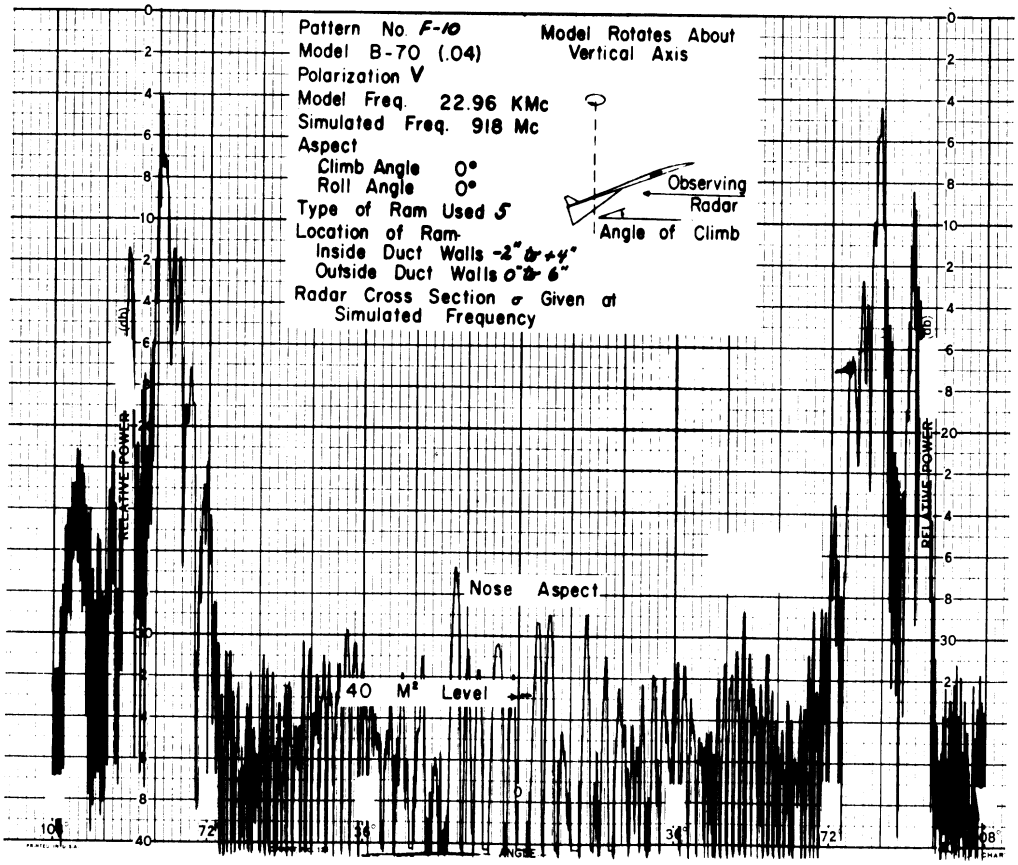
Pattern No. F-10
Model B-70 (.04)
Polarization V
Model Freq. 22.96 KMc
Simulated Freq. 918 Mc
Aspect
Climb Angle 0°
Roll Angle 0°
Type of Ram Used 5
Location of Ram
Inside Duct Walls -2" to +4"
Outside Duct Walls 0" to 6"
Radar Cross Section σ Given at Simulated Frequency
Model Rotates About Vertical Axis
Observing Radar
Angle of Climb
Nose Aspect
40 M² Level
RELATIVE POWER (db)
ANGLE

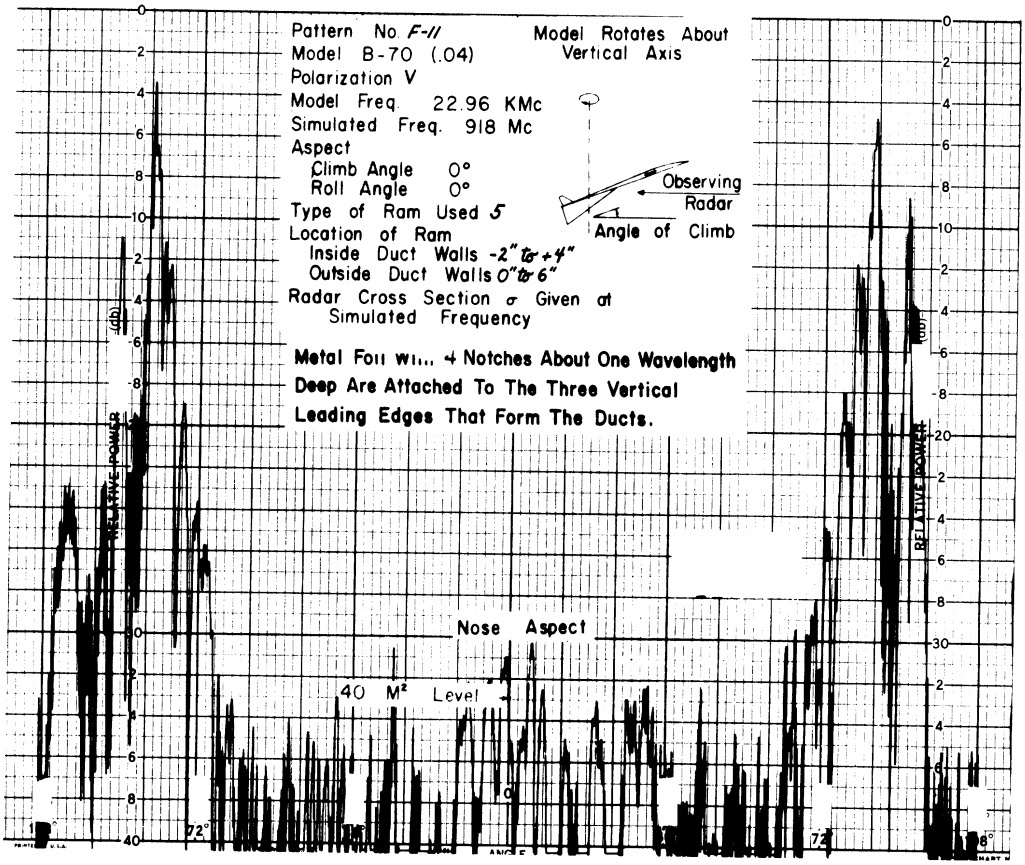
Pattern No. F-11
Model B-70 (.04)
Polarization V
Model Freq. 22.96 KMc
Simulated Freq. 918 Mc
Aspect
Climb Angle 0°
Roll Angle 0°
Type of Ram Used 5
Location of Ram
Inside Duct Walls -2" to +4"
Outside Duct Walls 0" to 6"
Radar Cross Section σ Given at Simulated Frequency
Metal Foil With 4 Notches About One Wavelength Deep Are Attached To The Three Vertical Leading Edges That Form The Ducts.
Model Rotates About Vertical Axis
Observing Radar
Angle of Climb
Nose Aspect
40 M² Level
RELATIVE POWER (db)
ANGLE

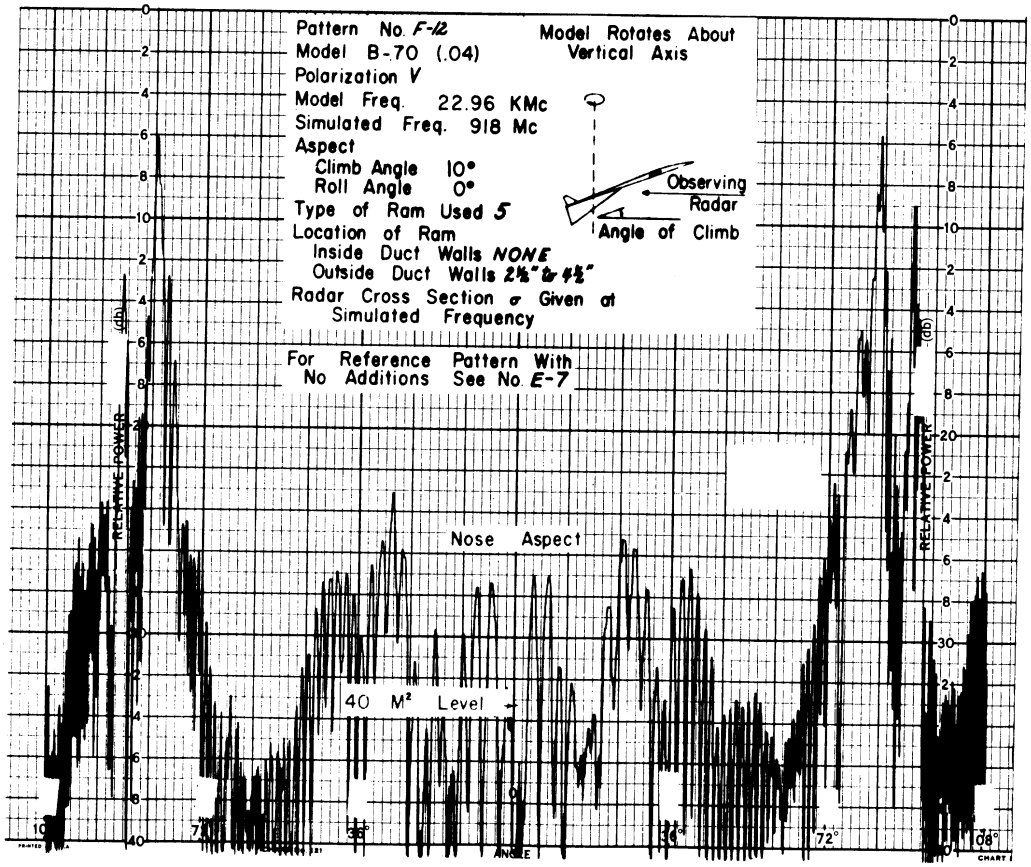
Pattern No. F-12
Model B-70 (.04)
Polarization V
Model Freq. 22.96 KMc
Simulated Freq. 918 Mc
Aspect
Climb Angle 10°
Roll Angle 0°
Type of Ram Used 5
Location of Ram
Inside Duct Walls NONE
Outside Duct Walls 2½" to 4½"
Radar Cross Section σ Given at Simulated Frequency
For Reference Pattern With No Additions See No. E-7
Model Rotates About Vertical Axis
Observing Radar
Angle of Climb
Nose Aspect
40 M² Level
RELATIVE POWER (db)
ANGLE

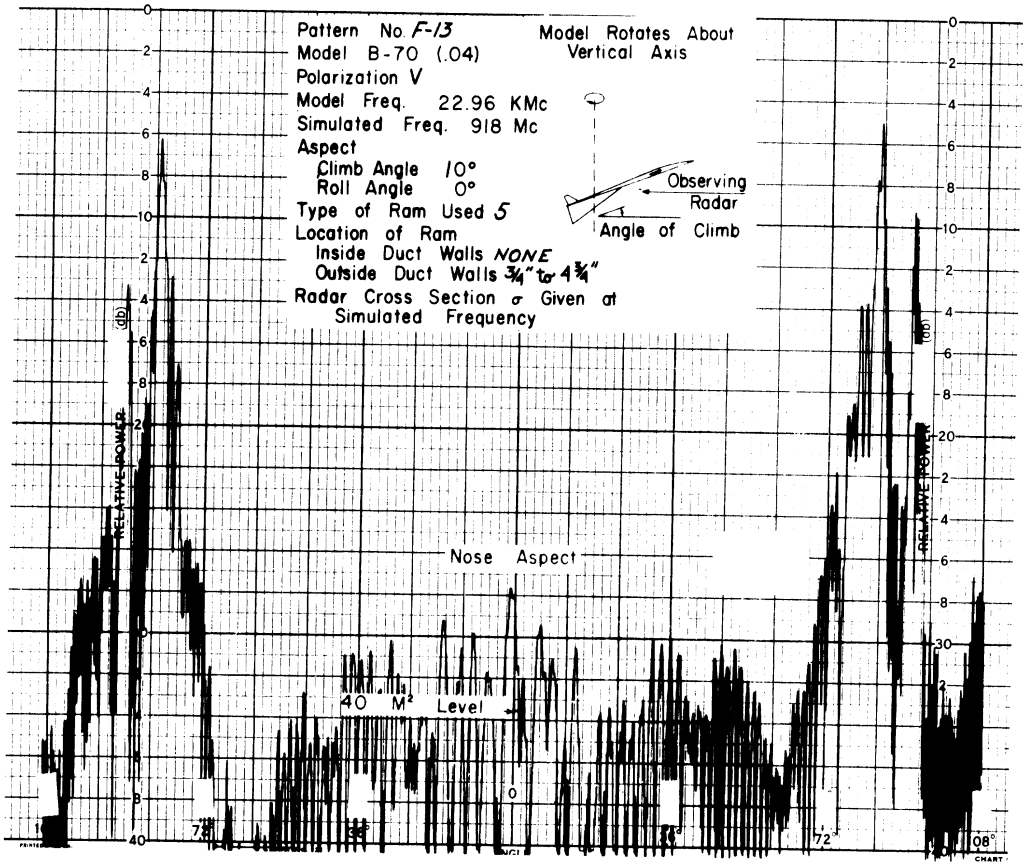
Pattern No. F-13
Model B-70 (.04)
Polarization V
Model Freq. 22.96 KMc
Simulated Freq. 918 Mc
Aspect
Climb Angle 10°
Roll Angle 0°
Type of Ram Used 5
Location of Ram
Inside Duct Walls NONE
Outside Duct Walls 3¼" to 4¾"
Radar Cross Section σ Given at
Simulated Frequency
Model Rotates About
Vertical Axis
Observing
Radar
Angle of Climb
Nose Aspect
40 M² Level
RELATIVE POWER
db
72°
108°

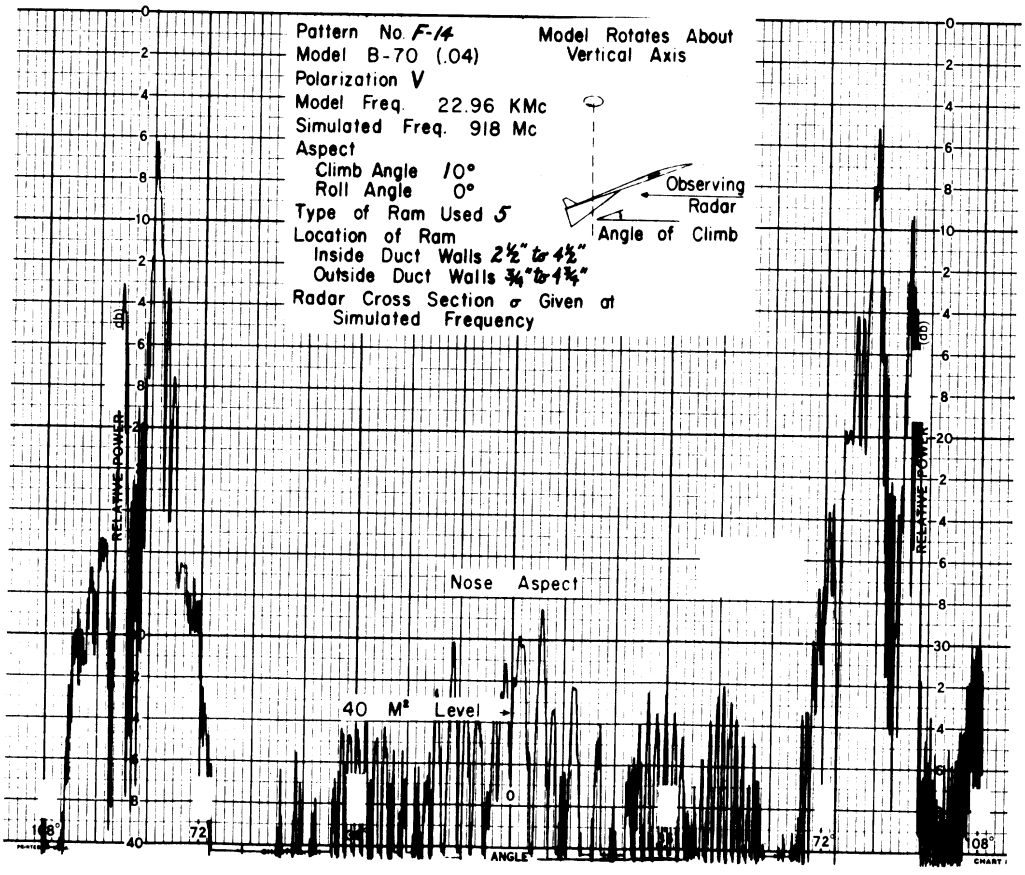
Pattern No. F-14
Model B-70 (.04)
Polarization V
Model Freq. 22.96 KMc
Simulated Freq. 918 Mc
Aspect
Climb Angle 10°
Roll Angle 0°
Type of Ram Used 5
Location of Ram
Inside Duct Walls 2½" to 4½"
Outside Duct Walls ¾" to 1¾"
Radar Cross Section σ Given at
Simulated Frequency
Model Rotates About
Vertical Axis
Observing
Radar
Angle of Climb
Nose Aspect
40 M² Level
RELATIVE POWER
db
72°
108°
ANGLE

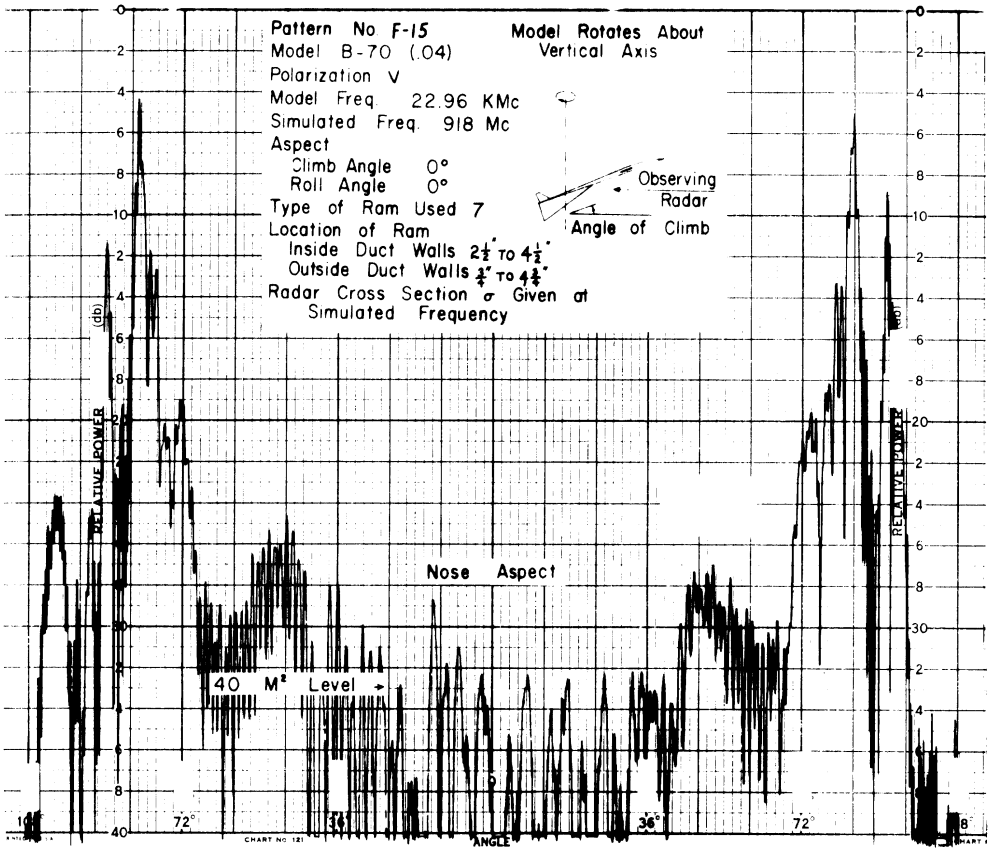
Pattern No F-15
Model B-70 (.04)
Polarization V
Model Freq. 22.96 KMc
Simulated Freq. 918 Mc
Aspect
Climb Angle 0°
Roll Angle 0°
Type of Ram Used 7
Location of Ram
Inside Duct Walls 2½" to 4½"
Outside Duct Walls ¾" to 4¾"
Radar Cross Section σ Given at
Simulated Frequency
Model Rotates About
Vertical Axis
Observing
Radar
Angle of Climb
Nose Aspect
40 M² Level
RELATIVE POWER
(db)
ANGLE
72°
36°

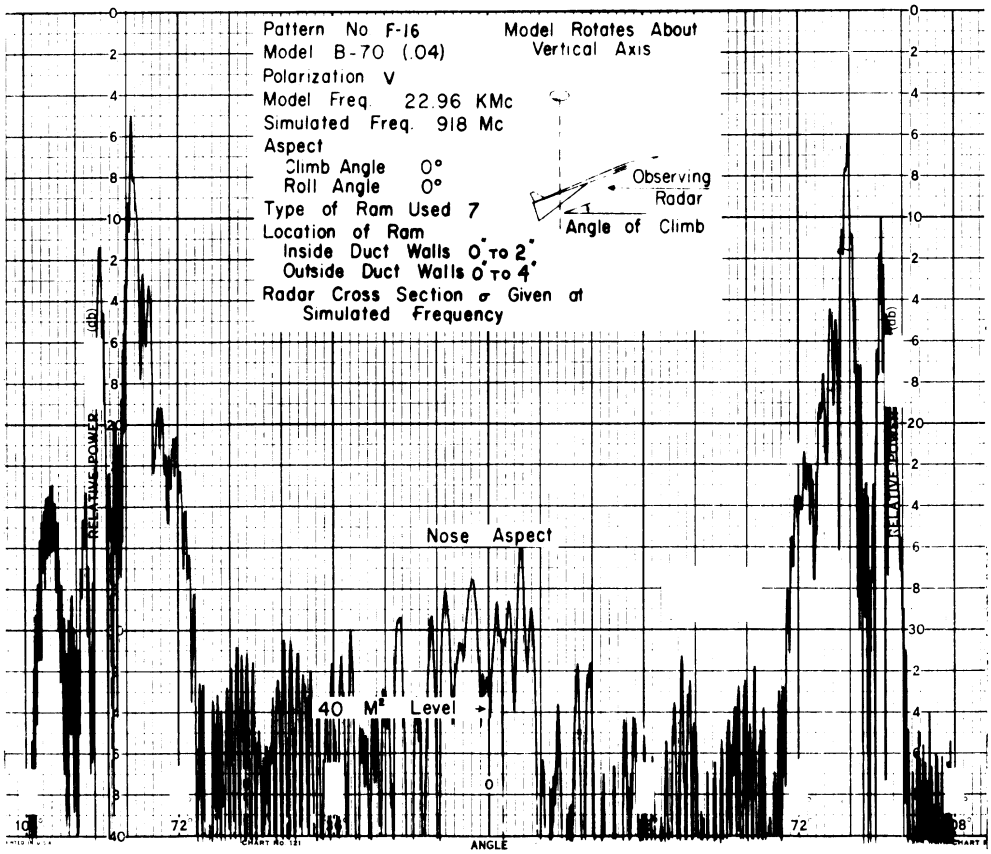
Pattern No F-16
Model B-70 (.04)
Polarization V
Model Freq. 22.96 KMc
Simulated Freq. 918 Mc
Aspect
Climb Angle 0°
Roll Angle 0°
Type of Ram Used 7
Location of Ram
Inside Duct Walls 0" to 2"
Outside Duct Walls 0" to 4"
Radar Cross Section σ Given at
Simulated Frequency
Model Rotates About
Vertical Axis
Observing
Radar
Angle of Climb
Nose Aspect
40 M² Level
RELATIVE POWER
(db)
ANGLE
72°

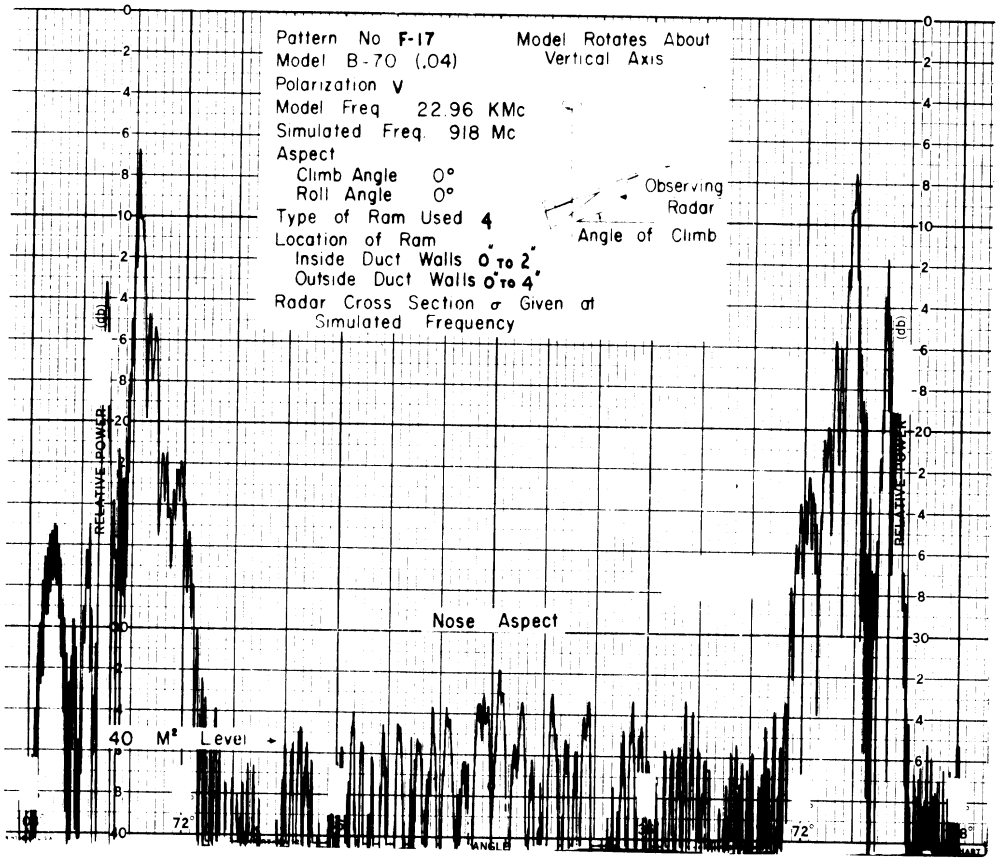
Pattern No F-17
Model B-70 (.04)
Polarization V
Model Freq 22.96 KMc
Simulated Freq. 918 Mc
Aspect
Climb Angle 0°
Roll Angle 0°
Type of Ram Used 4
Location of Ram
Inside Duct Walls 0" To 2"
Outside Duct Walls 0" To 4"
Radar Cross Section σ Given at Simulated Frequency
Model Rotates About Vertical Axis
Observing Radar
Angle of Climb
Nose Aspect
40 M² Level
RELATIVE POWER (db)
72°

4.3.7. Series G: Horizontal Polarization, Magnetic RAM, 918 Mc

This series is a continuation of the 918 Mc study started in the E group. The polarization is horizontal and the RAM is the magnetic material with a reflectivity of -9 db.

Patterns G-2 through G-7 show results for 0^{o} climb; first, for the three NAA preferred locations, and then for additional RAM on the inner duct wall. The last two patterns show the average level to be well below 40 m^2.

Patterns G-8 through G-14 show the results for the same conditions as above, but at 10^{o} climb angle. The average level of the cross section for the RAM locations in the last three patterns is well below 40 m^2.

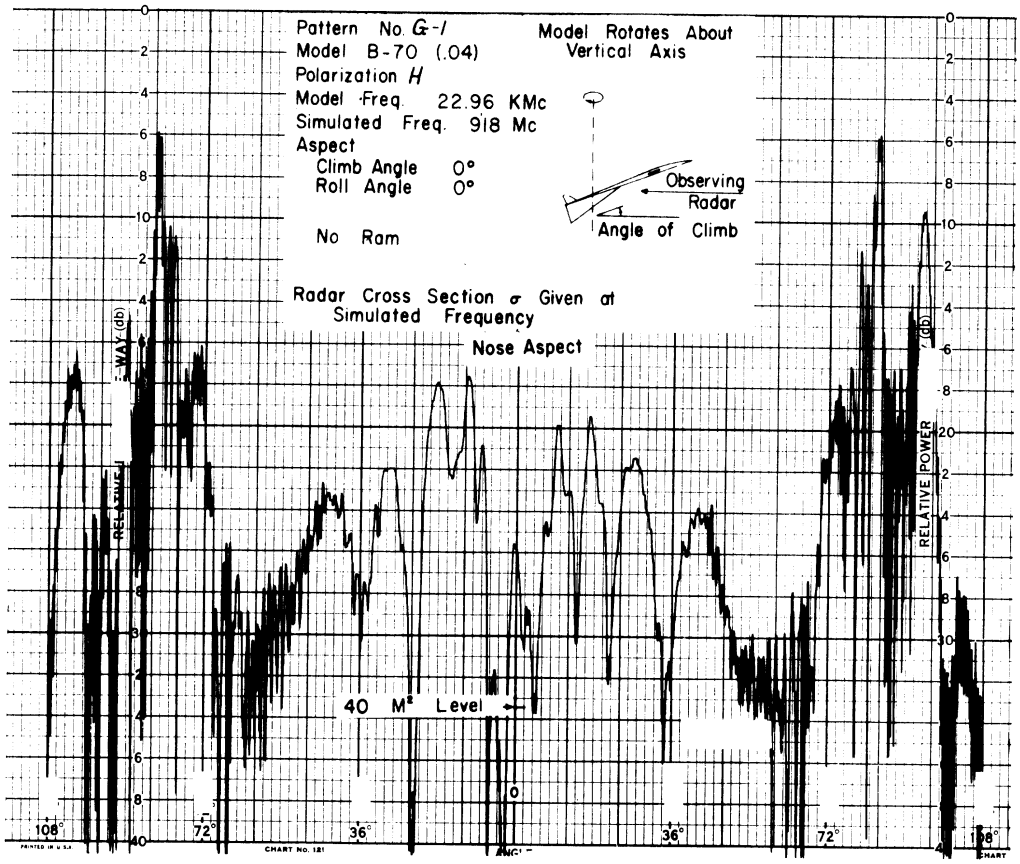
Pattern No. G-1
Model B-70 (.04)
Polarization H
Model Freq. 22.96 KMc
Simulated Freq. 918 Mc
Aspect
Climb Angle 0°
Roll Angle 0°
No Ram
Radar Cross Section σ Given at Simulated Frequency
Model Rotates About Vertical Axis
Observing Radar
Angle of Climb
Nose Aspect
40 M² Level
RELATIVE POWER (db)
108°
72°
36°
0
36°
72°
108°

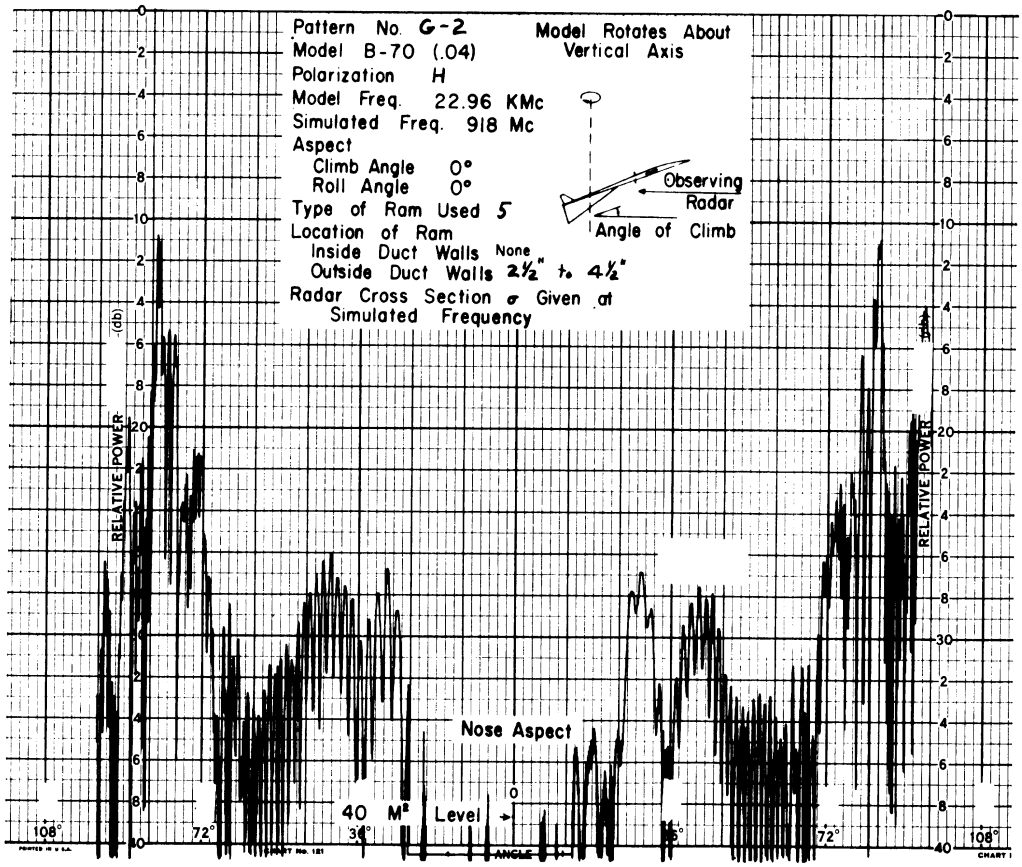
Pattern No. G-2
Model B-70 (.04)
Polarization H
Model Freq. 22.96 KMc
Simulated Freq. 918 Mc
Aspect
Climb Angle 0°
Roll Angle 0°
Type of Ram Used 5
Location of Ram
Inside Duct Walls None
Outside Duct Walls 2½" to 4½"
Radar Cross Section σ Given at Simulated Frequency
Model Rotates About Vertical Axis
Observing Radar
Angle of Climb
Nose Aspect
40 M² Level
RELATIVE POWER (db)
108°
72°
36°
0
36°
72°
108°

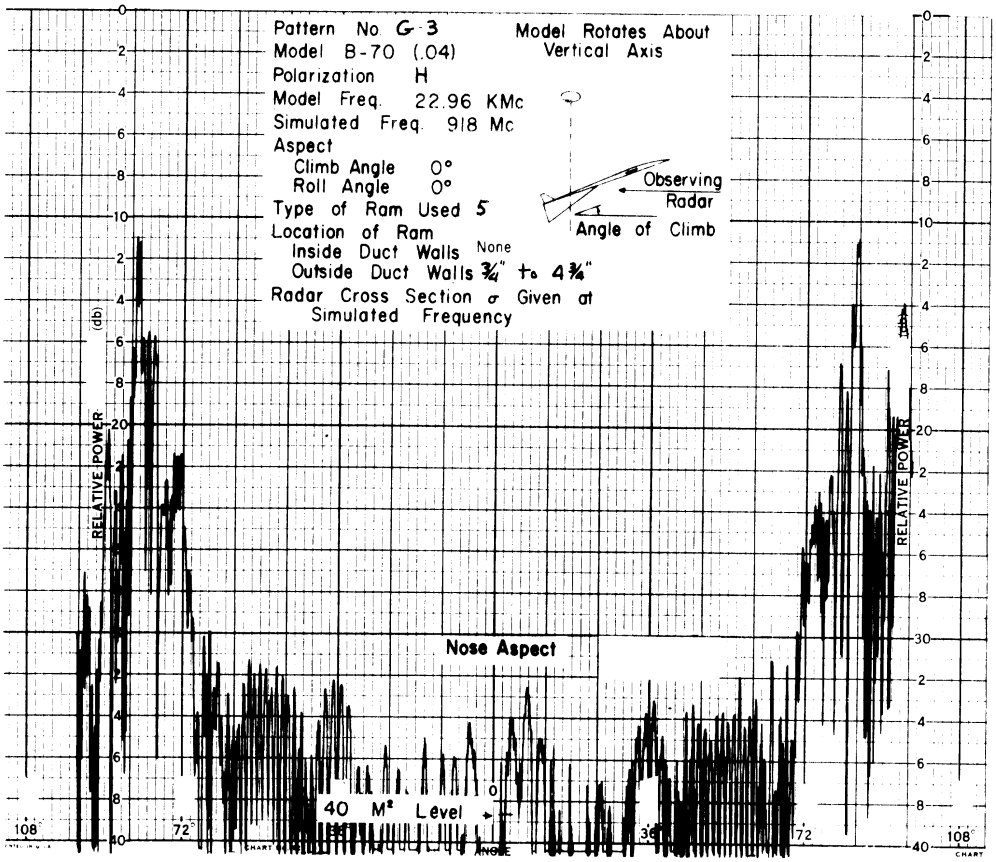
Pattern No. G-3
Model B-70 (.04)
Polarization H
Model Freq. 22.96 KMc
Simulated Freq. 918 Mc
Aspect
Climb Angle 0°
Roll Angle 0°
Type of Ram Used 5
Location of Ram
Inside Duct Walls None
Outside Duct Walls 3/4" to 4 3/4"
Radar Cross Section σ Given at
Simulated Frequency
Model Rotates About
Vertical Axis
Observing
Radar
Angle of Climb
RELATIVE POWER (db)
Nose Aspect
40 M² Level
108°
72°
36°
0
ANGLE
CHART

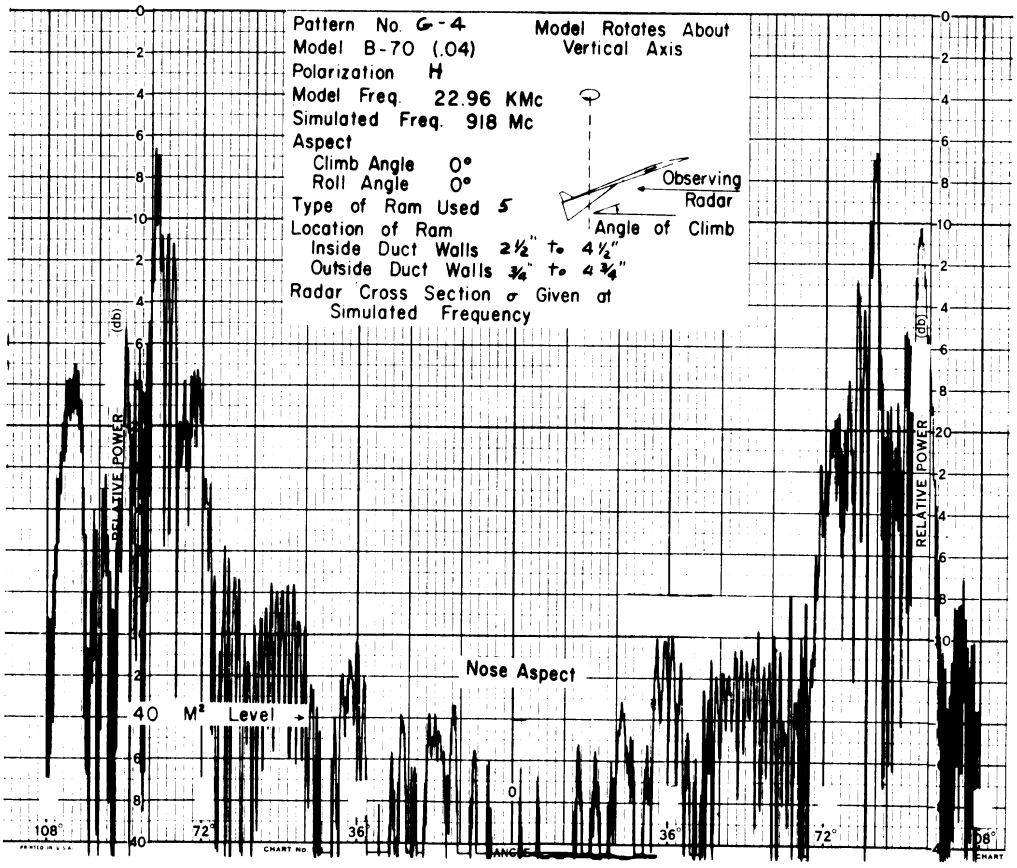
Pattern No. G-4
Model B-70 (.04)
Polarization H
Model Freq. 22.96 KMc
Simulated Freq. 918 Mc
Aspect
Climb Angle 0°
Roll Angle 0°
Type of Ram Used 5
Location of Ram
Inside Duct Walls 2 1/2" to 4 1/2"
Outside Duct Walls 3/4" to 4 3/4"
Radar Cross Section σ Given at
Simulated Frequency
Model Rotates About
Vertical Axis
Observing
Radar
Angle of Climb
RELATIVE POWER (db)
Nose Aspect
40 M² Level
108°
72°
36°
0
ANGLE
CHART

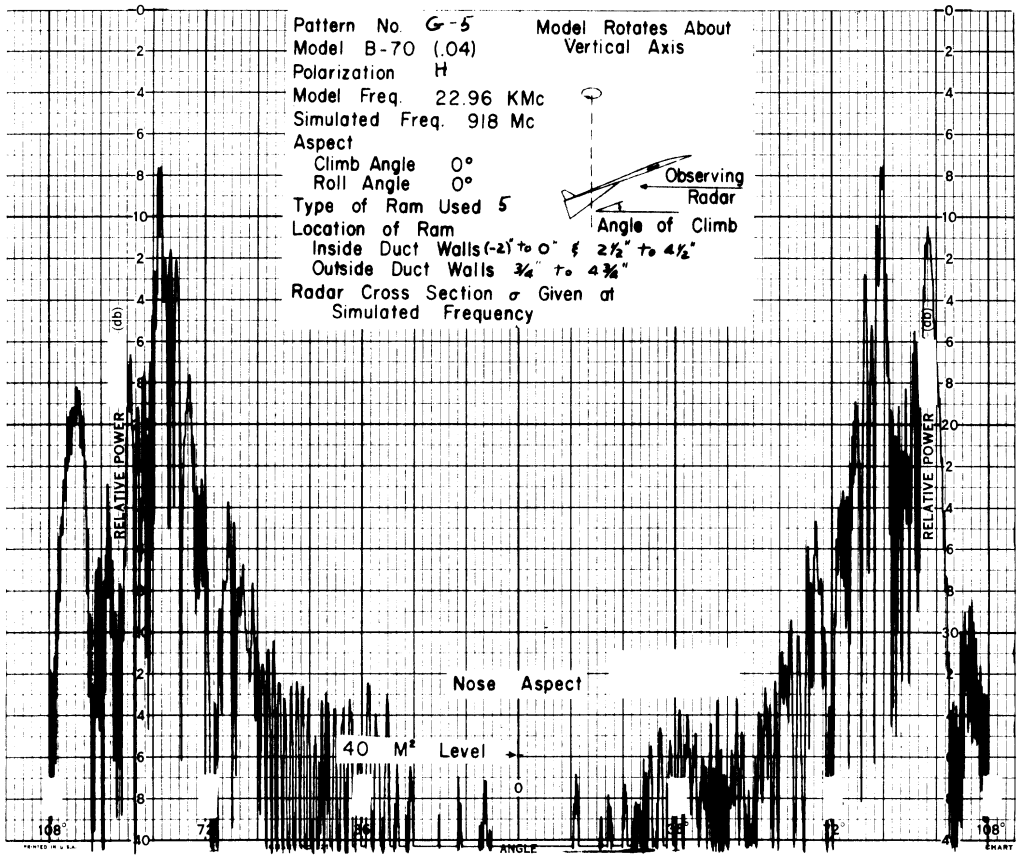
Pattern No. G-5
Model B-70 (.04)
Polarization H
Model Freq. 22.96 KMc
Simulated Freq. 918 Mc
Aspect
Climb Angle 0°
Roll Angle 0°
Type of Ram Used 5
Location of Ram
Inside Duct Walls (-2)" to 0" & 2½" to 4½"
Outside Duct Walls ¾" to 4¾"
Radar Cross Section σ Given at
Simulated Frequency
Model Rotates About
Vertical Axis
Observing
Radar
Angle of Climb
RELATIVE POWER (db)
Nose Aspect
40 M² Level
108°
72°
36°
0
ANGLE

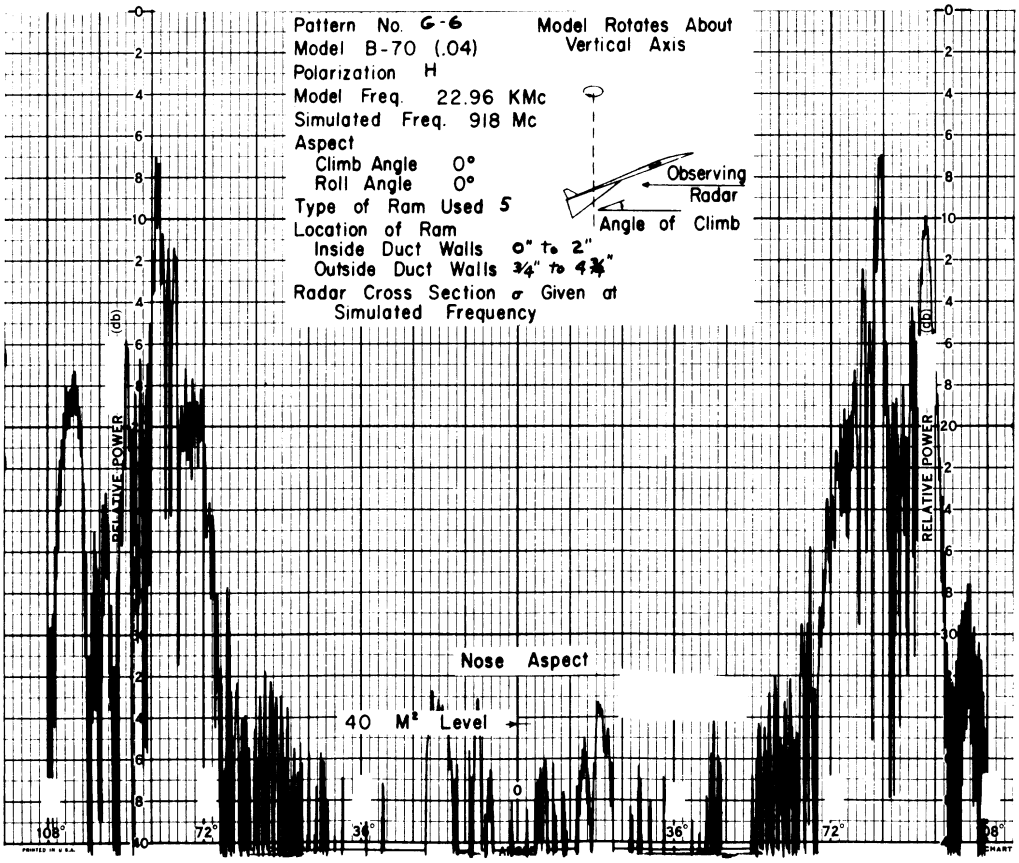
Pattern No. G-6
Model B-70 (.04)
Polarization H
Model Freq. 22.96 KMc
Simulated Freq. 918 Mc
Aspect
Climb Angle 0°
Roll Angle 0°
Type of Ram Used 5
Location of Ram
Inside Duct Walls 0" to 2"
Outside Duct Walls ¾" to 4¾"
Radar Cross Section σ Given at
Simulated Frequency
Model Rotates About
Vertical Axis
Observing
Radar
Angle of Climb
RELATIVE POWER (db)
Nose Aspect
40 M² Level
108°
72°
36°
0

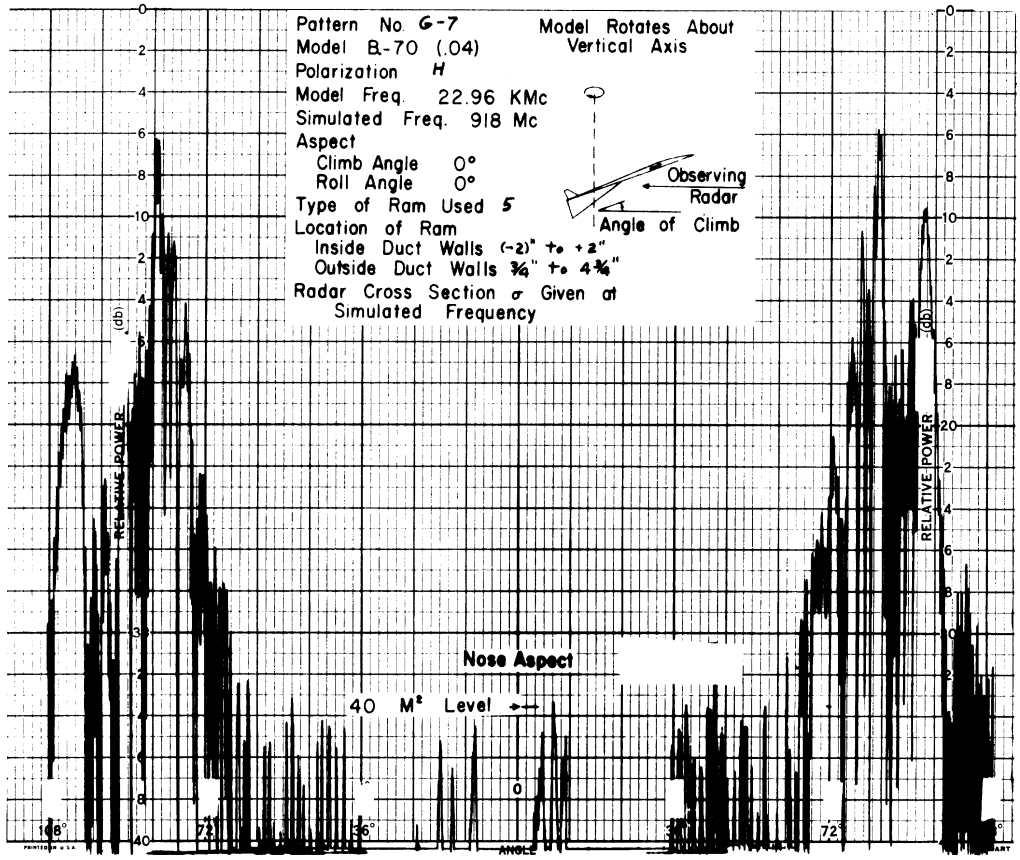
Pattern No. G-7
Model B-70 (.04)
Polarization H
Model Freq. 22.96 KMc
Simulated Freq. 918 Mc
Aspect
Climb Angle 0°
Roll Angle 0°
Type of Ram Used 5
Location of Ram
Inside Duct Walls (-2)" to +2"
Outside Duct Walls 3/4" to 4 3/4"
Radar Cross Section σ Given at Simulated Frequency
Model Rotates About Vertical Axis
Observing Radar
Angle of Climb
Nose Aspect
40 M² Level
RELATIVE POWER (db)
ANGLE

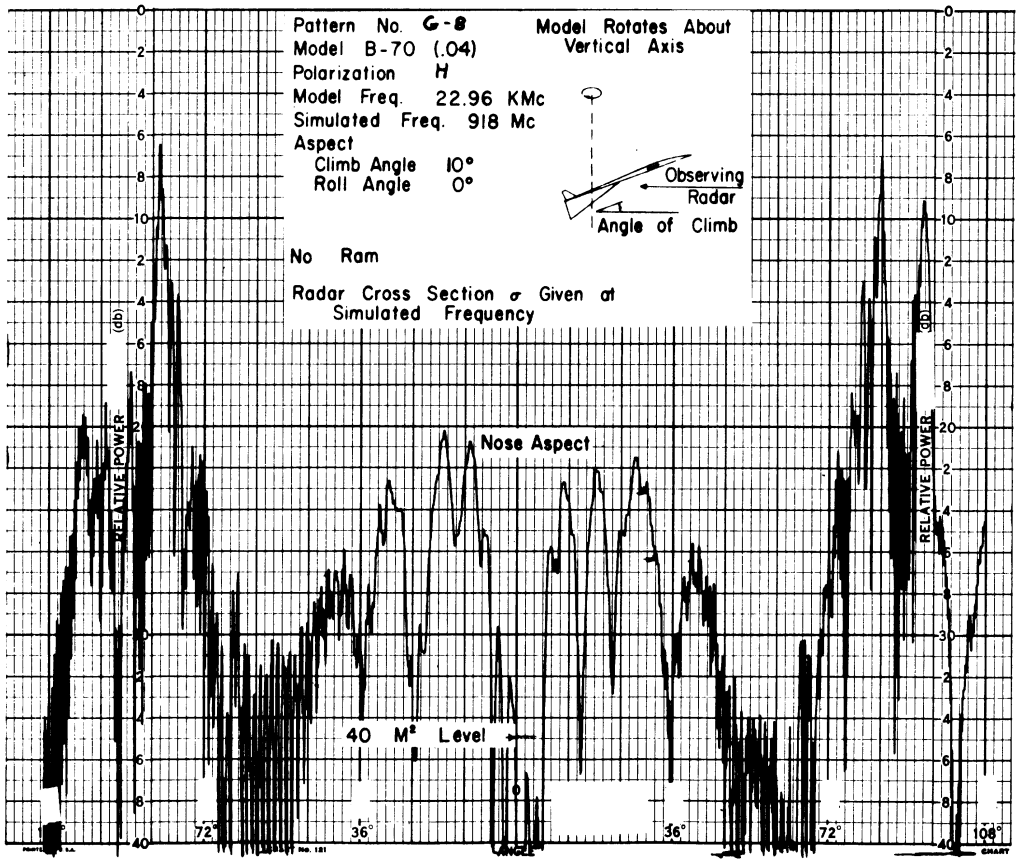
Pattern No. G-8
Model B-70 (.04)
Polarization H
Model Freq. 22.96 KMc
Simulated Freq. 918 Mc
Aspect
Climb Angle 10°
Roll Angle 0°
No Ram
Radar Cross Section σ Given at Simulated Frequency
Model Rotates About Vertical Axis
Observing Radar
Angle of Climb
Nose Aspect
40 M² Level
RELATIVE POWER (db)
ANGLE

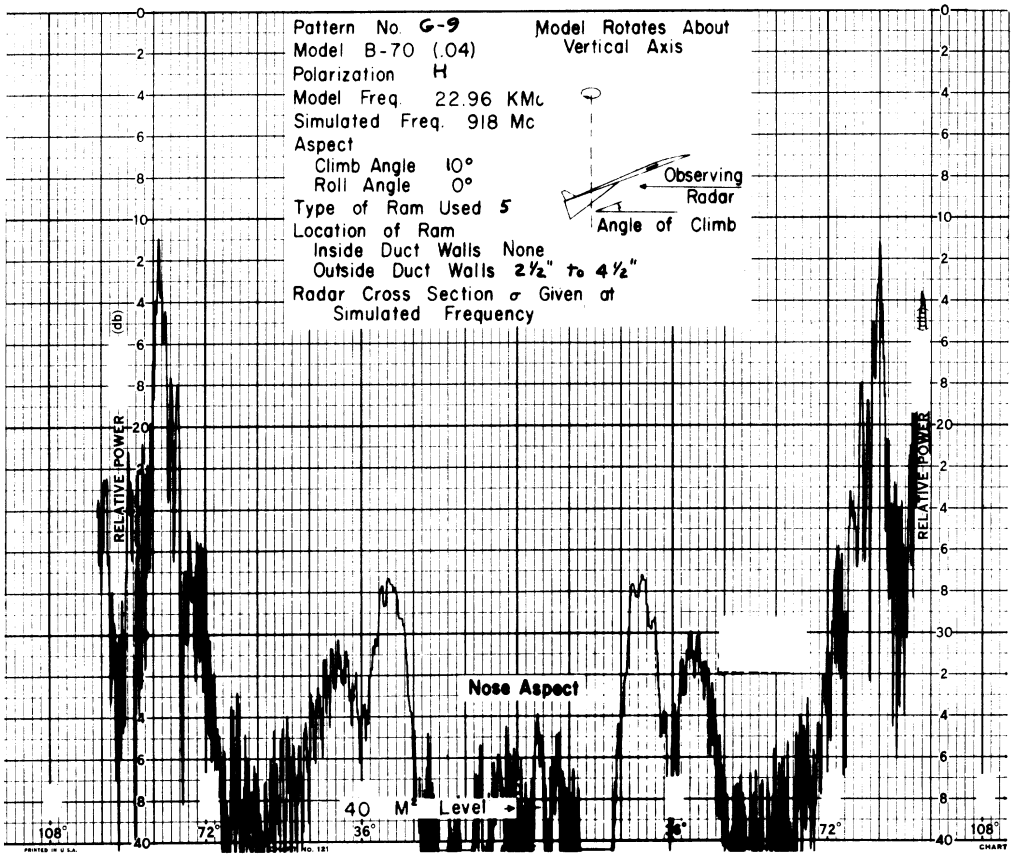
Pattern No. G-9
Model B-70 (.04)
Polarization H
Model Freq. 22.96 KMc
Simulated Freq. 918 Mc
Aspect
Climb Angle 10°
Roll Angle 0°
Type of Ram Used 5
Location of Ram
Inside Duct Walls None
Outside Duct Walls 2½" to 4½"
Radar Cross Section σ Given at Simulated Frequency
Model Rotates About Vertical Axis
Observing Radar
Angle of Climb
RELATIVE POWER (db)
Nose Aspect
40 M² Level
108°
72°
36°

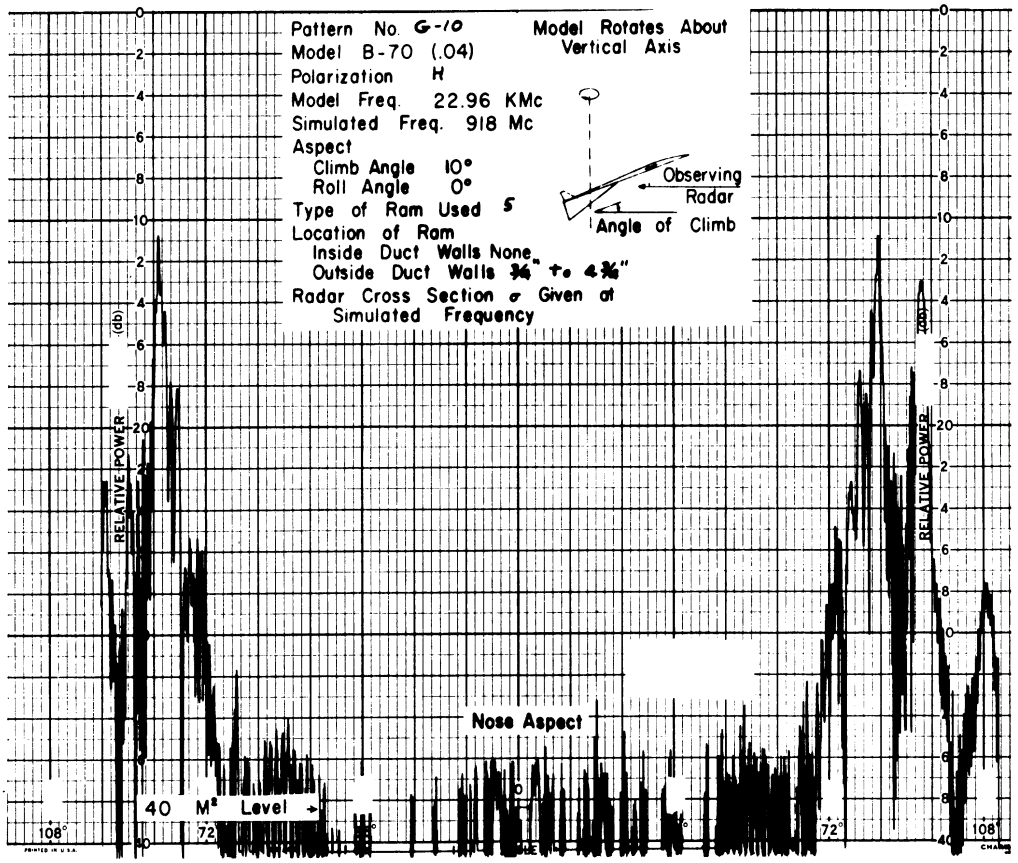
Pattern No. G-10
Model B-70 (.04)
Polarization H
Model Freq. 22.96 KMc
Simulated Freq. 918 Mc
Aspect
Climb Angle 10°
Roll Angle 0°
Type of Ram Used 5
Location of Ram
Inside Duct Walls None
Outside Duct Walls ¾" to 4¾"
Radar Cross Section σ Given at Simulated Frequency
Model Rotates About Vertical Axis
Observing Radar
Angle of Climb
RELATIVE POWER (db)
Nose Aspect
40 M² Level
108°
72°

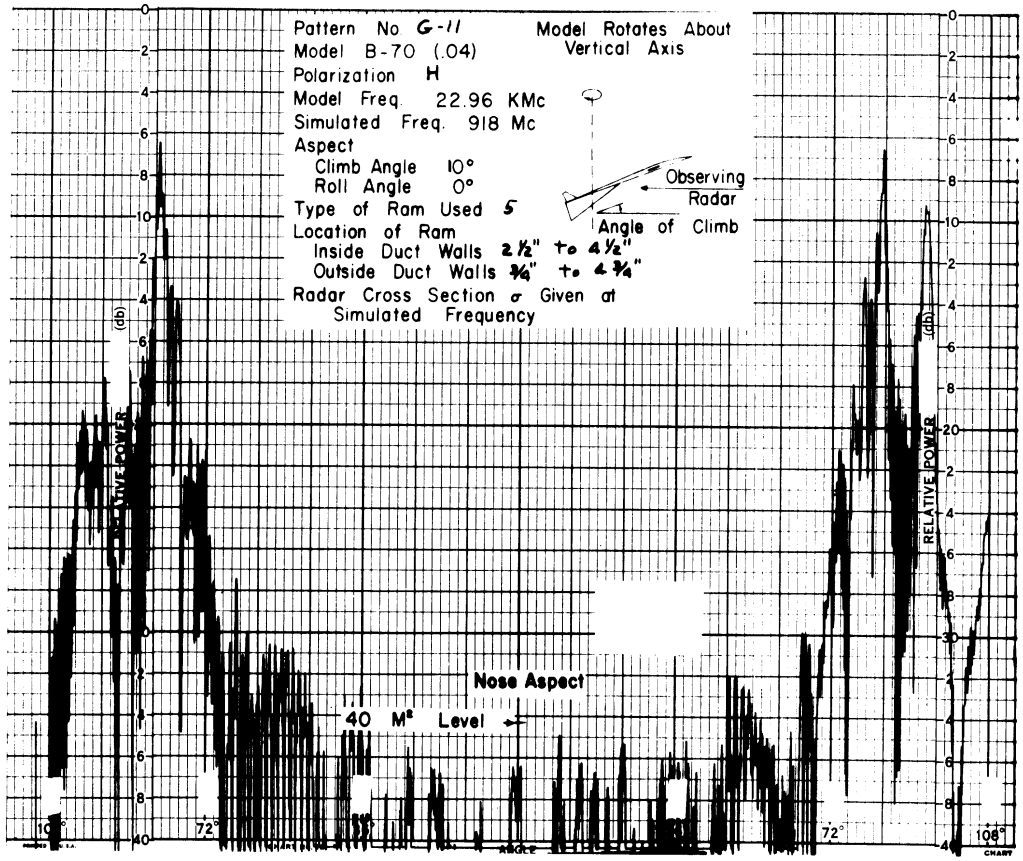
Pattern No. G-11
Model B-70 (.04)
Polarization H
Model Freq. 22.96 KMc
Simulated Freq. 918 Mc
Aspect
Climb Angle 10°
Roll Angle 0°
Type of Ram Used 5
Location of Ram
Inside Duct Walls 2 1/2" to 4 1/2"
Outside Duct Walls 3/4" to 4 3/4"
Radar Cross Section σ Given at
Simulated Frequency
Model Rotates About
Vertical Axis
Observing
Radar
Angle of Climb
RELATIVE POWER (db)
Nose Aspect
40 M² Level
10°
72°
108°

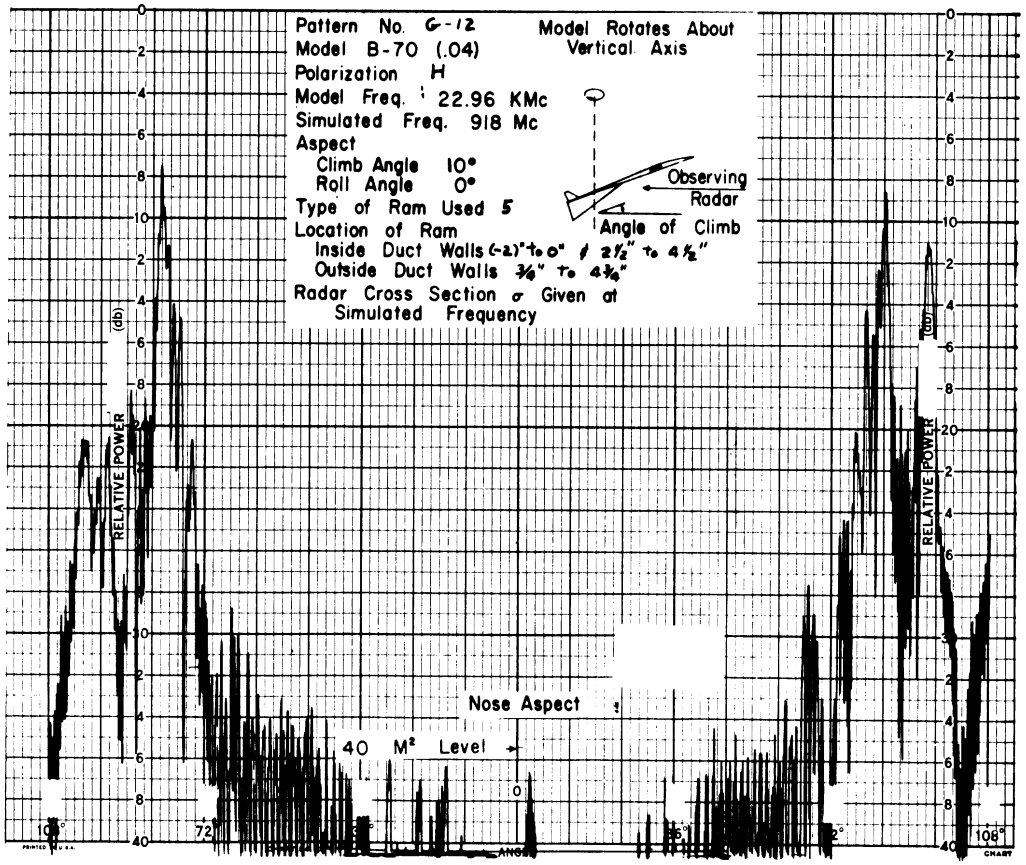
Pattern No. G-12
Model B-70 (.04)
Polarization H
Model Freq. 22.96 KMc
Simulated Freq. 918 Mc
Aspect
Climb Angle 10°
Roll Angle 0°
Type of Ram Used 5
Location of Ram
Inside Duct Walls (-2)° to 0° & 2 1/2" to 4 1/2"
Outside Duct Walls 3/4" to 4 3/4"
Radar Cross Section σ Given at
Simulated Frequency
Model Rotates About
Vertical Axis
Observing
Radar
Angle of Climb
RELATIVE POWER (db)
Nose Aspect
40 M² Level
10°
72°
108°

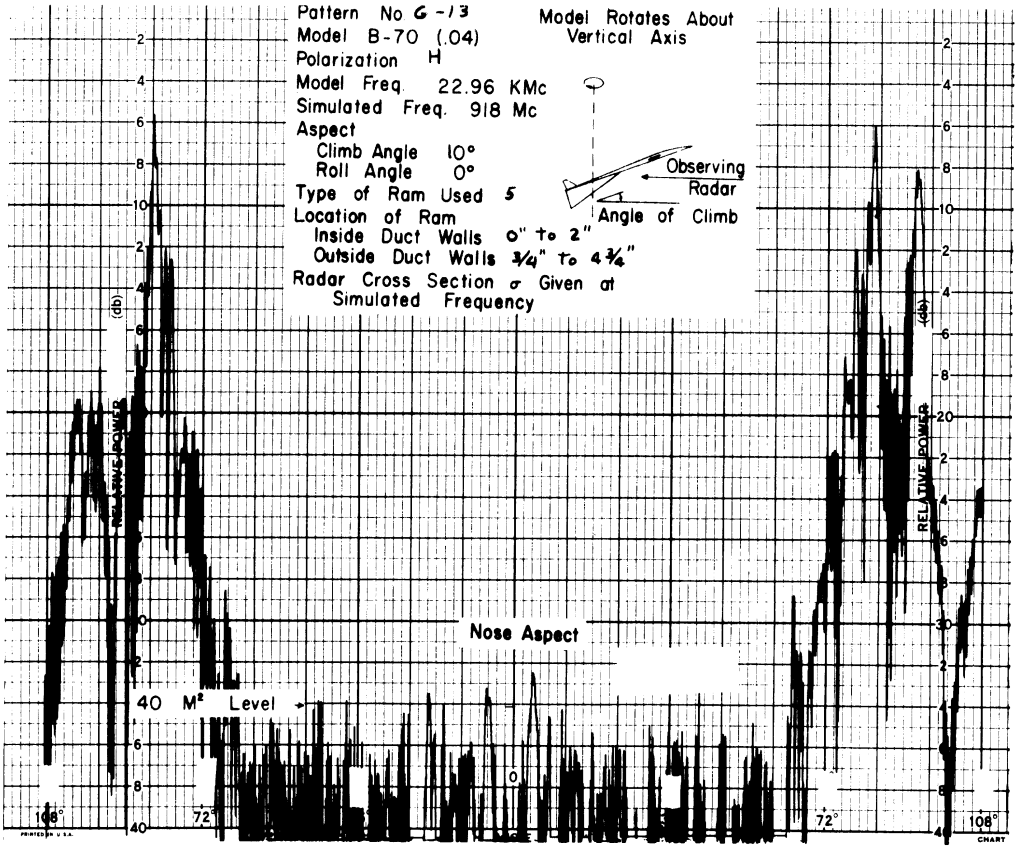
Pattern No G-13
Model B-70 (.04)
Polarization H
Model Freq. 22.96 KMc
Simulated Freq. 918 Mc
Aspect
Climb Angle 10°
Roll Angle 0°
Type of Ram Used 5
Location of Ram
Inside Duct Walls 0" to 2"
Outside Duct Walls 3/4" to 4 3/4"
Radar Cross Section σ Given at
Simulated Frequency
Model Rotates About
Vertical Axis
Observing
Radar
Angle of Climb
Nose Aspect
40 M² Level
RELATIVE POWER (db)
108°
72°
0
CHART

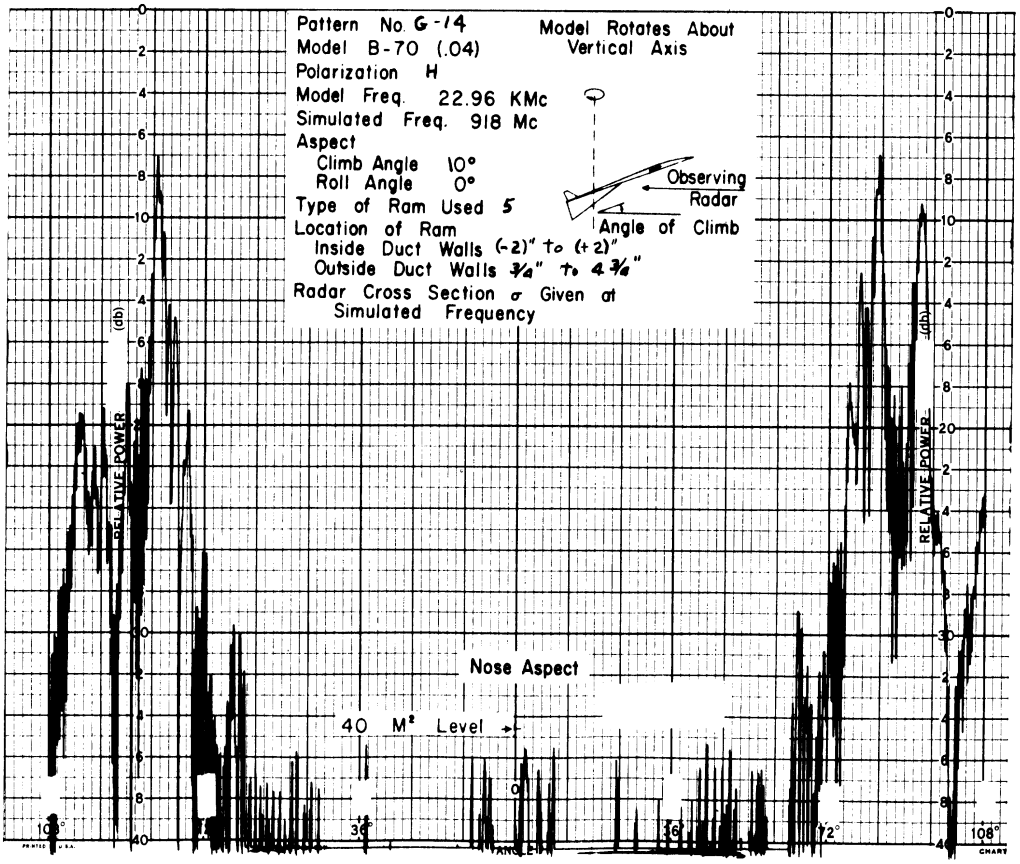
Pattern No G-14
Model B-70 (.04)
Polarization H
Model Freq. 22.96 KMc
Simulated Freq. 918 Mc
Aspect
Climb Angle 10°
Roll Angle 0°
Type of Ram Used 5
Location of Ram
Inside Duct Walls (-2)" to (+2)"
Outside Duct Walls 3/4" to 4 3/4"
Radar Cross Section σ Given at
Simulated Frequency
Model Rotates About
Vertical Axis
Observing
Radar
Angle of Climb
Nose Aspect
40 M² Level
RELATIVE POWER (db)
108°
72°
36°
0
ANGLE
CHART

4.3.8. Series H: Effect of Increased Climb Angle, 459 Mc

This group of patterns is presented for the sole purpose of showing the behavior at climb angles of 10^{o}, 20^{o} and 30^{o}. When using the 8 foot model (0.04 scale) it was not feasible to work at climb angles of more than 10^{o}, and consequently, for this series, the 4 foot model (0.02 scale) was used. The measurements were made with vertical polarization at a simulated frequency of 459 Mc. Four standard patterns with no RAM are shown for climb angles of 0^{o}, 10^{o}, 20^{o} and 30^{o}. The asymmetry in the lobes at $\pm$ 16^{o} (see Pattern H-1) was attributed to asymmetry in the ducts of the 2 foot model, and was verified by measurements made with the model inverted and by measuring the ducts only, both upright and inverted. An inspection of the model revealed a slight difference in the duct widths near the narrowest point.

Patterns H-2, H-4, H-6 and H-8 show results with RAM on both the duct walls from 0" to 2" (corresponding, of course, to 100" strips on the full-scale aircraft). The RAM used was the resonant dielectric absorber manufactured by McMillan Laboratories (type 3).

Judging from this series of patterns and the several patterns on the 0.04 model at 10^{o}, a cross section reduction to 40 m^2 for level flight will result in a similar or better reduction at climb angles up to 30^{o} at least.

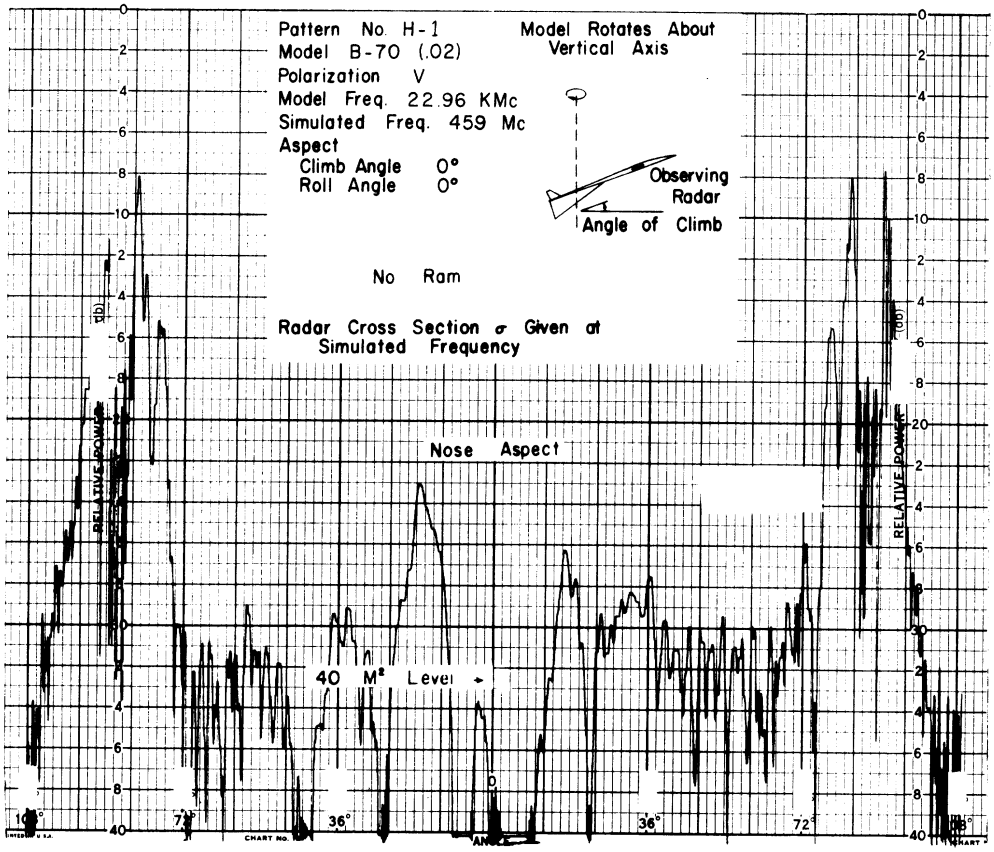
Pattern No. H-1
Model B-70 (.02)
Polarization V
Model Freq. 22.96 KMc
Simulated Freq. 459 Mc
Aspect
Climb Angle 0°
Roll Angle 0°
No Ram
Radar Cross Section σ Given at Simulated Frequency
Model Rotates About Vertical Axis
Observing Radar
Angle of Climb
Nose Aspect
40 M² Level
RELATIVE POWER (db)
ANGLE

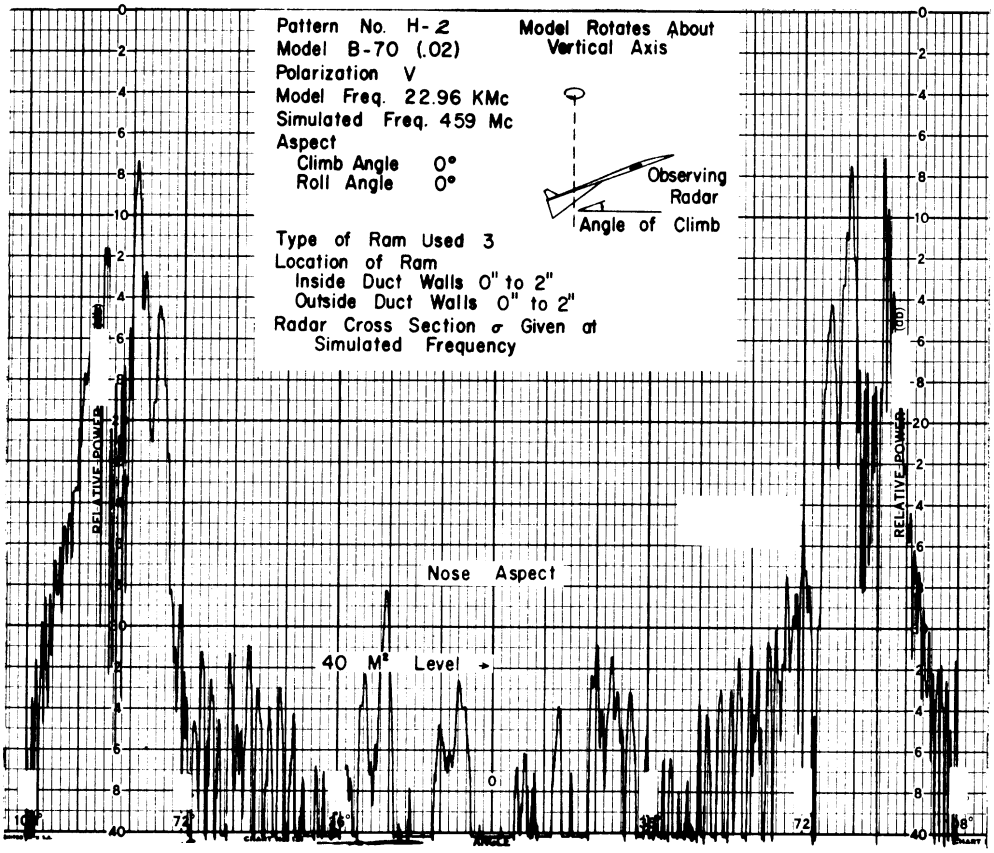
Pattern No. H-2
Model B-70 (.02)
Polarization V
Model Freq. 22.96 KMc
Simulated Freq. 459 Mc
Aspect
Climb Angle 0°
Roll Angle 0°
Type of Ram Used 3
Location of Ram
Inside Duct Walls 0" to 2"
Outside Duct Walls 0" to 2"
Radar Cross Section σ Given at Simulated Frequency
Model Rotates About Vertical Axis
Observing Radar
Angle of Climb
Nose Aspect
40 M² Level
RELATIVE POWER (db)
ANGLE

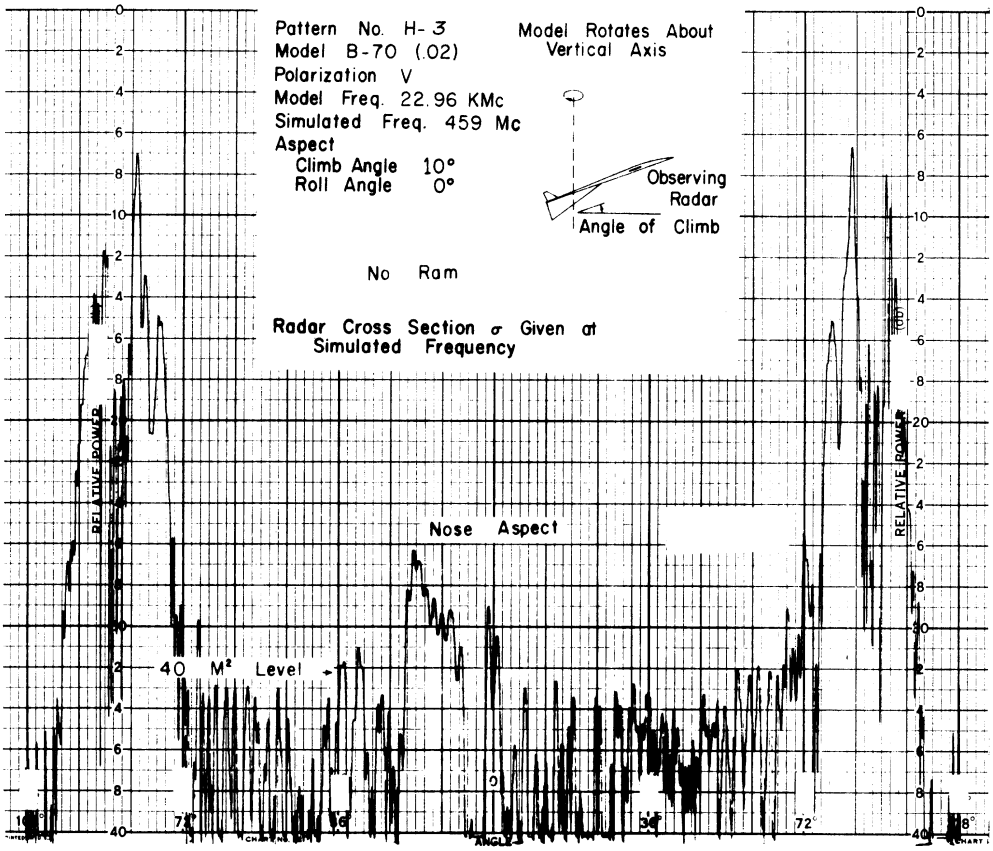
Pattern No. H-3
Model B-70 (.02)
Polarization V
Model Freq. 22.96 KMc
Simulated Freq. 459 Mc
Aspect
Climb Angle 10°
Roll Angle 0°
No Ram
Radar Cross Section σ Given at Simulated Frequency
Model Rotates About Vertical Axis
Observing Radar
Angle of Climb
Nose Aspect
40 M² Level
RELATIVE POWER
ANGLE

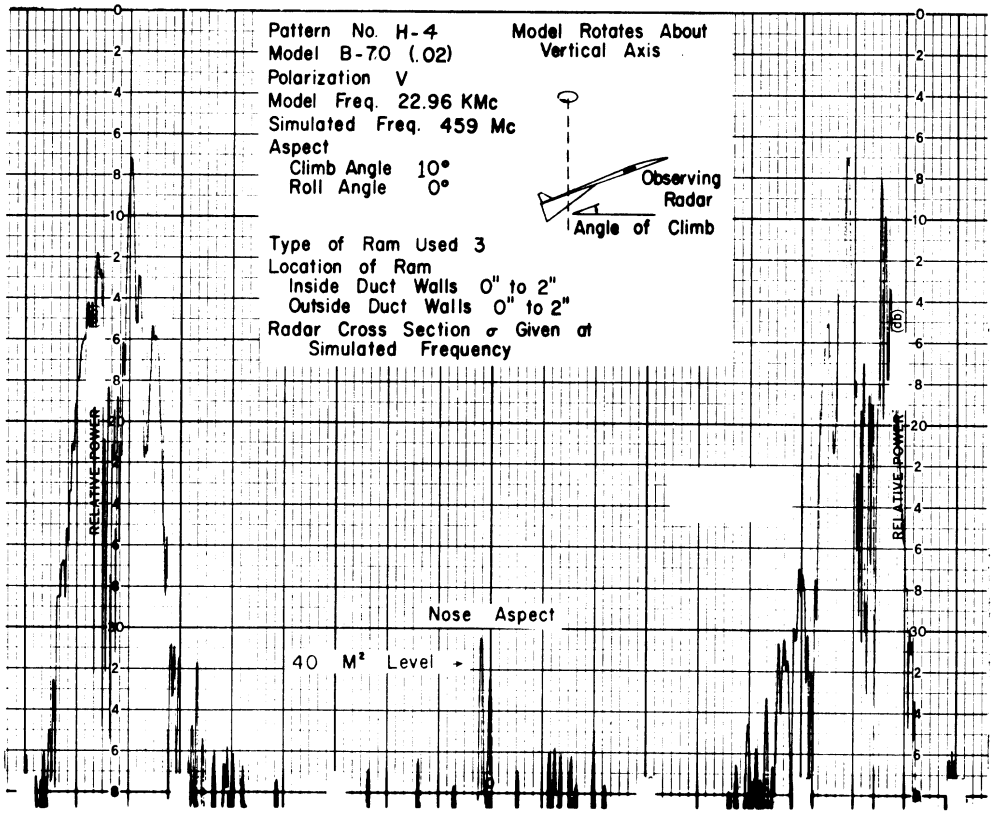
Pattern No. H-4
Model B-70 (.02)
Polarization V
Model Freq. 22.96 KMc
Simulated Freq. 459 Mc
Aspect
Climb Angle 10°
Roll Angle 0°
Type of Ram Used 3
Location of Ram
Inside Duct Walls 0" to 2"
Outside Duct Walls 0" to 2"
Radar Cross Section σ Given at Simulated Frequency
Model Rotates About Vertical Axis
Observing Radar
Angle of Climb
Nose Aspect
40 M² Level
RELATIVE POWER

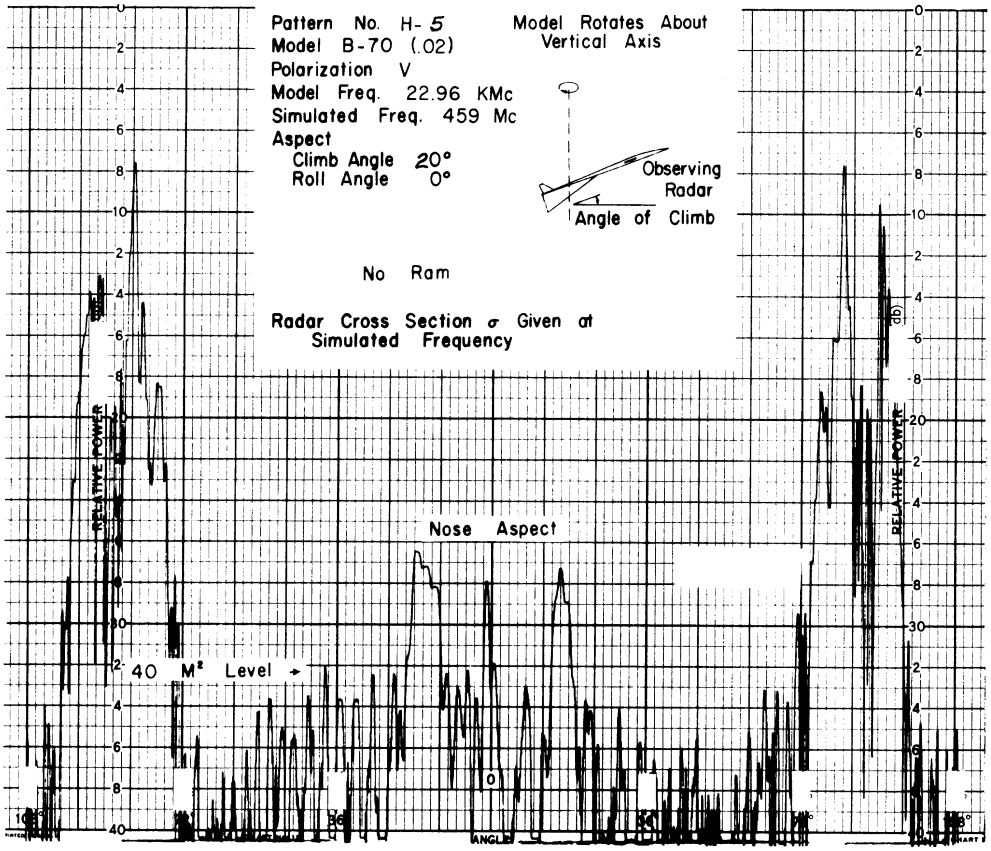
Pattern No. H-5
Model B-70 (.02)
Polarization V
Model Freq. 22.96 KMc
Simulated Freq. 459 Mc
Aspect
Climb Angle 20°
Roll Angle 0°
Model Rotates About Vertical Axis
Observing Radar
Angle of Climb
No Ram
Radar Cross Section σ Given at Simulated Frequency
Nose Aspect
40 M² Level
RELATIVE POWER
db
ANGLE

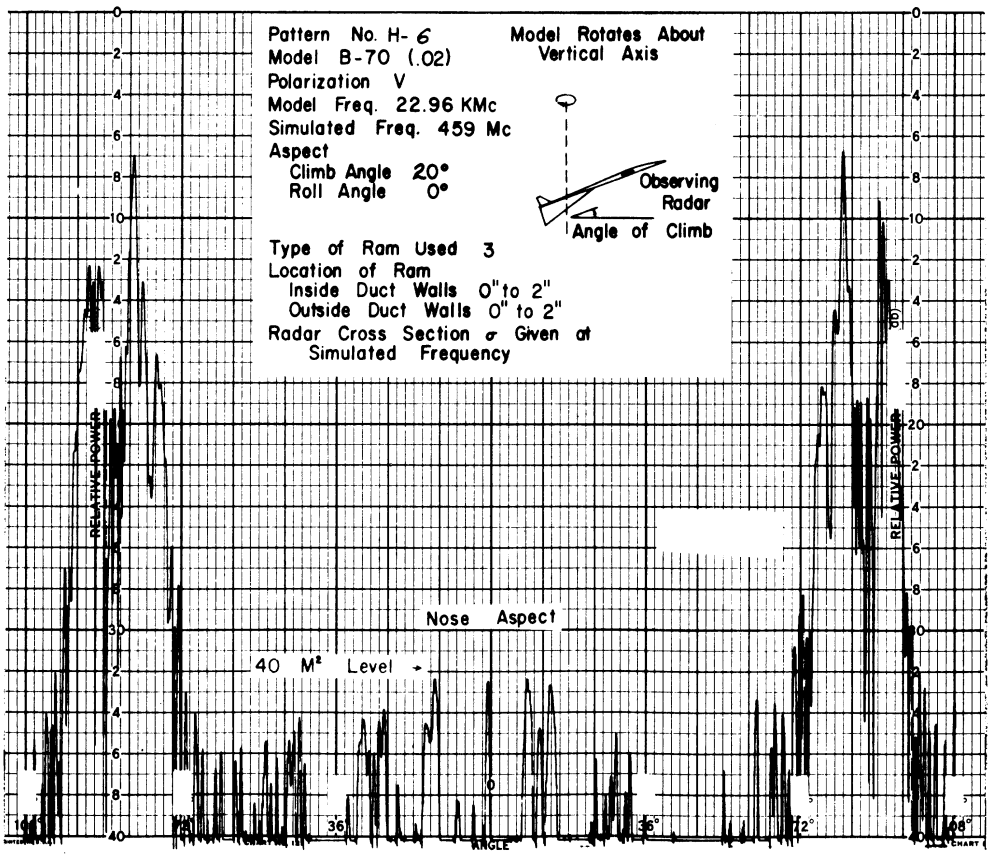
Pattern No. H-6
Model B-70 (.02)
Polarization V
Model Freq. 22.96 KMc
Simulated Freq. 459 Mc
Aspect
Climb Angle 20°
Roll Angle 0°
Model Rotates About Vertical Axis
Observing Radar
Angle of Climb
Type of Ram Used 3
Location of Ram
Inside Duct Walls 0" to 2"
Outside Duct Walls 0" to 2"
Radar Cross Section σ Given at Simulated Frequency
Nose Aspect
40 M² Level
RELATIVE POWER
db
ANGLE

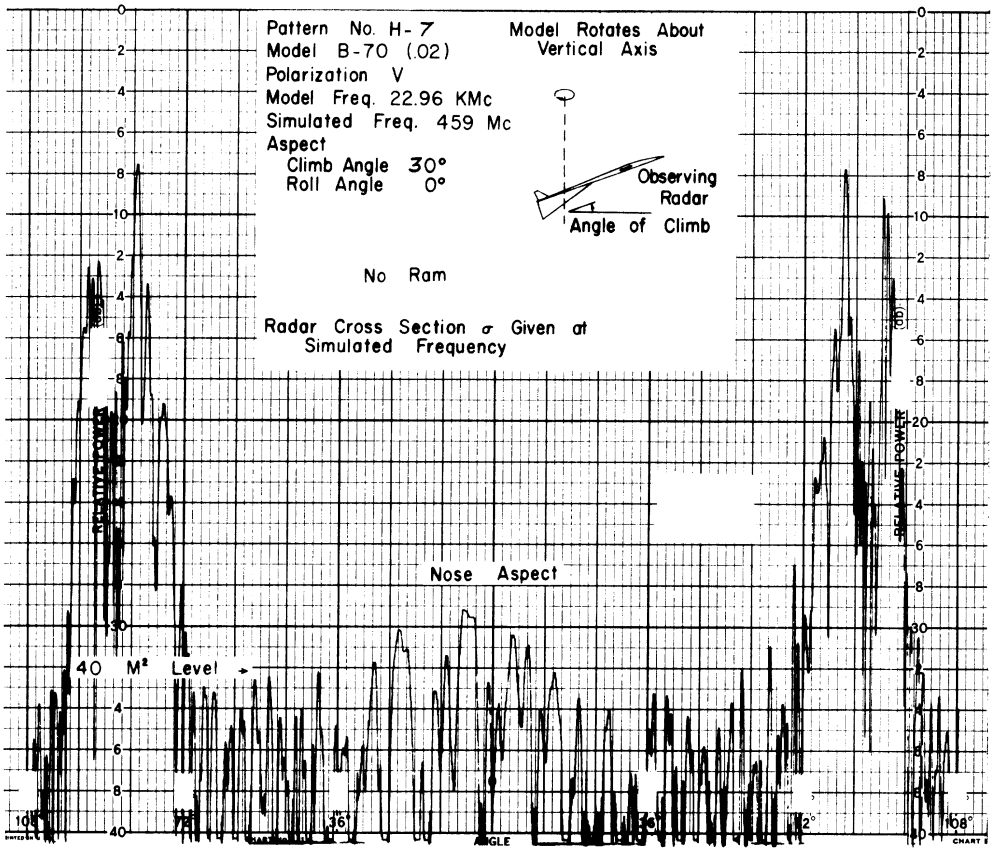
Pattern No. H-7
Model B-70 (.02)
Polarization V
Model Freq. 22.96 KMc
Simulated Freq. 459 Mc
Aspect
Climb Angle 30°
Roll Angle 0°
Model Rotates About Vertical Axis
Observing Radar
Angle of Climb
No Ram
Radar Cross Section σ Given at Simulated Frequency
Nose Aspect
40 M² Level
RELATIVE POWER (db)
ANGLE

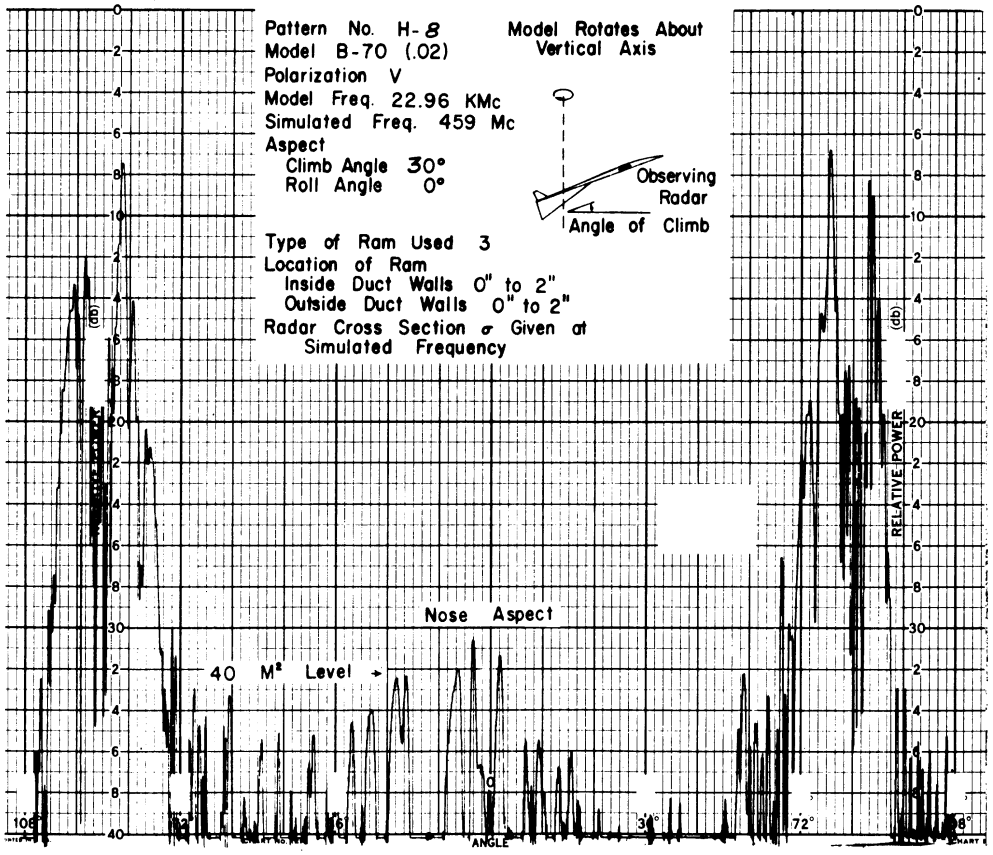
Pattern No. H-8
Model B-70 (.02)
Polarization V
Model Freq. 22.96 KMc
Simulated Freq. 459 Mc
Aspect
Climb Angle 30°
Roll Angle 0°
Model Rotates About Vertical Axis
Observing Radar
Angle of Climb
Type of Ram Used 3
Location of Ram
Inside Duct Walls 0" to 2"
Outside Duct Walls 0" to 2"
Radar Cross Section σ Given at Simulated Frequency
Nose Aspect
40 M² Level
RELATIVE POWER (db)
ANGLE

4.3.9. Series I: Effect of Inclined Duct Walls, 388 Mc

The four patterns in this series were made to check the effect of tilting the inside surfaces of the duct walls. Mr. D. Levine of NAA reported that ray tracing studies in their group indicated that a significant (10 to 15 db) reduction in cross section could be achieved if the inside duct walls were inclined at an angle of 2^{o} or 3^{o} to the vertical, resulting in a duct whose cross section is not rectangular. It was suggested that this reduction in the radar cross section is due to the scattering of much of the energy in directions other than backscattering. No absorbing material is, of course, involved. A brief analysis of this idea was made at the Radiation Laboratory and indicated that for certain aspects a small reduction might occur, but that it would be much less than 10 db and that the range of aspects over which the reduction occurred could be relatively small.

An experimental investigation of this question was made. To simulate the tilting of the ducts, wood wedges which had been metalized were inserted along the two vertical walls of each duct. These simulated a 2^{o} tilt in the duct walls. The wedges on the outer walls extended 8 inches into the ducts, while those on the inner walls extended 3.5 inches into the ducts (the curved inner walls made it more difficult to use a long wedge there).

The effect of the 2^{o} wall tilt is shown in Patterns I-1 through I-4. In each of the 4 patterns, the wall condition remains the same. The first two

patterns are for climb angles of 0^{o} and 10^{o} with vertical polarization. The second two are for 0^{o} and 10^{o} with horizontal polarization. An examination of the results shows a modest reduction of 2 or 3 db in some of the lobes (see I-1 for example). In other cases, the lobes are more narrow with little change in level. Pattern I-3 shows a 3 or 4 db increase in the first two lobes near 0^{o}.

From theoretical considerations and from these measurements, it is concluded that this approach will not provide the desired reduction in cross section.

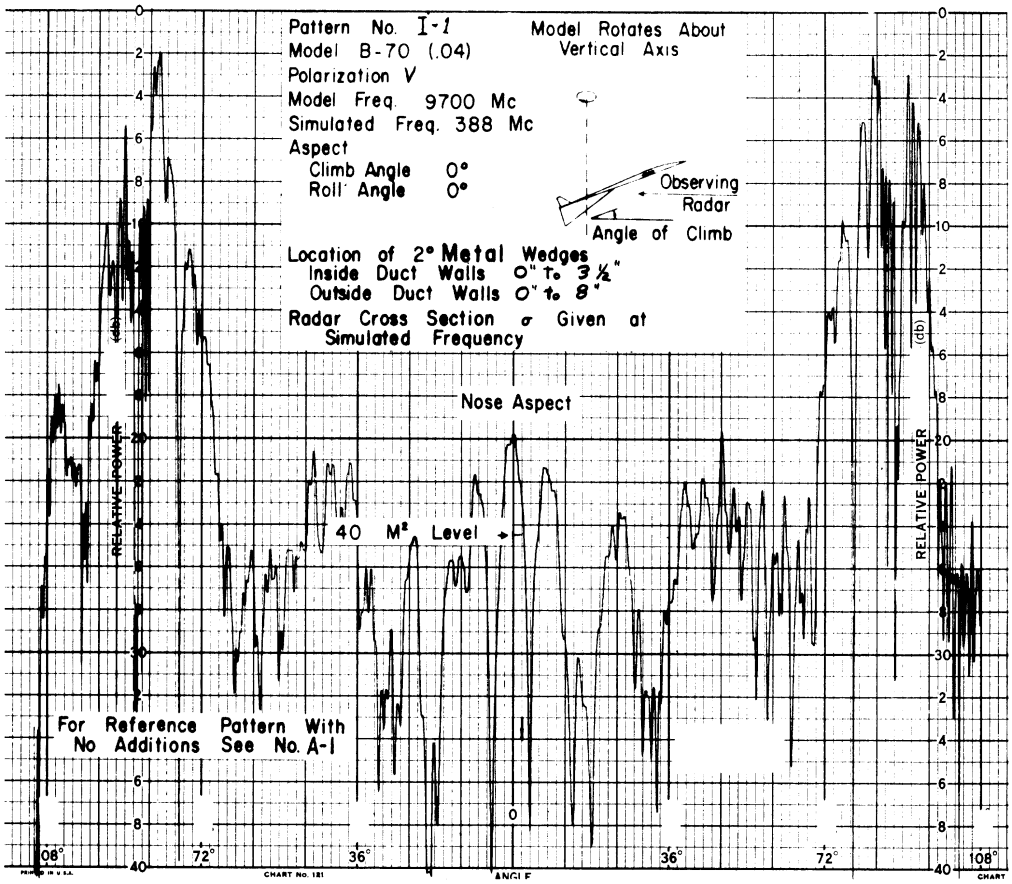
Pattern No. I-1
Model B-70 (.04)
Polarization V
Model Freq. 9700 Mc
Simulated Freq. 388 Mc
Aspect
Climb Angle 0°
Roll Angle 0°
Model Rotates About Vertical Axis
Observing Radar
Angle of Climb
Location of 2° Metal Wedges
Inside Duct Walls 0" to 3 ½"
Outside Duct Walls 0" to 8"
Radar Cross Section σ Given at Simulated Frequency
Nose Aspect
40 M² Level
For Reference Pattern With No Additions See No. A-1
RELATIVE POWER (db)
108° 72° 36° 0 36° 72° 108°
CHART NO. 121
ANGLE

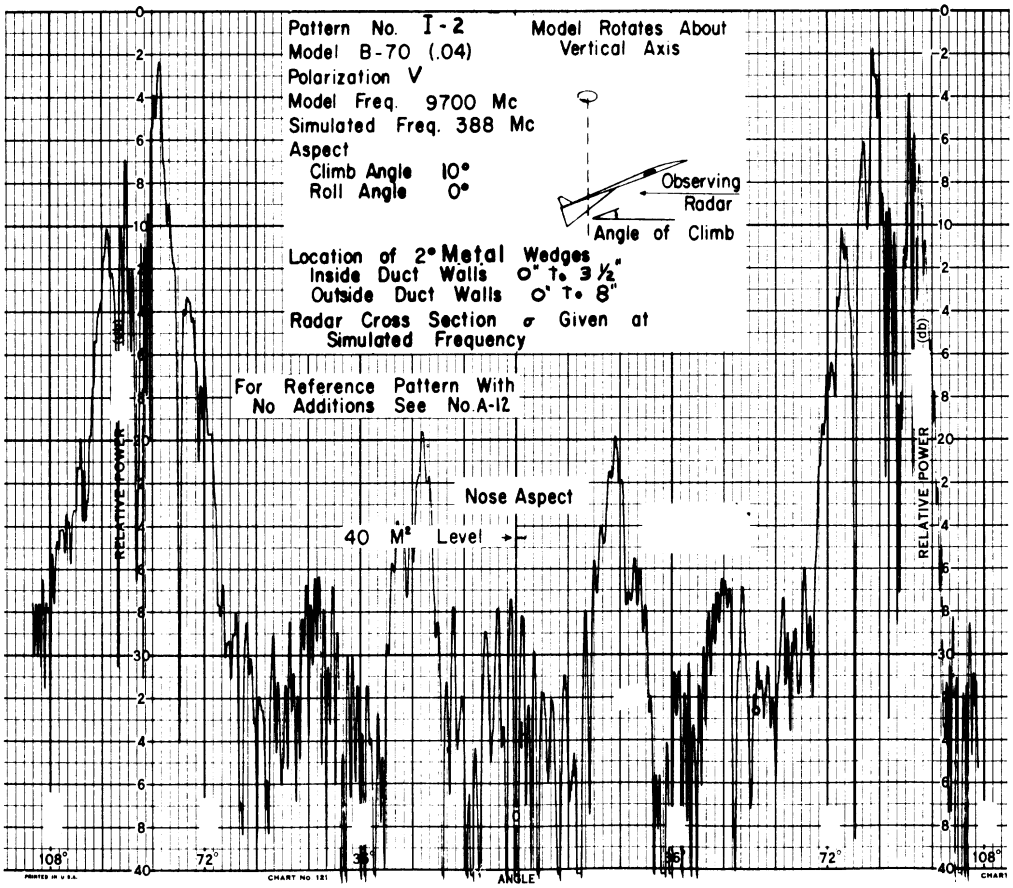
Pattern No. I-2
Model B-70 (.04)
Polarization V
Model Freq. 9700 Mc
Simulated Freq. 388 Mc
Aspect
Climb Angle 10°
Roll Angle 0°
Model Rotates About Vertical Axis
Observing Radar
Angle of Climb
Location of 2° Metal Wedges
Inside Duct Walls 0" to 3 ½"
Outside Duct Walls 0" to 8"
Radar Cross Section σ Given at Simulated Frequency
For Reference Pattern With No Additions See No. A-12
Nose Aspect
40 M² Level
RELATIVE POWER (db)
108° 72° 36° 0 36° 72° 108°
CHART NO. 121
ANGLE

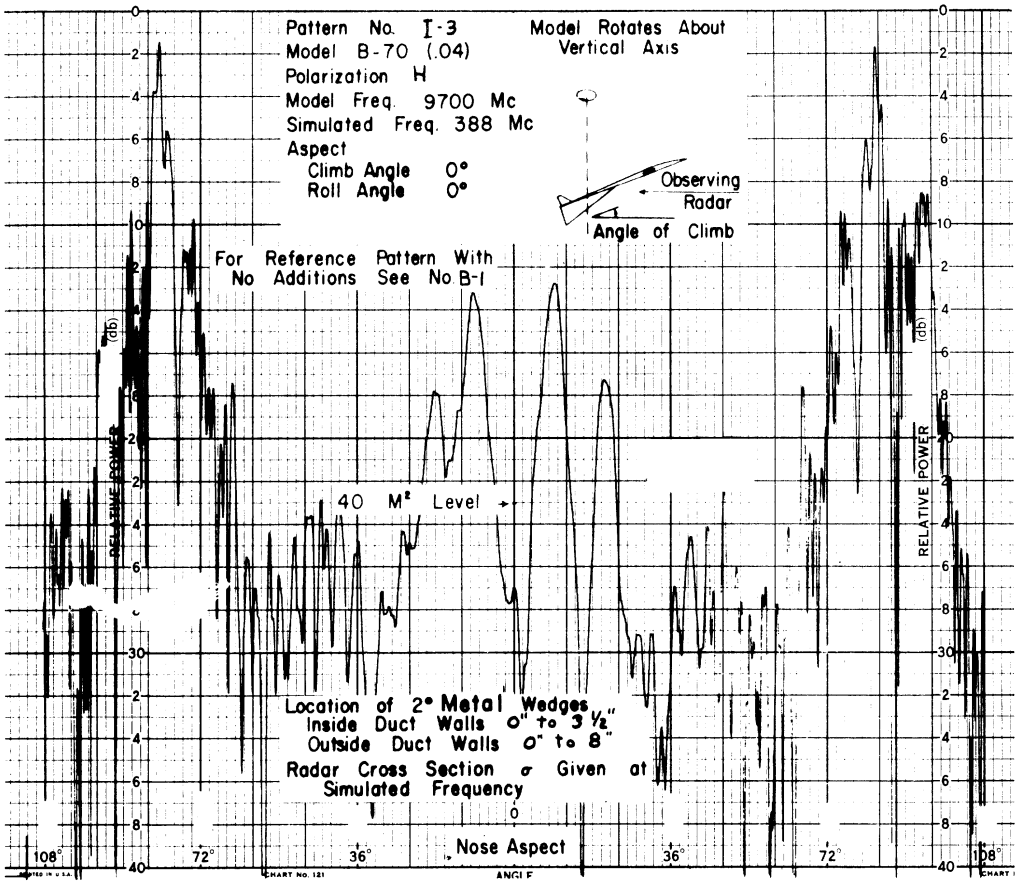
Pattern No. I-3
Model B-70 (.04)
Polarization H
Model Freq. 9700 Mc
Simulated Freq. 388 Mc
Aspect
Climb Angle 0°
Roll Angle 0°
Model Rotates About Vertical Axis
Observing Radar
Angle of Climb
For Reference Pattern With No Additions See No. B-1
40 M² Level
Location of 2° Metal Wedges
Inside Duct Walls 0" to 3 ½"
Outside Duct Walls 0" to 8"
Radar Cross Section σ Given at Simulated Frequency
Nose Aspect
RELATIVE POWER (db)
ANGLE
108° 72° 36° 0° 36° 72° 108°

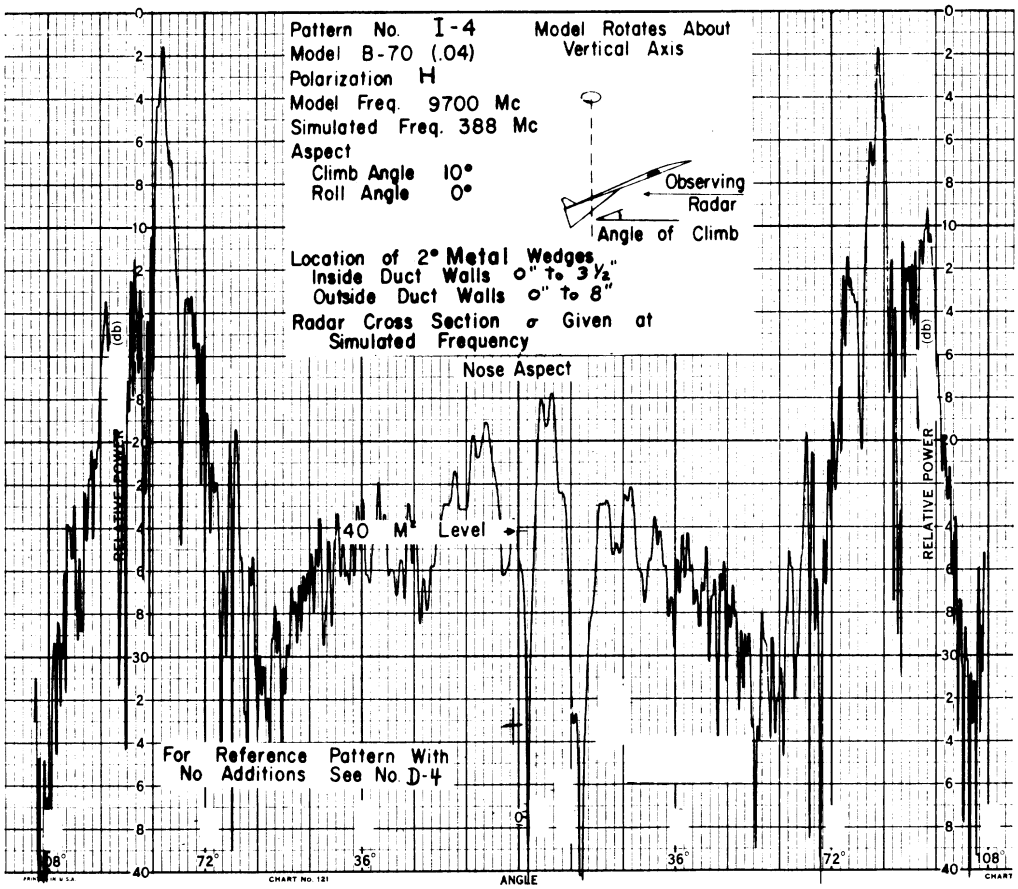
Pattern No. I-4
Model B-70 (.04)
Polarization H
Model Freq. 9700 Mc
Simulated Freq. 388 Mc
Aspect
Climb Angle 10°
Roll Angle 0°
Model Rotates About Vertical Axis
Observing Radar
Angle of Climb
Location of 2° Metal Wedges
Inside Duct Walls 0" to 3 ½"
Outside Duct Walls 0" to 8"
Radar Cross Section σ Given at Simulated Frequency
Nose Aspect
40 M² Level
For Reference Pattern With No Additions See No. D-4
RELATIVE POWER (db)
ANGLE
108° 72° 36° 0° 36° 72° 108°

4.4 Summary of Experimental Results

Over 100 patterns have been included to show the results of the experimental study. For the simulated frequencies covered (patterns not included give data at 230 Mc) measurements show that the radar cross section of the models can be reduced to what would correspond to an average of 40 m^2 or less by the use of RAM, at least in the laboratory. It is believed that reduction to this level is also possible and feasible on the full-scale plane.

The amount of RAM required to achieve the desired results varied considerably with the test conditions. For example, more RAM is required for vertical than for horizontal position; more RAM is required for 900 Mc than for 400 Mc; and more RAM is required for 0^o climb angle than for the 10^o. There is little or no question about the most effective locations for the RAM, assuming, of course, that the duct apertures are to be left open. These locations proved to be on the inner and outer duct walls at or near the beginning of the duct. To reduce the radar cross section to 40 m^2 for the more difficult condition, RAM was used as follows: on the outer duct walls 0 to 5", and on the inner walls from -2" to 4". (0 to 6" was actually used on the outer wall, but a 5" strip would probably be equally effective.) These locations are explained in Figure 35, and correspond on the full-scale aircraft to 125" linings on the outer walls starting at the beginning of the duct and 150" linings on the inner duct walls starting 50" before the beginning of the duct aperture. The resulting surface area of RAM is approximately 128 square feet per duct, making a total of 256 square feet for the

whole aircraft. The above tests were made with the -9 db RAM, and it is doubtful if one can be sure of having a RAM better than this at all the radar frequencies of interest. Since this amount of RAM is required for the most difficult condition tested, these locations are recommended for any future tests.

The tests also showed that the cross section reduction was greater with better RAM. Tests repeated with RAM having a reflectivity of -4 db, -9 db and -20 db showed a worthwhile reduction with the -4 db material, about the same with the -9 db RAM and better results with the -20 db RAM. (See Patterns F-6, F-16 and F-17.) For a less difficult condition, tests were made with a RAM having a reflectivity of -3 db and other tests were carried out with a -6 db RAM. As shown in Patterns B-13 and B-14, the results were quite satisfactory in each case.

5. RECOMMENDATIONS

To reduce the peak cross section of the broadside beam as observed at elevations up to 45° below the horizontal, the fins should be tilted upwards, the duct sides should be tilted inwards and the wings should be tilted upwards. A 5° tilt for the fins should be sufficient. With the same tilt for the ducts and a 10° tilt for the wings, the peak cross section will be reduced to approximately 10^4 square meters. The azimuthal beam width is essentially determined by the curvature (fore-and-aft) of the ducts, and will not be affected to any marked extent by the above changes.

As regards the forward aspects, work should be continued to find or develop the most suitable RAM for the B-70 application. Ferroxcube 105 is suggested as one material which is known to be satisfactory from a temperature point of view. It is believed to have a reflectivity which is nearly adequate, but it is doubtful if it is superior to many other high temperature ferrite absorbers which have not been investigated. Judging from the results already achieved with low temperature RAM (Ref. 4), it should be possible to develop a ferrite RAM whose power reflection coefficient is 10 % or less from 200 Mc to 10,000 Mc and whose thickness is no greater than 0.5 inches.

In an application where weight is more critical than thickness, materials of the silicone foam type, such as described in Reference 3, should be considered.

The experimental studies have shown that the radar cross section of the B-70 can be significantly reduced in the nose-on area. For all the conditions of polarization, aspect and frequency studied in the laboratory, it was possible to reduce the cross section to 40 square meters or less over a range of azimuth angle of $\pm$ 50° from nose-on. Caution should be exercised, however, in extrapolating these results to prove that the same reduction can be achieved on the full scale model for all frequencies of interest.

Since the tests described in this study have covered frequencies near 390, 460 and 920 Mc, there are still important regions in the frequency band of interest that have not been investigated. The methods used in this study will probably be satisfactory for all frequencies within the above limits of 400 to 1000 Mc. Above 1000 Mc, where the amount of reduction required tends to be greater, further experimental studies should be made.[+] These tests should simulate frequencies as near to the upper frequency limit as possible, and should be performed on a range long enough to eliminate any question concerning the far field requirement. Since the RAM to be used on the full scale aircraft will probably be most effective at these higher frequencies, one can be optimistic about the expected reduction in the cross section. Nevertheless, these tests should be made. In addition, the materials employed in future tests should approximate as closely as possible the RAM to be used on the full scale aircraft.

[+] The authors are aware that NAA, Columbus is investigating the cross section reduction problem at 3000 Mc.

At higher frequencies and with vertical polarization, difficulty may be experienced in obtaining a sufficient reduction of the echoes within 10^{o} or so of the nose. The use of an absorber, or perhaps a metal diffuser, placed in the center of the duct and far enough back to be in the non-critical flow region should prove to be effective in solving this problem.

Some attention should also be given to the frequencies below 400 Mc. Here the required amount of reduction is small but the performance of the RAM will itself be poor. Depending on the reflectivity of the RAM selected for the full scale aircraft it may or may not be necessary to use a wide mesh screen as an aid in the solution of the low frequency cross section reduction problem.[+]

[+] It is of interest to note that the cut-off frequencies at the beginning of the ducts are 122 Mc and 89 Mc for vertical and horizontal polarization, respectively.

6. ACKNOWLEDGEMENTS

The authors are indebted to Professor K. M. Siegel for his advice and guidance during the performance of the work described in this report; and to Mr. William Bahret of WADC and to workers at NRL, Battelle and Emerson and Cuming, Inc. for valuable information on radar absorbing materials.

Their thanks are also due to Professor D. M. Grimes for helpful discussions on ferrite absorbers in general, and for his measurements on specific ferrite materials; to Dr. F. B. Sleator and Mr. D. M. Raybin for their analysis of the dihedral reflector presented in the appendix; to Mr. R. L. Wolford who was responsible for most of the cross section measurements, and to other members of the Radiation Laboratory for assistance with both the theoretical and experimental programs.

7. REFERENCES

1. "Radar Reflection Characteristics of the B-70 Bomber", K. M. Siegel, September 1959. Prepared for the Scientific Advisory Board, U. S. A. F.

2. Rutgers University - RADC Contract AF 30(602)-2058, Ltr. report, October 1959.

3. Emerson and Cuming, Inc. Engineering Reports 1, 2, 3 and 4 on Contract AF 33(616)-6114, "Microwave Absorber Materials", December 1958, March 1959, June 1959 and September 1959.

4. NRL Report No. 4745, "Absorbent Materials for Electromagnetic Waves", R. W. Wright, May 1956, AD-99303.

5. Battelle Memorial Institute, "Research on Methods of Reducing Radar Cross Sections of Aircraft", Falkenbach and Harrison, Final Report on Contract AF 19(602)-1414, August 1957 and Battelle Memorial Institute, "Research Scientific Report No. 1, Contract AF 19(604)-3046, October 1958. ASTIA No. AD 304734.

6. University of Michigan Report No. 2799-4-T, "Hexagonal Ferromagnetic Absorbers", D. M. Grimes, W. W. Raymond and R. G. Wells, Contract AF 30(602)-1922.

7. NRL Report 5304, "Waveguide Dummy Loads and Attenuators Utilizing High-Loss Ferromagnetic Materials", W. H. Emerson, R. W. Wright, A. G. Sands and M. V. McDowell, June 1959.

APPENDIX

OPTICAL ANALYSIS OF THE DIHEDRAL REFLECTORS

by

D. M. Raybin and F. B. Sleator

We assume a dihedral reflector with rectangular sides of dimensions L_1 and L_2 normal to the intersection and interior angle $\frac{\pi}{2} + \theta$, struck by a plane wave with propagation vector normal to the intersection of the sides and making angle β with the side 2. If β is within the range $2\theta < \beta < \frac{\pi}{2} - \theta$, then part of this beam will be doubly reflected, the width of this part being determined by β and either L_1 or L_2, depending on certain relations between these three quantities noted below. The doubly reflected beam will be split into two beams separated by an angle 4θ, the part striking side 2 first leaving at an angle $\beta + 2\theta$ and that striking side 1 first leaving at an angle $\beta - 2\theta$, as shown in Figure A-1. It can be shown by the geometry of the figure that each doubly reflected beam has the same width as it had before the first reflection, and that at every point in a plane normal to the final direction of propagation its phase is the same.

Let B^i be the width of that part of the incident beam which suffers a double reflection, B_1^i, B_2^i be the widths of the parts striking sides 1 and 2 first, respectively. Then by the geometry of the setup, B_1^i is the lesser of the two quantities

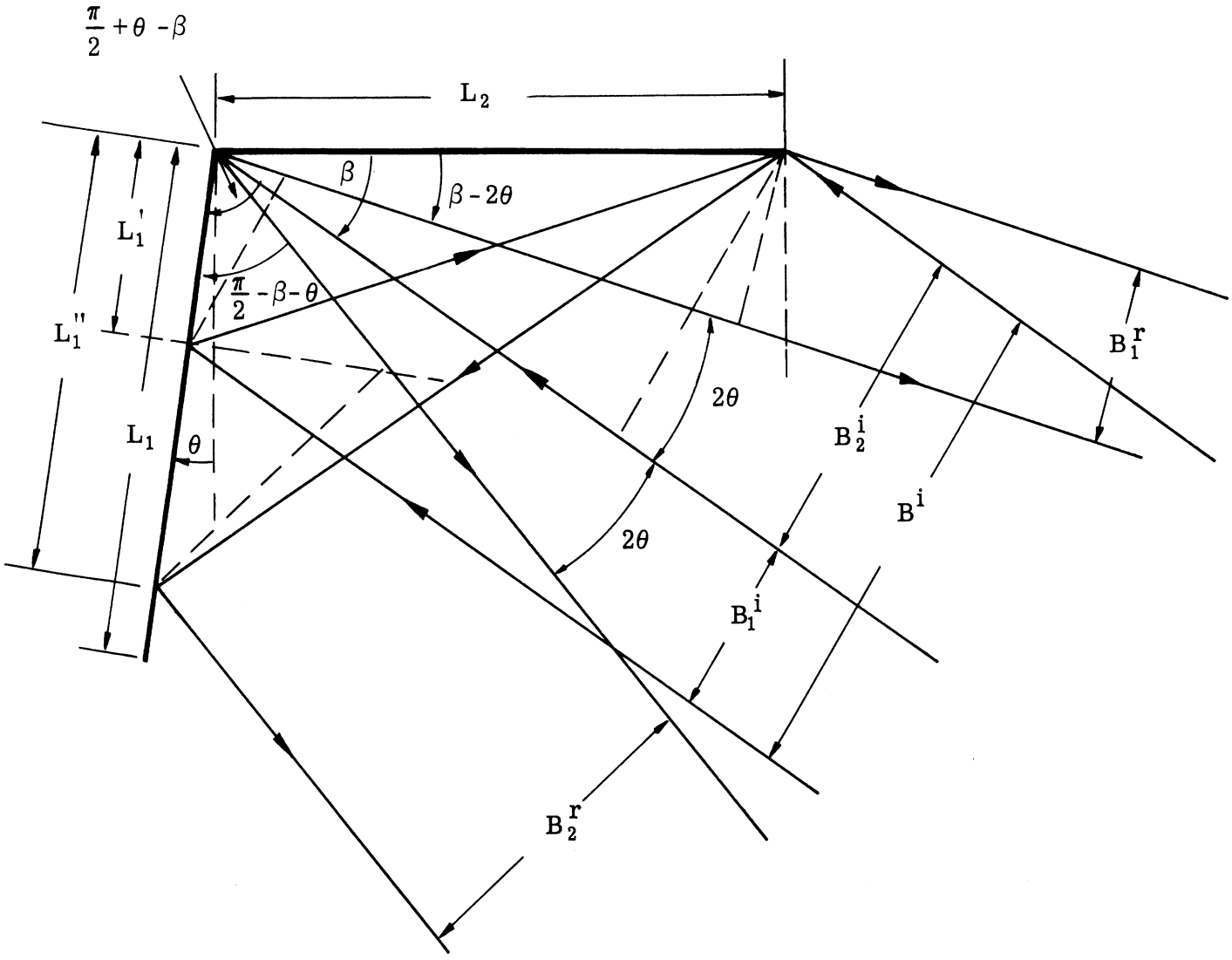
$\frac{\pi}{2}+\theta-\beta$
L_2
β
$\beta-2\theta$
L_1'
$\frac{\pi}{2}-\beta-\theta$
L_1''
L_1
θ
2θ
2θ
B_1^r
B_2^i
B^i
B_1^i
B_2^r

FIGURE A-1

$$\begin{cases} L_1 \sin\left(\frac{\pi}{2} + \theta - \beta\right) = L_1 \cos(\beta - \theta) \\ L_2 \sin(\beta - 2\theta) \end{cases}$$

and B_2^i is the lesser of the quantities

$$\begin{cases} L_1 \sin\left(\frac{\pi}{2} - \beta - \theta\right) = L_1 \cos(\beta + \theta) \\ L_2 \sin\beta. \end{cases}$$

(In the case illustrated, the second quantity is less in each bracket. It can be shown that both parts of B^i are necessarily limited by the same side, i.e. $L_1 \cos(\beta - \theta) < L_2 \sin(\beta - 2\theta) \Longleftrightarrow L_1 \cos(\beta + \theta) < L_2 \sin\beta.$)

Also, let L'_i, L''_i be the effective width of side i with respect to the first and second reflections respectively, i.e. L_1' be that part of side 1 struck by the part B_1^i of the incident beam and L_1'' be the part struck by the first reflection of B_2^i, with corresponding definitions of L_2' and L_2''. Then if side i is limiting (i = 1, 2) we have $L_i' = L_i'' = L_i$. (In the figure shown, i = 2). The above considerations then yield

$$B_1^i = B_1^r = L_1' \cos(\beta - \theta) = L_2'' \sin(\beta - 2\theta)$$

$$B_2^i = B_2^r = L_2' \sin\beta = L_1'' \cos(\beta + \theta).$$

Each part of the reflected beam is assumed to give the same diffraction pattern as an aperture of dimensions equal to those of the beam oriented normal to the direction of propagation of the reflected beam. Thus we write for the

amplitude of the field at a point on the axis of the incident beam due to B_1^r

$$A_1 = L_3 \cdot B_1^i \frac{\sin\left[\frac{kB_1^r}{2}\sin 2\theta\right]}{\frac{kB_1^r}{2}\sin 2\theta} = \frac{2L_3 \sin\left[\frac{kL_1'}{2}\cos(\beta-\theta)\sin 2\theta\right]}{k \sin 2\theta} \; +$$

where L_3 is the dimension of the dihedral parallel to the intersection of the sides, and for that due to B_2^r

$$A_2 = \frac{2L_3 \sin\left[\frac{kL_2'}{2}\sin\beta\sin 2\theta\right]}{k \sin 2\theta} .$$

In the case where L_1 is the limiting dimension, these can be written

$$A_1 = \frac{2L_3 \sin\left[\frac{kL_1}{2}\cos(\beta-\theta)\sin 2\theta\right]}{k \sin 2\theta}$$

$$A_2 = \frac{2L_3 \sin\left[\frac{kL_1}{2}\cos(\beta+\theta)\sin 2\theta\right]}{k \sin 2\theta} ,$$

and similarly if L_2 limits,

$$A_1 = \frac{2L_3 \sin\left[\frac{k}{2} L_2 \sin(\beta-2\theta)\sin 2\theta\right]}{k \sin 2\theta}$$

$$A_2 = \frac{2L_3 \sin\left[\frac{k}{2} L_2 \sin\beta\sin 2\theta\right]}{k \sin 2\theta} .$$

+ Note: This expression is reconciled with the usual form of the diffraction pattern for a flat plate, in which the factor of 2 is absent, by the observation that the angle used here is not that between incident beam and normal but between incident and specular beams.

The amplitudes A_1 and A_2 can be added directly only if the relative phases are considered. This could be done, but for present purposes we are interested in the maximum possible returns from the dihedral at the given angles of incidence, and these are given by the sums of the moduli of the two contributions. Thus the maximum total amplitude should in general be taken as

$$A_T = |A_1| + |A_2|$$

and the cross section proportional to the square of this quantity.

The above analysis holds for the dihedral with obtuse angle. If, instead of increasing the right angle, we diminish it by an angle θ, a similar situation prevails, with the incident beam being split into two parts separated by an angle 4θ as before, for a large part of the angular incidence range. The amplitude of the total backscattering return will thus be approximately as before, with differences occurring in certain ranges due to a switch in the limiting side of the dihedral.

These differences however may be insignificant in comparison to another effect which has not been mentioned, namely, that at certain angles of incidence, e.g. $\beta = \theta$ in the diagram above, there is a singly reflected beam (or if θ is negative, a triply reflected one) whose peak is exactly in the direction of the transmitter-receiver, and whose effective amplitude is thus in general much

larger than that of the doubly reflected beam in either case. The ultimate decision in the design of the dihedral may then be governed by the desirability of excluding this angle from the range of interest. We are led to a more specific analysis of the situation at hand, which can be outlined as follows.

With the dihedral oriented as shown in Figure A2, we assume first that the range of interest for β is from horizontal to 45^{o} below horizontal, and that we may change the orientation of either of the sides L_1, L_2 with respect to the horizontal and vertical. As shown in Case I, L_2 is maintained horizontal and L_1 inclined at angle $\pm\theta$ from the vertical. Here there is a specular return at the angle $\beta = \theta$ which is in general within the range of interest, and which in Case Ia) is singly reflected and limited only by L_1, and in Ib) is triply reflected and may be limited either by L_1 or L_2. Thus for given L_1, the specular return in Ia) is equal to or greater than that in Ib). In Case II, L_1 is maintained vertical and L_2 is rotated through an angle $\pm\theta$ from the horizontal. Here the specular return in IIa) occurs only at one extreme of the β range, i.e. $\beta = 0$, and is limited as before by L_1. In Case IIb) the specular return occurs at $\beta = 2\theta$, which is in general still within the range of interest, and is limited by either L_1 or L_2. The choice here then depends on which side limits and which position of the specular beam is less objectionable.

If it is deemed essential to remove the specular beam entirely from the range of interest, a configuration such as that shown in Case III should be considered,

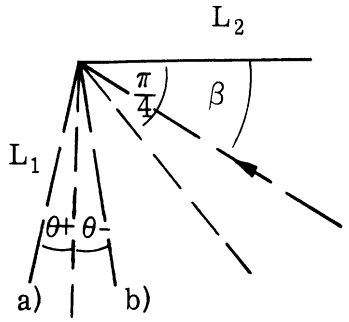

Case I

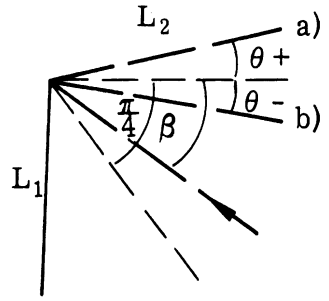

Case II

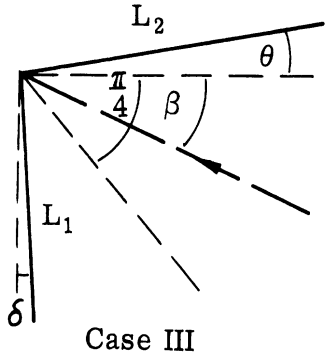

Case III

FIGURE A-2

in which both sides of the dihedral are rotated slightly through positive angles, with $\theta > \delta$, and the specular beam occurs at $\beta = -\delta$. With the permissible range of θ limited by other considerations, this configuration offers less reduction in the doubly-reflected backscattered return than either of the other two cases; however there may still be enough reduction available to make it preferable on the whole.